Impact of ageing on mitochondrial complex expression and islet cell composition in mtDNA mutator mice and human pancreas

Xuefei Yu

A thesis submitted for the degree of Doctor of Philosophy at Newcastle University

Newcastle University
Translational and Clinical Research Institute

September 2020

ABSTRACT

Age-related cumulative mitochondrial mutations can cause mitochondrial dysfunction. The mitochondrial DNA mutator mouse (*PolgA*$^{mut/mut}$) is a model of premature ageing and has been previously shown to develop impaired insulin secretion with age. Normal human ageing has been associated with islet β-cell dysfunction and the change of islet cell composition. The overall aim was to explore the impact of ageing on mitochondrial complex expression and islet cell composition in *PolgA*$^{mut/mut}$ mice and human pancreas.

Immunofluorescence was used to study mitochondrial respiratory chain protein expression (complex I and IV) by normalizing to mitochondrial mass marker (Tomm20). This technique was also applied to the study of islet cell composition with proliferation marker Ki67. Experiments were conducted on pancreas tissue from *PolgA*$^{mut/mut}$ mice and age-matched wild type (WT) mice at two ages: 3 months (young) and 11 months (old). Some of the *PolgA*$^{mut/mut}$ mice underwent exercise training from 4 months of age. Non-diabetic normal human pancreas tissue from two age groups: 20~40 years (young) and 60~80 years (old) were also studied for mitochondrial complex expression and islet cell composition.

The findings of the first three result chapters described the impact of ageing in mtDNA mutator mice model. Complex I expression was decreased in islets from young *PolgA*$^{mut/mut}$ mice, and it persisted with age in comparison with the WT mice. Investigation of islet cell composition identified an increase in absolute α-cell number with age in the *PolgA*$^{mut/mut}$ mice that contributed to a decreased β:α ratio in islets from the old *PolgA*$^{mut/mut}$ mice versus the age-matched WT mice. Ki67 examination showed that increased α-cell proliferation contributed to the increase in α-cell mass. Islet cell subtype analysis in old *PolgA*$^{mut/mut}$ mice revealed that the complex I deficiency was greater in the α-cells compared with the β-cells, suggesting that the increased α-cell proliferation observed in old *PolgA*$^{mut/mut}$ mouse islets maybe a direct response to complex I deficiency. Although none of these mice developed diabetes with age, decreased insulin expression was discovered in the pancreatic islets of the old *PolgA*$^{mut/mut}$ mice. Endurance exercise did not have significant impact on mitochondrial complex expression nor islet cell composition in old *PolgA*$^{mut/mut}$ mice. The last result chapter explored the impact of ageing in human pancreatic tissues from non-diabetic donors. Tomm20 expression was higher in pancreatic islets from old versus young donors, but there was no difference in complex I and IV expression. Whole islet cell number and absolute β-cell number were lower in the old versus young islets, but there was no significant difference in the β:α ratio. Taken together, my findings show that

mitochondrial dysfunction alters pancreatic islet cell composition in response to ageing in the *PolgA*$^{mut/mut}$ mice. In non-diabetic human islets, there is no evidence of altered mitochondrial subunit expression but Tomm20 expression was increased in the islets from old donors appears to reflect a compensatory increase in mitochondrial mass.

I would like to dedicate this thesis to my parents

Hongzhu Yu and Hongling Sun

Success is not final, failure is not fatal: it is the courage to continue that counts.

-Winston Churchill

DECLARATION OF ORIGINALITY

I hereby declare that all the work presented in this thesis is my own work. The data have not been submitted previously for any alternative degrees.

Xuefei Yu

Table of Contents

ABSTRACT 2
DECLARATION OF ORIGINALITY 6
LIST OF TABLES 13
LIST OF FIGURES 15
ACKNOWLEDGEMENTS 19
PUBLISHED WORK 20
LIST OF ABBREVIATIONS 21
CHAPTER 1. GENERAL INTRODUCTION 24
1.1. Diabetes 24
1.1.1. Diabetes Mellitus 24
1.1.2. Glucose homeostasis 25
1.1.2.1. Pancreas structure and function 25
1.1.2.2. The maintenance of blood glucose level 26
1.1.2.3. Glucose metabolism in pancreatic β-cells 26
1.1.2.4. Glucose-Stimulated Insulin Secretion 27
1.1.3. Diabetes Subtypes 31
1.1.4. T2DM risk factors 32
1.1.4.1. Metabolic risk factors 32
1.1.4.2. Genetic risk factors 33
1.2. Mitochondrial biology 34
1.2.1. Mitochondrion structure 34
1.2.2. Mitochondrial function 36
1.2.2.1. ATP generation 36
1.2.2.2. ROS generation 40
1.2.2.3. Calcium signaling and homeostasis 40
1.2.2.4. Apoptosis and necrosis 41
1.2.2.5. Mitochondrial quality control 42
1.2.3. Mitochondrial DNA 42
1.2.4. Mitochondria and ageing 44
1.2.5. Mitochondrial DNA mutation and the onset of diabetes/MIDD 47
1.2.6. T2DM and ageing 50
1.2.7. T2DM and mitochondrial dysfunction 51

1.2.8. MtDNA mutator mouse model 53
1.2.8.1. The *PolgA*$^{mut/mut}$ mice 55
1.2.8.2. The effect of exercise training 57
1.3. Islet beta cell physiology 60
1.3.1. Islet biology in mice and humans 60
1.3.1.1. The development of mouse islets. 62
1.3.1.2. The development of human islets. 62
1.3.2. Islet adaption to physiological and pathological stress. 63
1.3.2.1. The adaption of mouse islets. 64
1.3.2.2. The adaptation of human islets. 65
1.3.3. Islet dysfunction in T2DM 67
1.3.3.1. The β-cell dysfunction 68
1.3.3.2. The reduction of β-cell mass 69
CHAPTER 2. GENERAL MATERIALS AND METHODS 74
2.1. Mitochondrial DNA mutator mice model procurement. 74
2.1.1. Mouse husbandary and monitoring 74
2.1.2. Tissue harvest. 78
2.2. Human sample procurement. 78
2.3. Immunofluoresence staining 79
2.3.1. Sectioning 79
2.3.1.1. Fixed tissue sectioning 79
2.3.1.2. Frozen tissue sectioning 80
2.3.2. Staining 80
2.3.2.1. Formalin-fixed, paraffin-embedded sections. 80
2.3.2.2. Frozen sections. 85
2.3.3. Imaging 85
2.3.4. Image analysis 86
2.3.4.1. Mitochondrial complex expression analysis within islets 86
2.3.4.2. Expression of insulin secretion analysis within β cells. 87
2.3.4.3. Mitochondrial complex expression analysis within different islet endocrine cell types. 87
2.3.4.4. Islet cell composition analysis 90
2.3.4.5. Islet cell proliferation analysis. 90
2.3.5. Data analysis 90

2.3.5.1. Densitometry test for 3-month *PolgA*$^{mut/mut}$ and wild type mice 92
2.3.5.2. Densitometry test for 11-month *PolgA*$^{mut/mut}$ and wild type mice 92
2.4. Laser dissection microscopy 95
2.4.1. Preparation 95
2.4.2. Laser dissection 95
2.5. Real time PCR 96
2.5.1. DNA extraction 97
2.5.2. Make up standard curve 97
2.5.2.1. Preparation 97
2.5.2.2. Samples in serial dilutions 98
2.5.3. Loading samples and real time PCR 98
2.5.3.1. Making up mastermix 98
2.5.3.2. Real time PCR 99
2.5.4. After PCR analysis 100
2.5.4.1. Standard curve analysis method 100
2.5.4.2. △Ct analysis method 100
2.6. Blood glucose testing 100
2.7. HbA1c ELISA testing in mouse blood 101
2.7.1. Preparation of EDTA anticoagulant 101
2.7.2. Mouse blood collection 101
2.7.3. Mouse Haemoglobin A1c testing 102
2.7.3.1. Preparation of reagents, samples, calibrators and controls 102
2.7.3.2. Preparation of lysate 102
2.7.3.3. Preparation of the assay 102
2.7.3.4. Determining the HbA1c concentration 103
CHAPTER 3. IMPACT OF AGEING ON MITOCHONDRIAL RESPIRATORY CHAIN EXPRESSION BY COMPARING PANCREATIC ISLETS FROM *POLGA*$^{MUT/MUT}$ AND WILD TYPE MICE. 105
3.1 Introduction 105
Ageing and mitochondrial dysfunction. 105
The aims of the current chapter were to: 107
3.2 Methods 108
3.2.1 Quadruple immunofluorescence with mouse pancreas sections. 108
3.2.2 Immunofluorescence with mouse frozen sections. 108
3.2.3 Laser dissection microscopy 108

3.2.4 Real-time PCR and mitochondrial DNA copy number assay 109
3.3. Results 110
3.3.1. A significant mitochondrial complex I deficiency was found in islets from *PolgA*$^{mut/mut}$ mice compared to the wild type mice at 3 months. 110
3.3.2. A significant mitochondrial complex I deficiency but a significant increase of complex IV expression were found in islets from *PolgA*$^{mut/mut}$ mice compared to their wild type mice at 11 months. 113
3.3.3. A significant deficiency in mitochondrial complex IV expression was found in islets from 11-month wild type mice compared to 3-month wild type mice. 116
3.3.4. Tomm20 expression were significantly higher in islets from 11-month *PolgA*$^{mut/mut}$ mice compared to the 3-month *PolgA*$^{mut/mut}$ mice. 118
3.3.5. No significant differences in islet cell mtDNA copy number between *PolgA*$^{mut/mut}$ mice and wild type mice at 11 months 120
3.4. Summary 124
3.5. Discussion 125
CHAPTER 4: STUDY OF THE IMPACT OF AGEING ON PANCREATIC ISLET CELL COMPOSITION BY COMPARING *POLGA*$^{MUT/MUT}$ WITH WILD TYPE MICE. 131
4.1. Introduction 131
Ageing, mice β-cell mass and β-cell function. 131
The Aims of the current chapter were to: 132
4.2. Methods 133
4.2.1. Triple immunofluorescence staining on mouse pancreas sections. 133
4.3. Results 134
4.3.1. There were no significant differences in the α- and β-cell percentage, islet size and islet cell number between *PolgA*$^{mut/mut}$ mice and their wild type controls at 3 months. 134
4.3.2. *PolgA*$^{mut/mut}$ mice had a significantly lower β-cell percentage, higher α-cell percentage and higher absolute α-cell number versus their wild type controls at 11 months. 138
4.3.3. Islet size, whole islet cell number and absolute β-cell number all increased significantly in wild type mice from 3-month to 11-month. 142
4.3.4. Islet size, whole islet cell number, absolute α and β cell number all increased significantly in *PolgA*$^{mut/mut}$ mice from 3-month to 11-month. 145
4.3.5. The overall comparison between *PolgA*$^{mut/mut}$ and WT mice in two different ages. 148
4.4. Summary 150
4.5. Discussion 151
CHAPTER 5. THE STUDY OF ENDOCRINE CELL SUBTYPES IN *POLGA*$^{MUT/MUT}$ MICE COMPARED TO AGE-MATCHED WILD TYPE MICE. 155

5.1. Introduction 155
5.2. Methods 157
5.2.1. Mitochondrial complex expression analysis in different islet cell subtypes. 157
5.2.2. Proliferation assay immunofluorescence staining. 157
5.2.3. Monthly blood glucose and body weight measurement. 157
5.2.4. Endpoint HbA1c measurement. 157
5.3. Results 158
5.3.1. Increased α-cell proliferation in islets of 11-month *PolgA*$^{mut/mut}$ mice compared to the age-matched wild type mice. 158
5.3.2. Endocrine cell sub-types react differently to normal ageing and premature ageing. 162
5.3.3. Insulin expression in the pancreatic β-cells was significantly lower in the *PolgA*$^{mut/mut}$ versus their wild type controls at 11 months. 164
5.3.4. No increase in blood glucose levels in the 11-month-old *PolgA*$^{mut/mut}$ mice with age. 166
5.4. Summary 171
5.5. Discussion 172
CHAPTER 6. STUDY THE IMPACT OF AGEING ON MITOCHONDRIAL RESPIRATORY CHAIN FUNCTION AND ISLET CELL COMPOSITION IN NON-DIABETIC HUMAN PANCREATIC ISLETS. 180
6.1. Introduction 180
6.2. Methods 182
6.2.1. Human sample procurement. 182
6.2.2. Quadruple mitochondrial immunofluorescence staining on human pancreas sections 182
6.2.3. Triple immunofluorescence staining on human pancreas sections. 182
6.3. Results 183
6.3.1. There was no significant difference in BMI or gender between old and young non-diabetic donors. 183
6.3.2. The expression of mitochondrial mass marker (Tomm20) is significantly higher in islets from old versus young non-diabetic human donors. 184
6.3.3. Old human non-diabetic donors have significantly lower whole islet cell number and absolute β-cell number compared to the young non-diabetic donors. 187
6.4. Summary 191
6.5. Discussion 192
CHAPTER 7. GENERAL DISCUSSION 199
7.1. Discussion 199
7.1.1. Is *PolgA*$^{mut/mut}$ mice a good ageing model? 199
7.1.2. The difference in mitochondrial complex expression between α and β cells. 202

7.1.3. Altered pancreatic islet cell composition of *PolgA*$^{mut/mut}$ mice result from different mitochondrial complex expression in different endocrine cells. 202
7.1.4. *PolgA*$^{mut/mut}$ mice model compared to TFAM β-cell specific knockdown mice model. 203
7.1.5. The longitudinal comparison in mitochondrial complex expression and islet cell composition between human and mice. 205
7.2. Mitochondrial dysfunction and islet cell composition 208
7.2.1. Ageing 208
7.2.2. T2DM. 208
7.2.3. The interation between ageing and T2DM. 208
7.3. Innovations 211
7.4. Limitations 211
7.5. Future work 212
7.6. Conclusion 214
CHAPTER 8. APPENDIX 215
REFERENCES 222

LIST OF TABLES

Table 1-1. Percentage ratio of mtDNA point mutations in various tissues from the patient. 46

Table 1-2. Mutations of mitochondrial genes in patients with DM. 49

Table 2-1. Mitochondrial mutator mice in different ages and genotypes which were used in this study… 77

Table 2-2. The *PolgA*$^{mut/mut}$ and wild type mice datasheet. 77

Table 2-3. Patient information for 7 non-diabetic donors from University of Pisa. 79

Table 2-4. Patient information for 6 non-diabetic donors from Newcastle University. 79

Table 2-5. The choice of antigen retrieval buffer, washing buffer and blocking solution based on the primary antibody. 81

Table 2-6. Protocols for making 1×TBST and 1×PBS. 81

Table 2-7. Information for primary antibodies used in our study. 83

Table 2-8. Information for secondary antibodies used in our study. 83

Table 2-9. The optimized experimental procedure for quantifying mitochondrial OXPHOS function in pancreatic islets. 84

Table 2-10. The optimized experimental procedure for counting islet endocrinal cell and quantifying pancreatic hormone. 84

Table 2-11. The single cell lysis buffer protocol. 95

Table 2-12. The sequences for ND5 and β-actin forward and reverse primers. 99

Table 2-13. The information of mice used for blood glucose measurement and blood sample collection. 101

Table 4-1. The β/α ratio in wild type and *PolgA*$^{mut/mut}$ mice at two different ages 148

Table 5-1. The number of Ki67 (+) islets in each mouse. 161

Table 5-2. The endpoint body weight, HbA1c% and blood glucose level result summary. 170

Table 6-1. The age, BMI and gender information of human non-diabetic donors… 183

Table 6-2. The gender distribution in old and young age donors. 183

Table 7-1. The comparison between *PolgA*$^{mut/mut}$ mice and TFAM β cell specific knockdown mice. 204

Table 7-2. The age related changes in mitochondrial complex expression in mice and human islets. 205

Table 7-3. The age-related changes in islet cell composition in mice and human...... 206

Table 8-1. The endpoint body weight of 11 month *PolgA*$^{mut/mut}$ mice and wild type mice which used for mitochondrial expression and islet cell composition studies….....215

Table 8-2. Monthly glucose measurement results in newly recruited 5 *PolgA*$^{mut/mut}$ mice and 5 wild type mice (mmol/l). 216

Table 8-3. Monthly body weight measurement results in newly recruited *PolgA*$^{mut/mut}$ mice and wild type mice (g)...... 216

Table 8-4. Two times of HbA1c% measurement and average HbA1c% result in endpoint whole blood samples from newly recruited 5 *PolgA*$^{mut/mut}$ and 5 wild type mice. 216

LIST OF FIGURES

Figure 1-1. Dose response curves for insulin secretory rates against plasma glucose concentration. 29

Figure 1-2. Glucose induced insulin secretion in pancreatic β cells. 30

Figure 1-3. Mitochondrial electron transport chain. 39

Figure 1-4. Representative age ranges for mature life history stages in C57BL/6J mice compared to human beings. 54

Figure 1-5. The comparison between wild type and *PolgA*$^{mut/mut}$ mice both at 13 months of age. 56

Figure 1-6. The cytoarchitecture of rodent islets and primate islets. 61

Figure 1-7. The general outline of this study. 73

Figure 2-1. The survival curves for *PolgA*$^{mut/mut}$ and wild type mice 76

Figure 2-2. The comparison in signal intensity between mathematical and draw around methods. 89

Figure 2-3. The Pearson correlation analysis for mathematical and draw around methods. 89

Figure 2-3. The desitometric analysis and z-score result of 3-month old mice. 93

Figure 2-4. The densitometry analysis and z-score result of 11-month old mice. 94

Figure 2-7. 96 well plate layout for HbA1c measurement. 104

Figure 2-8. Summary of mouse hemoglobin A1C assay procedure. 104

Figure 3-1. The composite and separate quadruple mitochondrial immunofluorescence in pancreatic islets from 3-month sacrificed mice. 111

Figure 3-2. Changes of z-score expression in Tomm20 (mitochondrial mass), NDUFB8 (complex I) and MTCO1 (complex IV) in 3-month sacrificed *PolgA*$^{mut/mut}$ mice compared to the age-matched wild type mice. 112

Figure 3-3. The composite and separate quadruple mitochondrial immunofluorescence in pancreatic islets from 11 month sacrificed mice. 114

Figure 3-4. Changes of z-score expression in Tomm20 (mitochondrial mass), NDUFB8 (complex I) and MTCO1 (complex IV) in 11-month sacrificed *PolgA*$^{mut/mut}$ mice compared to age-matched wild type mice. 115

Figure 3-5. Changes of z-score expression in Tomm20 (mitochondrial mass), NDUFB8 (complex I) and MTCO1 (complex IV) in 11-month wild type mice compared to 3-month wild type mice. 117

Figure 3-6. Changes of z-score expression in Tomm20 (mitochondrial mass), NDUFB8 (complex I) and MTCO1 (complex IV) in 11-month *PolgA*$^{mut/mut}$ mice compared to 3-month *PolgA*$^{mut/mut}$ mice. 119

Figure 3-7. Standard curves of ND5 target gene and B-actin reference gene prepared using a series of 1 in 10 dilutions of wild type mouse pancreas DNA. 121

Figure 3-8. Pancreatic islet mtDNA copy number comparison between 11-month wild type and *PolgA*$^{mut/mut}$ mice. 123

Figure 3-9. Changes of mitochondrial complex expression in wild type and *PolgA*$^{mut/mut}$ mice in two age groups. 127

Figure 4-1. The separate and composite triple immunofluorescence staining images for endocrine hormones in pancreatic islets from 3 month mice… 135

Figure 4-2. Islet cell composition summary in 3 month sacrificed mice.. 136

Figure 4-3. Average value of islet cell composition summary in 3 month sacrificed mice. 137

Figure 4-4. The separate and composite triple immunofluorescence staining images for endocrine hormones in pancreatic islets from 11-month mice.. 139

Figure 4-5. Islet cell composition summary in 11 month sacrificed mice.. 140

Figure 4-6. Average value of islet cell composition summary in 11 month sacrificed mice. 141

Figure 4-7. The islet cell composition comparison between two different ages in wild type mice.. 143

Figure 4-8. Average value of islet cell composition summary in wild type mice between two different ages. 144

Figure 4-9. The islet cell composition comparison between two different ages in *PolgA*$^{mut/mut}$ mice. 146

Figure 4-10. Average value of islet cell composition summary in *PolgA*$^{mut/mut}$ mice between two different ages.. 147

Figure 4-11. The comparison of islet cell composition in two different mice groups in two different age. 149

Figure 4-12. Schematic representation of the change of islet cell composition in wild type and *PolgA*$^{mut/mut}$ mice in two age groups. 153

Figure 5-1. Representative image from 11 month old *PolgA*$^{mut/mut}$ mice. 160

Figure 5-2. Representative image from 11-month wild type mice. 160

Figure 5-3. The comparison in ratio of Ki67 (+) islets between *PolgA*$^{mut/mut}$ and wild type mice groups. 161

Figure 5-4. Different patterns of mitochondrial subunit expressions were found in different islet cell subtypes from *PolgA*$^{mut/mut}$ mice and the age-matched wild type mice at 44 weeks. 163

Figure 5-5. The insulin signal intensity summary in mice at 3 months. 165

Figure 5-6. The insulin signal intensity summary in mice at 11 months. 165

Figure 5-7. The comparison in endpoint blood glucose results between *PolgA*$^{mut/mut}$ and wild type mice.. 167

Figure 5-8. Monthly body weight measurement in wild type and *PolgA*$^{mut/mut}$ mice until 11 months of age.. 168

Figure 5-9. The comparison in endpoint body weight between *PolgA*$^{mut/mut}$ and wild type mice groups. 169

Figure 5-10. The average HbA1c% measurement result in endpoint whole blood samples from two groups of mice. 169

Figure 6-1. The composite and separate quadruple mitochondrial immunofluorescence in human pancreatic islets………185

Figure 6-2. Changes of z-score expression in Tomm20 (mitochondrial mass), NDUFB8 (complex I) and MTCO1 (complex IV) in old age non-diabetic human donors compared to young non-diabetic human donors. 186

Figure 6-3. The separate and composite triple immunofluorescence staining images for endocrine hormones in pancreatic islets human non-diabetic donors. 188

Figure 6-4. Islet cell composition summary in young and old non-diabetic donors. 189

Figure 6-5. Average Islet cell composition summary in young and old non-diabetic donors.. 190

Figure 6-6. The schematic representation of the change of mitochondrial complex expression and islet cell composition in non-diabetic donors in two age groups. 197

Figure 7-1. Different changing trend of mtDNA mutations between PolgA mutated ageing and normal ageing...... 201

Figure 7-2. The possible mechanisms behind the change of islet cell composition. 210

Figure 8-1. **The endpoint body weight of 11 month *PolgA*$^{mut/mut}$ sedentary and exercise mice and wild type mice**……215

Figure 8-2. Changes of signal intensity in mitochondrial mass marker, complex I (NDUFB8) and complex IV (MTCO1) in 3-month sacrificed *PolgA*$^{mut/mut}$ mice compared to age-matched wild type mice.. 217

Figure 8-3. Changes of signal intensity in mitochondrial mass marker, complex I (NDUFB8) and complex IV (MTCO1) in 11-month sacrificed *PolgA*$^{mut/mut}$ mice compared to age-matched wild type mice.. 218

Figure 8-4. Changes of signal intensity in mitochondrial mass marker, complex I (NDUFB8) and IV (MTCO1) in 11-month wild type mice compared to 3-month wild type mice. 219

Figure 8-5. Changes of signal intensity in mitochondrial mass marker, complex I (NDUFB8) and IV (MTCO1) in 11-month *PolgA*$^{mut/mut}$ mice compared to 3-month *PolgA*$^{mut/mut}$ mice. 220

Figure 8-6. Changes of signal intensity in Tomm20 (mitochondrial mass), NDUFB8 (complex I) and MTCO1 (complex IV) in old age non-diabetic human donors compared to young non-diabetic human donors. 221

ACKNOWLEDGEMENTS

Firstly, I would like to sincerely thank my supervisor, Professor Mark Walker, for giving me the opportunity to undertake my PhD in his research group. Professor Walker is a very responsible and capable supervisor who gave me a lot of good advice and support throughout my PhD. I learnt a lot from Mark's working attitude and mindset.

I would like to thank my second supervisor Dr. Laura Greaves. She provided the mouse model we used in our study and gave me a lot of technical support throughout my PhD. This PhD work can never be accomplished without her help and support.

I would like to thank all my colleagues in Diabetes Research Group and Mitochondrial Research Group for all the help and support throughout my PhD.

I would like to thank everyone in Translational and Clinical Research Insitute, Medical school and Newcastle University for friendly cooperation during my study time.

Finally, I would like to sincerely thank my parents for understanding and supporting my passion for science and research. I couldn't come here and finish my study without their financial and mental support.

PUBLISHED WORK

Published abstracts:

Impact of mitochondrial dysfunction on pancreatic islet cell composition in a mouse model of premature ageing.

Conference paper · September 2018

NuGO week. Mitochondria, Nutrition and Health. Newcastle, UK

Impact of mitochondrial dysfunction on pancreatic islet cell composition in a mouse model of premature ageing.

Conference paper · October 2018

European Association for the Study of Diabetes (EASD) conference, Berlin, Germany.

Impact of Aging on Mitochondrial Respiratory Chain Expression and Pancreatic Islet Cell Composition by Using a Mitochondrial DNA Mutator Mouse Model.

Conference paper · June 2019

American Diabetes Association (ADA) 79th Scientific Sessions, San Francisco, USA

LIST OF ABBREVIATIONS

AD	Alzheimer's disease
ADP	Adenosine Diphosphate
Apaf1	Apoptotic protease activating factor 1
ALS	Amyotrophic lateral sclerosis
ATP	Adenosine Triphosphate
B2M	β-2-microglobulin
BMI	Body mass index
CDKAL1	CDK5 regulatory subunit associated protein 1-like 1
CDKN2A/2B	Cyclin-dependent kinase inhibitor 2A/2B
CM	Cristae membrane
CT	Computerized tomography
CytC	Cytochrome *c*
ESRF	End stage renal failure
ETC	Eletron transport chain
$FADH_2$	Flavin adenine dinucleotide
FFA	Free fatty acid
FFPE	Formalin-fixed, paraffin-embedded
FMN	Flavin mononucleotide
FSGS	Focal segmental glomerular sclerosis
FTO	Fat mass and obesity-associated protein
GLP-1	Glucagon-like peptide 1
GLUT	Glucose transporters
GSIS	Glucose stimulated insulin secretion
GWAS	Genome wide association studies
HbA1c	Hemoglobin A1c
H_2O_2	Hydrogen peroxide
IBM	Inner boundary membrane

IMS	Intermembrane space
IRS1	Insulin receptor substrate 1
K_2EDTA	Ethylenediaminetetraacetic acid dipotassium salt dehydrate
LDM	Laser dissection microscope
LHON	Leber hereditary optic neuropathy
MELAS	Myopathy, encephalopathy, lactic acidosis and stroke
MERRF	Myoclonic Epilepsy with Ragged Red Fibres
MHC	Major histocompatibility complex
MIDD	Maternally inherited diabetes and deafness
MIM	Mitochondrial inner membrane
MODY	Maturity onset diabetes of the young
MOM	Mitochondrial outer membrane
mPTP	Mitochondrial permeability transition pore
MRI	Magnetic resonance imaging
MTCO1(COX1)	Cytochrome c oxidase subunit I
MtDNA	Mitochondrial DNA
NADH	Nicotinamide adenine dinucleotides
ND5	NADH dehydrogenase 5
NDUFB8	NADH dehydrogenase 1 beta subcomplex 8
NHANES	National Health and Nutrition Examination Survey
NRF-1/-2	Nuclear respiratory factor 1 and 2
OGTT	Oral glucose tolerance test
OXPHOS	Oxidative phosphorylation system
PBS	Phosphate buffer saline
PD	Parkinson’s disease
PDX1	Pancreatic duodenal homeobox 1
POLG	Polymerase-γ
PPARG	Peroxisome proliferator-activator receptor-γ protein

ROI	Region of interest
ROS	Reactive oxygen species
RT-PCR	Real time PCR
SI	Signal intensity
T2DM	Type 2 diabetes mellitus
TCA cycle	Tricarboxylic acid cycle
TCF7L2	Transcription factor 7-like 2
TD	Terminal differentiated
VDAC	Voltage-dependent anion-selective channel
TFAM	Mitochondrial transcription factor A
TFB1M	Mitochondrial transcription factor B1M
TPV	Total pancreas volume
WHO	World health organization

CHAPTER 1. GENERAL INTRODUCTION

1.1. Diabetes

1.1.1. Diabetes Mellitus

Diabetes mellitus, characterized by high blood glucose levels over a long period, is one of the most common non-communicable metabolic diseases (Alberti 1992). The World Health Organization (WHO) 2006 report (Organization 2006) indicated there were 171 million people diagnosed with diabetes worldwide in the year 2000 and this number was projected to increase to 366 million by 2030 (Wild, Roglic et al. 2004). This fact was recently updated by WHO that the number of people diagnosed with diabetes worldwide had risen to 422 million in 2014 (WHO 2016). In the UK, 4.7 million people are diagnosed with diabetes nationwide in 2018 and this number has been more than doubled since 1998 (Diabetes).

The normal glucose level is defined between the range of 4mM (72mg/dl) and 7mM (126mg/dl) before meals (NICE, 2008). Diabetes is diagnosed by a random venous plasma glucose concentration ≥ 11.1 mmol/l or a fasting plasma glucose concentration ≥ 7.0 mmol/l or plasma glucose concentration ≥ 11.1 mmol/l two hours after 75g anhydrous glucose in an oral glucose tolerance test (OGTT) (Organization 2006).

The clinical diagnosis of diabetes is made upon the presence of classical symptoms including polydipsia, polyphagia, and polyuria. In addition to this, the reduced ability to metabolize glucose caused by insulin deficiency and insulin resistance in human body can cause abnormalities of carbohydrate, fat and protein metabolism and induce abnormal weight loss (Organization 1999). The hyperglycaemic level leads to the occurrence of acute complications including diabetic ketoacidosis and nonketotic hyperosmolar coma. Long-term diabetic status can give rise to increased risks of chronic complications including microvascular damages (retinopathy, neuropathy and nephropathy) and macrovascular damages (ischaemic heart disease, stroke and peripheral vascular disease) (Organization 2006). Diabetes was regarded as the seventh leading cause of death in United States because of the large number of coexisting conditions and complications (Prevention. 2017) and the possibility of developing

diabetic complications is by the extent of hyperglycemia (Stratton, Adler et al. 2000). Apart from shortened life expectancy and significant morbidity, diminished quality of life is another major complaint of patients (IDF 2006, WHO 2016). The elevated blood glucose concentration provides a perfect incubating environment for the growth of bacteria and yeast, so hyperglycaemia is often accompanied by an increased chance of infection and delayed wound healing (Anderson and Hamm 2012).

1.1.2. Glucose homeostasis

1.1.2.1. Pancreas structure and function

The pancreas is located in the upper left part of the abdominal cavity, beneath the stomach, and attached to the duodenum of the small intestine. Anatomically, the pancreas is divided into the head of the pancreas, the body of the pancreas, and the tail of the pancreas (Drake, Vogl et al. 2009).

The most notable character of the pancreas is that it has both digestive (exocrinal) and endocrinal functions. As a part of the digestive system, the pancreas secretes pancreatic juice into the duodenum via the pancreatic duct. This pancreatic juice has the most important digestive function in the human body because it contains many digestive enzymes and bicarbonate. Digestive enzymes can break down protein, carbohydrates, and fat that come from the stomach. Bicarbonate can protect the duodenum membrane by neutralizing intestinal contents that come from the stomach during digestion (Mellanby 1925). The exocrine part takes up 96-99% of total pancreas volume (TPV) (Dolensek, Rupnik et al. 2015). Pancreas endocrinal function is achieved by pancreatic islets which are dispersed throughout the pancreas and surrounded by exocrine tissue (DeFronzo 2004). The pancreatic islet is a cluster of endocrine cells which first discovered by Paul Langerhans in 1868 (Langerhans 1869). Islet structure will be described in detail in paragraph **1.3.1.**

1.1.2.2. The maintenance of blood glucose level

Pancreatic islets only take up 2-5% of total pancreatic mass but they play important roles in maintaining blood glucose homeostasis (Carter, Dula et al. 2009). Pancreatic β-cells secrete insulin when blood glucose level increases. Insulin helps to transfer glucose from the blood into the liver, fat, and muscle, thus lowering the blood glucose level. The liver plays a central role by taking and converting glucose into glycogen via glycogenesis (Nordlie, Foster et al. 1999). The release of glucose from the liver is also regulated by insulin.

When the blood glucose levels fall below the normal glucose range, pancreatic α-cells are stimulated to secrete glucagon. The major function of glucagon is to stimulate the output of hepatic glucose (Jiang and Zhang 2003) by breaking down the glycogen stored in the liver into glucose, thus increasing the blood glucose concentration via a process called glycogenolysis or gluconeogenesis (Nordlie, Foster et al. 1999). Blood glucose levels are maintained by the balance in the secretion of insulin and glucagon.

1.1.2.3. Glucose metabolism in pancreatic β-cells

The insulin secretion from pancreatic β-cells happens after glucose stimulation in the cell. Glucose transporters (GLUT) facilitate the translocation of glucose across the β-cell membrane (Cholkar, Ray et al. 2013). Once inside the cells, glucose metabolism goes through different stages of cell respiration (Mader and Windelspecht 2003). The first step of glucose metabolism is to be phosphorylated by glucokinase which is a glucose sensor and a rate-limiting enzyme in β-cells (Fu, R Gilbert et al. 2013).

Glycolysis, the first and the most critical phase in glucose cell respiration, is an oxygen-independent metabolic pathway that transfers glucose into pyruvate. It occurs in the cytosol and includes a series of enzyme-catalyzed reactions (Romano and Conway 1996). Compared to the electron transport chain reaction, glycolysis is a low energy-generating process. Two molecules of ATP are yielded by breaking down one molecule of glucose into two molecules of pyruvate (Mader and Windelspecht 2003). Pyruvate transfers into the mitochondrial matrix

and is converted into acetyl-CoA in the oxygen-sufficient situation (Krebs and Eggleston 1940). Acetyl-CoA enters the tricarboxylic acid cycle (TCA cycle) for further metabolism. TCA cycle, also known as a citric acid cycle or Krebs cycle, was identified in 1937 by Hans Adolf Krebs and William Arthur Johnson (Krebs and Johnson 1937) (Krebs 1970). It is a series of aerobic reactions occurred in the matrix of mitochondria of eukaryotic cells that release the energy stored in acetyl-CoA into ATP. Carbon dioxide can be generated as a waste byproduct in this process and NAD+ can be reduced to NADH (Krebs and Johnson 1937). NADH can provide electrons to the electron transport chain which links the processes of metabolite oxidation and ATP generation together. Three NADH, one $FADH_2$, and one GTP are eventually generated from the TCA cycle (Lieberman and Marks 2009).

Electron transport chain (ETC), also known as oxidative phosphorylation, takes up electron carriers that are generated in the TCA cycle and generate a massive yield of ATP in the process. ETC will be further elaborated in paragraph **1.2.2.1**.

1.1.2.4. Glucose-Stimulated Insulin Secretion

In healthy subjects, insulin is secreted precisely to meet the metabolic demand. In the fasting state, circulating insulin acts primarily at the liver to regulate hepatic glucose release. Glucose is the primary stimulus for insulin secretion, but amino acid and fatty acid are also influencing factors (Fu, R Gilbert et al. 2013). The increasing circulating insulin in the postprandial state suppresses the release of hepatic glucose and promotes glucose uptake and metabolism in the peripheral insulin-sensitive tissues (particularly, skeletal muscle) (DeFronzo 2004). Insulin secretion has a specific characteristic biphasic pattern which is consisted of a rapid and transient first phase secretion and a sustained and slow developing second phase secretion (Fu, R Gilbert et al. 2013). In T2DM, the first-phase of insulin is secreted within 15 min after a sudden rise in plasma glucose level (Fehse, Trautmann et al. 2005). It plays the greatest role in postprandial plasma glucose control and the loss of first-phase insulin release is a common defect behind post-meal hyperglycemia (Fehse, Trautmann et al. 2005, Elder, Prigeon et al. 2006). A dose-response curve can be generated for insulin secretion against plasma glucose

levels after a glucose uptake (***Figure 1-1***). The slope of this curve decreases as glucose intolerance progresses to type 2 diabetes which means there is a progressive decrease in the insulin secretion rate for a given plasma glucose concentration (Byrne, Sturis et al. 1996).

The massive yield of ATP generated by a series of reactions of glycolysis, the TCA cycle, and the ETC can cause an increase in the ATP/ADP ratio from mitochondria into the cytosol. It promotes the closure of the ATP-dependent K^+ channels (K_{ATP}) on the pancreatic β-cell membrane and causes the depolarization of the cell membrane and the subsequent opening of voltage-gated Ca^{2+} channels (Lowell and Shulmanz 2005). The influx of Ca^{2+} after the opening of Ca^{2+} channels leads to an increase of cytosolic calcium and this important step induces the migration and fusion of insulin-containing granules to the cell membrane surface (Maechler and Wollheim 2001) (***Figure 1-2***). Insulin secretes from pancreatic β-cells into the bloodstream after insulin granules exocytosis (Lowell and Shulmanz 2005). The blockade of respiratory chain function can inhibit insulin secretion proves that mitochondria play a pivotal role in glucose-stimulated insulin secretion (Maechler and Wollheim 2001).

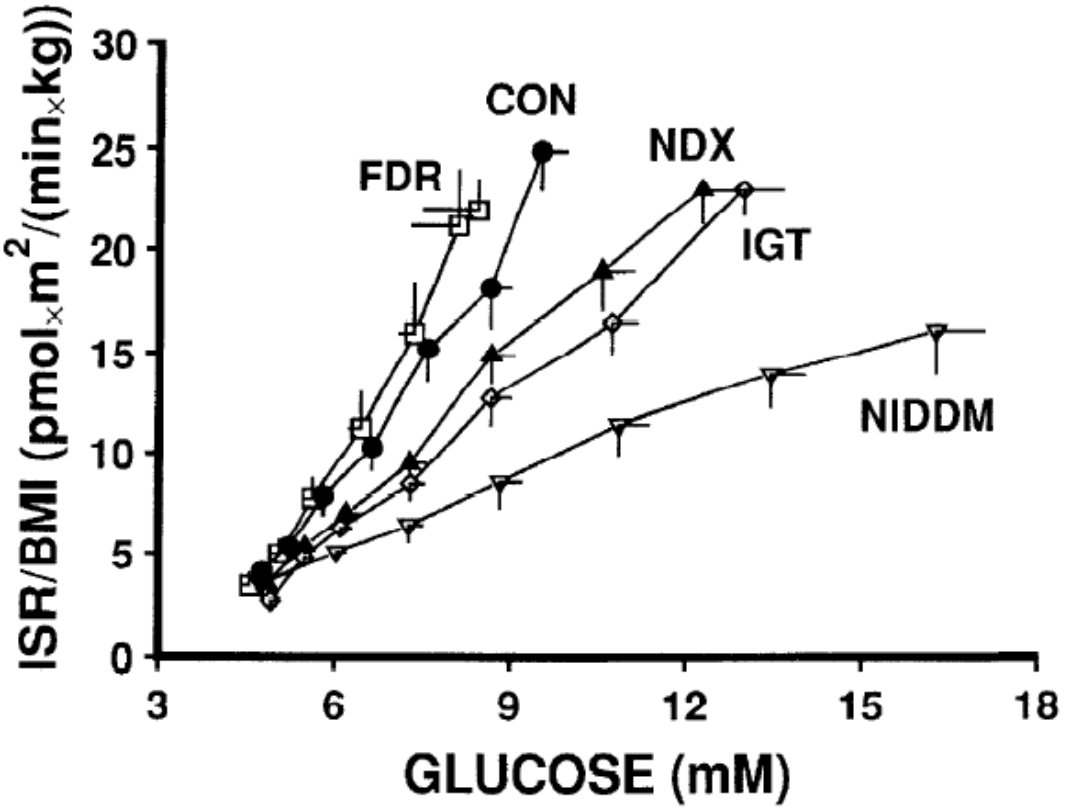

Figure 1-1. Dose response curves for insulin secretory rates against plasma glucose concentration. Curves are shown for subjects with different degrees of glucose tolerance, including those with normal glucose tolerance with (First degree relatives, FDR) and without (CON) a family history of diabetes, and those with established type 2 diabetes (Non-insulin-dependent diabetes mellitus, NIDDM). (Impaired glucose tolerance, IGT; Nondiagnostic oral glucose tolerance test, NDX; Control subject, CON). Figure is cited from (Byrne, Sturis et al. 1996).

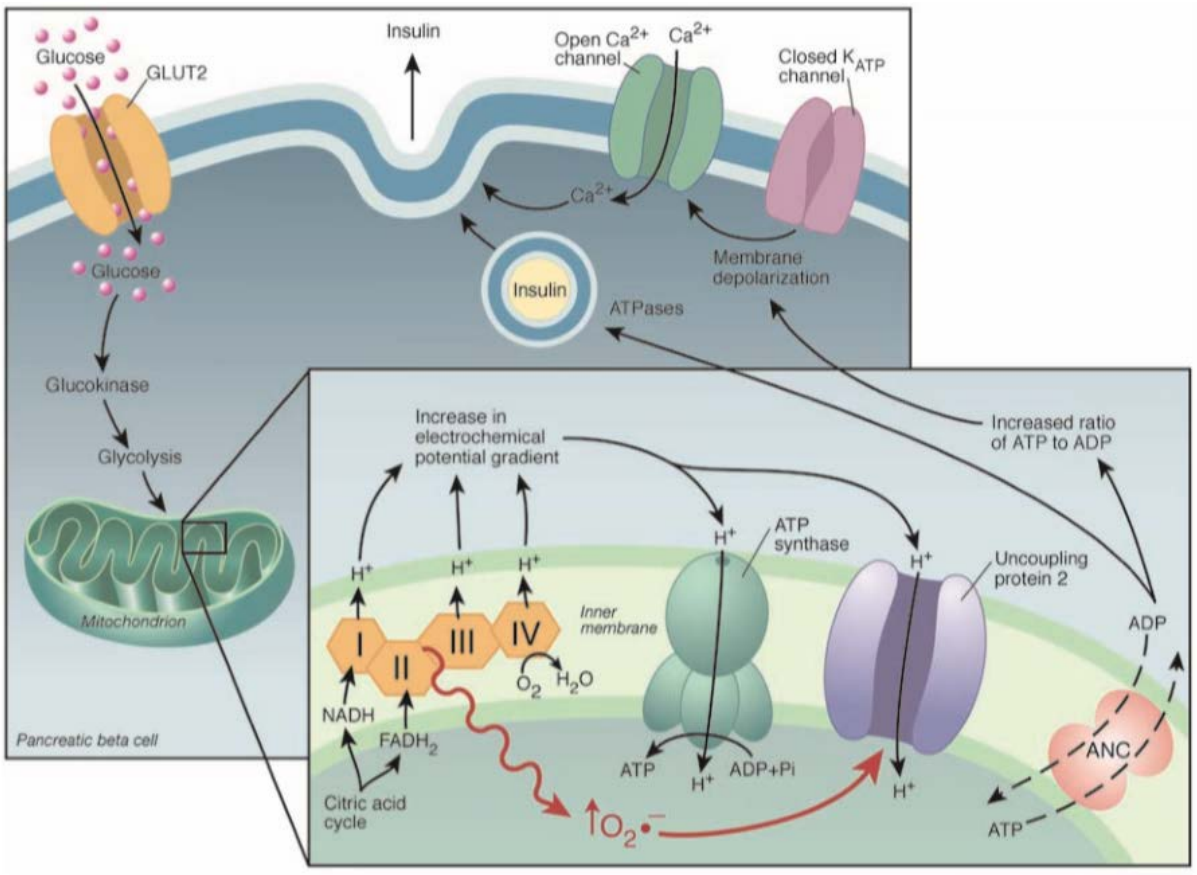

Figure 1-2. Glucose induced insulin secretion in pancreatic β cells. Figure is cited from (Lowell and Shulman 2005)**.**

1.1.3. Diabetes Subtypes

Diabetes occurs when there is either absolute insulin deficiency or insulin deficiency relative to the ambient level of insulin resistance (Alberti and Zimmet 1998). According to the different causes of diabetes, Lister and Nash characterized the two major subtypes of diabetes in their publication in 1951 (Lister, Nash et al. 1951). Type 1 Diabetes Mellitus (T1DM) is previously known as juvenile or childhood-onset diabetes because of the early onset age (usually before 40 years old) (Organization 2016). It takes up approximately 8% of the whole diabetes population (Care 2004). It is widely acknowledged that T1DM is triggered by a combinative interaction of genetic and environmental factors (Organization 2016). The presence of anti-GAD, islet cell, and insulin antibodies can drive the body's auto-immune attack and cause the loss of insulin-releasing pancreatic beta cells (Alberti and Zimmet 1998) (Pihoker, Gilliam et al. 2005) (Lieberman and DiLorenzo 2003, Pihoker, Gilliam et al. 2005, Pihoker, Lawrence et al. 2005), T1DM is thus characterized as severe and absolute insulin deficiency in the human body. The glucose homeostasis of T1DM patients is required to be maintained by daily injection of insulin (Organization 2016).

Type 2 Diabetes Mellitus (T2DM) is formerly named adult-onset diabetes or non-insulin-dependent diabetes. It accounts for approximately 90% of all diabetes cases worldwide and is regarded as the most common form of diabetes (Diabetes). T2DM has become increasingly prevalent over the past few decades and there has been an alarming increase in the number of children developing T2DM in recent years. 6 out of 10 people have no symptoms when they are diagnosed with T2DM. Because of this camouflaged early-stage feature, there are about 1 million people with T2DM have not been diagnosed yet (Diabetes). T2DM is characterized by decreased insulin secretion in the presence of insulin resistance (Alberti and Zimmet 1998). T2DM patients with predominant insulin resistance may have normal or elevated insulin levels to maintain glucose homeostasis. Because of this, the β cell insulin-secreting function can become insufficient to compensate for insulin resistance in the long term (Polonsky, Sturis et al. 1996). T2DM can thus be defined as an inability of the pancreatic beta cells to compensate for an increased functional demand caused by peripheral insulin

resistance (DeFronzo, Ferrannini et al. 2015). On the other hand, some individuals present with reduced β-cell secreting function with insulin action essentially normal (Kahn 2003). In T2DM subjects, the normal insulin secretion and action during fasting and postprandial processes are altered, with a blunted first phase response and a delayed second phase. This results in impaired suppression of hepatic glucose release and impaired peripheral glucose uptake (Luzi and DeFronzo 1989, DeFronzo 2004).

Some rarer causes of diabetes including gestational diabetes and genetic defect-induced diabetes take up 2% of diabetes cases. Gestational diabetes is a temporary high blood glucose condition that occurs in pregnancy (Organization 2013). During pregnancy and delivery, women diagnosed with gestational diabetes and their infants are more likely to develop metabolic complications. There are possibilities that these women can still carry the long-term risk of type 2 diabetes after delivery (Bellamy, Casas et al. 2009). Mitochondrial DNA point mutations have been proven to be associated with diabetes mellitus and deafness (Lowell and Shulmanz 2005). Several unusual causes of the diabetic state may be associated with genetic defects in beta-cell function (such as maturity-onset diabetes of the young, MODY) or genetic abnormalities of insulin action (Alberti and Zimmet 1998).

1.1.4. T2DM risk factors

An interplay of genetic and metabolic (smoke, physical inactivity, obesity and ageing) factors are driving the development of T2DM (Organization 2016).

1.1.4.1. Metabolic risk factors

Metabolic syndrome is associated with an increased risk of T2DM (Wilson, D'Agostino et al. 2005). Individual with a smoking habit, physical inactivity, overweight, obesity is more likely to develop T2DM (Chang 2012) (Organization 2016). Among them, being obese has the most important influence on the progression of T2DM. Insulin sensitivity can be enhanced by a healthy diet, increased physical activity, and antidiabetic treatment but it cannot be restored to a normal level (Simonson, Ferrannini et al. 1984). T2DM progression can be delayed or

even prevented by exercise intervention and calorie restriction (Tuomilehto, Lindström et al. 2001).

1.1.4.2. Genetic risk factors

The onset of T2DM also has a strong genetic predisposition. The risk of T2DM dramatically increases if there is a T2DM family history, especially in first-degree relatives (Viswanathan, Mohan et al. 1985). The risk of developing T2DM is 15 percent if either parent has the condition but this number increases to 75 percent if both parents are diagnosed. If a non-identical twin is diagnosed, the risk of developing T2DM is 10 percent but this number will dramatically increase up to 90 percent if an identical twin has the condition (Pickup and Williams 1991).

Candidate gene studies revealed the existence of various T2DM susceptibility genes including *PPARG* (encodes peroxisome proliferator-activator receptor-γ protein) and *KCNJ11* (encodes the Kir6.2 subunit of the β-cell ATP sensitive K^+ channel) (Gaulton, Willer et al. 2008) (Tabara, Osawa et al. 2009). *TCF7L2* (encodes transcription factor 7-like 2) gene allele has also been associated with increased risk of developing T2DM because it can defect insulin secretion by indirectly altering glucagon-like peptide 1 (*GLP-1*) level (Dayeh, Volkov et al. 2014) (Tong, Lin et al. 2009). The genome-wide association studies (GWAS) helped to identify more T2DM susceptibility genes. The risk allele of *CDKN2A/2B* (Cyclin-dependent kinase inhibitor 2A/2B) and *CDKAL1* (CDK5 regulatory subunit associated protein 1-like 1) are associated with decreased β-cell function and decreased glucose-stimulated insulin secretion (Tabara, Osawa et al. 2009). *IRS1* (Insulin receptor substrate 1) is involved with increasing insulin resistance and *FTO* (Fat mass and obesity-associated protein) is reported to cause the increased risk of obesity and increased body mass index (BMI) (Phani, Vohra et al. 2016) (Zeggini, Parkinson et al. 2004).

Ethnicity has also been associated with the onset of T2DM. South-Asian ethnic group is 6 times more likely to develop T2DM and people of African and African-Caribbean origin are 3 times more prone to have T2DM (Diabetes 2010).

1.2. Mitochondrial biology

1.2.1. Mitochondrion structure

Mitochondria are rod-shaped and double-membrane-encapsulated organelles and exist in the cytoplasm of almost all eukaryotic cells, including plants, animals, and fungi. Mitochondria, the powerhouse of the cell, are the main energy generator and supplier for all body functions and key regulators of cell survival and death. The number of mitochondria in one cell can range from none (erythrocytes) to 10000 (striated muscle cell) (Finsterer 2004). Tissues with higher metabolic activities and energy demand, such as neurons, skeletal muscle and islet cells usually have a higher number of mitochondria. The outer (OMM) and inner (IMM) mitochondrial membranes segregate mitochondria into two aqueous compartments which is the mitochondrial matrix and the intermembrane space (IMS) (Attardi and Schatz 1988). The two membranes differ from each other in structure and composition. The OMM is homogenous in structure whereas the IMM forms the distinct cristae structure which are invaginations within the mitochondria (Palade 1952, Walther and Rapaport 2009). The numerous transport proteins and metabolic enzymes on OMM make it become a permeable structure to transmit ions, adenosine triphosphate (ATP), and other cell signals. It serves as an important mediator of metabolic and genetic function between mitochondria and cytoplasm. For example, the most abundant OMM protein is porin, also known as the voltage-dependent anion-selective channel (VDAC). Porin allows the transfer of small molecules through the outer membrane and also contributes to mitochondrial membrane permeability (Walther and Rapaport 2009). For the larger proteins and nuclear-encoded proteins, the import of these proteins into the internal compartment of mitochondria depends on the translocase of the mitochondrial outer membrane (TOM complex)(Truscott, Brandner et al. 2003). The proper functioning of TOM partly relies on the presence of phosphatidylethanolamine (PE) which is the second most abundant phospholipid on the mitochondrial membrane (Mejia and Hatch 2016). Phosphatidylinositol (PI) which makes up 13% of phospholipid on OMM is responsible for several functions such as vesicle trafficking, actin rearrangement, and calcium regulation. PI also serves to allow mitochondria to communicate with other cellular components in the cytoplasm (Mejia and Hatch 2016).

Besides, the OMM integrity is important for controlling apoptosis. In the process of programmed cell death, mediators of apoptosis which participate in the activation of caspases and DNA degradation can be released from mitochondria through OMM. Among different OMM proteins, Bcl-2 family proteins can regulate VDAC function and form channels for coordinating the permeability of mitochondrial membranes (Harris and Thompson 2000). Unlike OMM which forms like an envelope that defends the macromolecules, IMM encloses the mitochondrial matrix and protects the inner content by strictly regulating the movement of small molecules through the various protein carriers (Vogel, Bornhövd et al. 2006). It was agreed that IMM is one of the most protein-rich lipid bilayers in the biological system (Vogel, Bornhövd et al. 2006). Two different membrane structures inner boundary membrane (IBM) and cristae membrane (CM) which are connected by cristae junction consists the IMM (Song, Park et al. 2013). IBM not only lies in parallel but also interacts functionally with OMM. However, CM which stretches out into the inner mitochondria makes up most of the mitochondrial inner membrane. This structure enables the greater capacity of OXPHOS because it increases the surface of IMM and it varies according to different energy states. Mitochondria of high respiratory activity cells have larger cristae whereas small cristae are usually found in low respiratory activity cells (Mannella 2008). CM is the major site for oxidative phosphorylation (OXPHOS) proteins, harboring the respiratory chain complexes and F_1F_O ATP synthase (Vogel, Bornhövd et al. 2006). There is a functional interplay between cristae architecture and mitochondrial DNA integrity. For example, skeletal muscle specific *Mfns* KO mice had growth defect and metabolic aberration when their cristae have compromised ultrastructural integrity. These mice also display a decrease of mtDNA copy number and defective respiratory function, again indicating that cristae integrity and mtDNA are interlinked. Another study also revealed the importance of cristae structure and dynamics because abnormal cristae structure is associated with various neurodegenerative diseases (Rampelt, Zerbes et al. 2017). It was discovered by immunoelectron microscopy on yeast mitochondria that the distribution of proteins are different on both subcompartments of IMM and they can change according to the physiological state of the cells. For example, components of the mitochondrial protein import machinery are preferentially found in the

IBM whereas OXPHOS components are present at higher levels in the CM and many components are in a dynamic behavior in the context of different functions (Vogel, Bornhövd et al. 2006).

1.2.2. Mitochondrial function

1.2.2.1. ATP generation

Mitochondria are involved in many important cell functions such as the generation of ATP, cell metabolism regulation, calcium transport, cell apoptosis and necrosis, generation of reactive oxygen species (ROS), mitochondrial quality control (fission, fusion and mitochondrial dynamics) and cell signaling (Murphy, Ardehali et al. 2016). Among them, the key and dominant mitochondrial function is to generate ATP (Finsterer 2004). ATP which is considered by biologist as the energy currency of life, is a high-energy molecule that stores the energy for all body functions and our daily activities (Zheng, Zychlinsky et al. 1991).

Energy from dietary intake is converted into ATP through OXPHOS facilitated by the electron transport chain (ETC) (***Figure 1-3***). The whole process starts from cytosol where pyruvate and reduced nicotinamide adenine dinucleotides (NADH) are produced. In the oxygen-deficient environment, pyruvate will go through anaerobic respiration and generate a small amount of ATP whereas in oxygen-sufficient situation, pyruvate will be transferred into the mitochondria and enter the tricarboxylic acid (TCA) cycle or the Krebs cycle. In this process, electron carriers such as NADH and reduced flavin adenine dinucleotide ($FADH_2$) are massively yielded (Maechler and Wollheim 2001). These electron carriers are utilized by ETC to shuttle electrons across the respiratory chain complexes. The electron transport chain, situated on the inner mitochondrial membrane, is composed of five respiratory chain complexes (also known as oxidative phosphorylation enzymes), with complex I (NADH ubiquinone oxidoreductase), II (succinate dehydrogenase), III (CoQ-cytochrome c oxidoreductase), IV (cytochrome c oxidase) as electron transport chain and final complex V (ATP synthase). These complexes are subject to dual genetic control of mitochondrial genome and nuclear genome. Apart from complex II, all the other complexes are encoded by both nuclear and mitochondrial DNA (Wallace 1992).

Complex I which is the largest ETC complex and also the largest membrane-bound protein assembly has a classic L-shaped structure formed by a hydrophilic peripheral arm and a hydrophobic membrane arm (Mimaki, Wang et al. 2012). Bovine and human mitochondrial CI has 45 different subunits, among them 7 subunits ND1, ND2, ND3, ND4, ND4L, ND5, and ND6 are encoded by mtDNA and the remaining 38 subunits are encoded by nuclear DNA (nDNA) (Mimaki, Wang et al. 2012). There are three functional modules, N-module, Q-module and P-module within complex I. The electron accepter flavin mononucleotide (FMN) in the N-module can transfer two electrons from NADH to FMN, oxidizing NADH and reducing FMN into $FMNH_2$ (Brandt 2006). The electrons are subsequently transferred from FMN to ubiquinone in the Q-module through an electron transfer chain made up by seven iron-sulfur clusters, reducing ubiquinone to ubiquinol at the same time. The transfer of two electrons from NADH to ubiquinone is coupled with the transfer of four protons across the IMM to the inter-membrane space facilitated by the P-module (Brandt 2006, Moser, Farid et al. 2006). Complex II, which is the smallest respiratory chain complex with only four subunits, is the only complex that is entirely nDNA encoded. It serves as another entry point for electrons to transfer from succinate into the ETC through the reduction of ubiquinone, converting succinate to fumarate (Cecchini, Schroder et al. 2002, Yankovskaya, Horsefield et al. 2003). Complex III is composed of 11 subunits and only one subunit, cytochrome b, is encoded by mtDNA. Complex III reoxidise ubiquinone by transferring two electrons from ubiquinol to cytochrome *c* (CytC), coupled with the translocation of two protons into the inter-membrane space (Mitchell 1975). Complex IV, as a terminal electron acceptor, consists of three mitochondrial encoded subunits; COXI, COXII and COXIII. It is one of the most important study target since it was discovered because it reduces molecular O_2 to H_2O by using electrons delivered by cytochrome c. Four electrons are required for reduction of one molecule of oxygen, making this the rate-limiting step in the ETC (Huttemann, Pecina et al. 2011). This electron transfer process is usually accompanied by pumping four protons per reduced O_2 from the matrix into the intermembrane space (Tsukihara, Aoyama et al. 1996, Faxen, Gilderson et al. 2005). As the final OXPHOS step, complex V catalyse the ADP and inorganic phosphate (P_i) into ATP. Among all the 16 complex V subunits, two of them (ATPase 6 and

ATPase 8) are mtDNA encoded. Complex V compose of two domains such as F0 and F1 domains (Elston, Wang et al. 1998). The F0 domain which is located in the IMM can serve as a proton channel whereas F1 domain which is found on the matrix side of the IMM is the binding site for ADP and P_i (Elston, Wang et al. 1998). With the protons constantly being pumped across the inner membrane into the intermembrane space during the previous steps, an electrochemical gradient which is negative inside is formed (Maechler and Wollheim 2001). Complex V generates ATP driven by the formed electrochemical proton gradient by bringing extruded protons back into the matrix (Lowell and Shulman 2005). This process of producing ATP through the mitochondrial respiratory chain is defined as oxidative phosphorylation. By the large amount of ATP it produces, this process is known as the most efficient energy-generating machinery in cells (Rich 2003).

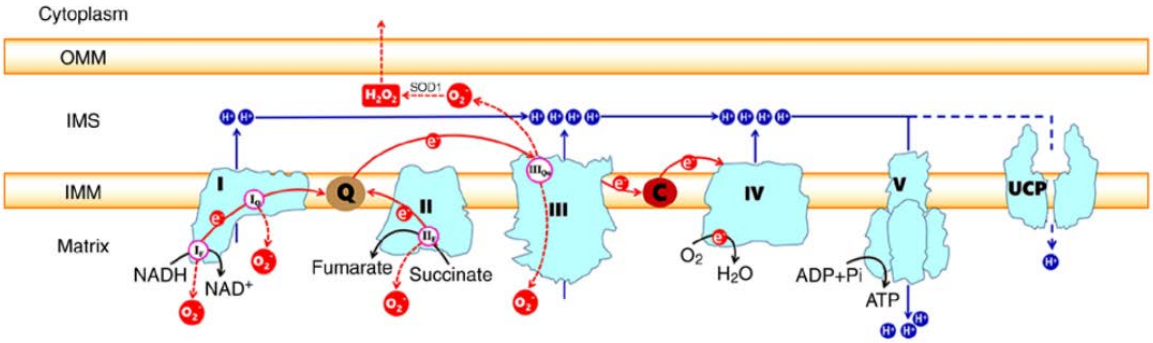

Figure 1-3. Mitochondrial electron transport chain. Figure is cited from (Zhao, Jiang et al. 2019).

1.2.2.2. ROS generation

ROS, which is predominantly (90%) generated by mitochondria, are very small and highly reactive molecules. The major sites of ROS generation are at mitochondrial complex I and complex III of the respiratory chain (Balaban, Nemoto et al. 2005). During electron transport procedure, a small fraction of electrons that leak from the complex I and III of ETC can react with free molecular oxygen and cause partial reduction of oxygen to create superoxide anions, O_2- (Murphy 2009), which are converted to hydrogen peroxide (H_2O_2) within mitochondria (Loschen, Azzi et al. 1974, Sastre, Pallardo et al. 2000) and then be released to the external medium. By comparing different mammal species, it was discovered that the rate of mitochondrial ROS generation is inversely correlated to maximum life span of species (Ku, Brunk et al. 1993). Mitochondria from shorter-lived species produced greater amounts of hydrogen peroxide than those from longer-lived species (Ku, Brunk et al. 1993, Sohal 2002).

Historically, ROS were considered harmful, especially at high level because of the irreversible damage that was caused to tissue and cells (Murphy 2009). Excessive levels of ROS cannot be buffered by the mitochondrial antioxidant system (reduced glutathione, GSH), thus can cause damage to lipids, proteins and nucleotides and eventually lead to cell death by necrosis or apoptosis (Sena and Chandel 2012). However, ROS serves as a signaling molecule at the basal level and it has been proven that it is crucial for response to a physiological and pathological stimulus (Murphy 2009). Apart from the role it plays in the cell signaling pathway, ROS can also regulate and facilitate many other functions such as metabolic adaptation, immune cell activation and autophagy, cell differentiation (Sena and Chandel 2012).

1.2.2.3. Calcium signaling and homeostasis

Mitochondria play an important role in balancing cytosolic Ca^{2+} levels (Kirichok, Krapivinsky et al. 2004). Cytosolic Ca^{2+} diffuses across OMM by VDAC and crosses IMM into matrix by ion channels and transporters (Clapham 2007). One of the Ca^{2+} uptake systems on the IMM is named as MiCa (Mitochondrial Ca^{2+} channel) and is considered as a highly Ca^{2+}-selective ion

conductance channel because it can bind Ca^{2+} with high affinity and high selectivity despite relatively low cytoplasmic Ca^{2+} concentration (Clapham 2007).

This intracellular Ca2+ signaling process makes mitochondria take up a significant amount of Ca^{2+} from the cytosol (Kirichok, Krapivinsky et al. 2004). Once Ca^{2+} enters the mitochondrial matrix, the Kreb's cycle can be stimulated because increasing cytosolic Ca^{2+} can boost up ATP production (Clapham 2007). The gradual accumulation of Ca^{2+} can trigger the abrupt opening of mitochondrial permeability transition pore (mPTP), leading to the mitochondrial swelling, the release of cytochrome c and eventual cell apoptosis (Mattson and Chan 2003).

1.2.2.4. Apoptosis and necrosis

Apoptosis is a programmed and targeted cellular death that occurs in both physiological and pathological situations. Due to the necessity of eliminating damaged or unwanted cells during development, apoptosis is involved in the normal cell cycle in tissues from healthy individuals (Kerr, Wyllie et al. 1972). In contrast, necrosis is an unprogrammed cell injury which caused by harmful external factors (Proskuryakov, Konoplyannikov et al. 2003), thus it is always detrimental and fatal. Apoptosis and necrosis can be induced through two general pathways: extrinsic pathway and intrinsic pathway. The extrinsic pathway is mediated by the extracellular ligand activation of death receptors. Mitochondria have been regarded as key mediators of apoptosis and necrosis via intrinsic pathways (Murphy, Ardehali et al. 2016). Pro-apoptotic BAX and BAK from the Bcl-2 family trigger the permeabilization of OMM and release the cytochrome c from mitochondria into the cytosol. The assembly of apoptosome is formed by cytosolic cytochrome c binding to apoptotic protease activating factor 1 (Apaf1). Precaspase-9 is subsequently activated by apoptosome, triggering a downstream signaling cascade and eventually leading to cell death (Wei, Zong et al. 2001, Murphy, Ardehali et al. 2016). The triggering event of mitochondria-mediated necrosis is the abrupt opening of mPTP in the IMM and this is accompanied by dissipation of proton gradient across IMM (Murphy, Ardehali et al. 2016). As a result, the abrupt cessation of new ATP generation and

mitochondrial matrix swelling follows the opening of mPTP, triggering the caspase activation and necrosis (Kroemer, Dallaporta et al. 1998, Murphy, Ardehali et al. 2016).

1.2.2.5. Mitochondrial quality control

Mitochondria divide to increase the number with the reproduction of cells and organisms, and they can also fuse back together. The continual fission and fusion cycle make up a process called mitochondrial dynamics which is essential for their host cells and organism (Murphy, Ardehali et al. 2016). On the cellular level, mitochondrial fission can produce damaged debris through segregation, so the mitophagy after fission can clear up the damaged mitochondria and proteins (Liesa and Shirihai 2013). Mitophagy, as a part of the overall mitochondrial quality control process, can remove dysfunctional mitochondria and prevent the accumulation of cytotoxic ROS (Murphy, Ardehali et al. 2016). Also the mitochondrial fusion helps compensate the damage on organelles by exchanging proteins and genome, avoiding the serious accumulation of mutations (Tondera, Grandemange et al. 2009, Youle and Van Der Bliek 2012).

1.2.3. Mitochondrial DNA

In animal cells, the mitochondrial genome is the only extranuclear source of DNA. Mitochondrial DNA (mtDNA), which is transcribed and translated in the mitochondria, is a circular, double-stranded DNA molecule of 16.6 kb in length in humans. In humans, maternally inherited mtDNA comprises of only 37 genes, including 13 essential polypeptides for the OXPHOS system, 2 ribosomal RNAs (12S and 16S) and 22 tRNAs (Falkenberg, Larsson et al. 2007). For example, the regulation of OXPHOS is subject to dual genetic control of mitochondrial genome and nuclear genome (Larsson, Wang et al. 1998). 13 mtDNA encoded respiratory chain subunits constitute the important part of the OXPHOS whereas the nuclear DNA encodes the majority of respiratory chain subunits (Larsson, Wang et al. 1998, Baines, Stewart et al. 2014). According to previous literature, mtDNA has a 10 fold higher mutation rate compared to nuclear DNA (Zheng, Khrapko et al. 2006). This is due to the close proximity of mtDNA to the generation of ROS during the OXPHOS process, the lack of histone protection

and poor DNA repair mechanism in mtDNA compared to nuclear DNA (Sastre, Pallardo et al. 2000, Greaves and Turnbull 2009). It has been found that in mammals, mtDNA oxidative damage load is inversely related to the maximum life span, whereas this relationship between oxidative damage and maximum life span doesn't exist in the case of nuclear DNA (Barja and Herrero 2000). Also, there is a random mtDNA genome distribution known as mitotic segregation happening during cell division, resulting in the changes of mutation between generations (Greaves and Taylor 2006). So mtDNA point mutations that start early in life can clonally expand to a level that can cause mitochondrial dysfunction (Kauppila, Baines et al. 2016). This explains the occurrence of the age-related, progressive accumulation of mtDNA point mutations and deletions and the development of later-on clinical phenotypes (Greaves and Taylor 2006). A single mutation or different mutations in the same gene may present with different clinical manifestations (genetic phenocopy) whereas the same clinical manifestation may be caused by different mutations (genetic heterogeneity) (Finsterer 2004). MtDNA has a multicopy nature and the copy number varies between different cells. Mutations in mitochondrial genome coexist with wild type genome and this situation is known as heteroplasmy (Greaves and Turnbull 2009). These mtDNA mutations will not cause biological defects and trigger clinical pathological expressions until they reach a critical threshold level. This threshold level depends on the type of mutation and the cell energy requirement (Coller, Khrapko et al. 2001, Taylor, Barron et al. 2003, Greaves and Turnbull 2009). A threshold for deleted mtDNA is expected to be around 50–60% and this value tends to be higher for mtDNA point mutations. For tRNA point mutation, the level has been suggested to be as high as 90% (Greaves and Turnbull 2009). The complement of cell mtDNA function depends on both the mitochondrial genome copy number and the integrity of each mtDNA molecule (Miller, Rosenfeldt et al. 2003) and this has been proved by many previous studies that age-related mtDNA point mutations and deletions can cause reduced complement of fully functional mtDNA in different tissues (Welle, Brooks et al. 2004, Kaaman, Sparks et al. 2007, Cree, Patel et al. 2008). Apart from the impact of ageing, various physiological and pathological conditions can also influence the mtDNA copy number. For example, cardiac hypertrophy was found to increase mtDNA content in chickens and rats (Rajamanickam, Merten et al. 1979)

and endurance exercise can increase mtDNA content in mice and human skeletal muscle (Menshikova, Ritov et al. 2006, Safdar, Bourgeois et al. 2011). A lot of mitochondrial transcription factors, including mitochondrial transcription factor A (TFAM), TFB1M, TFB2M, nuclear respiratory factor 1 and 2 (NRF-1/-2), and polymerase-γ (POLG), regulate mitochondrial copy number and they are all essential for mitochondrial biogenesis and embryonic development (Larsson, Wang et al. 1998).

1.2.4. Mitochondria and ageing

Ageing is characterized as a time-dependent loss of an organism's physiological function and increased vulnerability to death (Greaves and Taylor 2006) (López-Otín, Blasco et al. 2013). The free radical theory of ageing was firstly raised by Harman: he postulated that age-related dysfunction at cellular and tissue level can be caused by the generation of oxygen-derived free radicals (Sastre, Pallardó et al. 2000) (Harraan 1955). So far, much experimental pieces of evidence have supported this theory. For example, the degradation of cognitive function and motor skills can be associated with protein damage caused by oxidative stress in different regions of the brain (Forster, Dubey et al. 1996). There is also an inverse relationship between the producing rate of ROS and the maximum species life span (Sohal 2002).

Because mitochondria consume almost 90% of the oxygen taken in by aerobic cells, oxygen-derived free radicals (a.k.a reactive oxygen species, ROS) and hydrogen peroxide can be generated continuously from the mitochondrial respiratory chain. However, a very small amount of ROS is produced during the normal process of oxidative phosphorylation (Greaves and Taylor 2006).

It was Harman proposed in 1972 again that the mitochondria are the biological clock of ageing in humans (Harman 1972). Miquel and co-workers refined Harman's idea and proposed the mitochondrial theory of ageing later in 1980 (Miquel, Economos et al. 1980). Since then, mitochondria have been put into a crucial position in ageing research. The mitochondrial theory of ageing postulates that lifelong continuous accumulation of mtDNA point mutations

and deletions can lead to mitochondrial dysfunction (Greaves and Turnbull 2009). Because most of the respiratory chain complexes are encoded by mtDNA, OXPHOS function can be impaired by accumulative mtDNA mutations and deletions. Dysfunctional respiratory chain complexes can generate and accumulate an increasing amount of ROS with age (Greaves and Turnbull 2009) and can in turn exert chronic stress on mitochondria. The oxidative stress can defect the mitochondrial respiration function by majorly affecting the activities of respiratory chain complex I, II and especially IV (Benzi and Moretti 1995). MtDNA is considered by Miquel as the major target of free radical attack due to the proximity to the respiratory chain and the lack of protective histone protein (Miquel, Economos et al. 1980, Sastre, Pallardo et al. 2000).

As a consequence, increasing point mutations and deletions in mtDNA are found late in life in tissues (Brossas, Barreau et al. 1994) (Lezza, Boffoli et al. 1994), causing a vicious cycle between ROS generation and mitochondrial dysfunction and eventually leading to cell death. Many studies revealed that different mtDNA deletion loads exist within different tissues (***Table 1-1***). Postmitotic tissues such as the brain, heart, and muscle own the most severe mtDNA deletions later in life (Gadaleta, Kadenbach et al. 1999), and these mtDNA deletions are usually associated with the onset of age-related degenerative diseases such as Alzheimer's disease (AD), Parkinson's disease (PD) and amyotrophic lateral sclerosis (ALS) (Greaves and Taylor 2006) (Wallace 1994). By comparing mtDNA copy number in single substantia nigra neurons from patients diagnosed with Parkinson's disease and age-matched healthy controls, 52.3% ± 9.3% mtDNA deletion was detected in Parkinson's patients compared to 43.3% ± 9.3% in the age-matched controls (Bender, Krishnan et al. 2006). 60% of heteroplasmy of mitochondrial DNA A3243G mutations were detected in skeletal muscle tissues from patients. However in the pancreas, the mutation load was relatively low (only 31%) compared to other post-mitotic tissues and this low ratio of heteroplasmy was also found in the individual β-cells (Lynn, Borthwick et al. 2003). The extent of mtDNA deletion doesn't remain similar even within the same tissue, with some cells having a higher level of deletion compared to others. For example, the mutation ratio of mtDNA was low in pancreatic islet tissue (20±9%) compared to pancreatic acinar tissue (27±5%) (Lynn, Borthwick et al.

2003). This uneven distribution of mtDNA deletion is called mosaic distribution and it is one of the peculiar characteristics of the age-related mtDNA deletion (Gadaleta, Kadenbach et al. 1999). More severe mtDNA deletions were discovered in COX deficient cells compared to the COX normal cells, indicating that mtDNA deletion is the driving cause of COX deficiency (Bender, Krishnan et al. 2006) (Herbst, Pak et al. 2007).

Table 1-1. Percentage ratio of mtDNA point mutations in various tissues from the patient. Table is cited from (Lynn, Borthwick et al. 2003).

	Patient
Skeletal muscle	60%
Occipital Cortex	78%
Cerebellum	66%
Liver	60%
Pancreas	31%
Kidney	75%
Myocardium	58%
Blood	8%

It was hypothesized by many studies that mtDNA mutations can accumulate in stem cells. The colonic stem cells were widely studied because of the ease of identifying and detecting the mutations in the progeny of the colonic stem cells. It was found out that mutation load was very high in colonic stem cells. If a significant number of stem cells are developing mutations, the tissue function will be negatively influenced within the individual (Taylor, Barron et al. 2003). Also, colonic crypts of mice and humans are clonal populations. If one of several colonic stem cells acquires a mutation in the mitochondrial genome, the mutation can quickly expand, resulting in a detectable cytochrome c oxidase deficiency after the age of 40 (Greaves, Preston et al. 2006, Kauppila, Kauppila et al. 2017). The stem cell functionality of homozygous mtDNA mutator mice were used to further study the connection between mtDNA mutations and stem cell dysfunction. It can be concluded that mtDNA mutations directly affect stem cell functionality by bioenergetics deficiency and/or ROS-signaling-mediated mechanisms (Kauppila, Kauppila et al. 2017).

Apart from age-related mtDNA point mutations and deletions, the role of protein oxidative damage and lipid peroxidation in mitochondria are also important in the ageing process (Sastre, Pallardo et al. 2000). Some enzymes become catalytically less active or even inactive during ageing because of the age-related oxidative stress (Gershon and Gershon 2002). The cell membrane of old animals is more vulnerable and susceptible to oxidative damage than that of young individuals because of the existence of greater amounts of polyunsaturated fatty acids (Shigenaga, Hagen et al. 1994) (Laganiere and Byung 1993). An inverse relationship exists between the sensitivity of mitochondrial lipids to oxidative damage and the maximum life span of species (Sastre, Pallardo et al. 2000). The combinative effects of lipid peroxidation and protein oxidative modification in mitochondria can negatively influence the oxidative damage to mtDNA with increasing age (Wei 1998), thus aggravating the vicious cycle in mitochondrial ageing. The accumulation of oxidative stress can also cause changes in mitochondrial structure and membrane potential and can in turn modulate mitochondrial function and metabolism (Scalettar, Abney et al. 1991).

1.2.5. Mitochondrial DNA mutation and the onset of diabetes/MIDD

More than 250 mtDNA point mutations and rearrangements have already been reported in a wide range of clinical diseases, underlining the importance of mtDNA replication, transcription and translation. (Greaves and Taylor 2006). The m. A3243G mutation associated with the onset of mitochondrial myopathy, encephalopathy, lactic acidosis and stroke (MELAS) was the first recorded mtDNA point mutation in ageing individuals (Greaves and Turnbull 2009). Other point mutations such as m.8344A>G transition is linked to Myoclonic Epilepsy with Ragged Red Fibres (MERRF) and m.11778G>A is linked to Leber hereditary optic neuropathy (LHON) (Greaves and Taylor 2006).

As mentioned in chapter 1.2.4, the insulin secretion from pancreatic beta cells is closely related to the ATP generation in the mitochondria. An age-related functional decline in pancreatic beta cells was found in the normal populations and many studies have concluded that the reason is mtDNA depletion (Soejima, Inoue et al. 1996) (Kennedy, Maechler et al.

1998). Due to the loss of mtDNA encoded subunits following mtDNA depletion, the defect of the electron transport chain and the impairment of mitochondrial ATP generation can lead to the decrease of glucose-stimulated insulin secretion (Soejima, Inoue et al. 1996) (Kennedy, Maechler et al. 1998). Previous studies about transcriptional knockout of the pancreatic duodenal homeobox 1 (pdx1) gene and mitochondrial transcription factor A (TFAM) in pancreatic tissue revealed that mtDNA depletion can cause mitochondrial dysfunction as well as impaired insulin secretion (Gauthier, Wiederkehr et al. 2009) (Silva, Köhler et al. 2000) (Nile, Brown et al. 2014).

MtDNA mutation accounts for around 1% of all diabetes cases and the most common diabetes associated mtDNA mutation is m.3243A>G (A to G substitution at position 3243 of the mitochondrial DNA) mutation in the tRNA (Leu,UUR) gene (Maassen, t Hart et al. 2004, Schaefer, Walker et al. 2013). Association of other mtDNA mutations with diabetes have also been intensively studied in the past a few decades and have been listed in ***Table 1-2***. Apart from having associative relationship with the MELAS syndrome, m.3243A>G point mutation has also been linked to the onset of maternally inherited diabetes and deafness (MIDD) (Murphy, Turnbull et al. 2008) (Schaefer, Walker et al. 2013). The mean age of MIDD diagnosis is 37 ± 11 years (Guillausseau, Dubois-Laforgue et al. 2004). It was estimated from studies carried out in north-east England that m.3242A>G mutation prevalence ranges from 1.4 to 16.3 per 100000 people (Chinnery, Johnson et al. 2000).

Diabetic patients with mtDNA abnormalities have a characteristic feature of impaired insulin secretion because the mtDNA mutation involves in the attenuation of cytosolic ATP/ADP level (Lynn, Borthwick et al. 2003). Carriers of the m.3243A>G mutation show a significant reduction in first and second-phase insulin secretion in response to a 10mmol/l hyperglycaemic clamp compared with non-mutation carriers (Maassen, t Hart et al. 2004). Apart from the diabetes features, patients with MIDD also have other clinical manifestations such as central neurological and psychiatric features, ophthalmic disease, myopathy, cardiac disorders and renal disease. It was reported that among young adults who are less than 45 years of age, 1% of patients with clinical diagnosis of stroke and 6% of patients with brain

infarcts can be attributed to m.3243A>G mutation (Majamaa, Turkka et al. 1997) (Murphy, Turnbull et al. 2008). More than half of the MIDD patients have bilateral basal ganglia calcification scanned by brain computerized tomography (CT) and basal ganglia high signal lesions shown by magnetic resonance imaging (MRI) (Lien, Lee et al. 2001) (Suzuki, Shibuya et al. 1996). The macular retinal dystrophy is the most common ophthalmic feature of m.3243A>G mutation because it is observed in 86% of examined MIDD adult patients (Massin, Virally-Monod et al. 1999). Approximately 43% of MIDD patients were observed with muscular abnormalities and the clinical myopathy generally involves with proximal limb muscles and present as exercise-induced muscle cramps. Cardiac death which is one of the most severe clinical features of MIDD patients has raised a grand concern because of the rapid progression to heart failure in young patients (Nishikai, Shimada et al. 2001) (Silveiro, Canani et al. 2003). End-stage renal failure (ESRF) is also prevalent in MIDD patients, with focal segmental glomerular sclerosis (FSGS) as the most common finding (Guillausseau, Dubois-Laforgue et al. 2004). Besides, many MIDD patients have major depression and phobia syndromes (Murphy, Turnbull et al. 2008). It is very impressive that various clinical phenotypes are associated with one single m.3243A>G mutation and the clinical phenotypes presented on individuals vary between cases (Remes, Majamaa et al. 1993). Different tissues have different heteroplasmic mutation loads and mutated genome segregations can explain this phenotype variation (Murphy, Turnbull et al. 2008). The diabetes-related mitochondrial gene mutations are described in ***Table 1-2***.

Table 1-2. Mutations of mitochondrial genes in patients with DM.

	Clinical manifestations apart from diabetes	References	Other
$tRNA^{Leu}$(3243)A→G	The bilateral hearing impairment The presence of maternal transmission Lower BMI Higher FPG	(Maassen, t Hart et al. 2004) (Wang, Wu et al. 2013) (Crispim, Tschiedel et al. 2002)	The most common mutation
$tRNA^{Leu}$(3256) C→T	MERRF and chronic progressive external ophthalmoplegia (CPEO)	(Kawarai, Kawakami et al. 1997) (Wang, Wu et al. 2013)	
$tRNA^{Glu}$(14709)T→C	Adult onset myopathy mental retardation cerebellar ataxia	(Perucca-Lostanlen, Taylor et al. 2002) (Hao, Bonilla et al. 1995)	It presents at high levels in the patient's muscle and white blood cells
tRNALys(8344)A→G	MERRF syndrome Neurosensory deafness	(Suzuki, Hinokio et al. 1994)	

ND1(3316)G→A	Leber's hereditary optic neuropathy (LHON) syndrome	(Crispim, Tschiedel et al. 2002) (Wang, Wu et al. 2013) (Chalmers and Schapira 1999) (Crispim, Tschiedel et al. 2002)	Prevalence of this mutation is 2-4% in DM patients
ND1(3394)T→C	Leber's hereditary optic neuropathy (LHON) syndrome	(Crispim, Tschiedel et al. 2002) (Yu, Yu et al. 2004)	
ND_4(12026)A→G	Early onset disease High prevalence of family history Require insulin therapy	(Wang, Wu et al. 2013) (Tawata, Ohtaka et al. 1998) (Wang, Wu et al. 2006)	

1.2.6. T2DM and ageing

It was widely acknowledged that the onset of T2DM is closely associated with metabolic and genetic influencing factors. There are also evidence that T2DM prevalence is linked to the ageing effect. The National Health and Nutrition Examination Survey (NHANES) is a national study that lasts for 5 decades and it has become an important authority for health and nutrition instruction (Harris, Hadden et al. 1987). The T2DM prevalence in the elder age group (>65 years) has increased from 17.7% in 1976-1980 (Harris, Hadden et al. 1987), to 21.6% in 1999-2002 (Cowie, Engelgau et al. 2006) and to 30% in 2005-2006 (Cowie, Rust et al. 2009). In the 2005-2006 report, almost three-quarters of the elder population had diabetes or pre-diabetes (Cowie, Rust et al. 2009). This increase of T2DM prevalence in the elder population with time is possible because of more elder people are living longer. It was reported in their 1976 – 1980 study that the diabetes prevalence increases from 2.0% in individuals of 20-44 years to 17.7% in individuals of 65-74 years in American populations (Harris, Hadden et al. 1987), indicating the increase of prevalence with age. Another 8 years follow-up study with 1163 men and 1386 women shows that the prevalence of metabolic syndrome increases with the time. The prevalence of metabolic syndrome in men with an average age of 50 at baseline was 21.4% but increases to 38.8% at the end of the 8-year study. The prevalence rate in women starts from 12.5% and ends up with 30.6% after 8 years follow-up (Wilson, D'Agostino et al. 2005). The reason why T2DM prevalence increases with age (Harris, Hadden et al. 1987) (Paulweber, Valensi et al. 2010) can be blamed to the age-related β-cell dysfunction and

insulin resistance. Age-related insulin resistance is also associated with changes in body composition and physical inactivity.

Old-age T2DM patients also have higher chances of developing microvascular and macrovascular diseases and geriatric syndromes including falls and fractures, and hearing impairment, and urinary incontinence (Chang and Halter 2003). Old age adults with diabetes also have greater declines in physical and cognitive function. The consequences of overtreatment for hyperglycemia in older adults such as hypoglycaemia are common and significant. They also have significantly higher long-term mortality after hyperglycemia (Alagiakrishnan and Mereu 2010).

Due to the high prevalence of T2DM and higher chances of diabetes-related complications in older adults, this challenge need to be addressed urgently by both clinician and researchers in the future.

1.2.7. T2DM and mitochondrial dysfunction

Many pieces of evidences have shown that decreased β-cell mitochondrial function can impact on insulin secretory capacity and predispose to diabetes because insulin secretion is dependent on ATP generation. As mentioned in **chapter 1.2.5**, m.3243A>G point mutation is linked to the onset of maternally inherited diabetes and deafness (MIDD) (Schaefer, Walker et al. 2013). Apart from causing mitochondrial diabetes, mitochondrial dysfunction also contributes to pancreatic β-cell dysfunction and decreased insulin secretion in T2DM.

Two different mechanisms could link decreased mitochondrial function and decreased insulin secretion. First, mitochondrial respiratory chain dysfunction can generate an increasing amount of ROS which is closely related to the onset, progression and pathological consequences of diabetes (Rolo and Palmeira 2006, Greaves and Turnbull 2009). At the same time, chronic hyperglycaemia status of diabetes can increase glucose metabolism through oxidative phosphorylation which causes increased production of ROS with age (Rolo and Palmeira 2006, Chang-Chen, Mullur et al. 2008, Volpe, Villar-Delfino et al. 2018). Cellular

oxidative stress generated along with other insulin resistance inducing reagents can negatively regulate the function of insulin receptor substrate 1 (IRS1). IRS1 is an important protein involved in insulin signaling (Valko, Leibfritz et al. 2007). Glucose intolerance begins to be seen because the age-related dysfunction of β-cells is unable to secrete enough insulin to compensate the insulin resistance (Gastaldelli, Ferrannini et al. 2004). β-cells are especially sensitive to the attack by reactive oxygen species (ROS) because lack of antioxidant enzymes (Valko, Leibfritz et al. 2007). Therefore, it can be explained that age-related ROS generation in mitochondria can blunt insulin secretion gradually. This increasing amount of ROS can also activate the β-cell apoptosis and dysfunction and cause the progression of important diabetes-related metabolic disorders (Chang-Chen, Mullur et al. 2008, Volpe, Villar-Delfino et al. 2018). The role of impaired β-cell function in the progress of T2DM has been proved in many human studies. In a study conducted on 131 T2DM patients, a mathematical linear regression model was used to study the β-cell function with the increasing age. It was shown that β-cell function declines at a rate of 1.5% per year (Rudenski, Hadden et al. 1988). This age-dependent character even exists in the general, non-diabetic population (Chang and Halter 2003) (Basu, Breda et al. 2003).

Secondly, it was established several decades ago that blockade of the respiratory chain inhibits glucose-stimulated insulin secretion (GSIS) (Maechler and Wollheim 2001). Age-related mtDNA mutation and deletion can cause the dysfunction of respiratory chain complexes. The following loss of mitochondrial ATP production inhibits the closure of ATP-sensitive K^+ channels and the opening of voltage-sensitive Ca^{2+} channels. As a result, cytosolic Ca^{2+} which is the main trigger for exocytosis decreases and the GSIS is decreasing or even absent (Maechler and Wollheim 2001). Through these two mechanisms, a vicious cycle was caused between the increasing T2DM prevalence and ageing.

To study the impact of mitochondrial dysfunction on insulin secretion, a model of partial mtDNA depletion and mitochondrial dysfunction was created in MIN6 cells. They express decreased COX1 expression, decreased mitochondrial respiration and ATP synthesis and

produced decreased GSIS in response to glucose (Nile, Brown et al. 2014)(Bensch, Degraaf et al. 2007).

1.2.8. MtDNA mutator mouse model

House mice have been long served as models of human biology and disease because of their phylogenetic relatedness and physiological similarity to humans (Perlman 2016). The reason why mice are so popular is also due to the availability of different mouse strains and ease of breeding and genetically modifying them in the laboratory (Morse 2007). So far, many age-related diseases such as T2DM, cancer, heart disease, arthritis, osteoporosis and cognitive decline have been modeled in mice, prompting questions about how the life history of mice correlates with humans. The life phases and maturational rates of mice and humans were compared in ***Figure 1-4*** which is a survival curve based on a large cohort of C57BL/6J mice (150 males and 150 females) (Laboratory) (Fox, Barthold et al. 2006). Most studies focus on two or three specific life phases: mature adult, middle age, and old. The mice maturational rate does not linearly correlate with humans—it occurs 150 times faster during the first month of life. Mature adult mice range in age from 3 - 6 months and this life phase is equivalent for 20 – 30 years in human age range. The mature adult group is often used as a reference group for any change in ageing studies because this group is post-development but not yet affected by ageing. After 6 months of age, the maturational rate of mice is 25 times faster compared to humans. A middle-aged group (aged from 10 to 14 months) can help determine if an age-related change is progressive. Mice ranging from 18 - 24 months of age correlate with age range of 56 ~69 years of age in humans. This age range can be defined as the old age group. And the upper limit for this group is ~24 months for C57BL/6J mice (Fox, Barthold et al. 2006).

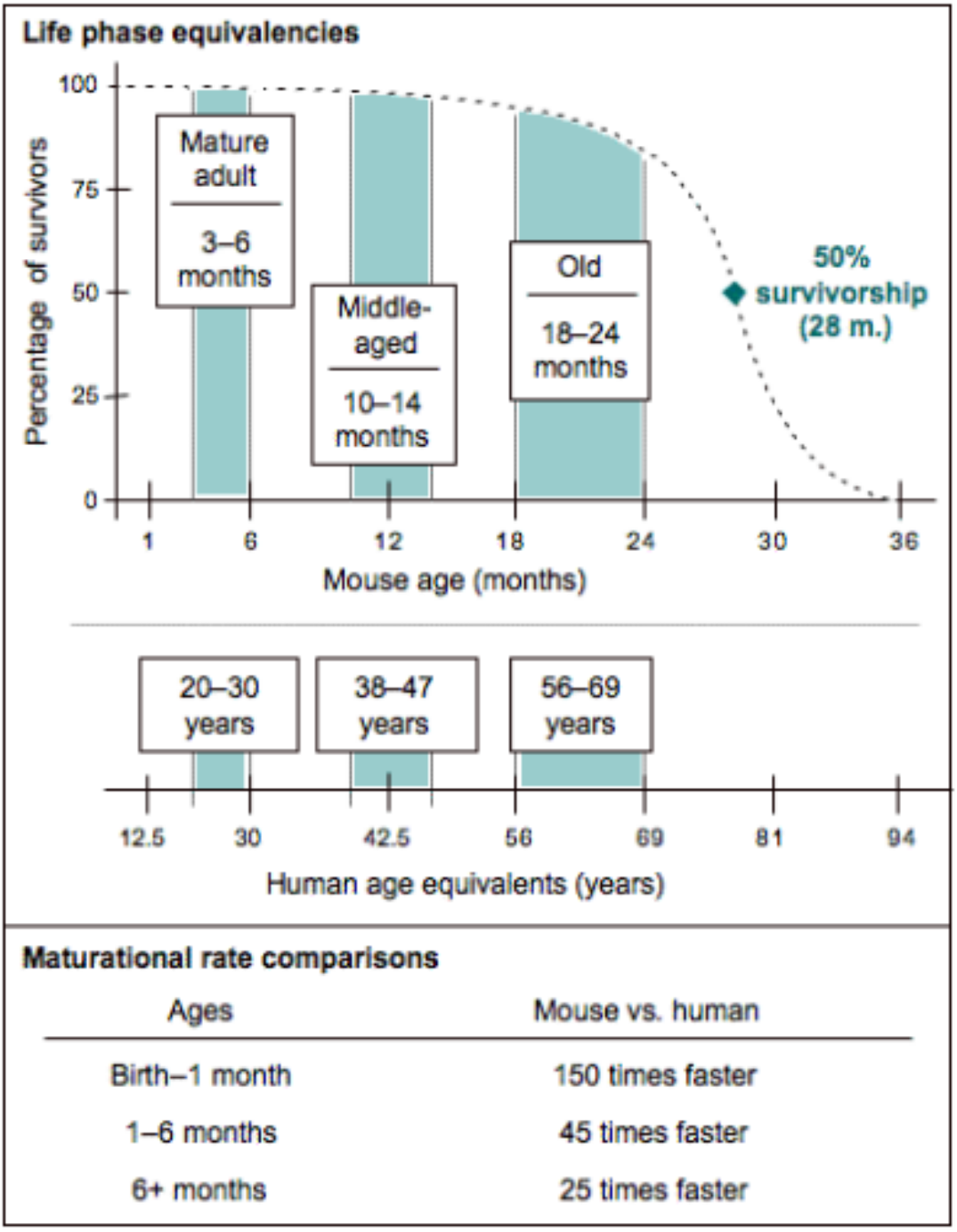

Figure 1-4. Representative age ranges for mature life history stages in C57BL/6J mice compared to human beings. Figure was cited from https://www.jax.org/research-and-faculty/research-labs/the-harrison-lab/gerontology/life-span-as-a-biomarker

1.2.8.1. The *PolgA$^{mut/mut}$* mice

Although it has been widely discussed that mtDNA has cumulative deletions and mutations with increasing age, whether mitochondria are the driving cause of ageing is still waiting to be further discovered. So far, several mouse models have been generated to serve as a link between mtDNA mutations and ageing phenotypes (Greaves and Turnbull 2009). One of the mutator mouse model that has been paid a great amount of attention is the homozygous knock-in mice which express a proof-reading-deficient mtDNA polymerase gamma (POLG) (Kujoth, Hiona et al. 2005) (Trifunovic, Wredenberg et al. 2004). This mtDNA mutator mice (*PolgA$^{mut/mut}$*) were generated by inserting a knock-in missense mutation (D257A) in the second endonuclease proofreading domain of the PolgA catalytic subunit of the mtDNA polymerase, using a C57BL/6 background mouse (Dobson, Rocha et al. 2016). It was shown in *PolgA$^{mut/mut}$* have 3 to 5-fold increase in mtDNA point mutations and an increase in mtDNA deletions compared to their age-matched controls (Trifunovic, Wredenberg et al. 2004). Unlike mtDNA deletions which present at early life don't increase over time, mtDNA mutations increase linearly with the increasing age in the mutator mice (Trifunovic, Wredenberg et al. 2004). This increase in mtDNA mutations has been shown to be associated with reduced lifespan and the onset of classic ageing phenotypes such as hair loss, weight loss, reduced subcutaneous fat, osteoporosis and reduced fertility in *PolgA $^{mut/mut}$* mice (shown in ***Figure 1-5***) (Trifunovic, Wredenberg et al. 2004). In our study, it was found out that *PolgA$^{mut/mut}$* mice have significant changes in mitochondrial respiratory chain complex expression and islet cell composition compared to the age-matched controls. However, the accumulation of mtDNA mutations in the mutator mice starts from the embryonic period and builds up to a very high extent compared to their wild-type controls (Ross, Coppotelli et al. 2014). However, this model is a 'whole body' mutator mice model, mtDNA mutation remains equally between different tissues within the mice which is different from normal ageing (Greaves and Turnbull 2009).

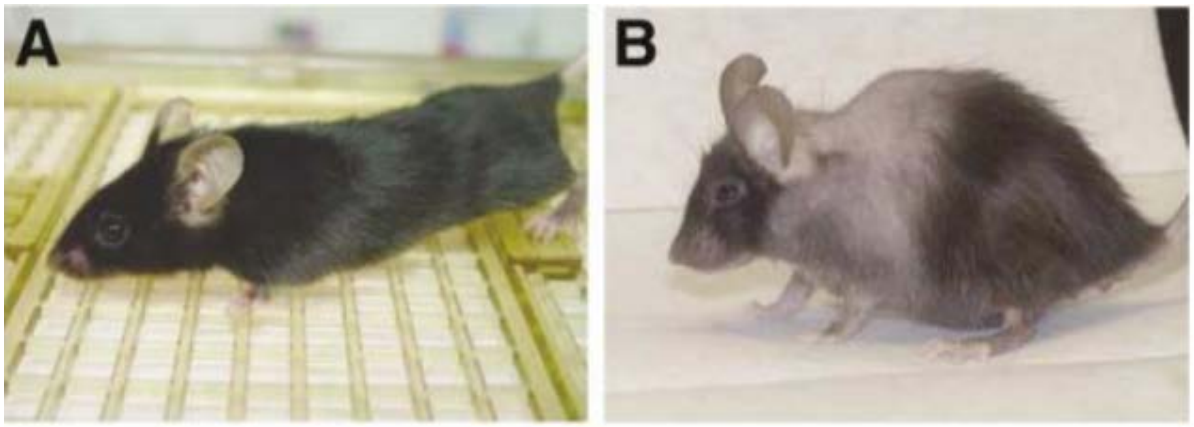

Figure 1-5. The comparison between wild type and *PolgA*$^{mut/mut}$ mice both at 13 months of age. (A) Wild type mice. (B) *PolgA*$^{mut/mut}$ mice. *PolgA*$^{mut/mut}$ mice shows progeroid ageing phenotypes, including hair loss, graying, and kyphosis. Figure is cited from (Kujoth, Hiona et al. 2005).

.

1.2.8.2. The effect of exercise training

1.2.8.2.1. Exercise induced cell adaptations

The emergence of modern chronic diseases mostly stems from the sedentary life and excessive energy intake (Holloszy and Booth 1976). Exercise has always been regarded as the first-line lifestyle intervention. As a physiological stress, exercise requires a synchronised response from different systems. Many types of research have documented the beneficial effects of exercise in rodent models and humans. Epidemiologic studies have demonstrated that exercise training reduces the risk of chronic diseases and extends life expectancy in humans (Johannsen and Ravussin 2009, Warburton, Charlesworth et al. 2010). Many molecular and cellular adaptations occur to improve work capacity because of fatigue during exercise training. Causes of fatigue range from ATP depletion, low cellular PH, glycogen depletion, limited oxygen flux and insufficient mass of skeletal muscle. Enhanced glucose transporter response and mitochondrial adaptations are the major adaptations to exercise-related fatigue (Booth and Thomason 1991).

Mitochondria play an important role in providing the enhanced ATP source to the working muscle during exercise and only enough healthy mitochondria can satisfy increased energy demand. Cardiac mitochondrial oxygen consumption increases by at least 10-fold to accommodate the greater energy demand of working muscles (Olver, Ferguson et al. 2015). Endurance exercise is the most potent physiological inducer of mitochondrial biogenesis which helps to increase the quality and quantity of mitochondria in skeletal muscle and many other tissues such as liver, brain and adipose tissue (Holloszy and Booth 1976, Boveris and Navarro 2008, Sutherland, Bomhof et al. 2009). Exercise promotes mitochondrial biogenesis in cardiac muscle by increasing the expression of PGC-1α which is the master regulator of mitochondrial metabolism (Tadaishi, Miura et al. 2011). The activities of the mitochondrial complex enzymes doubled in the skeletal muscles of the trained rats. And this has been verified in many other species including humans (Booth and Thomason 1991). Also, the restoration and protection of mitochondrial quality and quantity in trained animals have increased the capacity to oxidize fat and carbohydrates which it can lead to the reduction of

multi-organ pathology and postpone the overall ageing progress (Safdar, Bourgeois et al. 2011).

Accompanied with increase in mitochondrial number and energy production capacity, the cellular adaptations of muscle cells induced by exercise include physiological cardiac hypertrophy. This accommodates the increased reliance on the cardiac muscle during exercise and to meet the increased basal metabolic rate and energy demand (De Biase, De Rosa et al. 2014). Since cardiac muscle is a post-mitotic tissue just like pancreatic islet cells, the growth in the size of cardiomyocytes is more likely to occur than cellular proliferation.

1.2.8.2.2. Exercise in mice.

Treadmill running in mice has been a subject of exercise investigation since the 1970s and most of the work was carried out discerning its role and effects on cardiac and skeletal muscle (Kemi, Loennechen et al. 2002, Avila, Kim et al. 2017). Positive and negative consequences of exercise were all reported before. A mouse model of colitis suffered an exacerbation of systemic inflammation after forced treadmill running (Cook et al., 2014). The induction of stress in another mouse model of cerebral ischaemia was associated with forced treadmill running (Svensson, Rosvall et al. 2016). It can be concluded that mice with a predisposed disease burden may suffer from the added pressure of forced exercise. On the other hand, Luccetti et al proved that moderate forced treadmill running provides better cardiac function and resistance against the infection. A study by Narath, Skalicky and Viidik reported running in rat increases their survival rate and reduces body fat to muscle ratio (Narath, Skalicky et al. 2001).

Apart from the impact of the predisposed disease, the type of exercise, intensity, frequency and duration play an essential role in the outcome of exercise (Nebiker, Lichtenstein et al. 2018, Sarabia Marín, Agustín et al. 2018). From previous epidemiological studies, it is known that endurance and moderate exercise can restore body function, extend life expectancy and quality in mice (Safdar, Abadi et al. 2009, Logan, Shabalina et al. 2014). However, compared

to endurance exercise, there are more debates and conflicts regarding the impact of high-intensity exercise. Some studies suggest that high-intensity exercise imposes some potential health and safety concerns by adding extra stress on body function whereas other people insisted that it will bring equal or even superior improvement to body function. It was reported by Davies in 1982 that strenuous acute exercise in mice increased oxidative stress and led to tissue damage because of enhanced tissue oxygen consumption by 3.6-fold in the heart (Davies, Quintanilha et al. 1982). However, one study carried on aged mice revealed that high-intensity exercise benefited brain function (E, Burns et al. 2014).

As for the mitochondrial *PolgA*$^{mut/mut}$ mice model I used in my study, it was discussed in a previous study that endurance exercise could decrease mitochondrial superoxide generation and delay the onset of ageing. It attenuated the decline in mtDNA copy number and reduced the mtDNA point mutation frequency in *PolgA*$^{mut/mut}$ mice. Besides, it promoted systemic mitochondrial oxidative capacity by enhancing COX activity in *PolgA*$^{mut/mut}$ mice (Logan, Shabalina et al. 2014). Another study carried by Safdar showed that 5 months of treadmill running mitigate stress intolerance, multisystem degeneration and increase body weight, fertility rate and lifespan. They also proved that endurance exercise can not only induce mitochondrial biogenesis and reduce the frequency of mtDNA mutations in skeletal muscle, it also profoundly rescues mtDNA mutations and increase COX assembly in non-exercised tissues include heart, brain, adipose tissue, and liver, indicating multisystem mitochondrial restoration by endurance exercise (Safdar, Bourgeois et al. 2011). It was the main reason why I induced endurance exercised *PolgA*$^{mut/mut}$ mice in my study because I want to see if endurance exercise impact on mitochondrial function and cell composition of pancreatic islet which is another non-exercised tissue.

1.3. Islet beta cell physiology

1.3.1. Islet biology in mice and humans

The exocrine pancreas takes up 96-99% of total pancreas volume (TPV) (Dolenšek, Rupnik et al. 2015) and the rest is the endocrine part. Pancreatic islets, a cluster of endocrine cells, were first discovered by Paul Langerhans in 1868 is the basic unit of pancreatic endocrine function (DeFronzo 2004) (Langerhans 1869). Pancreatic islets are composed of four different endocrine cells and each cell type secretes a different type of hormone: β-cells form up to 50-70% and 60-80% of the islet mass in humans and mice, respectively, secreting insulin. α-cells make up 20-40% and 10-20% of the islet mass in humans and mice, respectively, secreting glucagon. δ-cells form 2-8% of the islet mass and secrete somatostatin and PP cells, or γ cells, secrete pancreatic polypeptide (DeFronzo, Ferrannini et al. 2015). In the human pancreas, the number of islets has been estimated to range from 10,000 to 1000,000 whereas in rodents, this number is around 1000-5000 islets per pancreas (Rosenberg, Vinik et al. 1996, Dolenšek, Rupnik et al. 2015). The structure of islets also differs between species. In rodents, β-cells are located mainly in the islet centre and surrounded by a discontinuous mantle of non- β-cells that are one to three cells thick (Erlandsen, Hegre et al. 1976). In human and some primateislets, the endocrine cells disperse throughout the islets and make up a disorganized cellular composition (Cabrera, Berman et al. 2006). More recently, human islets were described as composites of several mantle-core subunits (Erlandsen, Hegre et al. 1976). This is partly due to the different capillary networks that support the islets between human and rodents (DeFronzo, Ferrannini et al. 2015). Different islet structure between human and rodent is shown in ***Figure 1-6***. β-cells have the protective and compensatory capacity to respond to the high blood glucose level and adapt to the insulin resistance in the prediabetes stage (Puri and Hebrok 2012). In the physiological situation, transient increases in glucose level within a normal range after meals stimulate insulin secretion (Chang-Chen, Mullur et al. 2008). β-cell mass is determined by the size and number of β-cells, and the number of β-cells depends on the dynamic balance of β-cell life cycle such as β-cell neogenesis, β-cell proliferation, transdifferentiation and replication, and β-cell death (Montanya, Nacher et al. 2000).

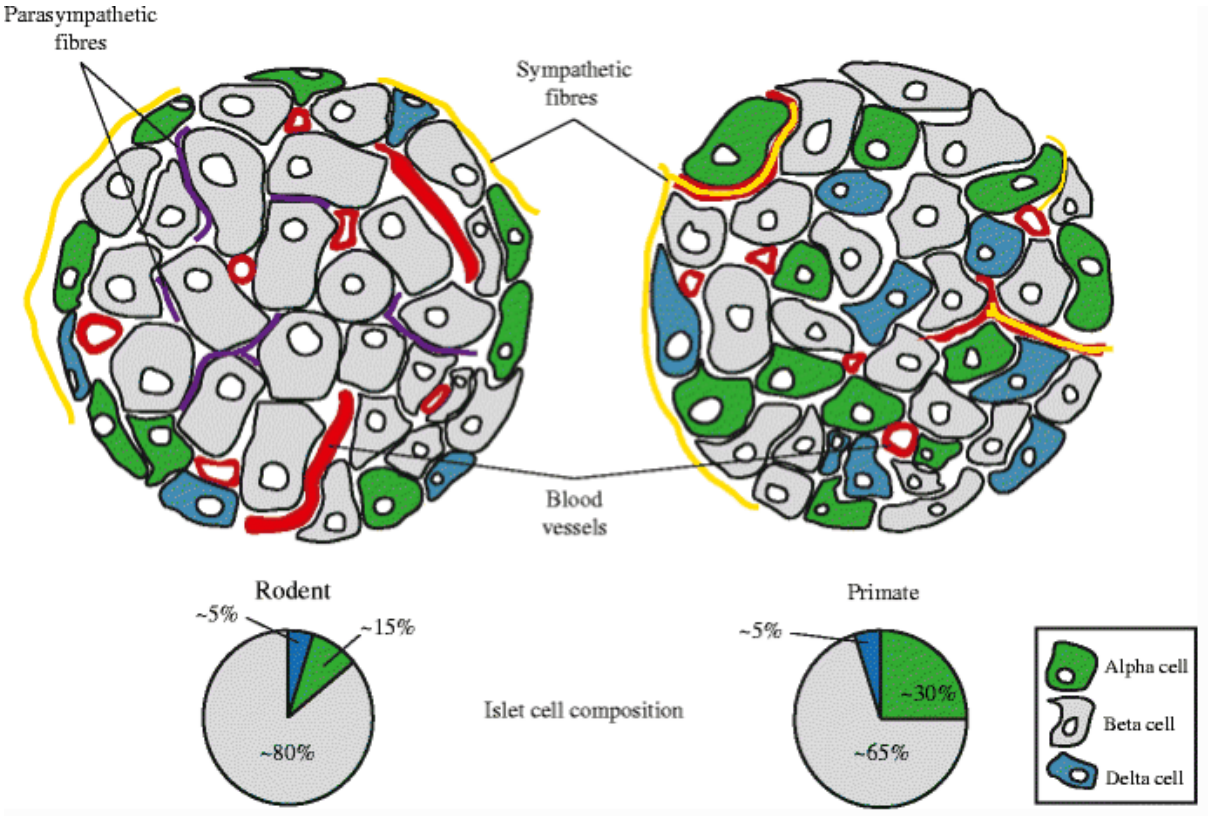

Figure 1-6. The cytoarchitecture of rodent islets and primate islets. Figure is cited from (Arrojo e Drigo, Ali et al. 2015).

1.3.1.1. The development of mouse islets.

In rodents, the β-cell number is determined in a certain window phase, which is in the last quarter of fetal gestation and in the first few days after birth. It is generally accepted that in this stage, β-cell population is mainly developed by the neogenesis process that is the formation of new β-cells from differentiated precursor cells (Bouwens and Rooman 2005). The β-cell mass generated from this process defines the baseline β-cell mass. It is the critical starting β-cell population from which a compensatory β-cell expansion may occur later (Perl, Kushner et al. 2010). After birth, only a small number of β-cells proliferation including replication and neogenesis in the normal situation and most of them are coming from the replication of pre-existing β-cells (Montanya, Nacher et al. 2000, Bonner-Weir, Li et al. 2010). There are also some of the β-cells forming from the progenitor cells and ductal cells. This discovery has been proved by studies using different mouse models (Bonner-Weir, Taneja et al. 2000, Ramiya, Maraist et al. 2000, Chang-Chen, Mullur et al. 2008, Gregg, Moore et al. 2012). The developmental biology of murine α-cells is similar to that of β-cells. They both expand via self-renewal and their growth rates both experience age-related declines (Lam, Rankin et al. 2019).

1.3.1.2. The development of human islets.

Human islets usually have proportionally fewer β-cells and more α-cells than do mouse islets. Mice islet cell division reduces over time and are largely post-mitotic by 12 months (Rankin and Kushner 2009). However, in humans, the islet β-cell replication rate which is estimated to be 10- fold less than in adult mice peaks at the age of 5 (Kassem, Ariel et al. 2000). The human baseline β-cell population is established by 5 years of age (Gregg, Moore et al. 2012). Also, very little replication of human α and β-cell is observed after the age of 20 (Perl, Kushner et al. 2010). This fact was also proved by a Japanese study that islet density was markedly high in the first decade of life span (Mizukami, Takahashi et al. 2014). Human β cells turn over very slowly, it happens once every 25 years (Gregg, Moore et al. 2012). Because of these above facts, human endocrine cells in islets aged more than 20 years are unlikely to divide and replicate, thus can be regarded as mature islets. The study about ageing impact is more

often starting from this time point because they are less likely affected by other influencing factors.

1.3.2. Islet adaption to physiological and pathological stress.

Striking plasticity in islet architecture and composition not only exists among species but also within the same species in response to different physiological and pathological changes (Miller, Kim et al. 2009). Pancreatic β-cells, which take up 70% of islet cell numbers, are highly sophisticated cells that respond to blood glucose concentration by rapidly and constantly secreting insulin, helping maintain the blood glucose homeostasis. β-cells can respond to the high glucose level and adapt to the insulin resistance in the prediabetes stage (Puri and Hebrok 2012). Glucose is an important modulator of β-cell function (Chang-Chen, Mullur et al. 2008). In the physiological situation, transient increases in glucose level within a normal range after each meal can stimulate insulin secretion and send out beneficial signals to coordinate the functions of body organs (Chang-Chen, Mullur et al. 2008). A strong and intense stimulus such as experimental surgical or chemical pancreatic injury can trigger the β-cell regeneration in T1DM children or young diabetic mice (Wang, Bouwens et al. 1996, Thorel, Nepote et al. 2010). Long-term physiological and pathological demands such as ageing, pregnancy, excessive nutrition and obesity can also accumulate stress in β-cells and overwhelm the morphological and functional compensation of β-cells, causing reduced β-cell mass and function (Puri and Hebrok 2012). There is a strong correlation between reduced β-cell mass and β-cell dysfunction because the increased insulin demand caused by decreased β-cell mass can exhaust β-cell secreting function. β-cell failure which is characterized by β-cell dysfunction and decreased β-cell mass is considered as a central contributor of type 2 diabetes (Group 1995, Bouwens and Rooman 2005).

However, whether the decrease of β-cell mass is due to β-cell death or loss of β-cell identity remains controversial (Puri and Hebrok 2012, Talchai, Xuan et al. 2012). There is evidence that mature β-cells can lose their differentiated phenotype and the cellular identity and regress to a less differentiated and precursor-like state or even convert to different endocrine

cell types subsequently. These β-cells although maintain the endocrine cell characters don't contribute to the glucose homeostasis because they are no longer secreting insulin (Talchai, Xuan et al. 2012, Bensellam, Jonas et al. 2018). A multitude of controlling factors such as cell cycle proteins during fetal and postnatal life govern β-cell mass and improve the adaptation of β-cells in response to stressed conditions, helping to achieve a balance of maintaining the β-cell mass and function (Rooman, Lardon et al. 2002, Ouziel-Yahalom, Zalzman et al. 2006, Chang-Chen, Mullur et al. 2008).

1.3.2.1. The adaption of mouse islets.

It is proved by different mouse model studies that β-cell respond to high glucose concentration by increasing β-cell mass, including the hypertrophy and proliferation of β-cells and even the formation of new β-cells from the progenitor cells and ductal cells (Bonner-Weir, Taneja et al. 2000, Ramiya, Maraist et al. 2000, Chang-Chen, Mullur et al. 2008). For example, a continuous increase of β-cell mass was reported throughout the lifespan in normal Lewis rat. In young rats, the increase in β-cell mass was contributed by hypertrophy and hyperplasia whereas only hypertrophy was responsible for β-cell increment in old animals (Montanya, Nacher et al. 2000). The reasons behind this phenomenon may be first, the continuous increase of β-cell mass is a compensation of the age-related glucose intolerance because glucose tolerance progressively decreases in the ageing process. This can result in a high prevalence of type 2 diabetes in the older population (Chang and Halter 2003); secondly, the increase of β-cell mass is a response to the increase of insulin secretory demand as the size of the animals increase with age (Clark 2008).

To study the underlying reason behind the islet cell proliferation, we can stain the islets by using Ki67 proliferation marker. Ki67 is a nuclear protein, which is only expressed during the active phases of the cell cycle. Therefore, it can mark cells that undergo proliferating process (Perl, Kushner et al. 2010). In immunofluorescence staining, it has a unique nucleus-staining distribution. Ki-67 protein is absent in resting phase of cell cycle (G_0) but present during all active phases of the (Gerdes, Schwab et al. 1983, Scholzen and Gerdes 2000). The expression of Ki67 protein is also an absolute requirement for progression through the cell-division cycle.

This special characteristic makes Ki67 an excellent marker for determining the growth fraction of a-cell population and in many cases, it was used in the diagnosis of human tumors, such as prostate and breast cancer (Bettencourt, Bauer et al. 1996, Stattin, Damber et al. 1997).

1.3.2.2. The adaptation of human islets.

Similar to mouse β-cells, human β-cell mass and function can also adapt to the impact of long term physiological and pathological demands.

1.3.2.2.1. The adaptation of human islets to obesity.

Unlike two- to three-fold expansion in mouse islets during pregnancy and obesity, human islet cell plasticity is less evident and more modest (Cnop, Igoillo-Esteve et al. 2011). In human studies, it was reported back in 1933 by Ogilvie that there is a higher percentage of islet tissue in the pancreas of obesity cases compared to lean controls (Robertson. 1933). More recently, Bonner-Weir et al found out there is β-cell neogenesis from pancreatic ductal cells by in vitro cultivation of pancreatic ductal tissue (Bonner-Weir, Taneja et al. 2000). A very interesting study conducted on 124 human autopsy tissue by Butler and colleagues shows that the β-cell volume is found to be about 50% higher in obese non-diabetic subjects (BMI ≈ 38) compared to the lean controls (BMI ≈ 22) (Butler, Janson et al. 2003). Butler et al also pointed out the underlying mechanism was β-cell neogenesis rather than proliferation because of the increasing occurrence of insulin-positive ductal cells in the obese patient pancreas. Later on, the Rahier group also shows that β-cell mass increases with the BMI and a difference of 20% increase in β-cell mass was observed between obese European subjects (BMI ≈ 30) and the lean controls (BMI ≈ 22) (Rahier, Guiot et al. 2008). Adiposity influences whole-body insulin sensitivity. It was reported in previous studies that average insulin sensitivity is lower in obese subjects compared to their lean controls (Kahn, Prigeon et al. 1993). Some human studies found islets isolated from obese subjects have a two to three-fold increase in insulin secretion compared to the lean controls in order to defend insulin resistance (Polonsky, Given et al. 1988, Ferrannini, Natali et al. 1997). However, this compensatory effect of stressed β-cells

can lead to β-cell mass exhaustion and trigger accelerated hyperglycemia progression as side effects in the long term (Talchai, Xuan et al. 2012).

1.3.2.2.2. The adaptation of human islets to ageing.

Apart from the obese situation, ageing also impacts on islet function and composition. It was documented in previous studies that normal human ageing has been associated with impaired glucose tolerance, insulin resistance, hyperinsulinemia, defect islet β-cell function and changes of islet endocrine cells composition (DeFronzo 1979, DeFronzo 1981, Fink, Kolterman et al. 1983, Chen, Bergman et al. 1985, Kahn, Larson et al. 1992, Ihm, Matsumoto et al. 2006, Mizukami, Takahashi et al. 2014). An in vitro study shows that with the increase of donor age, islet ATP content/DNA decreases accordingly. This result backs up the hypothesis that age-related decline in intracellular ATP metabolism and mitochondrial function in β-cells (Ihm, Matsumoto et al. 2006). A human study shows that β-cell secretory function was 48% lower and insulin sensitivity index was diminished 63% in the older men (Chen, Bergman et al. 1985). This impaired tissue sensitivity to insulin is the factor that is responsible for age-related decrease in glucose tolerance (DeFronzo 1981). Although these phenomena mentioned above are recognized to represent an inherent phenotypic characteristic of the ageing process, they are also contributed by other controversial age-related variations in dietary habits, exercise, lean body mass and total body fat (Rowe, Minaker et al. 1983). Diets low in carbohydrates will impair glucose tolerance (Fink, Kolterman et al. 1983). The change of body composition such as the decrease in lean body mass and increases in total body fat can accompany normal human ageing (Rowe, Minaker et al. 1983) and impair insulin secretion and action. Endurance exercise can improve the degree of insulin sensitivity (Rowe, Minaker et al. 1983). In adult humans, the pancreatic β-cell mass has a certain degree of plasticity and can expand to compensate for insulin resistance with age (Gregg, Moore et al. 2012). According to one recent Japanese study, the density of whole islets, β-cells and non-β-cells were all high in the maturation period but they progressively declined with the increase of age. However, β-cell size which increased during the maturation period continues increasing with age. The β-cell occupancy in the islets started from 54.4% in

the first decade. It kept increasing until the fifth decade and then went down to 60.2% in the eighth decade (Mizukami, Takahashi et al. 2014). However, another American study pointed out that in a group of donors aged between 16 to 66 years, the average β: α ratio is 1.3 in donors aged <40 years and 1.8 in donors aged 40 or older. The result suggested that older donors' islets have more β-cells relative to α cells (Blodgett, Carroll et al. 2013).

In human islets, islet cell composition and islet cell mass constantly change with the increase of age. In a recent study, human pancreas donors were grouped into four age categories: 1-5 days, 2-3months, 10-20 months and 5-10 years. From 1-5 days to 5-10 years, the β-cell population increased from 41±9% to 57±6%, the α-cell population increased from 20±5% to 25±2% whereas δ-cell population decreased from 38±5% to 17±4%. β, α-cell mass increased gradually with age from 1-5 days to 5-10 years (Hart, Aramandla et al. 2014). In another human study with a donor age range between 16 to 66 years, the average β: α cell ratio was 1.3 in donors aged <40 years and 1.8 in donors aged 40 or older. It suggests older donors' islets have more β-cells relative to α cells (Blodgett, Carroll et al. 2013). However, according to a recent Japanese study, the average β-cell size which obtained by division of the β-cell area by the number of β-cells increased from 83.3 μm^2 in the first decade of life (0-9yrs age) to 129.4 μm^2 in the eighth decade of life (70- 79yrs age). The β-cell occupancy which obtained by division of the β-cell area by the total islet area started from 54.4% in the first decade (0-9yrs age). It kept increasing until the fifth decade (40-49yrs age) and then went down to 60.2% in the eighth decade (70-79yrs age). As a result, the number of β-cells per islet decreased since the fifth decade of life (40-49yrs age) to eighth decade of life (70-79yrs age) (Mizukami, Takahashi et al. 2014). Compared to rodent donors, human islets have greater variability and lower β: α cell ratio (4 in rodent islets). There is also greater donor-to-donor variability in human donors (Blodgett, Carroll et al. 2013).

1.3.3. Islet dysfunction in T2DM

If these original physiological and pathological stress continue, the protective and compensatory response of β-cells to the initial stress would in turn gradually cause a negative impact on β-cell mass and function (Chen, Cohrs et al. 2017) (Wajchenberg 2007). The

reduced β-cell mass and β-cell dysfunction are strongly correlated because the increased insulin demand caused by loss of β-cell mass can exhaust β-cell secreting function. The hyperglycemia status after the β-cell loss can also deteriorate β-cell function at the same time (Donath and Halban 2004). A reduction of β-cell mass and a substantial deficit in beta cell function are hallmarks of T2DM (Group 1995).

1.3.3.1. The β-cell dysfunction

The sign of functional decrease seems to start at around 10 years before diagnosis and can be further aggravated by increasing fasting plasma glucose level (Holman 1998). At the time of diagnosis, the pancreatic islet function was found to be 50% of normal level (Holman 1998).

In the pathogenesis of type 2 diabetes, lipotoxicity and glucotoxicity may both be implicated (Sivitz 2001). It was proved by previous human and animal studies that glucotoxicity, lipotoxicity, proinflammatory cytokines and potentially islet cell amyloid all serve as mediators of decreased β-cell function (Wajchenberg 2007). Glucotoxicity is the diabetogenic effect caused by elevated blood glucose levels (Sivitz 2001). Glucotoxicity can adversely affect β-cell function through mitochondrial dysfunction with excessive production of reactive oxygen species (ROS) and the activation of the endoplasmic reticulum (ER) because of the increased oxidative phosphorylation (Poitout and Robertson 2008). This glucotoxicity induced apoptosis is specifically related with β-cells not only because of their extreme sensitivity towards glucose change but also because of limited defense against excess ROS production (Wajchenberg 2007). The normal GSIS can be affected accordingly and the β-cell fate will be governed in a different way (Wajchenberg 2007).

Another key contributor of β-cell failure is lipotoxicity which is caused by increased circulating free fatty acids (FFA) and increased cellular fat content. Lipotoxicity can be regarded as a beneficial stimulus for insulin secretion in healthy individuals and may result in β-cell failure in genetically predisposed diabetes patients (Wajchenberg 2007, Chang-Chen, Mullur et al. 2008). Even worse, excessive glucose and lipid can interact with each other adversely, causing

mutual damage between these two important regulators. Previous studies have proved that in the background of hyperglycemia, the toxic effect of FFA becomes apparent (Prentki, Joly et al. 2002). It is also revealed lipid infusion in type 2 diabetes patients are associated with impaired insulin secretion (El-Assaad, Buteau et al. 2003). Many human studies showed that insulin secretion capacity in T2D patients reduced 50%-97%, revealing the existence of β-cell dysfunction (Butler, Janson et al. 2003) (Chen, Cohrs et al. 2017) (Ferrannini, Gastaldelli et al. 2005). Another indication of β-cell dysfunction lies in the changes of the dynamics of insulin releases, for example, the irregular oscillatory release patterns and the loss of first-phase insulin response (Brunzell, Robertson et al. 1976, Lang, Matthews et al. 1981). However, the recuperation of β-cell sensitivity, early insulin response and insulin sensitivity can serve as a reversal for the β-cell dysfunction. Many positive metabolic outcomes were observed by clinical treatments such as bariatric surgery and caloric restriction in T2D patients (Malandrucco, Pasqualetti et al. 2012, Schauer, Mingrone et al. 2016).

1.3.3.2. The reduction of β-cell mass

In response to continuous physiological and pathological stress, β-cell also experiences morphological changes by reducing their mass (Chang-Chen, Mullur et al. 2008, Puri and Hebrok 2012, Chen, Cohrs et al. 2017). Long-term exposure of human and rodent islets to excessive glucose and saturated fatty acid can induce β-cell apoptosis (Wajchenberg 2007). Many studies reported that a significant reduction of β-cell mass is evident in long-term T2D patients. It was reported in Rahier's study that the average β-cell mass is about 39% lower in T2DM subjects compared with controls (Rahier, Guiot et al. 2008). It also concluded that there was a positive correlation between the reduction of β-cell mass and the diabetes duration. The mean β-cell mass has an average of 24% loss in patients with 5 years of diabetes onset, this number increases to 54% in patients diagnosed with diabetes for more than 15 years. This extent of β-cell mass reduction in T2DM patients was agreed by most studies (Sakuraba, Mizukami et al. 2002, Butler, Janson et al. 2003). The β-cell mass is also determined by combined factors in humans with T2DM. One study reported that obese and lean T2DM patients had a 63% and 41% deficit in relative β-cell volume compared with nondiabetic obese

and lean cases, respectively (Butler, Janson et al. 2003). However, Rahier reported that the deficiency of β-cell mass in T2DM subjects went down with the increase of BMI compared with non-diabetic controls (Rahier, Guiot et al. 2008).

However, it remains controversial whether the decrease of β-cell mass is due to death or dedifferentiation (Puri and Hebrok 2012, Talchai, Xuan et al. 2012). Recent studies show another contributing factor behind the loss of functional β-cell mass is that mature β-cell can lose their differentiated phenotype and the cellular identity and regress to a less differentiated or precursor-like state, also known as the loss of β-cell identity. These β-cells can't contribute to glucose homeostasis because they are no longer insulin positive (Talchai, Xuan et al. 2012, Bensellam, Jonas et al. 2018). By using a linage tracing technique on a different hyperglycemic mouse models, Talchai finds out that there is a loss of β-cell gene expression and reprogramming to other islet cell types, secreting glucagon and somatostatin. This finding was proved by seeing that the endocrine cell mass is maintained. A recent human study conducted on isolated human pancreatic islets concludes that 31.9% β-cells are dedifferentiated in type 2 diabetics compared to only 8.7% in controls. There is also a significant decrease of β-cells but a significant increase of α cells in diabetic donors, causing a decrease in β: α cell ratio in diabetic donors (Cinti, Bouchi et al. 2016). Also, β-cell specific transcription factors were found in glucagon and somatostatin producing cells in T2DM subjects (Cinti, Bouchi et al. 2016). This idea is further proved by another study that β-cell dedifferentiation could be an adaptive mechanism to escape cell death when chronic hyperglycemia happens (Bensellam, Jonas et al. 2018).

The possible mechanisms behind the β-cell dedifferentiation involve (1) the down-regulation of β-cell enriched genes, including key transcription factors (PDX1, PAX6, Nkx6.1 and FOXO1) (Talchai, Xuan et al. 2012, Chen, Cohrs et al. 2017, Bensellam, Jonas et al. 2018), islet β-cell gene, glucose metabolism genes and signal pathway genes (Swisa, Glaser et al. 2017); (2) the up-regulation of β-cell forbidden genes (Ngn3, Myc) and the progenitor cell genes (Talchai, Xuan et al. 2012). Due to the fragile identity of β-cells and the epigenetic similarity between

islet cells, the transitions between β-cells and non- β-cells within islet can easily happen in different directions caused by different stimuli. Interestingly, a previous mouse study has demonstrated that the loss of β-cell identity and dysfunction are reversible when the blood glucose level is normalized by insulin therapy during disease pathogenesis (Wang, York et al. 2014). This provides a plausible method to save the exhausted β-cells. Recently, Ouziel-Yahalom et al published a study by isolating and culturing human islet with betacellulin (BTC) in vitro. An increase of β-cell replication and redifferentiation was observed. Also, the expression of key β-cell transcription factors such as PDX1 and Nkx6.1 was observed to be induced, stimulating insulin synthesis after treating with BTC (Ouziel-Yahalom, Zalzman et al. 2006).

Understanding the mechanisms of reduced β-cell mass and dysfunction is important for β-cell preservation at early stages (Wajchenberg 2007). Many clinical interventions such as short-term intensive insulin therapy, modulation of β-cell K_{ATP} channel and application of anti-apoptotic drugs all have the positive effects of preventing and rejuvenating β-cells (Wajchenberg 2007). This opens up many new questions and new ideas in the diabetes study. For example, the relative importance of compromised βcell identity in T2D, compared to β-cell dysfunction and β-cell death, is still in need to be further discovered, requiring more investigations in both human and animals for the significance and mechanism of β-cell transdifferentiation and dedifferentiation (Chen, Cohrs et al. 2017).

Project hypothesis

Dysfunction of mitochondria is associated with various age-related degenerative diseases, including diabetes. The homozygous knock-in mtDNA mutator mouse is a model of premature ageing due to the accumulation of mitochondrial DNA mutations.

Using pancreas sections from this mouse model, we explored the hypothesis that age-related mitochondrial dysfunction can affect islet cell composition and the possible mechanisms behind this change of cell composition in mice islets.

Moreover, I further investigated the hypothesis that ageing affects mitochondrial complex expression and cell composition in human islets from non-diabetic ageing human non-diabetic donors were.

Project aims

The overall aim of my project is to study the impact of ageing on mitochondrial complex expression and islet cell composition by using mtDNA mutator mice model and non-diabetic human donors. The general outline of my study is shown in ***Figure 1-7***. This aim can be further separated into following aims:

- Study the nature and extent of changes in mitochondrial ETC expression in pancreatic islets in response to ageing in *PolgA*$^{mut/mut}$ and wild type control mice, and determine whether exercise training impacts upon these changes.
- Study the changes in islet size and cellular composition in response to ageing in *PolgA*$^{mut/mut}$ and wild type control mice, and determine whether exercise training impacts upon these changes.
- Study the potential drivers and mechanisms underlying changes in islet cell composition in the *PolgA*$^{mut/mut}$ mouse.
- Characterize the differences in mitochondrial ETC complex expression and islets cell composition in pancreatic islets from young and old non-diabetic human donors.

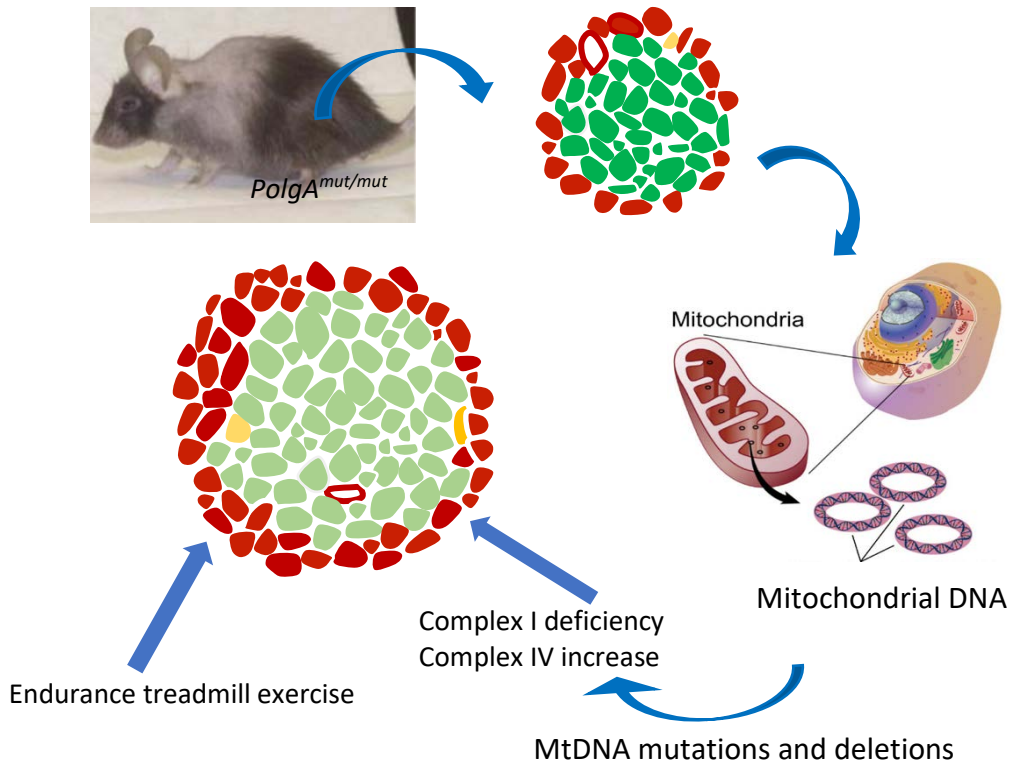

Figure 1-7. The general outline of this study.

CHAPTER 2. GENERAL MATERIALS AND METHODS

2.1. Mitochondrial DNA mutator mice model procurement.

PolgA$^{mut/mut}$ mutator mice were kindly offered by Dr Laura Greaves (Mitochondrial research group, Newcastle University). The mitochondrial mutator mice experiment was approved by the Newcastle University Animal Welfare Ethics Board, no 325 on 1st, December, 2016. All animal experimental procedures were conducted in accordance with the UK Home Office guidelines and under its approval (PPL60/4540).

2.1.1. Mouse husbandary and monitoring

Mice were kept at a temperature controlled room (25°C) and cages (25°C) with 12hrs light/dark cycle. They all have constant access to water and RM3 chow diet. Enrichment materials such as pieces of wood and cardboard tunnels were placed in the cages. Mice were monitored and their data were recorded on a weekly basis by Carla Bradshaw from Mitochondrial Research Group in Newcastle University.

Two age groups of mice (3 month and 11 month) were used in our study ***Table 2-1*** and ***Table 2-2***. It was reported before that heterozygous mtDNA mutator mice don't harbour ageing phenotypes and have normal lifespan because their mtDNA abnormalities are not sufficient enough (Mito, Kikkawa et al. 2013). The homozygous *PolgA*$^{mut/mut}$ mice was generated by intercrossing heterozygous *PolgA*$^{mut/+}$ mice and further investigate the impact of ageing. The reasons behind the choice of these two time points are: firstly, according to the survival curves (***Figure 2-1***) that median lifespan of *PolgA*$^{mut/mut}$ mice are around 48 weeks and all of them died before age of 61 weeks (Trifunovic, Wredenberg et al. 2004). *PolgA*$^{mut/mut}$ mice used in my study were presented with severe ageing phenotypes when they reached 11 months of age so I decided to sacrifice them at this age; secondly, according to the original Trifunovic study, the mtDNA mutational load was already substantial by the age of 2 months. 3 month is an intial time point to observe the impact of substantial accumulation of mtDNA

mutations. Also 3 month is comparatively younger compared to 11 months, I can further investigate the difference between young and old age.

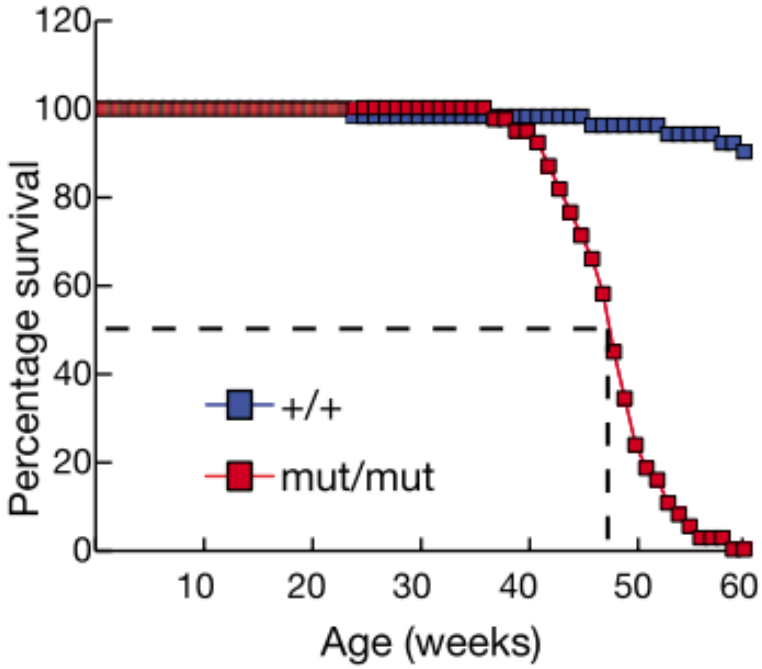

Figure 2-1. The survival curves for *PolgA*$^{mut/mut}$ and wild type mice. Figure was cited from (Trifunovic, Wredenberg et al. 2004)

Exercise intervention in *PolgA*$^{mut/mut}$ mice started at 4 months of age and terminated at 11 months of age. The speed of treadmill running remained at 20cm/s for 40 minutes, 4 times per week from week 2 onwards for the duration of six months. A 5 minutes warm up and cool down periods were included in each run at 12cm/s. Sedentary mice were allowed to remain their normal cage activity while exercised mice were running on the treadmill. In my study, the gender of mice I recruited are all male because it can exclude the impact of changes in hormones.

Table 2-1. Mitochondrial mutator mice in different ages and genotypes which were used in this study.

	3 months (12 weeks)	11 months (44 weeks)
Wild type (C57BL/6J)	4	5
PolgA$^{mut/mut}$ sedentary	4	5
PolgA$^{mut/mut}$ exercise		4

Table 2-2. The *PolgA*$^{mut/mut}$ and wild type mice datasheet.

Harvest number	Exercise/ Sedentary	Genotype	Gender	Age	Case number
PolG1622	Sedentary	WT	Male	3 months	C1-Y
PolG1624	Sedentary	WT	Male	3 months	C2-Y
PolG1626	Sedentary	WT	Male	3 months	C3-Y
PolG1629	Sedentary	WT	Male	3 months	C4-Y
PolG1681	Sedentary	*PolgA*$^{mut/mut}$	Male	3 months	P1-Y
PolG1682	Sedentary	*PolgA*$^{mut/mut}$	Male	3 months	P2-Y
PolG1683	Sedentary	*PolgA*$^{mut/mut}$	Male	3 months	P3-Y
PolG1709	Sedentary	*PolgA*$^{mut/mut}$	Male	3 months	P4-Y
GA0002	Sedentary	WT	Male	11 months	C1-O
GA0004	Sedentary	WT	Male	11 months	C2-O
GA0005	Sedentary	WT	Male	11 months	C3-O
GA0007	Sedentary	WT	Male	11 months	C4-O
GA0008	Sedentary	WT	Male	11 months	C5-O
LG0002	Sedentary	*PolgA*$^{mut/mut}$	Male	11 months	P1-OS
LG0004	Sedentary	*PolgA*$^{mut/mut}$	Male	11 months	P2-OS
LG0006	Sedentary	*PolgA*$^{mut/mut}$	Male	11 months	P3-OS
LG0011	Sedentary	*PolgA*$^{mut/mut}$	Male	11 months	P4-OS
LG0036	Sedentary	*PolgA*$^{mut/mut}$	Male	11 months	P5-OS

LG0005	Exercise	*PolgA*$^{mut/mut}$	Male	11 months	P1-OE
LG0009	Exercise	*PolgA*$^{mut/mut}$	Male	11 months	P2-OE
LG0023	Exercise	*PolgA*$^{mut/mut}$	Male	11 months	P3-OE
LG0024	Exercise	*PolgA*$^{mut/mut}$	Male	11 months	P4-OE
Polg1909	Sedentary	*PolgA*$^{mut/mut}$	Female	11 months	
Polg1918	Sedentary	*PolgA*$^{mut/mut}$	Male	11 months	
Polg1923	Sedentary	*PolgA*$^{mut/mut}$	Female	11 months	
Polg1937	Sedentary	*PolgA*$^{mut/mut}$	Male	11 months	
Polg1940	Sedentary	*PolgA*$^{mut/mut}$	Female	11 months	
Polg1967	Sedentary	WT	Male	11 months	
Polg1997	Sedentary	WT	Male	11 months	
Polg1999	Sedentary	WT	Male	11 months	
Polg2029	Sedentary	WT	Female	11 months	
Polg2034	Sedentary	WT	Male	11 months	

2.1.2. Tissue harvest.

Pancreas tissues were harvested from *PolgA*$^{mut/mut}$ exercise, *PolgA*$^{mut/mut}$ sedentary and wild type (C57BL/6J) mice. Animals were sprayed with 70% ethanol then followed by dissection. Whole pancreas tissues were dissected from mice and the half of tissue was put immediately into liquid nitrogen and stored in the -80° C freezer. The other half of pancreas was fixed in 10% normal buffered formalin (Sigma Aldrich) for 72 hours at room temperature and then embedded in paraffin.

2.2. Human sample procurement.

Human pancreas blots were kindly given by Professor Piero Marchetti (Islet Cell Laboratory University of Pisa, Italy) and Professor James Shaw (Diabetes Research Group, Newcastle University). Individual consent was obtained from the relatives of the donors. Pancreas were procured at the time of deceased donor organ donation and paraffin embedded and fixed. Detailed clinical data of non-diabetic pancreas samples from University of Pisa and Newcastle University are listed in ***Table 2-3*** and ***Table 2-4*** separately. In the experiment, only 6 out of 7 donors were used from Italian donors. I excluded one young donor (09/04/2013) from the

donors because of the bad staining quality, only studied 2 young donors and 4 old donors for all the following studies.

Table 2-3. Patient information for 7 non-diabetic donors from University of Pisa.

Pancreas ID	Diabetes status (ND/T2D)	Gender (M/F)	Age (years)	BMI (Kg/m^2)	Region	Case number
HP_04/05/2013	ND	M	31	23.1	Tail	ND-Y1
HP_09/04/2013	ND	M	25	24.7	Tail	Excluded
HP_20/05/2013	ND	M	24	27.8	Tail	ND-Y2
HP_11/6/11	ND	F	68	27.3	Tail	ND-O1
HP_09/03/2013	ND	F	72	22.0	Tail	ND-O2
HP_20/12/10	ND	F	75	23.4	Tail	ND-O3
HP_25/3/11	ND	F	85	24.7	Tail	ND-O4

Table 2-4. Patient information for 6 non-diabetic donors from Newcastle University.

Pancreas ID	Diabetes status (ND/T2D)	Gender (M/F)	Age (years)	BMI (Kg/m^2)	Region	Case number
LDIS087	ND	M	27	26	Tail	ND-Y3
LDIS158	ND	F	35	29.98	Tail	ND-Y4
LDIS167	ND	M	39		Tail	ND-Y5
LDIS161	ND	F	63	24	Tail	ND-O5
LDIS174	ND	M	71	26.73	Tail	ND-O6
LDIS193	ND	M	71	30.86	Tail	ND-O7

2.3. Immunofluoresence staining

2.3.1. Sectioning

2.3.1.1. Fixed tissue sectioning

All the paraffin-embedded fixed blots of pancreas tissues were placed on ice for at least 1 hour before sectioning. 5 μm thickness of sections were cut by blades and they were immediately placed floating on the water bath (37° C). Carefully load these sections on the labelled superfrost slides (ThermoFisher Scientific, UK). In order to dry out the slides, all the formalin-fixed, paraffin-embedded (FFPE) sections were put into a 37° C oven for 24 hours. Most of our blots were sent to cell pathology department in Royal Victoria Infirmary (Newcastle) to section. PhD student Anna Smith from Mitochondrial Research Group,

Newcastle University also kindly undertook a small amount of paraffin tissue sectioning for my study.

2.3.1.2. Frozen tissue sectioning

All the frozen tissue sectioning was done in cell pathology department in Royal Victoria Infirmary. 15µm thickness of sections were cut on membrane slides (ThermoFisher Scientific) and then stored in the -80°C freezer for later use.

2.3.2. Staining

2.3.2.1. Formalin-fixed, paraffin-embedded sections.

2.3.2.1.1. Deparaffinisation

The formalin-fixed, paraffin-embedded slides were first deparaffinised in 60-degree oven for 45 minutes to 1 hr. The slides were deparaffinised by putting directly in Histoclear solutions (National diagnostics) for 10 min and then followed by another Histoclear wash for 10 min. Then slides were rehydrated through graded alcohols from 100% (5 min) to 95% (5 min) to 70% (5 min) and washed with deionised water (10 min) to remove the ethanol. I then put slides into the 2100 antigen retriever (Pickcell laboratories B.V. Kruislaan 406, Amsterdam, Netherlands) for antigen retrieval process to recover the epitope. I filled the retriever's body with 750ml of deionised water and then put deparaffinised slides and appropriate buffer into the slides chamber and placed the slides chamber into the rack. After closing the lid, it was necessary to make sure that the depressurizing valve was closed. The whole antigen retrieval cycle run for 20 minutes. I let the retriever unit cool down for 2 hours when the cycle was completed because the cooling down time was also part of the processing cycle.

2.3.2.1.2. Immunofluorescence staining

The choice of antigen retrieval buffer, washing buffer, blocking solution and the antibody diluting solution depends on what types of primary antibody were used (***Table 2-5***).

Table 2-5. The choice of antigen retrieval buffer, washing buffer and blocking solution based on the primary antibody.

Category	Antigen retrieval buffer	Washing buffer	Blocking solution	Diluting solution	Mounting media
Mitochondrial antibodies	EDTA buffer (pH 8.0)	TBST (pH 7.4)	10% normal goat serum in TBST	10% normal goat serum in TBST	Prolong™ Gold Antifade Mountant
Pancreatic hormone antibodies	Sodium citrate buffer (pH 6.0)	PBS (pH 7.4)	20% FBS (Gibco) in PBS	0.05% FBS in PBS	Vectashield mounting medium with DAPI

Sodium citrate (Sigma, Belgium) buffer (2.94g sodium citrate in 1 litre of dH_2O, pH6) is often used for antibodies targeted at pancreatic hormones or transdifferentiation markers whereas EDTA (ThermoScientific) buffer (0.416g EDTA in 1 litre of dH_2O, pH8) is used for antibodies targeted at mitochondrial complexes. However, EDTA buffer is chosen when mitochondrial and pancreatic antibodies are stained at the same time. When the whole antigen retrieval process was finished, slides were then transfer to either TBST or PBS to cool down and hydrate. The protocol of making up 2L 1×TBST (pH 7.4) and 1L 1×PBS (pH 7.4) are listed in ***Table 2-6***.

Table 2-6. Protocols for making 1×TBST and 1×PBS.

1×TBST	1×PBS (phosphate buffer saline)
1.2g Trizma base (Sigma, USA)	Start with 800 ml of distilled water:
17g NaCl (Sigma, USA)	8 g of NaCl.
2 ml Tween 20 (Sigma, UK)	0.2 g of KCl.
	1.44 g of Na_2HPO_4.
	0.24 g of KH_2PO_4.
Add 1L distilled water	Adjust the pH to 7.4
Adjust the pH to 7.4	Add distilled water to a total volume of 1L

The sections were bordered by using a hydrophobic PAP pen (Vector Laboratory). Sections were incubated in 10% normal goat serum (Sigma) in TBST or 20% FBS (Gibco) in PBS for 1 hour at room temperature to avoid false-positive staining and the remaining serum was rinsed off using 1×TBST or 1×PBS. The samples were then incubated with primary antibody diluted in a volume of 100 µl either 10% normal goat serum in TBST or 0.05% FBS in PBS.

Primary antibodies used in our study are listed in ***Table 2-7***. Negative controls were incubated with according blank blocking buffer. After overnight incubation at 4°C or 1h incubation at room temperature in a dark and humidified box, slides were washed three times using washing buffer (1×TBST or 1×PBS) for 5 minute each wash. The tissue were then incubated with secondary antibodies (***Table 2-8***) diluted in a volume of 100 µl 10% normal goat serum in TBST or 0.05% FBS in PBS for 2 hours in the dark and followed by three 5-minute washes with washing buffer (1×TBST or 1×PBS). After the final wash, tissue which used for counting the endocrine cells and quantifying pancreatic hormones were incubated with DAPI nuclear marker (1:50000 in PBS) (Bio-Rad) for 15 minutes before the quick PBS wash. We mounted the slides using vectashield mounting medium with DAPI (4,6-diamidino-2-phenylindole) (Vector laboratories Ltd, UK). For tissue used for assessing mitochondrial OXPHOS function were incubated for another 2 hours with Streptavidin-conjugated tertiary antibody in the dark and followed by three 5-minute washes with washing buffer. Then they were mounted with Prolong™ Gold Antifade Mountant (Invitrogen, P36930, USA) directly after the final wash of tertiary antibodies. The optimized protocol for quantifying mitochondrial OXPHOS function is listed in ***Table 2-9***. Mitochondrial import receptor subunit Tomm20 can be used as a mitochondrial mass marker. Complex I (NADH dehydrogenase 1 beta subcomplex 8, NDUFB8) and Complex IV (Cytochrome c oxidase subunit I, MTCO1) are important parts of mitochondrial respiratory chain. Insulin can be regarded as a β-cell marker. By immunofluorescence detecting these antibodies, I can quantitatively calculate and compare the mitochondrial complex expression between *PolgA*$^{mut/mut}$ and wild type mice. Every time when I run the experiment, each donor was analyzed with a corresponding no primary antibody slide from the same donor in order to eliminate the effect of background signals. The protocol for counting the islet endocrinal cells and quantifying pancreatic hormones is listed in the ***Table 2-10***. To avoid drying of the mounting media, a coverslip was carefully and quickly applied to the sample immediately after adding mounting media and sealed with nail varnish. Then slides were left to dry in the dark, covered with foil and stored in a -20°C freezer until ready to be viewed by Nikon A1 confocal microscope. 50 islets were studied for each mouse. All the camera and microscope settings remain the same between mice and between

different batches of experiments. Follow up analysis will be further elaborated in result chapters.

Table 2-7. Information for primary antibodies used in our study.

Category	Primary Antibody	Species raised in	Clonality	Isotype	Confirmed specificity	Dilution	Supplier & catalogue number
Mitochondrial primary antibodies	Tomm20	Rabbit	monoclonal	IgG	Mouse, Rat, Human	1:100	Abcam ab186734
	MTCO1	Mouse	monoclonal	IgG2a	Mouse, Rat, Goat, Cow, Human	1:100	Abcam ab14705
	NDUFB8	Mouse	monoclonal	IgG1	Mouse, Rat, Cow, Human, Pig	1:100	Abcam ab110242
Pancreatic hormone primary antibodies	Insulin	Guinea pig	Polyclonal		Human, Mouse, Rat	1:200	DAKO IR00261-2
	Glucagon	Mouse	Monoclonal	IgG1	Rat, Pig, Guinea pig, Mouse, Canine, Human, Rabbit	1:200 (1:100 for human)	Sigma G2654
	Glucagon	Rabbit	Monoclonal	IgG	Mouse, Rat, Human	1:200	Abcam ab92517
	Ki67	Rabbit	Monoclonal	IgG	Human, Mouse, Rat	1:400	Cell signaling D3B5

Table 2-8. Information for secondary antibodies used in our study.

Category	Species raised in and isotype	Antibody against	Conjugation	Dilution	Supplier and catalogue number	Corresponding primary antibody
Mitochondrial secondary antibodies	Rabbit IgG	Goat	FITC	1:200	Invitrogen A11008	Tomm20
	Mouse IgG2a	Goat	TRITC	1:200	Invitrogen A21133	MTCO1
	Mouse IgG1	Goat	Biotin	1:200	Invitrogen A10519	NDUFB8
			Streptavidin Alexa 647	1:100	Invitrogen S32357	
Pancreatic hormone secondary antibodies	Guinea pig IgG	Goat	DAPI	1:200	Abcam ab175678	Insulin
	Guinea pig IgG	Goat	Alexa 647	1:250	Life Technologies A21450	Insulin
	Mouse IgG	Donkey	TRITC	1:250	Life Technologies A10037	Glucagon
	Rabbit IgG1	Goat	FITC	1:500	Invitrogen A11008	Ki67

Table 2-9. The optimized experimental procedure for quantifying mitochondrial OXPHOS function in pancreatic islets.

Primary antibody		Secondary antibody		Tertiary antibody	
Name	Dilution	Name	Dilution	Name	Dilution
Rabbit anti-Tomm20	1:100	Goat anti-rabbit IgG Alexa Fluor 488	1:200	NA	
Mouse anti-MTCO1	1:100	Goat anti-mouse IgG2a Alexa Fluor 546	1:200	NA	
Mouse anti-NDUFB8	1:100	Biotinylated goat anti-IgG1	1:200	Streptavidin-conjugated Alexa Fluor 647	1:100
Guinea pig anti-insulin	1:200	Goat anti-guinea pig Alexa Fluor 405	1:250	NA	

Table 2-10. The optimized experimental procedure for counting islet endocrinal cell and quantifying pancreatic hormone.

Primary antibody		Secondary antibody		Tertiary antibody		DAPI
Name	Dilution	Name	Dilution	Name	Dilution	
Guinea pig anti-insulin	1:200	Goat anti-guinea pig Alexa Fluor 647	1:250	NA		
Mouse anti-glucagon	1:200 (1:100 for human)	Donkey anti-mouse Alexa Fluor 546	1:250	NA		1:50000 in PBS
Rabbit anti-urocortin3	1:500	Poly-HRP-conjugated 1×goat anti-rabbit IgG secondary		Alexa Fluor 488 tyramide reagent	1:100	
Rabbit anti-Ki67	1:400	Goat anti-rabbit Alexa Fluor 488	1:500	NA		

2.3.2.2. Frozen sections.

After sections were taken out of the freezer, they were dried at normal temperature for 1 hour at a hygienic and dark area. For each section, 100 µl of 4% cold paraformaldehyde (PFA) solution in PBS (TissuePro) was applied and incubated for 5 minutes to preserve and fix tissue for immunofluorescence staining later (PFA is a formaldehyde releasing agent and has potentially carcinogenic effect. Applying and incubating under laboratory hood is necessary). Three 5-minute washes using PBS were followed by the PFA incubation. Slides went through a series of methanol gradients from 70%, 95%, 100%, 100%, 95% to 70%. I put slides in each methanol gradient for 10 minutes and finally washed with PBS for 3 times. Tissues were incubated with 10% normal goat serum in PBS for 1 hour. After three times of PBS washes, primary antibodies were applied overnight at 4°C or 90 minutes at room temperature in a humidified and dark box. Laser dissection would be performed on the frozen stained tissue to cut off islets for mtDNA copy number quantification, so the identification and location of islets on the pancreas section is important. As a result, the primary antibody we chose was glucagon because it marked the alpha cells located on the outside of the islets. After three 5-minute PBS washes after the overnight primary antibody incubation, secondary antibody diluted in 10% normal goat serum was applied for 2 hours in a humidified and dark box. If the nuclei were needed to be stained, the tissue needed to be incubated for 15 minutes with hoechst diluted in 1:400 in 10% normal goat serum. After three 5-minute PBS washes, slides were stored at -20°C freezer to preserve fluorescence and wait for following laser dissection microscopy.

2.3.3. Imaging

Imaging was performed using a Nikon A1 confocal microscope at 20 × optical magnification, using 4 channels such as DAPI, FITC, TRITC and Alexa 647, detecting wavelength at 405 nm, 488 nm, 546 nm and 647 nm. For mitochondrial staining, insulin, Tomm20, MTCO1 and NDUFB8 stains were excited under Alexa fluor 405, Alexa fluor 488, Alexa fluor 546 and Alexa fluor 647 filters separately. Wild type mice sections with primary antibodies were used to calibrate laser power settings in each of the 4 channels which can be further applied to mutant

mice sections. By adjusting z-axis of the object stage, I could find out the brightest scan surface of the tissue. I set up optimal confocal camera setting (High voltage, offset and laser power) based on the brightest surface can avoid under or over pixel saturation in the whole tissue. Besides, the corresponding no primary antibody slides were used to calculate non-specific background fluorescence in order to remove the effect of background staining. After the optimal camera laser power setting was done, this was then maintained across all mice cases, and across experiments. In order to achieve more accurate and consistent results, 50 different islets per case in mice sections were captured for mitochondrial staining whereas 25 islets per case were captured for cell composition study. For human samples, again 50 islets per case were captured for mitochondrial staining whereas 25 islets were captured for cell composition staining.

2.3.4. Image analysis

Two main analysis processes were done on mouse and human stained tissue in this study. They are signal intensity analysis (mitochondrial complex expression analysis and insulin expression analysis) and islet cell counting.

2.3.4.1. Mitochondrial complex expression analysis within islets

Because all the images were taken by the same camera settings between mouse and human cases and between different batches of experiments, the comparison of staining signal intensity can be done directly by image analysis. Image analysis software (NIS-Element viewer) was used to detect islets and areas within islets that were positive for the insulin (DAPI, 405 nm), mitochondrial mass marker Tomm20 (FITC, Alexa fluor 488 nm), MTCO1 (TRITC, Alexa fluor 546 nm) and NDUFB8 (Alexa fluor 647, Alexa fluor 647 nm). 50 islets were studied for each case. Tomm20 staining exists in the whole islet area and the staining intensity is different from the exocrine tissue. By drawing the region of interest (ROI) around the whole islet area based on the Tomm20 staining, the average signals intensity values within individual islet from all three mitochondrial channels were calculated and generated from the Nikon.

2.3.4.2. Expression of insulin secretion analysis within β cells.

In the quadruple immunofluorescence staining, apart from the Tomm20, MTCO1 and NDUFB8 staining signals, we also analyze the insulin staining signal intensity in order to understand insulin secretion function of β-cells in *PolgA*$^{mut/mut}$ and wild type mice. I used two different methods to compare, the first method is to directly compare insulin signal intensity and second method is to compare insulin signal intensity normalized by Tomm20 signal intensity. The only difference compared to the mitochondrial signal analysis is that the insulin signal intensity area is analyzed based on islet β-cell area instead of whole islet area. By drawing the region of interest (ROI) around the β-cell area based on insulin staining, the average signal intensity values of insulin and Tomm20 from β-cell area were calculated and generated from the Nikon. This is a novel method of comparing insulin secreting function but it needs to be validated by functional test such as insulin secretion ELISA test.

2.3.4.3. Mitochondrial complex expression analysis within different islet endocrine cell types.

In order to study the impact of ageing on different endocrine cell types, I separately analyzed the mitochondrial complex expression in α and β cell types.

Step 1: β-cell validation

I compared the mathematical method with the gold standard machine method.

- The gold standard method is to draw the region of interest (ROI) around the β-cell area based on insulin staining (as we stated in chapter 2.3.4.2), the mean signal intensity values of insulin (Alexa fluor 405mm), Tomm20 (Alexa fluor 488mm), MTCO1 (Alexa fluor 546mm) and NDUFB8 (Alexa fluor 647mm) can be generated from β-cell area by the Nikon image analysis software (NIS-element).
- The mathematical method is based upon the general principle (Mean SI: Mean signal intensity; Sum SI: Summary signal intensity):

  Mean SI = $\frac{sum\ SI\ in\ ROI}{size\ of\ ROI}$.

- The mathematical method has to be validated after identifying pixel correction factor. In NIS element, pixel size is 2.67.
- The equations of mathematical method in β-cells

Mean SI of Tomm20 in β-cells = $\frac{Sum\ SI\ of\ Tomm20\ in\ \beta-cell\ area}{Size\ of\ \beta-cell\ area \times Pixel\ size\ (2.67)}$

Mean SI of MTCO1 in β-cells = $\frac{Sum\ SI\ of\ MTCO1\ in\ \beta-cell\ area}{Size\ of\ \beta-cell\ area \times Pixel\ size\ (2.67)}$

Mean SI of NDUFB8 in β-cells = $\frac{Sum\ SI\ of\ NDUFB8\ in\ \beta-cell\ area}{Size\ of\ \beta-\ cell\ area \times Pixel\ size\ (2.67)}$

Step 2: α-cell validation

It's more difficult to calculate the signal intensity within α-cells because I didn't stain the islets with glucagon. I compared the mathematical method with the gold standard draw around method.

- The gold-standard draw around method is to trace between the borders of whole islets and β-cell area and form a ROI. Then Tomm20 (Alexa fluor 488), MTCO1 (Alexa fluor 546) and NDUFB8 (Alexa fluor 647) can be generated from β-cell area by the Nikon image analysis software (NIS-element).
- The equations I used here are listed below (Mean SI: mean signal intensity; Sum SI: summary signal intensity).

Mean SI of Tomm20 in α-cells = $\frac{(Sum\ SI\ of\ Tomm20\ in\ whole\ islet - Sum\ SI\ of\ Tomm20\ in\ \beta-cell\ area\ )}{(Size\ of\ whole\ islet - size\ of\ \beta-cell\ area) \times Pixel\ size\ (2.67)}$

Mean SI of MTCO1 in α-cells = $\frac{(Sum\ SI\ of\ MTCO1\ in\ whole\ islet\ - Sum\ SI\ of\ MTCO1\ in\ \beta-cell\ area\ )}{(Size\ of\ whole\ islet - size\ of\ \beta-cell\ area) \times Pixel\ size\ (2.67)}$

Mean SI of NDUFB8 in α-cells = $\frac{(Sum\ SI\ of\ NDUFB8\ in\ whole\ islet - Sum\ SI\ of\ NDUFB8\ in\ \beta-cell\ area)}{(Size\ of\ whole\ islet - size\ of\ \beta-cell\ area) \times Pixel\ size\ (2.67)}$

I analzyed 10 islets from the same *PolgA*$^{mut/mut}$ mouse by using mathematical method and draw around method (P-D). Mathematical method (P-M) validated against draw around method (P-D) based on correlation and paired t-test analyses (***Figure 2-2*** and ***Figure 2-3***).

In conclusion, the mathematical method replicated the machine generated measurements and was strongly correlated with the draw around measurements for the β-cell and α-cell mitochondrial subunit expression measurements, respectively.

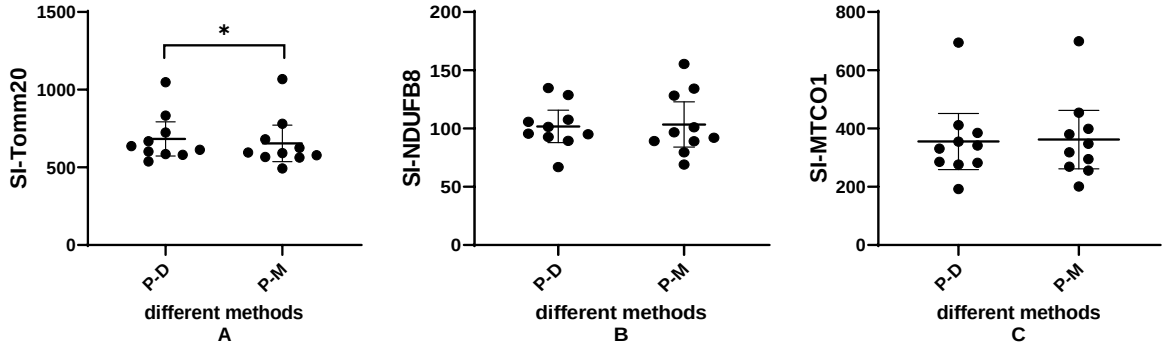

Figure 2-2. The comparison in signal intensity between mathematical and draw around methods (SI: signal intensity; P-M: mathematical method; P-D: draw around method). (**A) The comparison in SI-Tomm20.** Paired t-test: P<0.05. **(B) The comparison in SI-NDUFB8.** Paired t-test: P>0.05. **(C) The comparison in SI-MTCO1.** Paired t-test: P>0.05.

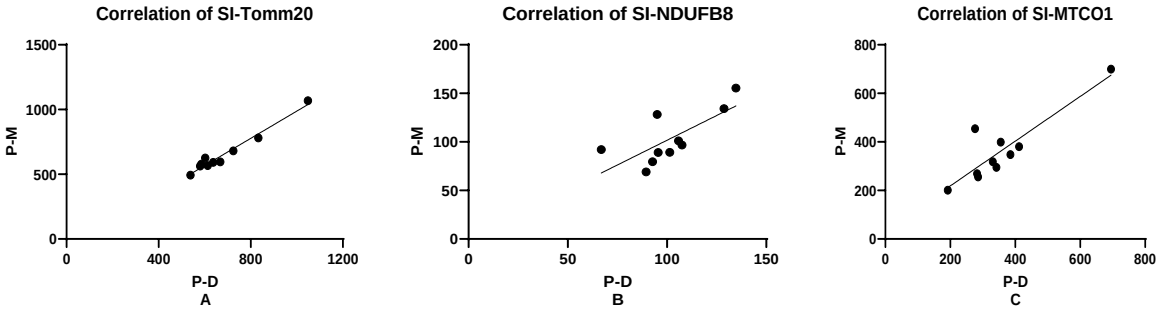

Figure 2-3. The Pearson correlation analysis for mathematical and draw around methods (SI: signal intensity; P-M: mathematical method; P-D: draw around method). **(A) Correlation of SI-Tomm20 between P-M and P-D.** Y = 1.052*X - 64.34. P<0.0001. **(B) Correlation of SI-NDUFB8 between P-M and P-D.** Y = 1.018*X - 0.1650. P<0.05. **(C) Correlation of SI-MTCO1 between P-M and P-D.** Y = 0.9211*X + 34.49. P<0.01.

2.3.4.4. Islet cell composition analysis

In order to study the islet cell composition, triple immunofluorescence staining was applied to mice and human islets. Again, NIKON image analysis software (NIS-Element viewer) was used to detect islets which are positive for nucleus (DAPI, 405nm), glucagon (TRITC, 568nm) and Insulin (Alexa fluor 647, 647nm). α-cell number was counted in islets of mouse and human cases by overlapping nucleus and glucagon channels. β-cell number was counted by overlapping nucleus and insulin channels. Because α- and β-cell number take up more than 90% of the islet total endocrine cell number, the whole islet cell number can be roughly calculated by adding α- and β- cell number together. α- and β- cell percentage were calculated by dividing absolute α- and β- cell number by the whole islet cell number, respectively. By drawing around a region of interest (ROI) based on the pheripheral side of islets, I can calculate the islet size. β/α ratio can be calculated by dividing absolute β-cell number by absolute α-cell number. 25 islets were studied per case.

2.3.4.5. Islet cell proliferation analysis.

In order to study the islet cell proliferation in mice, quadruple immunofluorescence staining was applied to mice islets. Again, NIKON image analysis software was used to detect islets which are positive for nucleus (DAPI, 405nm), Ki67 (FITC, 488nm), glucagon (TRITC, 568nm) and Insulin (Alexa fluor 647, 647nm). I stained and calculated at least 40 islets for each mouse case. I calculated the number of Ki67 (+) islets and divided it by the number of all islets in each case and generated a ratio of Ki67 (+) islet. The distribution of Ki67 (+) stained nuclei differs between different mouse genotypes. I further calculated the number of islets with Ki67 (+) α-cells and Ki67 (+) β-cells and divided them by the number of all islets in each case, generating a ratio of islets with Ki67 (+) stained α-cells and a ratio of islets with Ki67 (+) β-cells.

2.3.5. Data analysis

By using the Nikon software, the average signal intensity (SI) are calculated and automatically measured in each islet from pancreas section with primary antibodies (SI-Tomm20, SI-MTCO1 and SI-NDUFB8). The average background intensities (BI) of no primary antibody control (BI-

Tomm20, BI-MTCO1 and BI-NDUFB8) were measured to determine the levels of non-specific fluorescence. For each islet, SI-Tomm20, SI-MTCO1 and SI-NDUFB8 were corrected for background signals by subtracting the mean BI-Tomm20, BI-MTCO1 and BI-NDUFB8 of the no primary control respectively. Both corrected SI-MTCO1 and SI-NDUFB8 were normalized by corrected SI-Tomm20 and log transformed in the OXPHOS quadruple immunofluorescence analysis tool. This analysis tool was developed and optimized by Wellcome Trust Mitochondrial Research Group and website for this analysis tool is https://research.ncl.ac.uk/mitoresearch/. This analysis tool will generate a Z-score excel datasheet for Tomm20, MTCO1 and NDUFB8.

2.3.5.1. Densitometry test for 3-month *PolgA$^{mut/mut}$* and wild type mice

The signal intensity values of Tomm20, MTCO1 and NDUFB8 from 3-month old mice islets were imported into an OXPHOS quadruple immunofluorescence z-score analysis software. By analysing z-score excel datasheet generated from 3-month mice data, a densitometry test can be formed by putting z-score of Tomm20, MTCO1 and NDUFB8 from wild type mice together (***Figure 2-3***). It can be found out that most of the wild type islet z-scores (all Tomm20, MTCO1 and NDUFB8) fall within the range of -2 to 2 and almost all the wild type z-scores are located between -2.5 to 2.5. As a result, a wild type mice z-score range of -2 to 2 was set up as a reference for 3-month mice. By comparing *PolgA$^{mut/mut}$* z-score to wild type z-score reference, the changes of mitochondrial complex expression in islets of 3-month *PolgA$^{mut/mut}$* can be accurately quantified. It was shown in ***Figure 2-3*** that a significant down-shift of complex I expression is shown in 3-month *PolgA$^{mut/mut}$* sedentary mice compared to the wild type mice, but the complex IV expression doesn't have difference between these two groups.

2.3.5.2. Densitometry test for 11-month *PolgA$^{mut/mut}$* and wild type mice

The signal intensity values of Tomm20, MTCO1 and NDUFB8 from 11-month old mice islets were imported into an OXPHOS quadruple immunofluorescence z-score analysis software. A densitometry test can be formed by putting z-score of z-Tomm20, z-MTCO1 and z-NDUFB8 from WT mice together (***Figure 2-4***). Again, a wild type mice z-score range of -2 to 2 was set up as a reference for 11-month-old mice. By comparing *PolgA$^{mut/mut}$* z-score to wild type z-score reference, the changes of mitochondrial complex expression in islets of 11-month-old *PolgA$^{mut/mut}$* mice can be accurately quantified. A down-shift of complex I expression is shown in both *PolgA$^{mut/mut}$* exercise and sedentary mice compared to the wild type mice. However, there is a surprising right-shift of complex IV expression in *PolgA$^{mut/mut}$* mice (***Figure 2-4***).

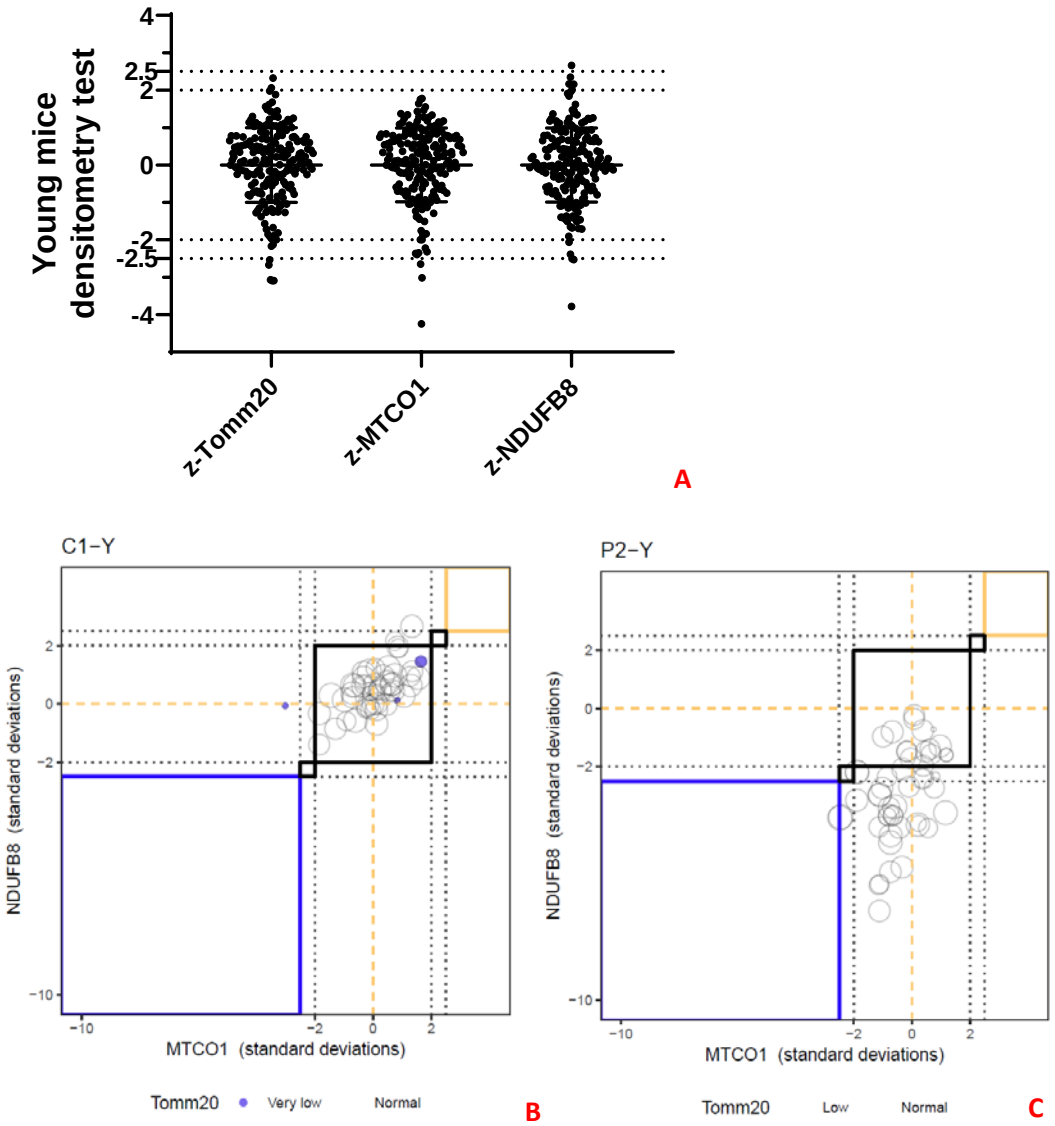

Figure 2-4. The desitometric analysis and z-score result of 3-month old mice. (A) The densitometric analysis of each fluorophore at single islet level from 3-month wild type mice. Five level of protein expression were categorized based on the Z-score in wild type islets. The standard deviation value was defined that over 2.5 as very high, 2 to 2.5 as high, -2 to 2 as normal, -2.5 to -2 as low and below -2.5 as very low. **(B-C) The mice Z-score result graph created by MRG OXPHOS quadruple immunofluorescence analysis software for mice sacrificed at 3 months.** (B) wild type 1622; (C) *PolgA*$^{mut/mut}$ 1709.

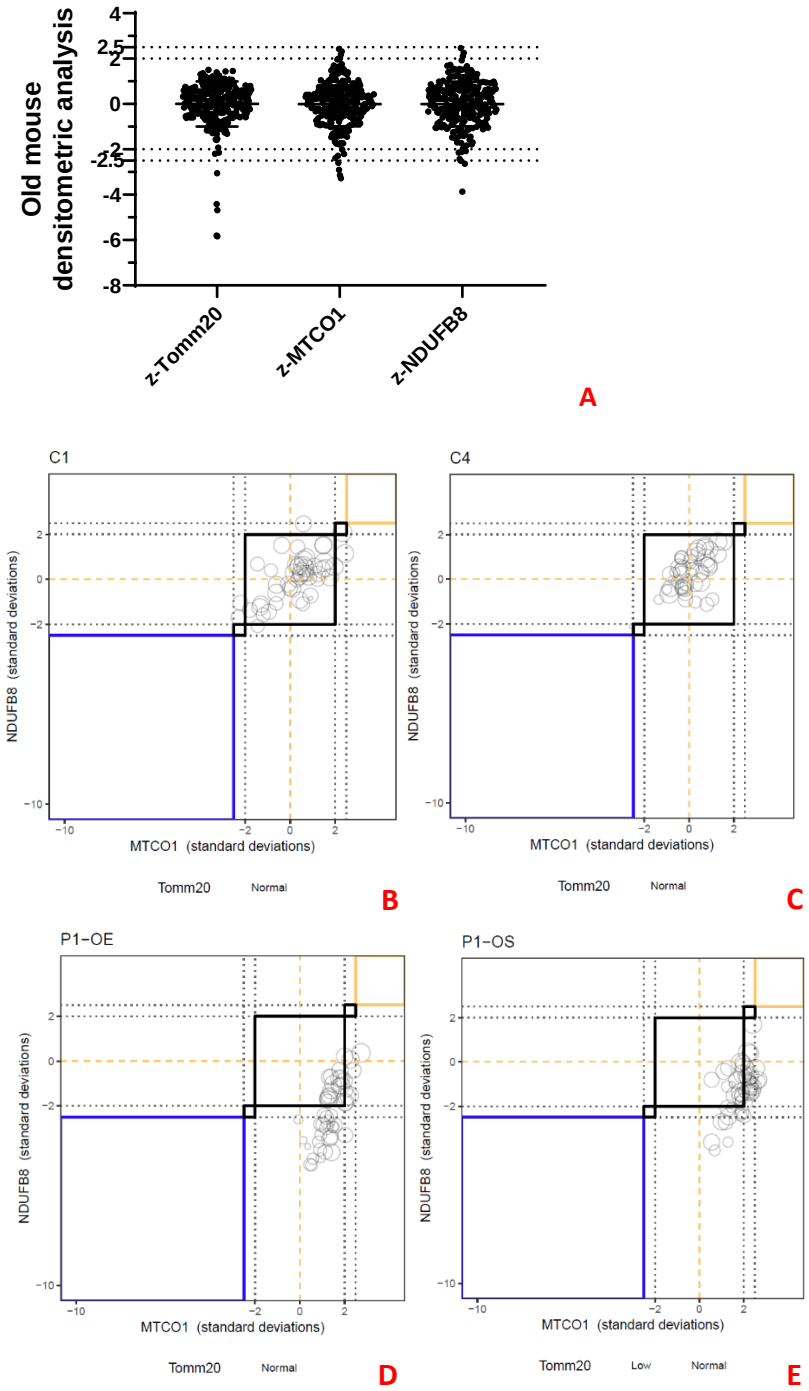

Figure 2-5. The densitometry analysis and z-score result of 11-month old mice. (A) The densitometric analysis of each fluorophore at single islet level from 11-month wild type mice. Five level of protein expression were categorized based on the Z-score in wild type islets. The standard deviation value was defined that over 2.5 as very high, 2 to 2.5 as high, -2 to 2 as normal, -2.5 to -2 as very low and below -2.5 as very low. **(B-D) The 11 month sacrificed mice Z-score result graph created by MRG OXPHOS quadruple immunofluorescence analysis software.** (B) wild type GA0002; (C) wild type GA0007; (D) *PolgA*$^{mut/mut}$ exercise LG0005 (E) *PolgA*$^{mut/mut}$ sedentary LG0002.

2.4. Laser dissection microscopy

2.4.1. Preparation

Before starting the actual experiment, I used 70% ethanol to wipe the table, pipettes and UV hood and autoclaved 1ml water, some 200 µl and 500 µl tubes. A clean lab coat was specifically prepared for laser dissection experiment. 1ml water, one 500 µl tube, one aliquot of sterilized Tris-HCl and one aliquot of Tween 20 were put into the UV hood for 30 minutes. After the UV sterilization, single cell lysis buffer (Protocol is listed in ***Table 2-11***) was made in the clean PCR hood. The use of proteinase K (ThermoFisher Scientific) is to digest protein and remove contamination from nucleic acid preparation because it can rapidly inactivate nucleases that might otherwise degrade the DNA or RNA during purification. Tris-HCl and Tween 20 were also used (Trizma base: Sigma; HCl: VMR; Tween 20: Sigma) to make up the single cell lysis buffer.

Table 2-11. The single cell lysis buffer protocol.

Ingredient	Amount needed per one unit	Amount needed for 50 units
Tris HCL	10	500
Tween 20	50	2500
dH_20	38	1900
Proteinase K	1	50
Whole volume	99µl	4950µl

Frozen stained tissue was taken from -20°C freezer and went through 75%, 95%, 100% and 100% ethanol gradients and stayed in each gradient for 10 minutes. After the ethanol dehydration, slides were put in an air-dry lab hood for at least 1 hour for a complete dry out.

2.4.2. Laser dissection

Wiped the pipette, keyboard, desk and laser dissection microscope platform with disinfect spray (Starlab, TM328, UK). Put dried and stained slide on the microscope platform and scan the tissue from top-left to the bottom-right under the TRITC immunofluorescence laser channel to get a general mapping area of the tissue. Because islets on the pancreas tissue were stained with glucagon, they are very easy to identify from the background. A blank tissue

area was chosen to calibrate the laser energy and focus. Once the most suitable laser energy and focus were set up, it should be remained the same between cases and experiments.

Put 10µl lysis buffer into the cap of the 200µl Eppendorf tube and put tubes onto the collector. Islets were found by targeting glucagon staining on the tissue under the 20× microscope magnification and cut off by laser power which set up previously. After laser dissection, one islet was flicked into the cap of one 200µl tube on the collector. Once islets were collected into the tubes, they were taken off from the collector and put downsided onto the ice for temporary storage. 10 islets for each mouse case (wild type GA0007 and GA0008; *PolgA*$^{mut/mut}$ LG0002 and LG0011) were dissected and processed with lysis buffer.

A quick centrifuge is needed to bring all the liquid down to the tube bottom from the cap. In our lab, 15800 rcf for 2min is used on the centrifuge machine (Eppendorf). Then they were put into the PCR machine (Applied Biosystems) to run the protocol (55°C 1h × 3 times----95°C 10 min---- 4 °C ∞). On the next day, samples were collected from the machine and put into the -20°C freezer for storage and 30 µl sterile dH_2O was added into each sample.

2.5. Real time PCR

Real-time PCR (RT-PCR) is also called quantitative PCR or qPCR. The DNA amplification is detected by the use of fluorescence reporter in real time as the progress of PCR. In other words, the signal strength of fluorescence can reflect the number of amplified DNA molecules, which is also the key feature of real time PCR (Jia 2012). There are two detection methods of RT-PCR, the first one is based on sequence-specific probe such as TaqMan probe; the second is based on generic non-sequence-specific double-stranded DNA-binding dye such as SYBR green. RT-PCR is a very sensitive and powerful DNA analysis tool. RT-PCR can be divided into four stages: linear ground phase, early exponential phase, linear exponential phase (log phase) and plateau phase. In our study, I used SYBR green fluorescence dye. The principle of SYBR Green is that the fluorescence of SYBR dyes increases by 20 to 100-fold when they bind to double-stranded DNA and also SYBRE green fluorescence signal can proportionally and

correspondingly increase as the amount of double-stranded DNA increases during PCR process.

Real time PCR can be quantified in absolute quantification or in relative quantification. The determination of mtDNA copy number is usually done by absolute quantification by serially diluting samples of known concentrations to create a standard curve. For relative quantification, changes in sample quantity are measured based on a reference sample, the results are usually expressed as a target/reference ratio. In the interest of the mitochondrial DNA copy number assay, it was thought that relative quantification would be better, simply because of the vast number of samples to be processed. Relative quantification can be done in two ways which are standard curve method and comparative Ct ($2^{-\Delta\Delta Ct}$) method. In my studies, I started with standard curves serially diluted in 1:10 which were amplified for both the target and reference genes to test the reaction efficiency. Then I used both analysis methods (standard curve and comparative Ct) to compare the difference in mtDNA copy number between groups.

2.5.1. DNA extraction

I defrosted one wild type mouse pancreas from the -80°C freezer on ice. After adding in 10 units of lysis buffer (protocol is in ***Table 2-11***) to make sample immersed in the buffer, I grinded it completely with a small sterilized stick. The tube was placed onto the thermomixer (Applied Biosystems) at 55°C, 300 rpm for an overnight incubation. On the next day, the sample tube was taken away from the thermomixer and heat up in the hot plate machine (Techne) at 90°C for 10 min. Aliquot the wild type mouse pancreas DNA sample into 10 µl per tube and stored them in the -20°C freezer.

2.5.2. Make up standard curve

2.5.2.1. Preparation

Autoclaved dH_2O and some 1.5ml tubes. Defrosted one 10 µl aliquot mouse pancreas DNA sample (collected in step 2.6.1) on the ice and test DNA concentration by using the Nanodrop spectrophotometer. By using the equation below, I can work out how much water should be

added into the sample to make up 50 µl DNA sample with a starting concentration of 1000 ng/µl.

$1000\ ng/\mu l \times 50 = \text{test concentration} \times X_{(DNA)}$ $\quad X_{(DNA)} = \dfrac{1000 \times 50}{\text{Test concentration}}$

$X(water) = 50 - X_{(DNA)}$

2.5.2.2. Samples in serial dilutions

The second sample was made up by adding 10 µl DNA from the first DNA sample (1000 ng/µl concentration) and 90 µl dH_2O. Mix the sample well by repeated pipetting and doing vortex. In this way, a series of eight 1 in 10 dilutions of wild type control DNA samples were made up with the concentrations of 1000, 100, 10, 1, 0.1, 0.01ng/µl and standard curves were prepared using these samples. The concentration from 100 to 0.01 ng/µl were more often used for RT-PCR analysis.

2.5.3. Loading samples and real time PCR

2.5.3.1. Making up mastermix

MtDNA copy number level was detected by using the mtDNA copy number assay, which was optimized by Dr. Laura Greaves (Mitochondrial Research Group, Newcastle University). ND5 (NADH dehydrogenase 5) is a mtDNA encoded subunit of Complex I (NADH Dehydrogenase). The ND5 gene is situated on the heavy strand of mtDNA and is approximately 1.8 kb in length, producing a protein of 607 amino acids in length. B-actin (B2M) also known as β2 microglobulin and this gene encodes a serum protein found on the surface of nearly all nucleated cells because it is in association with the major histocompatibility complex (MHC) class I heavy chain (Güssow, Rein et al. 1987). The sequences for ND5 and β-actin forward and reverse primers were detailed in ***Table 2-12***. After DNA was extracted from islet samples, real-time PCR reaction was set up using a LightCycler 480 detector.

For each reaction, 10 µl Platinum SYBR Green qPCR SuperMix-UDG (Invitrogen, Cat. No. 11733-038), 0.6 µl forward primer (10 µM) (Eurofin), 0.6 µl reverse primer (10 µM), 3 µl dH_2O and 5 µl DNA sample are needed. Primers for mitochondrial gene NADH Dehydrogenase 5 (ND5) were used to quantify mitochondrial DNA copy number and were normalized by housekeeping gene β-actin. A 20µl sample containing 15 µl mastermix and 5 µl DNA samples (from standard curve samples achieved in step 2.5.2.2 and laser-dissected islet DNA samples achieved in step 2.4.2) were loaded in triplicate into a 96-well RT-PCR plate and the loaded plate was briefly vortexed and centrifuged. Forward and reverse primers were diluted in TE buffer.

Table 2-12. The sequences for ND5 and β-actin forward and reverse primers.

<table>
<tr><td rowspan="2">Gene product</td><td rowspan="2">Transcript Genbank accession number</td><td rowspan="2">Primer sequence</td><td colspan="3">Cycling parameters</td></tr>
<tr><td>Procedure</td><td>Temperature</td><td>Time</td></tr>
<tr><td rowspan="3">ND5</td><td rowspan="3">NC_005089.1</td><td>Forward: CCACGCATTCTTCAAAGC (22)</td><td>Denaturation</td><td>95°C</td><td>10 min</td></tr>
<tr><td rowspan="2">Reverse:
TCGGATGTCTTGTTCGTC (20)</td><td rowspan="2">Extension (40 cycles)</td><td>95°C</td><td>15s</td></tr>
<tr><td>60°C</td><td>1 min</td></tr>
<tr><td rowspan="2">B-actin</td><td rowspan="2">NC_000071.6</td><td>Forward: CCATCTTGTCTTGCTTTCTTCA (20)</td><td colspan="3">Melting curve analysis</td></tr>
<tr><td>Reverse: CCACCGATCCACACAGAGTA(20)</td><td colspan="3">Final hold at 4°C</td></tr>
</table>

2.5.3.2. Real time PCR

Real time PCR was carried out in the StepOnePlus Real-time PCR system (Applied Biosystems) using the cycling conditions: 10-minute initial denaturation at 95°C followed by 40 cycles of 95°C for 15s and 60°C for 1 minute. The cycling condition was ended with a melting curve analysis.

2.5.4. After PCR analysis

2.5.4.1. Standard curve analysis method

The Ct value for each sample on the Y-axis versus the corresponding concentration on the X-axis can form a standard curve. ND5 and β-actin standard curve equations can be generated separately. The concentrations of mouse pancreas dissected islets can be calculated by interpolating the Ct values into the standard curve. Later, I normalized the islet concentrations achieved from ND5 standard curve by islet concentrations achieved from β-actin standard curve. Finally, I compared the normalized value of dissected islet concentrations between wild type and *PolgA*$^{mut/mut}$ mice.

2.5.4.2. △Ct analysis method

△Ct was generated by subtracting ND5 Ct values of islets by β-actin Ct values. MtDNA copy number of wild type and *PolgA*$^{mut/mut}$ islets were generated by calculating 2*(2^(-△Ct)).

2.6. Blood glucose testing

Another 5 wild type and 5 *PolgA*$^{mut/mut}$ mice were recruited for this part of study. The information of mice used for blood glucose measurement is in the ***Table 2-13***. After wiping the tip of the mice tail with 70% ethanol, I used a fine disposable sterile needle to perform a tiny puncture at the tip of the tail. After squeezing out the first blood drop, the second fresh blood drop was placed on test strips, I used Alphatrak glucometer (Abbott Laboratories) to determine the glucose content and make notes about the readings. The blood glucose levels were measured between 1pm to 3pm, when mice were not fasted. This monthly blood glucose measurement started from March 2019 and stopped in September 2019. When these mice reached 11 months of age, they were sacrificed, and their endpoint blood samples were collected (further elaborated in the next method). Apart from blood glucose measurement, I also measured mice body weight monthly.

Carla Bradshaw (Mitochondrial Research Group, Newcastle University) kindly helped me with all the monthly blood glucose measurement.

Table 2-13. The information of mice used for blood glucose measurement and blood sample collection.

Mouse	Sex	Genotype	Date of birth
1909	F	HOM	12/06/2018
1918	M	HOM	03/07/2018
1923	F	HOM	03/07/2018
1937	M	HOM	26/07/2018
1940	F	HOM	26/07/2018
1967	M	WT	04/09/2018
1997	M	WT	26/09/2018
1999	M	WT	26/09/2018
2029	F	WT	01/11/2018
2034	M	WT	01/11/2018

2.7. HbA1c ELISA testing in mouse blood

2.7.1. Preparation of EDTA anticoagulant

Ethylenediaminetetraacetic acid dipotassium salt dehydrate (K_2 EDTA) was used in our study (BDH laboratory supplies, England) as an anticoagulant. The optimal anticoagulant concentration is 1.5 mg per ml of blood. In order to make up 10% EDTA, 10g EDTA is dissolved in 100 ml of distilled water.

2.7.2. Mouse blood collection

When these 10 mice reached 11-month of age, they were sacrificed and an average of 1-2ml whole blood can be collected from each mouse at endpoint. 30 µl 10% EDTA solution is prepared for every 2ml of mouse blood and is stored in 2ml Eppendorf tube. Vortexed the tubes intensely so EDTA can be evenly coated inside the tubes. A 1000ml pipette was used in collecting mouse blood and I rinsed the 1000 ml tip with EDTA solution that had been made up before. After cutting the mouse skin on the abdomen, I immediately collected mouse blood and inject into the EDTA coated tube and mixed the blood with EDTA thoroughly by gentle inversion. Mouse whole blood was stored in the -80°C freezer. Carla Bradshaw (Mitochondrial Research Group, Newcastle University) kindly offered me help for raising, catching and sacrificing mice. Divided 2ml blood into two 1.5ml Eppendorf tubes.

2.7.3. Mouse Haemoglobin A1c testing

2.7.3.1. Preparation of reagents, samples, calibrators and controls

When blood glucose level increases, glucose will be glycosylated haemoglobin in the red blood cells, also known as HbA1c. The average life span for red blood cell is around 8 ~12 weeks. By measuring the level of HbA1c it will give out information about how blood glucose level has been managed in the past two to three months. For quantitatively determination of haemoglobin A1c (HbA1c) in mouse whole blood, an Elisa kit was used in our study (Crystal Chem, Cat 80310, USA). All the reagents provided in this kit need to be brought to room temperature for at least 30 minutes prior to use. For the calibrators, controls provided by the kit, they were reconstituted by adding 0.5 ml distilled water and stayed at room temperature for 30 minutes before use. Whole blood sample should be taken out from -80°C freezer and defrosted on ice. Prior to testing, all the blood samples, calibrators and controls should be thoroughly mixed by gentle inversion. Especially for whole blood samples, they should be mixed at least 5 times to resuspend the settled erythrocytes and achieve the most accurate result of the assay.

2.7.3.2. Preparation of lysate

Dispensed 62.5 µl of lysis buffer provided by the kit into a 1.5 ml Eppendorf tube. Added in 5 µl fully resuspended whole blood or calibrator or control sample into the tube and mixed gently with pipette without creating foam. Vortexed the mixture and incubated at room temperature (25°C) for 10 minutes to lyse the red blood cells until the mixture became a clear dark red solution without any particles.

2.7.3.3. Preparation of the assay

A microplate and a microplate reader (ThermoFisher) were used in this procedure. 112 µl of reagent CC1a and 48 µl of reagent CC1b were added into each well of the microplate. Each sample, calibrator and control was tested in duplicate and mixed well by repeated pipetting (***Figure 2-7***). It's better to mix without creating bubbles because it will affect the accuracy of plate reading. 25µl lysate of sample, calibrator or control was added into each well and mixed by repeated pipetting. The microplate absorbance was incubated at 37°C for 5 minutes before

it was read by a Multiskan Spectrum (Thermo labsystems) at A700 wavelength. 70 µl reagent CC2 was added into each well and mixed by repeated pipetting. The microplate absorbance was read again after 3 minute incubation at 37°C using Multiskan Spectrum at A700 wavelength (***Figure 2-8***).

2.7.3.4. Determining the HbA1c concentration

Use the equation below to calculate the change in absorbance ΔA (5 min ~ 8 min). After calculating the absorbance for each calibrator, the absorbance value for each calibrator on the Y-axis versus the corresponding HbA1c concentration on the X-axis can form a calibration curve. And the mouse whole blood HbA1c concentration can be calculated by interpolating the absorbance values into the calibration curve.

$\Delta A = (OD_{700nm,\ 8min}) - [(OD_{700nm,\ 5min}) \times (185/255)]$

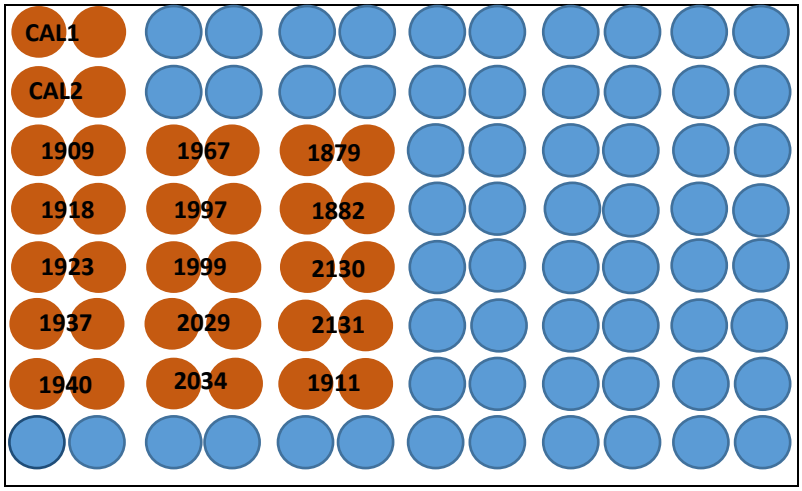

Figure 2-6. 96 well plate layout for HbA1c measurement.

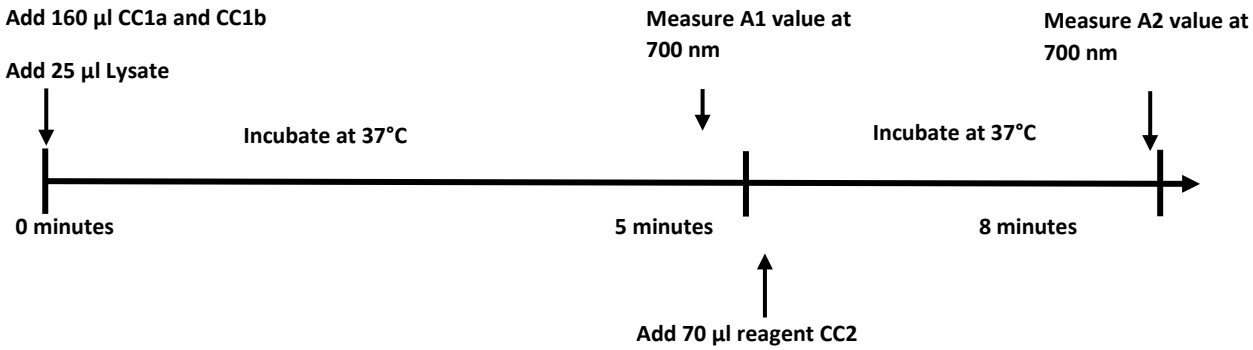

Figure 2-7. Summary of mouse hemoglobin A1C assay procedure.

CHAPTER 3. IMPACT OF AGEING ON MITOCHONDRIAL RESPIRATORY CHAIN EXPRESSION BY COMPARING PANCREATIC ISLETS FROM *POLGA*$^{MUT/MUT}$ AND WILD TYPE MICE.

3.1 Introduction

Ageing and mitochondrial dysfunction.

Ageing is characterized as a time-dependent loss of an organism's physiological function and increased vulnerability to death. Mitochondria are important in the ageing process because they consume almost 90% of oxygen that is taken in by aerobic cells thus they become the principal source of ROS (Maechler and Wollheim 2001, Sanz 2017). Complex I and III are the major ROS generators in mitochondrial OXPHOS. Normally, only 0.1% of total oxygen consumption leaks to ROS generation, but this number is higher in the ageing tissue (Beckman and Ames 1998). The cellular oxidative damage caused by ROS is not only on macromolecules but also in cell signaling, especially when the level of ROS has exceeded the capacity of the antioxidant enzymatic defenses (for example, catalase and superoxide dismutase). The reason why β-cells are particularly susceptible to ROS action is due to the low expression of these protective enzymes (Maechler, Jornot et al. 1999). ROS generation is closely linked to ageing and ageing-related diseases. Endurance exercise and N-acetyl cysteine treatment can decrease mitochondrial superoxide generation and delay the onset of ageing (Logan, Shabalina et al. 2014).

It was first proposed by Harman in 1972 that the mitochondrion is the biological clock of ageing in humans. The age-related cumulative mtDNA mutations and deletions can cause mitochondrial OXPHOS dysfunction because mitochondrial respiratory chain complexes are mostly encoded by mtDNA. Most pathogenic mtDNA mutations have to exceed a threshold level of 60%~90% in order to cause OXPHOS dysfunction (Kauppila, Kauppila et al. 2017). Dysfunctional respiratory chain complexes can generate enhanced amount of ROS with age (Linnane, Ozawa et al. 1989, Greaves and Turnbull 2009) and can in turn exert a chronic stress on mitochondria, especially on mtDNA, because of the close proximity to the OXPHOS (Greaves and Turnbull 2009). This accumulation of oxidative stress can also change

mitochondrial structure and membrane potential which in turn modulate mitochondrial function and metabolism. Thus, a vicious cycle between ageing and mitochondrial dysfunction is produced, ultimately leading to cell death (Greaves and Turnbull 2009, Logan, Shabalina et al. 2014). This correlation between ageing and mitochondrial dysfunction can be studied by measuring mitochondrial complex function and expression. MtDNA point mutations which accumulated in stem cells can lead to complex IV deficiency in differentiated cells, thus contributing to the ageing process (Kauppila, Kauppila et al. 2017). The stem cells functionality of homozygous mtDNA mutator mice were used to further study the connection between mtDNA mutations and stem cell dysfunction. It can be concluded that mtDNA mutations directly affect stem cell functionality by bioenergetics deficiency and/or ROS-signaling-mediated mechanisms (Kauppila, Kauppila et al. 2017).

In order to study the impact of ageing on mitochondrial complex expression and function, a specific mouse model was used in my study. The mitochondrial mutator mice (*PolgA*$^{mut/mut}$) was created by inserting a knock-in mutation (D257A) into the second endonuclease proofreading domain of PolgA catalytic subunit of the mtDNA polymerase, using a C57BL/6 background mouse, shows accelerated premature ageing phenotypes. The mitochondrial complex dysfunction or deficiency have been studied in different organs and published in previous studies on this a mouse model before (Dobson, Rocha et al. 2016, Houghton, Stewart et al. 2017). However, the pancreas tissue of *PolgA*$^{mut/mut}$ mice hasn't been tested, I want to begin my studies by examining the mitochondrial respiratory chain complex expressions in pancreatic islets.

The diagnosis of mitochondrial function is usually dependent on histopathological assessment of tissue biopsy samples and molecular genetic testing. A novel quadruple immunofluorescence assay to assess mitochondrial respiratory chain defect was used in our study.

The aims of the current chapter were to:

Study the nature and extent of changes in mitochondrial ETC complex expression in pancreatic islets in response to ageing in mutator and control mice, and determine whether exercise training impacts upon these changes.

It can be further separated into following aims:

1. Characterize the mitochondrial complex expression in pancreatic islets from mtDNA mutator mice and age-matched wild type mice at two different ages.
2. Investigate whether exercise training impact on the change of mitochondrial ETC complex expression in mtDNA mutator mice.
3. Characterize the mitochondrial complex expression between two different age groups within each genotype.
4. Investigate the mtDNA copy number at single islet level in mtDNA mutator mice and wild type mice.

3.2 Methods

3.2.1 Quadruple immunofluorescence with mouse pancreas sections.

Quadruple immunofluorescence staining protocol was used in our study. Insulin, Tomm20 (mitochondrial mass marker), MTCO1 (Complex IV) and NDUFB8 (Complex I) stains were excited under Alexa fluor 405, Alexa fluor 488, Alexa fluor 546 and Alexa fluor 647 separately. NDUFB8 is a nuclear-DNA encoded subunit of Complex I and COX-I is a mtDNA-encoded subunit of Complex IV. Complex I is the largest ETC complex and it has been reported before that complex I served as an early indicator of mitochondrial pathology because was commonly and initially affected in mitochondrial disease (Janssen, Nijtmans et al. 2006, Rygiel, Miller et al. 2015). Complex IV is a terminal electron accetor on the ETC. The histochemical assessment of cytochrome c oxidase (Complex IV, COX) has been a standard methodology to assess OXPHOS function in tissue sections (Old and Johnson 1989, Sciacco and Bonilla 1996). 50 islets were studied for each pancreas sample and Nikon image analysis software was used for signal intensity measurement. Graphpad prism 8 was used to generate graphs and different analysis.

3.2.2 Immunofluorescence with mouse frozen sections.

After frozen pancreas sections were taken from -80^{o}C freezer, they were defrosted, dried, fixed and dehydrated, monoclonal mouse antibody against glucagon was applied on pancreas sections as a marker for islets. The glucagon marker makes following laser dissection microscope become easier to perform. After PBS washing, glucagon stained sections were stored in -20^{o}C freezer.

3.2.3 Laser dissection microscopy

Laser dissection microscope (LDM) was used to detect islets and cut off islets to test the mtDNA copy number. Single cell DNA lysis buffer was made up to extract DNA from the islet sample (Detailed in Method chapter 2.4.1). Each islet was cut off and collected in one 200µl tube. All the samples were stored in -20 freezer for following real time PCR.

3.2.4 Real-time PCR and mitochondrial DNA copy number assay

After DNA was extracted from islet samples, real-time PCR reaction was set up using a LightCycler 480 detector. DNA sample was amplified using either ND5 or B2M primers using the PCR parameters detailed in method chapter. Standard curves of ND5 target gene and B2M reference gene prepared using a series of five 1 in 10 dilutions of wild type mouse pancreas DNA (from 100 to 0.01 ng/ul). 10 islets for each mouse case (wild type and *PolgA*$^{mut/mut}$) were dissected and processed with lysis buffer. Standard curve analysis and delta Ct quantification were performed to calculate the mtDNA copy number.

3.3. Results

3.3.1. A significant mitochondrial complex I deficiency was found in islets from *PolgA$^{mut/mut}$* mice compared to the wild type mice at 3 months.

I identified pancreatic islets from pancreas tissue and quantified the protein abundance of complex I and complex IV relative to mitochondrial mass from 3-month wild type (WT) and *PolgA$^{mut/mut}$* mice. 4 WT and 4 *PolgA$^{mut/mut}$* mice were studied. Composite and separate images were shown in ***Figure 3-1***. ***Figure 3-2*** shows the z-score expression of Tomm20, complex I and IV of individual islets and average value in each mouse. Unpaired t-test showed us that there was significant difference in complex I expression between wild type and *PolgA$^{mut/mut}$* mice groups ($p<0.0001$), but there were no significant differences in Tomm20 and complex IV expression between two mice groups ($p>0.05$). The signal intensity comparison and graphs are listed in ***Figure 8-2*** in Appendix chapter.

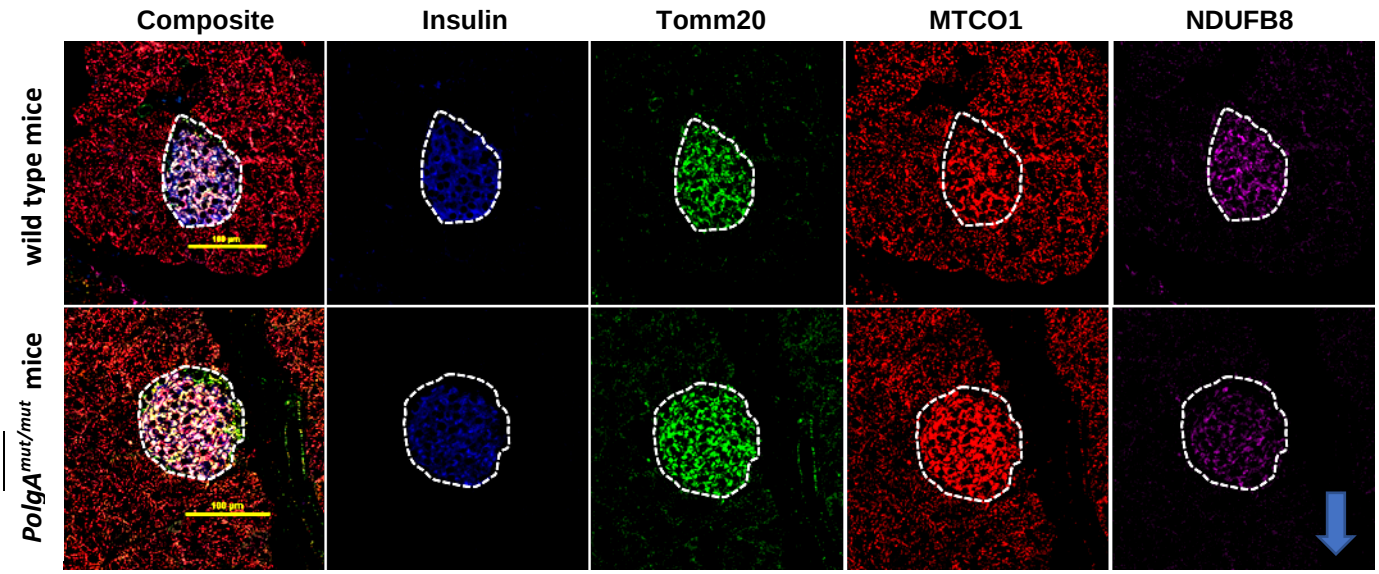

Figure 3-1. The composite and separate quadruple mitochondrial immunofluorescence in pancreatic islets from 3-month sacrificed mice. (Top) wild type mice Polg1624. (Bottom) *PolgA*$^{mut/mut}$ sedentary mice Polg1681. From left to right, immunofluorescence labeling of Insulin (Alexa fluor 405); Tomm20 (Mitochondrial mass marker, Alexa fluor 488); MTCO1 (Complex IV, Alexa fluor 546); NDUFB8 (Complex I, Alexa fluor 647). Pictures were taken by A1 confocal with 20 times magnification. Scale bar, 100 µm. The blue arrow indicates the decrease of signal intensity in NDUFB8 in *PolgA*$^{mut/mut}$ mice through an eyeball test.

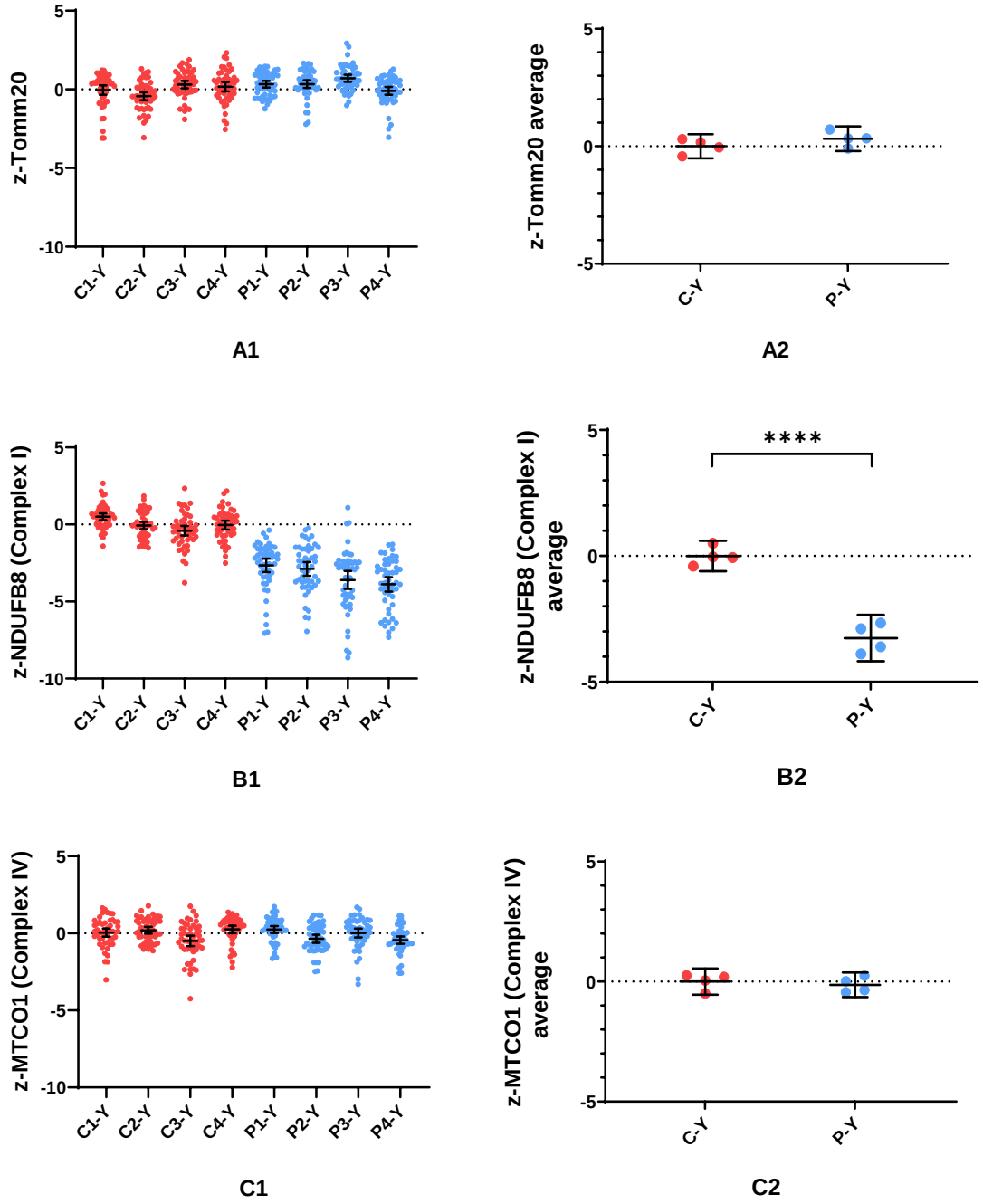

Figure 3-2. Changes of z-score expression in Tomm20 (mitochondrial mass), NDUFB8 (complex I) and MTCO1 (complex IV) in 3-month sacrificed *PolgA*$^{mut/mut}$ mice compared to the age-matched wild type mice. Data are presented as mean ± 95%CI. **(A1, B1, C1) Case analysis.** In all graphs: wild type mice (C1-Y to C4-Y) and *PolgA*$^{mut/mut}$ sedentary mice (P1-Y to P4-Y). Each dot represents one islet and 50 islets were studied for each mouse. (A1) z-Tomm20; (B1) z- NDUFB8; (C1) z- MTCO1. **(A2, B2, C2) Group average comparison.** In all graphs, wild type mice (C-Y), *PolgA*$^{mut/mut}$ sedentary mice (P-Y). Each point represents an average data of 50 islets from one mouse and each group consists of 4 mice. (A2) z-Tomm20 group average. Unpaired t-test, $p>0.05$. (B2) z-NDUFB8 group average. Unpaired t-test, $p<0.0001$; (C2) z-MTCO1 group average. Unpaired t-test, $p>0.05$. ****$p<0.0001$.

3.3.2. A significant mitochondrial complex I deficiency but a significant increase of complex IV expression were found in islets from *PolgA$^{mut/mut}$* mice compared to their wild type mice at 11 months.

Another 5 WT and 5 *PolgA$^{mut/mut}$* sedentary mice were sacrificed at age of 11 months for further study. Also, in order to test whether endurance exercise can reverse the impact of ageing on mitochondrial function, we also studied 4 *PolgA$^{mut/mut}$* mice which started exercise training at age of 4 months but also sacrificed at age of 11 months (exercise protocol was explained in method chapter 2.1). Again 50 islets were studied for each mouse. The composite and separate staining results were shown in ***Figure 3-3***. ***Figure 3-4*** shows the z-score expression of Tomm20, complex I and IV of individual islets and average value in each mouse. Unpaired t-test showed there was significant difference in complex I and IV expression between wild type and *PolgA$^{mut/mut}$* mice group (both $p<0.001$), *PolgA$^{mut/mut}$* mice group had significantly lower complex I but higher complex IV expression compared to the wild type mice group at 11 months. Tomm20 expression didn't have significant difference between wild type and *PolgA$^{mut/mut}$* mice group ($p>0.05$). Besides, unpaired t-test between sedentary and exercise group showed that there was no significant difference in any of these three mitochondrial indexes between sedentary and exercise group ($p>0.05$). It showed that endurance exercise didn't improve the mitochondrial expression in *PolgA$^{mut/mut}$* mice. The signal intensity comparison and graphs are listed in ***Figure 8-3*** in Appendix chapter.

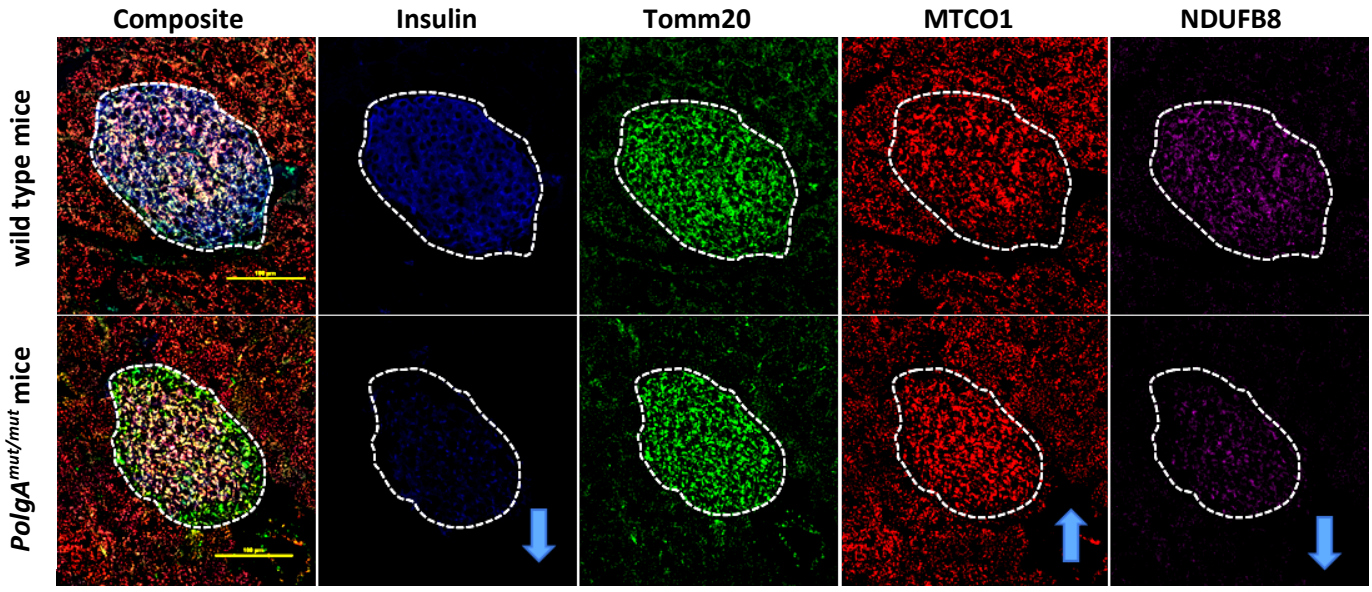

Figure 3-3. The composite and separate quadruple mitochondrial immunofluorescence in pancreatic islets from 11 month sacrificed mice. (Top) wild type mice GA0007; (Bottom) *PolgA*$^{mut/mut}$ sedentary mice LG0011. From left to right, immunofluorescence labelling of Insulin (Alexa fluor 405), Tomm20 (Mitochondrial mass, Alexa fluor 488), MTCO1 (Complex IV, Alexa fluor 546) and NDUFB8 (Complex I, Alexa fluor 647). Pictures were taken by A1 confocal with 20 times magnification. Scale bar, 100µm. The blue arrows indicate the changes of signal intensities in islets of *PolgA*$^{mut/mut}$ mice compared to the wild type mice through an eyeball test.

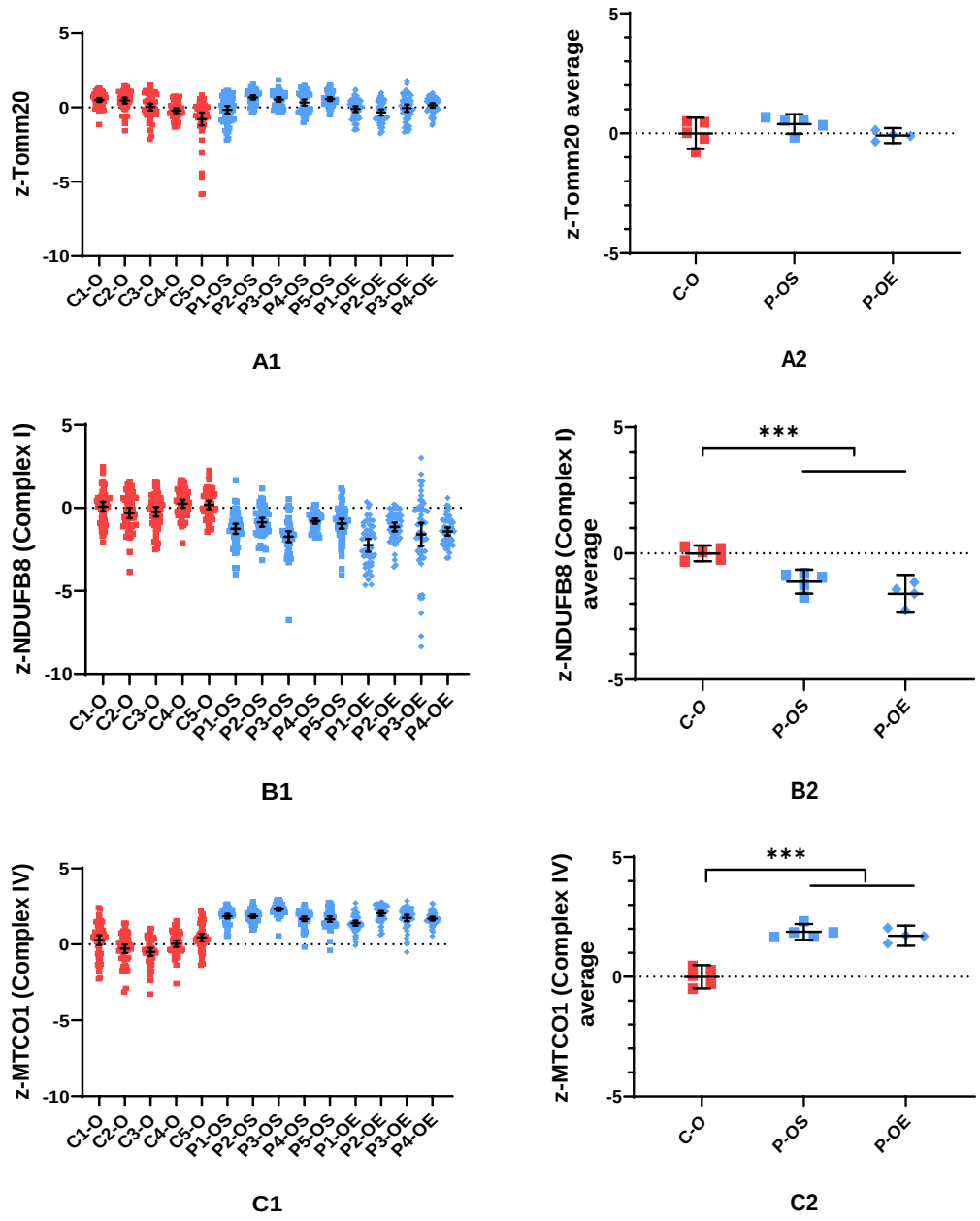

Figure 3-4. Changes of z-score expression in Tomm20 (mitochondrial mass), NDUFB8 (complex I) and MTCO1 (complex IV) in 11-month sacrificed *PolgA*$^{mut/mut}$ mice compared to age-matched wild type mice. Data are presented as mean ± 95%CI**. (A1, B1, C1) Case analysis.** Wild type mice (C1-O to C5-O); *PolgA*$^{mut/mut}$ sedentary mice (P1-OS to P5-OS); *PolgA*$^{mut/mut}$ exercise mice (P1-OE to P4-OE). Each dot represents one islet and 50 islets were studied for each mouse. (A1) z-Tomm20; (B) z-NDUFB8; (C) z-MTCO1. **(A2, B2, C2) Group average comparison.** Wild type mice (C-O); *PolgA*$^{mut/mut}$ sedentary mice (P-OS); *PolgA*$^{mut/mut}$ exercise mice (P-OE). Each point represents average data of 50 islets from one mouse. (A2) z-Tomm20 group average. Unpaired t-test, p>0.05. (B2) z-NDUFB8 group average. Unpaired t-test between wild type and *PolgA*$^{mut/mut}$ group, p<0.001; Unpaired t-test between *PolgA*$^{mut/mut}$ sedentary and exercise group, p>0.05; (C2) z-MTCO1 group average. Unpaired t-test between wild type and *PolgA*$^{mut/mut}$ mice group, p<0.001; Unpaired t-test between *PolgA*$^{mut/mut}$ sedentary and exercise group, p>0.05. ***p<0.001.

3.3.3. A significant deficiency in mitochondrial complex IV expression was found in islets from 11-month wild type mice compared to 3-month wild type mice.

By comparing the mitochondrial antibodies signals between young (3 month) and old (11 month) mice within wild type and *PolgA*$^{mut/mut}$ genotypes, the changes of mitochondrial respiratory chain complex expressions during natural ageing and mutated ageing process can be further studied.

8 wild type mice were studied in this part of study; 4 were sacrificed at age of 3 months and the other 4 were sacrificed at age of 11 months. This time, 25 islets were studied for each case. ***Figure 3-5*** shows the z-score expression of Tomm20, complex I and IV of individual islets and average value in each mouse. Unpaired t-test showed there was significant difference in complex IV expression between 3-month and 11-month wild type mice group ($p<0.01$). Tomm20 and complex I expression did not differ significantly between young and old wild type mice group (both $p>0.05$). With the increase of age, old wild type mice group had significantly lower complex IV expression compared to the young wild type mice group. Although Tomm20 expression didn't show significant difference between young and old wild type mice, there was an increasing trend of Tomm20 expression in wild type mice with increase of age (***Figure 3-5***). The signal intensity comparisons and graphs are listed in ***Figure 8-4*** in Appendix.

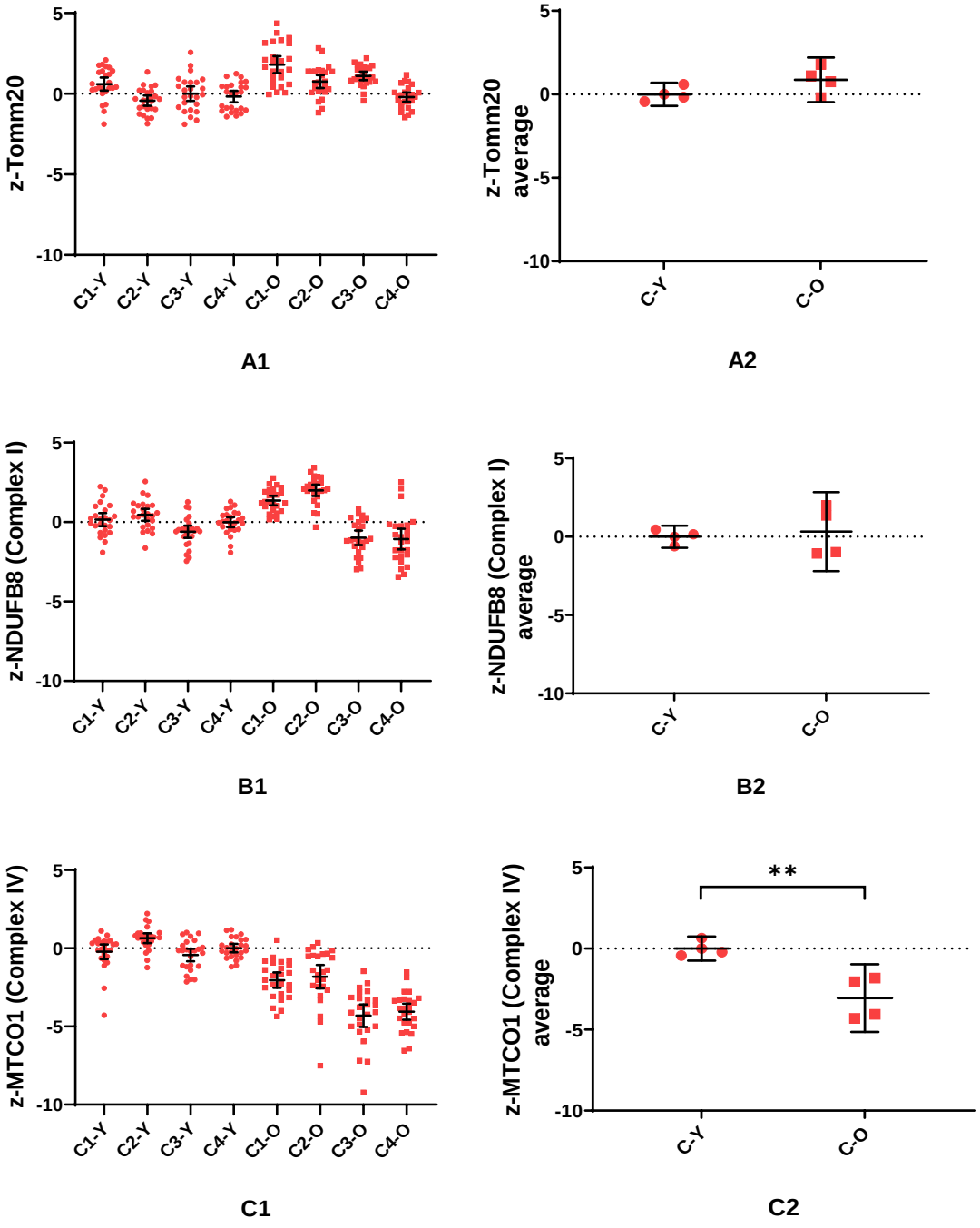

Figure 3-5. Changes of z-score expression in Tomm20 (mitochondrial mass), NDUFB8 (complex I) and MTCO1 (complex IV) in 11-month wild type mice compared to 3-month wild type mice. Data are presented as mean ± 95%CI. **(A1, B1, C1) Case analysis**. 3-month mice (C1-Y to C4-Y); 11-month mice (C1-O to C4-O). Each dot represents one islet and 25 islets were studied for each mouse. (A1) z-Tomm20; (B1) z-NDUFB8; (C1) z-MTCO1. **(A2, B2, C2) Group average comparison.** 3-month young mice (C-Y); 11-month mice (C-O). Each point represents an average data of 25 islets from one case and each group consists of 4 mice. (A2) z-Tomm20 group average. Unpaired t-test, $p>0.05$. (B2) z-NDUFB8 group average. Unpaired t-test, $p>0.05$; (C2) z-MTCO1 group average. Unpaired t-test, $p<0.01$. **$p<0.01$.

3.3.4. Tomm20 expression were significantly higher in islets from 11-month *PolgA$^{mut/mut}$* mice compared to the 3-month *PolgA$^{mut/mut}$* mice.

8 mice were studied in this part of study; 4 were sacrificed at age of 3 months and the other 4 were sacrificed at age of 11 months. Again, 25 islets were studied for each case. ***Figure 3-6*** shows the z-score expression of Tomm20, complex I and IV of individual islets and average value in each mouse. Unpaired t-test showed that there was significant difference in Tomm20 expression between 3-month and 11-month *PolgA$^{mut/mut}$* mice group ($p<0.01$) but complex I and IV expression did not differ significantly between young and old *PolgA$^{mut/mut}$* mice group (both $p>0.05$). With the increase of age, older *PolgA$^{mut/mut}$* mice had significantly higher Tomm20 expression but they didn't show significant difference in complex I and IV expression compared to the younger *PolgA$^{mut/mut}$* mice. The signal intensity comparison and graphs are listed in ***Figure 8-5*** in Appendix chapter.

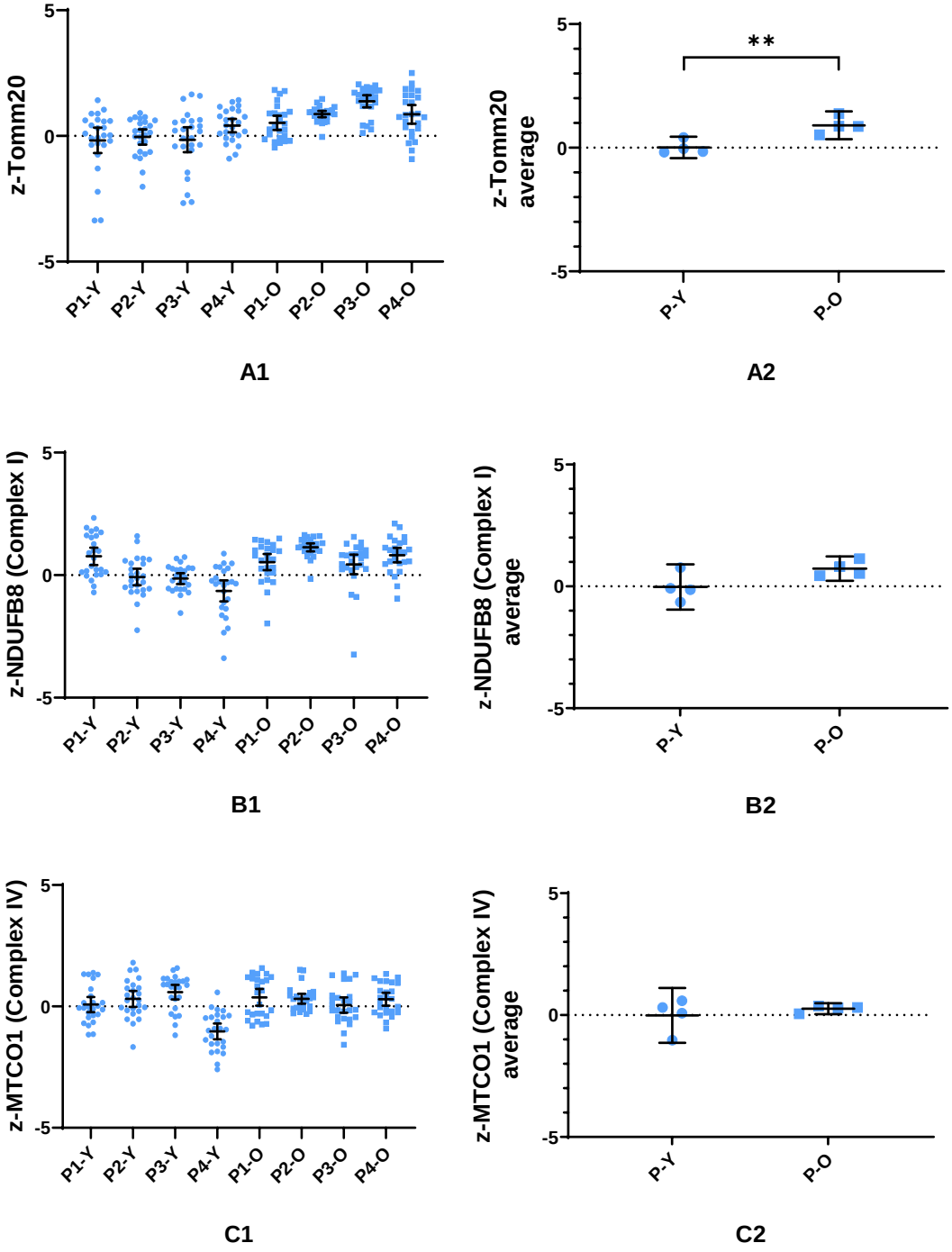

Figure 3-6. Changes of z-score expression in Tomm20 (mitochondrial mass), NDUFB8 (complex I) and MTCO1 (complex IV) in 11-month *PolgA*$^{mut/mut}$ mice compared to 3-month *PolgA*$^{mut/mut}$ mice. Data are presented as mean ± 95%CI**. (A1, B1, C1) Z-score case comparison.** In all graphs, 3-month mice (P1-Y to PY-4); 11-month mice (P1-O to P4-O). Each dot represents one islet and 25 islets were studied for each mouse. (A1) z-Tomm20; (B1) z-NDUFB8; (C1) z-MTCO1. **(A2, B2, C2) Z-score group average comparison**. In all graphs, young mice (P-Y); old mice (P-O). Each point represents average data of 25 islets from one case. (A2) z-Tomm20 group average. Unpaired t-test, $p<0.01$. (B2) z-NDUFB8 group average. Unpaired t-test, $p>0.05$; (C2) z-MTCO1 group average. Unpaired t-test, $p>0.05$. **$p<0.01$.

3.3.5. No significant differences in islet cell mtDNA copy number between *PolgA*$^{mut/mut}$ mice and wild type mice at 11 months

In my study, an original concentration of 1000 ng/µl DNA was extracted from wild type mice pancreas. A serial 1:10 diluted samples of ND5, B-actin were made up to construct standard curves in real time PCR. The real time PCR for each gene was repeated many times in order to achieve a better standard curve efficiency. The closer the efficiency is to 1, the better it illustrates and calculates the mitochondrial copy number of each sample. The standard curve result for ND5 and B-actin genes are listed in the ***Figure 3-7***.

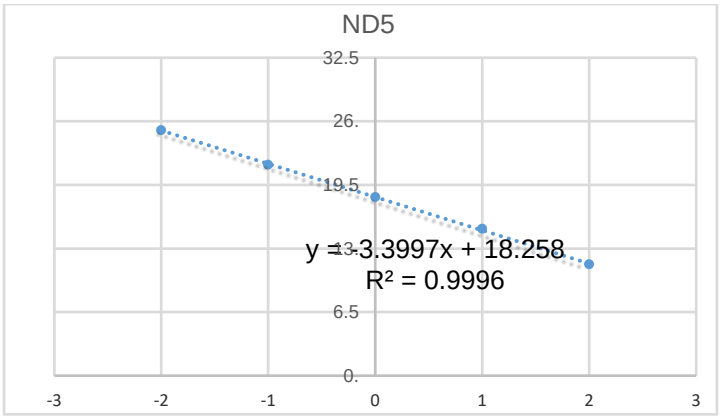

A

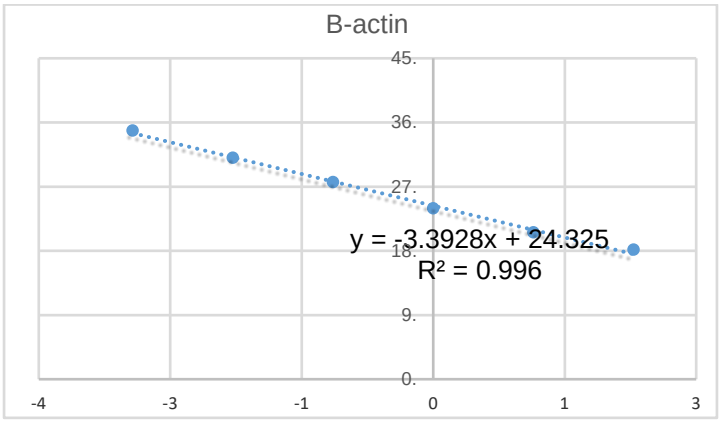

B

Figure 3-7. Standard curves of ND5 target gene and B-actin reference gene prepared using a series of 1 in 10 dilutions of wild type mouse pancreas DNA. (A) The amplification curve starts from the first dilution of ND5 (concentration 100 ng/µl) and ends with the fifth dilution (concentration 1×10^{-2} ng/µl). ND1: R^2: 0.9996. Slope: -3.3997. Y-intercept: 18.258. (B) The amplification curve starts from the first dilution of B-actin (concentration 100 ng/µl) and ends with the sixth dilution (concentration 1×10^{-3} ng/µl). B-actin: R^2: 0.996. Slope: -3.3928. Y-intercept: 24.325.

The frozen pancreas slides from two 11-month wild type (GA0007 and GA0008) and two 11-month *PolgA*$^{mut/mut}$ mice (LG0002 and LG0011) were studied in this part of study. At least 10 islets were studied from each case. The pancreatic islet mtDNA copy number results from 11-month wild type and *PolgA*$^{mut/mut}$ mice are shown in ***Figure 3-8***. The results were analyzed in both standard curve method and 2*(2^ (-ΔCt)) method. It can be concluded from unpaired t-test that there was no significant difference in islet mtDNA copy number between 11-month wild type and *PolgA*$^{mut/mut}$ mice in both analysis methods. Tomm20 represents mitochondrial mass marker in previous mitochondrial quadruple immunofluorescence staining. It was stated that in the ***Paragraph 3.3.2*** that there was no significant difference in islet Tomm20 signal intensity value between 11-month wild type and *PolgA*$^{mut/mut}$ mice. The mtDNA copy number result is therefore consistent with the quadruple staining analysis result.

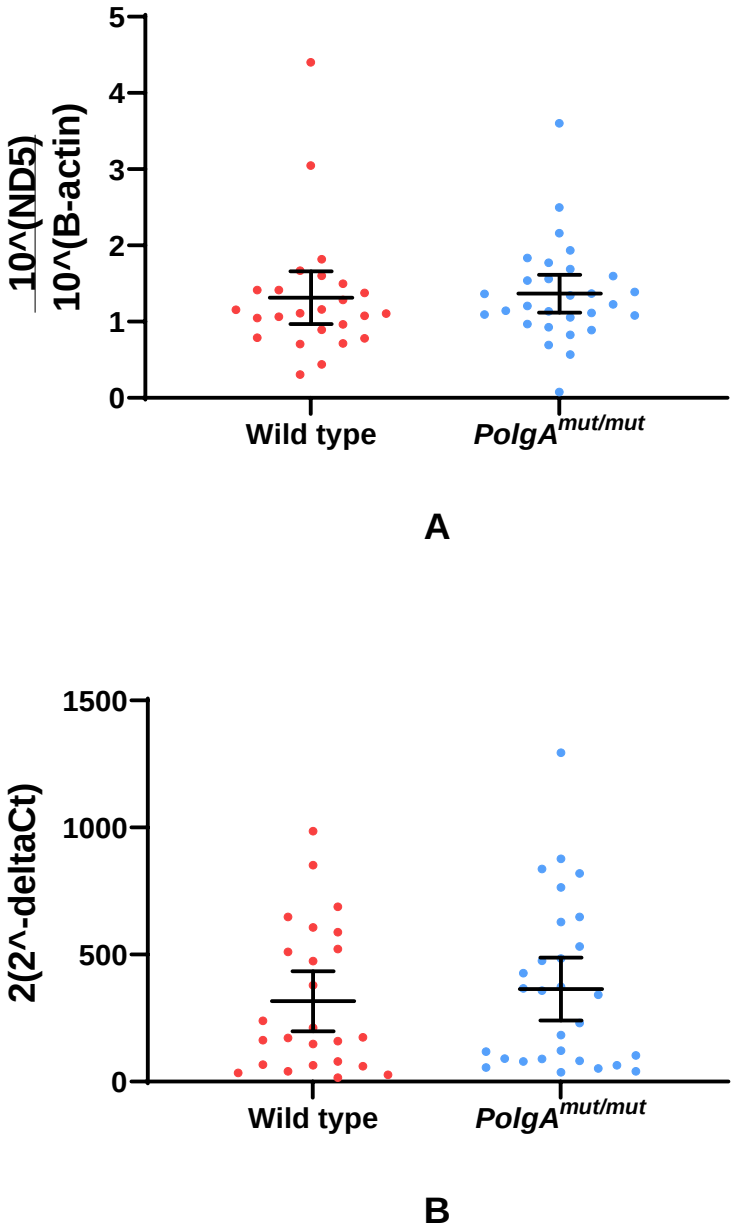

Figure 3-8. Pancreatic islet mtDNA copy number comparison between 11-month wild type and *PolgA*$^{mut/mut}$ mice. Data are presented as mean ± 95%CI**.** (A) Standard curve analysis method; each dot represents one islet. Unpaired t-test, p>0.05. (B) 2*(2^ (-ΔCt)) analysis method; each dot represents one islet. Unpaired t-test, p>0.05

3.4. Summary

1. A significant mitochondrial complex I deficiency was found in islets from *PolgA*$^{mut/mut}$ mice compared to the age-matched wild type mice at 3 months.

2. A significant mitochondrial complex I deficiency but a significantly higher complex IV expression were detected in islets from *PolgA*$^{mut/mut}$ mice compared to the age-matched wild type mice at 11 months.

3. In wild type mice, a significant mitochondrial complex IV deficiency was detected in islets from 11-month mice compared to 3-month mice.

4. In *PolgA*$^{mut/mut}$ mice, a significant increase of Tomm20 expression was detected in islets from 11-month mice compared to the 3-month mice but there were no significant differences in mitochondrial complex I and IV expression between young and old *PolgA*$^{mut/mut}$ mice.

5. Endurance exercise didn't have significant impact on mitochondrial complex expression and no significant difference in expression of Tomm20, complex I and IV were found in islets between *PolgA*$^{mut/mut}$ sedentary mice and exercise mice at 11 months.

6. No significant differences in islet cell mtDNA copy number between *PolgA*$^{mut/mut}$ mice and WT mice at 11 months

3.5. Discussion

By doing quadruple immunofluorescence staining on wild type and *PolgA*$^{mut/mut}$ mice from two age groups, it can be clearly found out the difference in expression of mitochondrial complex I and IV between *PolgA*$^{mut/mut}$ mice and wild type mice in both age groups. Mitochondrial research group from Newcastle University innovated this quantifiable quadruple immunofluorescence technique. It was used to apply this on many tissues from *PolgA*$^{mut/mut}$ such as bone, heart and neuro tissues and most of them have been observed to show deficiencies in either complex I and IV expression (Trifunovic, Wredenberg et al. 2004, Vermulst, Wanagat et al. 2008, Dobson, Rocha et al. 2016, Houghton, Stewart et al. 2017). I adapted this technique to further study the mitochondrial complex expression on pancreatic islet tissue.

Our experiments started from pancreas slides from *PolgA*$^{mut/mut}$ mice and wild type mice at 3 months. A significant deficiency in complex I expression was discovered in islets from *PolgA*$^{mut/mut}$ mice compared to their wild type counterparts at 3 months. When I studied the mitochondrial complex expression on pancreas slides from *PolgA*$^{mut/mut}$ mice and wild type mice at 11 months, the significant complex I deficiency persisted but complex IV expression significantly increased in islets from *PolgA*$^{mut/mut}$ mice compared to their wild type counterparts. This complex I deficiency was also observed in osteoblast of elder *PolgA*$^{mut/mut}$ mice before (Dobson, Rocha et al. 2016).

Complex I and complex IV are the first and fourth components of mitochondrial electron transport chain. The functionality of each electron transport chain complex is important for generating sufficient amount of ATP. In order to find out whether the increase of complex IV expression is caused by a compensatory response after the complex I expression deficiency in the pancreatic islets, or is driven by other reasons, I further test the change of mitochondrial mass (Tomm20) and mitochondrial complex I and IV expression between different ages but within the same genotype. I firstly studied the Tomm20, complex I and IV

expression in wild type mice at 3 and 11 months and a significant mitochondrial complex IV deficiency was detected in islets from 11-month mice compared to 3-month mice. This result was also observed in a previous study on human skeletal muscle (Rocha, Grady et al. 2015). The expression of Tomm20, although didn't have a significant difference between two ages, show an increasing trend in wild type mice with ageing. When I compare the Tomm20, complex I and IV expression in *PolgA*$^{mut/mut}$ mice at 3 and 11 months, no significant differences in mitochondrial complex I and IV expression were found in islets from 11-month *PolgA*$^{mut/mut}$ mice compared to the 3-month *PolgA*$^{mut/mut}$ mice. However, older *PolgA*$^{mut/mut}$ mice had significantly higher Tomm20 expression compared to younger *PolgA*$^{mut/mut}$ mice. The changes of mitochondrial complex expression in wild type and *PolgA*$^{mut/mut}$ mice in two age groups were illustrated in the ***Figure 3-9*** below.

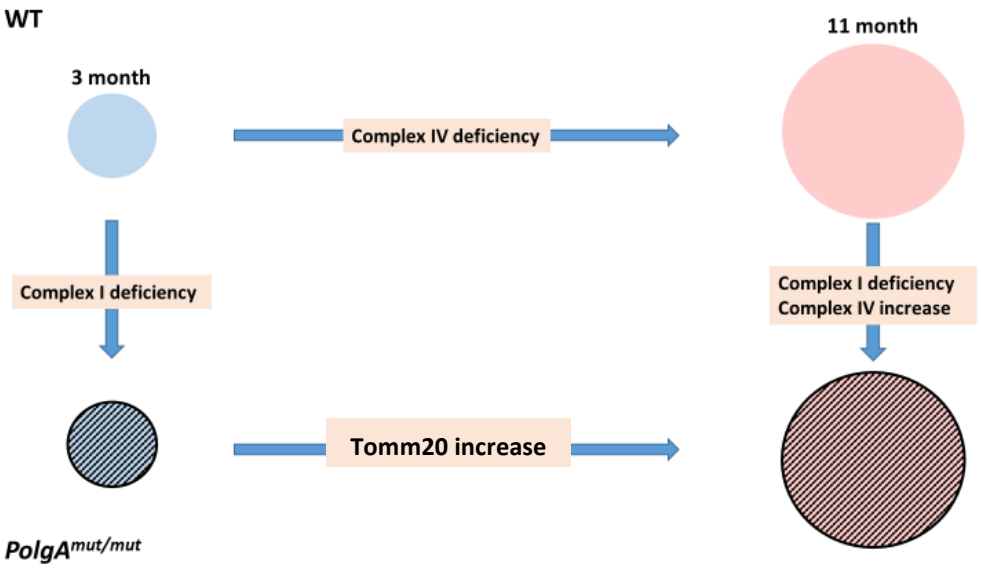

Figure 3-9. Changes of mitochondrial complex expression in wild type and *PolgA*$^{mut/mut}$ mice in two age groups.

From ***Figure 3-9***, I can see the normal ageing process from 3 months to 11 months in the wild type mice and the normal ageing on the background of altered mitochondrial function from 3 months to 11 months in the *PolgA*$^{mut/mut}$ mice. Mitochondrial dysfunction can accelerate the ageing process in the *PolgA*$^{mut/mut}$ mice.

I can conclude that different mitochondrial complex dysfunction can be contributed by different ageing process. The normal ageing process mainly causes the complex IV deficiency whereas mitochondrial dysfunction can accelerate the normal ageing process and lead to the complex I deficiency. However, the age-related decrease in complex IV expression see in the control mice islets was not apparent in the *PolgA*$^{mut/mut}$ mice. This raises the possibility that the age-related increase of Tomm20 expression helps to maintain complex IV expression with age in the *PolgA*$^{mut/mut}$ islets. It reflects a compensatory response in the face of the early and persistent complex I deficiency. This has been observed in other tissues such as brain, kidney and liver tissue (DiMauro and Schon 2003).

In human, mtDNA mutations were initially detected in ageing human post-mitotic tissues, with a mosaic pattern of COX deficiency in heart, muscle and brain tissue (Baines, Turnbull et al. 2014). Post-mitotic tissue is defined as mature and terminally differentiated tissue which are no longer able to undergo mitosis process (Aranda-Anzaldo 2012). Pancreatic endocrine cells which differentiate from progenitors cells also belong to post-mitotic tissue (Dhawan, Georgia et al. 2007). However, although high mutation loads were found in skeletal muscle and brain tissue of patients, a surprisingly low percentage ratio of heteroplasmy was detected in pancreas (Lynn, Borthwick et al. 2003). A possible explanation is that β-cells are particularly sensitive to mtDNA mutations so a very low levels of mutations can cause biochemical defects in β-cells.

PolgA$^{mut/mut}$ mice were created by inserting knock-in mutation in the proofreading domain of PolgA catalytic subunit of the mtDNA polymerase, using a C57BL/6 background mouse. It was

reported before that the accumulation of mtDNA mutations may start occur during embryonic and/or fetal development in these mice because the mutation load was already substantial by 2 month of age (Trifunovic, Wredenberg et al. 2004). These mutations can cause similar or even more severe mitochondrial dysfunction compared to human because of its 3-5 times higher mutation rate in these mice (Baines, Turnbull et al. 2014). All these above findings were consistent with my results that a significant complex I deficiency was detected in the islets of *PolgA*$^{mut/mut}$ mice from 3-month age and persisted to 11-month age. However, the onset of premature ageing is not accompanied until around 6 months of age. The stronger accumulation of mtDNA mutations in different tissues and cells, once beyond a critical threshold, can lead to the death of vital cells. This is the critical process of driving the onset of premature ageing phenotypes and reduce life span (Trifunovic, Wredenberg et al. 2004).

There is an increasing trend of Tomm20 in wild type mice and a significant increase of Tomm20 expression in *PolgA*$^{mut/mut}$ mice with increase of age. The reason behind maybe because this was a compensatory response to maintain the normal mitochondrial function under the ageing condition. Mitochondrial biogenesis is most likely the underlying mechanism of this compensatory response. Mitochondrial biogenesis can be regarded as an efficient strategy to delay mitochondrial ageing because it is the expansion of mitochondria by either expanding mitochondrial mass or increasing mitochondrial number (Chistiakov, Sobenin et al. 2014). Mitochondrial biogenesis will also contribute to a larger number of mtDNA genome which can buffer the mitochondrial dysfunction caused by mtDNA mutations (Kaufman, Li et al. 2015).

There are several limitations in this part of study: firstly, normal control C57BL/6J mice as old as 3 months can be regarded as mature adults and mice will start exhibiting some age-related changes (Laboratory). *PolgA*$^{mut/mut}$ mice born with mtDNA mutations age significantly faster compared to the normal C57BL/6J mice. The time when significant age-related changes happen may have already been missed when mice were studied at 3 months. In order to further study the impact of premature ageing, it's better to recruit some mice which sacrificed

younger than 3-month (Fox, Barthold et al. 2006). Secondly, in *PolgA*$^{mut/mut}$ mice, although I didn't see a significant difference in complex I and IV expression between 3-month and 11-month, very big standard deviations were observed in z-score value from each case. A more accurate comparison result can be achieved if we can recruit more wild type and *PolgA*$^{mut/mut}$ mice from different ages and repeat the mitochondrial staining in the future.

It was discussed in a previous study that endurance exercise could decrease mitochondrial superoxide generation and delay the onset of ageing. It attenuated the decline in mtDNA copy number and reduced the mtDNA point mutations frequency in *PolgA*$^{mut/mut}$ mice. Besides, it promoted systemic mitochondrial oxidative capacity by enhancing COX activity in *PolgA*$^{mut/mut}$ mice (Logan, Shabalina et al. 2014). Another study also proved that endurance exercise can not only induce mitochondrial biogenesis in skeletal muscle, it also profoundly improve metabolism in non-exercised tissues, including heart, brain, adipose tissue, and liver (Safdar, Bourgeois et al. 2011). It was the main reason why I induced endurance exercised *PolgA*$^{mut/mut}$ mice in my study because I want to see if endurance exercise impact on islet which is another non-exercised tissue (Menshikova, Ritov et al. 2006, Safdar, Bourgeois et al. 2011). However, this improvement in mitochondrial subunit expression was not observed in our study. There are no significant differences in the expression of mitochondrial mass, complex I and IV between *PolgA*$^{mut/mut}$ sedentary and exercise mice at 11 months. Similar results were reported by my colleague Dr. Ghazaleh Alimohammadiha, she agreed that endurance exercise had no effect on complex I and complex IV expression in the cardiac muscle of *PolgA*$^{mut/mut}$ mice, it also didn't impact on mitochondrial biogenesis demonstrated by mitochondrial mass (porin) expression level.

Complex I deficiency and complex IV increase were found in the islets of 11-month *PolgA*$^{mut/mut}$ mice. I want to further discover the age-related change in islet cell composition of 11-month *PolgA*$^{mut/mut}$ mice.

CHAPTER 4: STUDY OF THE IMPACT OF AGEING ON PANCREATIC ISLET CELL COMPOSITION BY COMPARING *POLGA*$^{MUT/MUT}$ WITH WILD TYPE MICE.

4.1. Introduction

Ageing, mice β-cell mass and β-cell function.

β-cell mass is determined by the size and number of β-cells. The number of β-cells was achieved by a balance among the neogenesis, replication and death of β-cell (Montanya, Nacher et al. 2000). In rodents, β-cell number is determined in a certain window phase, which is from the last quarter of fetal gestation period to the first few days after birth. It is generally accepted that in this stage, β-cell population is mainly developed by neogenesis which is the formation of new β-cells from differentiated precursor cells (Bouwens and Rooman 2005). The β-cell mass generated from this process defines the baseline β-cell mass. It is the critical starting β-cell population from which a compensatory β-cell expansion may occur later (Perl, Kushner et al. 2010). After birth, only a small number of β-cells replicate in the normal situation and most of them are coming from the replication of pre-existing β-cells (Montanya, Nacher et al. 2000). There are also some of the β-cells forming from the progenitor cells and ductal cells. This discovery has been proved by studies using different mouse models (Bonner-Weir, Taneja et al. 2000, Ramiya, Maraist et al. 2000, Chang-Chen, Mullur et al. 2008, Gregg, Moore et al. 2012). A similar neonatal burst of β-cell proliferation has been described in human studies, but normal human β-cells replication is unusual and it is estimated that human β-cells turn over once every 25 years (Perl, Kushner et al. 2010, Gregg, Moore et al. 2012).

In response to postnatal physiological and pathological stress, an interplay of beta cell replication, proliferation and apoptosis is contributing to the adaptation of β-cell population in rodents. For example, a continuous increase of β-cell mass was reported throughout the lifespan in normal Lewis rat. In young rats, the increase in β-cell mass was contributed by hypertrophy and hyperplasia whereas hypertrophy alone was responsible for β-cell increment in old animals (Montanya, Nacher et al. 2000). The reasons behind this phenomenon may be

firstly, the continuous increase of β-cell mass is a compensatory response to an age-related tendency for the development of glucose intolerance (Chang and Halter 2003). Secondly, the increase of β-cell mass is a response to the increase of insulin secretory demand as animals grow in size with an increase in age (Clark 2008).

The continued accumulation of physiological and pathological stresses over time will tend to overwhelm the morphological and functional compensation of β-cells (Wajchenberg 2007, Chen, Cohrs et al. 2017) and lead to the reduced β-cell mass. There is also a strong correlation between reduced β-cell mass and β-cell dysfunction because the increased insulin demand caused by decreased β-cell mass can exhaust β-cell secreting function. β-cell failure which characterized by β-cell dysfunction and decreased β-cell mass is considered as a central contributor of type 2 diabetes (Group 1995, Bouwens and Rooman 2005).

The Aims of the current chapter were to:

Study the changes in islet size and cellular composition in response to ageing in *PolgA*$^{mut/mut}$ and wild type control mice, determine whether exercise training impacts upon these changes.

It can be further separated into following aims:

1. Characterize the pancreatic cell composition in *PolgA*$^{mut/mut}$ mice and their age-matched wild type mice at two different ages.

2. Investigate whether exercise training impact on the change of pancreatic islet cell compositionin mtDNA mutator mice.

3. Characterize the pancreatic cell compositional change between two different ages in each genotype.

4.2. Methods

4.2.1. Triple immunofluorescence staining on mouse pancreas sections.

Triple immunofluorescence staining protocol was used in our study. Glucagon and insulin stains were excited under TRITC and Alexa fluor 647 separately. Stained sections were mounted with nuclei staining DAPI. After staining, β-cells can be counted when we overlap insulin and DAPI channel and α-cells can be counted when I overlap glucagon and DAPI channel. In this study, only α- and β-cells are counted in each islet and other endocrine cell types are not counted. 25 islets were counted for each case. Graphpad prism was used to generate graphs and different analysis.

4.3. Results

4.3.1. There were no significant differences in the α- and β-cell percentage, islet size and islet cell number between *PolgA*$^{mut/mut}$ mice and their wild type controls at 3 months.

4 wild type and 4 *PolgA*$^{mut/mut}$ sedentary mice were sacrificed at 3 months and 25 islets were studied per mouse. Representative composite and separate staining images are shown in ***Figure 4-1***. ***Figure 4-2*** shows the α- and β-cell percentages, islet size, whole islet cell number, absolute α- and β-cell number, and the β/α cell ratio for the individual islets for each mouse. ***Figure 4-3*** shows the mean values for each animal and unpaired t-test was used for intergroup analysis. It can be concluded from the staining images and the data analysis that in 3 month sacrificed mice, there were no differences in α- and β-cell percentage, islet size, whole islet cell number, absolute α- and β-cell number between *PolgA*$^{mut/mut}$ mice compared with their age-matched wild type mice.

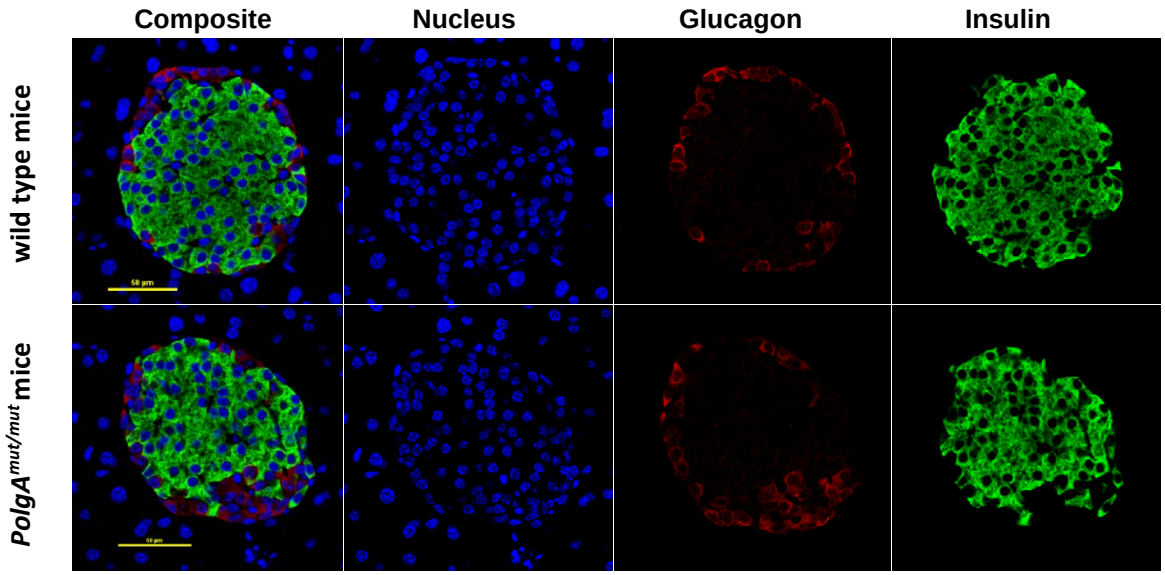

Figure 4-1. The separate and composite triple immunofluorescence staining images for endocrine hormones in pancreatic islets from 3 month mice. (Top) wild type mice; (Bottom) *PolgA*$^{mut/mut}$ mice. DAPI stain for nucleus; Glucagon stain for α-cells, Alexa fluor 568; Insulin stain for β-cells, Alexa fluor 488. Pictures were all taken by A1 confocal with 20 times magnification. Scale bar, 50μm.

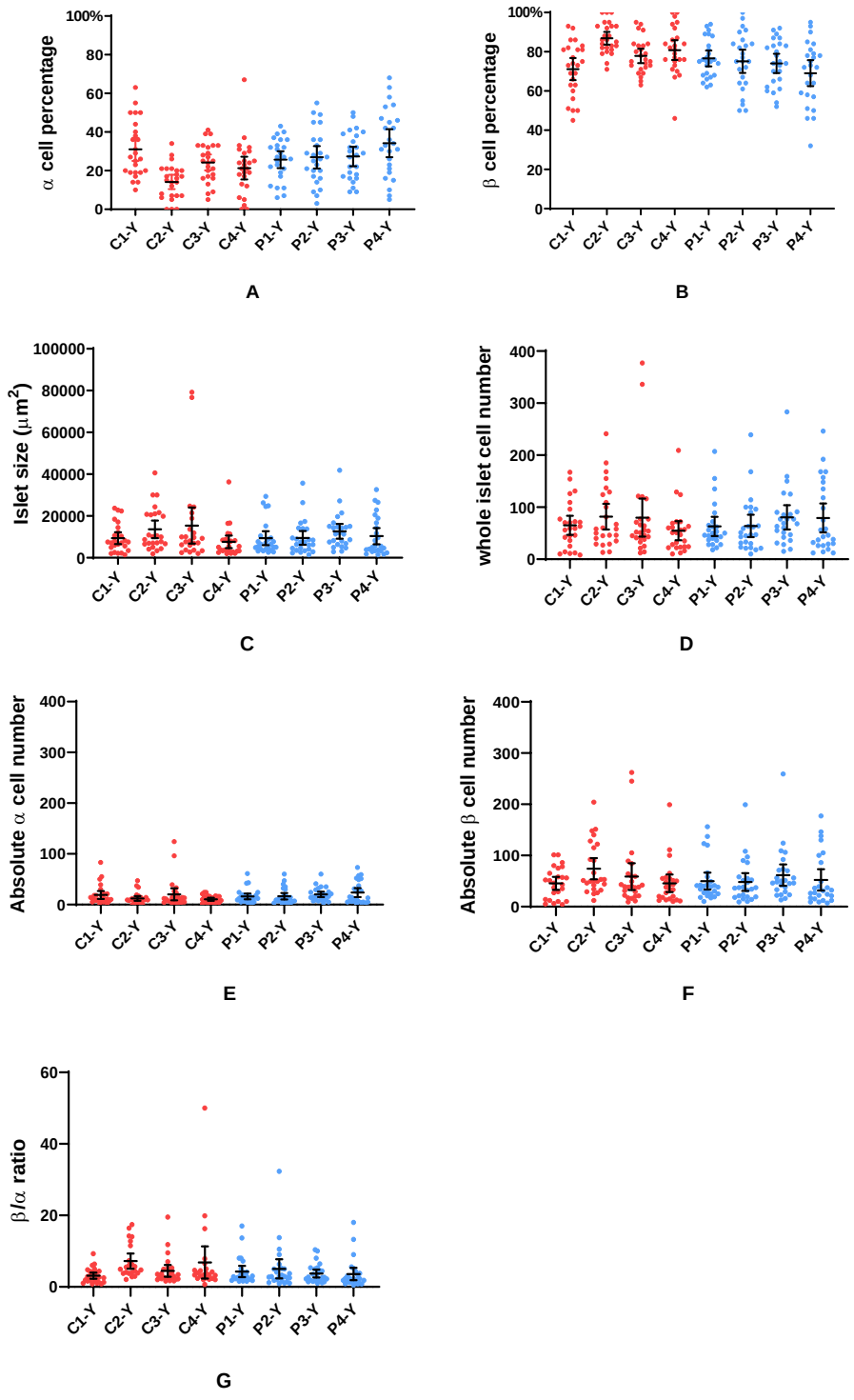

Figure 4-2. Islet cell composition summary in 3 month sacrificed mice. Data are presented as mean ± 95% CI**.** In all graphs: wild type mice (C1-Y to C4-Y) and *PolgA*$^{mut/mut}$ sedentary mice (P1-Y to P4-Y). 25 islets were studied per mouse and each dot represents one islet in the above graphs. (A) α-cell percentage; (B) β-cell percentage; (C) Islet size. (D) Whole islet cell numbe; (E) Absolute α-cell number; (F) Absolute β-cell number; (G) β/α ratio.

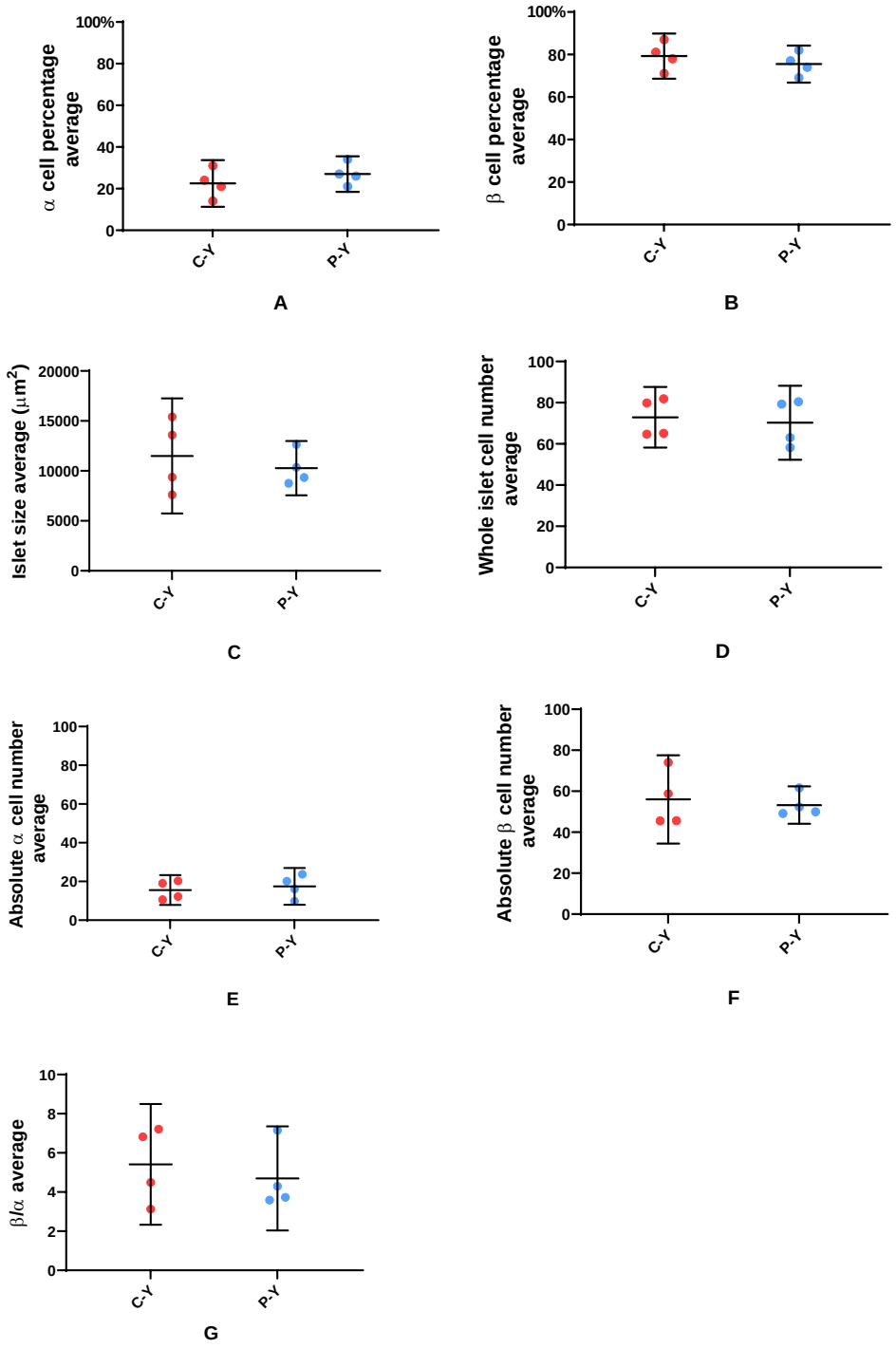

Figure 4-3. Average value of islet cell composition summary in 3 month sacrificed mice. Data are presented as mean ± 95% CI. In all graphs, wild type mice(C-Y), *PolgA*$^{mut/mut}$ sedentary mice (P-Y). One dot represents the average value of 25 islets from each case. (A) Average α-cell percentage. Unpaired t-test, p>0.05; (B) Average β-cell percentage. Unpaired t-test, p>0.05; (C) Average islet size. Unpaired t-test, p>0.05; (D) Average whole islet cell number. Unpaired t-test, p>0.05; (E) Average α-cell number. Unpaired t-test, p>0.05; (F) Average β-cell number. Unpaired t-test, p>0.05. (G) Average β/α ratio. Unpaired t-test, p>0.05.

4.3.2. *PolgA*$^{mut/mut}$ mice had a significantly lower β-cell percentage, higher α-cell percentage and higher absolute α-cell number versus their wild type controls at 11 months.

4 wild type, 4 *PolgA*$^{mut/mut}$ exercise and 5 *PolgA*$^{mut/mut}$ sedentary mice were sacrificed at 11 months, and 25 islets were studied per mouse. Representative composite and separate staining images are shown in ***Figure 4-4***. ***Figure 4-5*** shows the α- and β-cell percentages, islet size, whole islet cell number, absolute α- and β-cell number, and the β/α cell ratio for the individual islets for each mouse. The average values of islet cell composition for each animal are listed in ***Figure 4-6*** and unpaired t-test was used for intergroup analysis. It can be concluded from the staining images and the data analysis in 11-month sacrificed mice, *PolgA*$^{mut/mut}$ mice had significantly higher α-cell percentage (29.95% ± 4.14% vs 13.02% ± 4.67%, mean±SEM, P<0.001) but lower β-cell percentage (71.4% ± 4.29% vs 88.84% ± 4.51%, mean±SEM, P<0.001) compared to their age-matched wild type mice. Besides, 11-month *PolgA*$^{mut/mut}$ mice had significantly higher absolute α-cell number (44.41 ± 12.14 vs 15.2 ± 8.02, mean±SEM, P<0.01) and lower β/α ratio (2.97 ± 0.67 vs 13.73 ± 5.44, mean±SEM, P<0.01) compared to their age-matched wild type mice. However, there were no significant differences in islet size and whole islet cell number between 11-month *PolgA*$^{mut/mut}$ and wild type mice. In addition, endurance exercise didn't have significant impact on cell composition indexes when exercise versus sedentary *PolgA*$^{mut/mut}$ mice were compared.

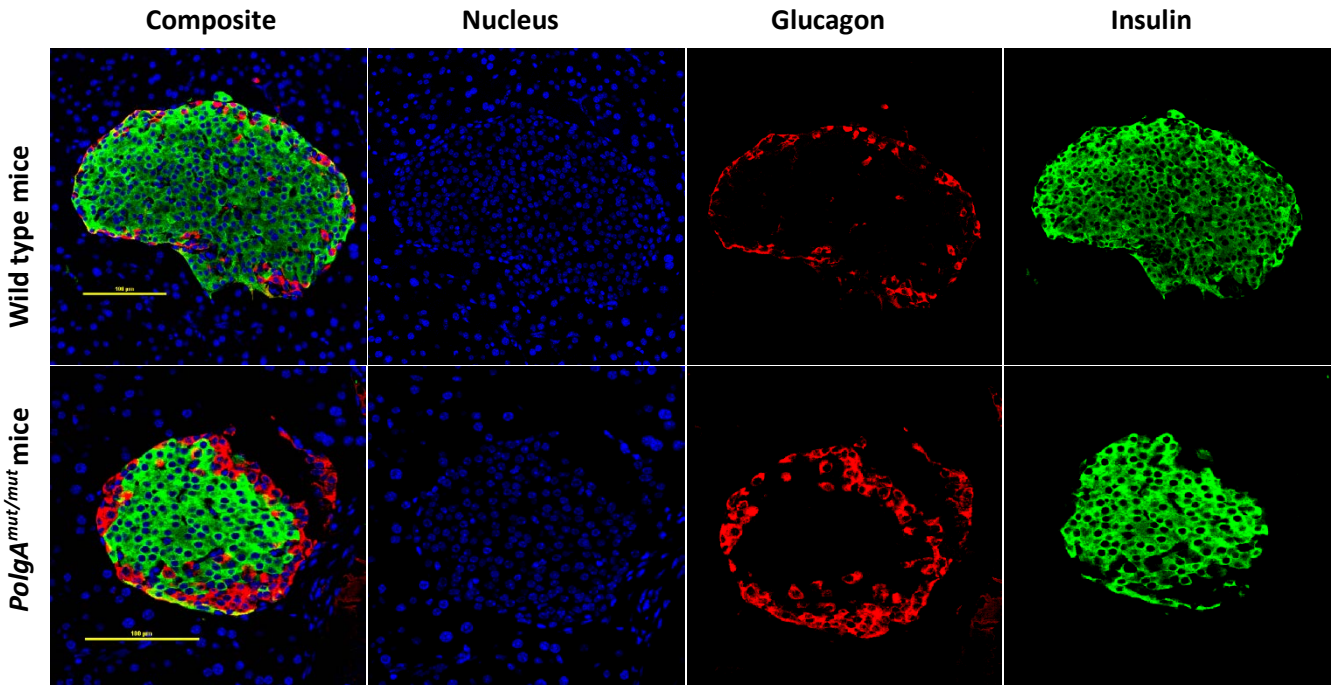

Figure 4-4. The separate and composite triple immunofluorescence staining images for endocrine hormones in pancreatic islets from 11-month mice. (Top) wild type mice; (Bottom) *PolgA*$^{mut/mut}$ mice. DAPI stain for nucleus; Glucagon stain for α-cells, Alexa fluor 568; Insulin stain for β-cells, Alexa fluor 488. Pictures were all taken by A1 confocal with 20 times magnification. Scale bar, 100μm.

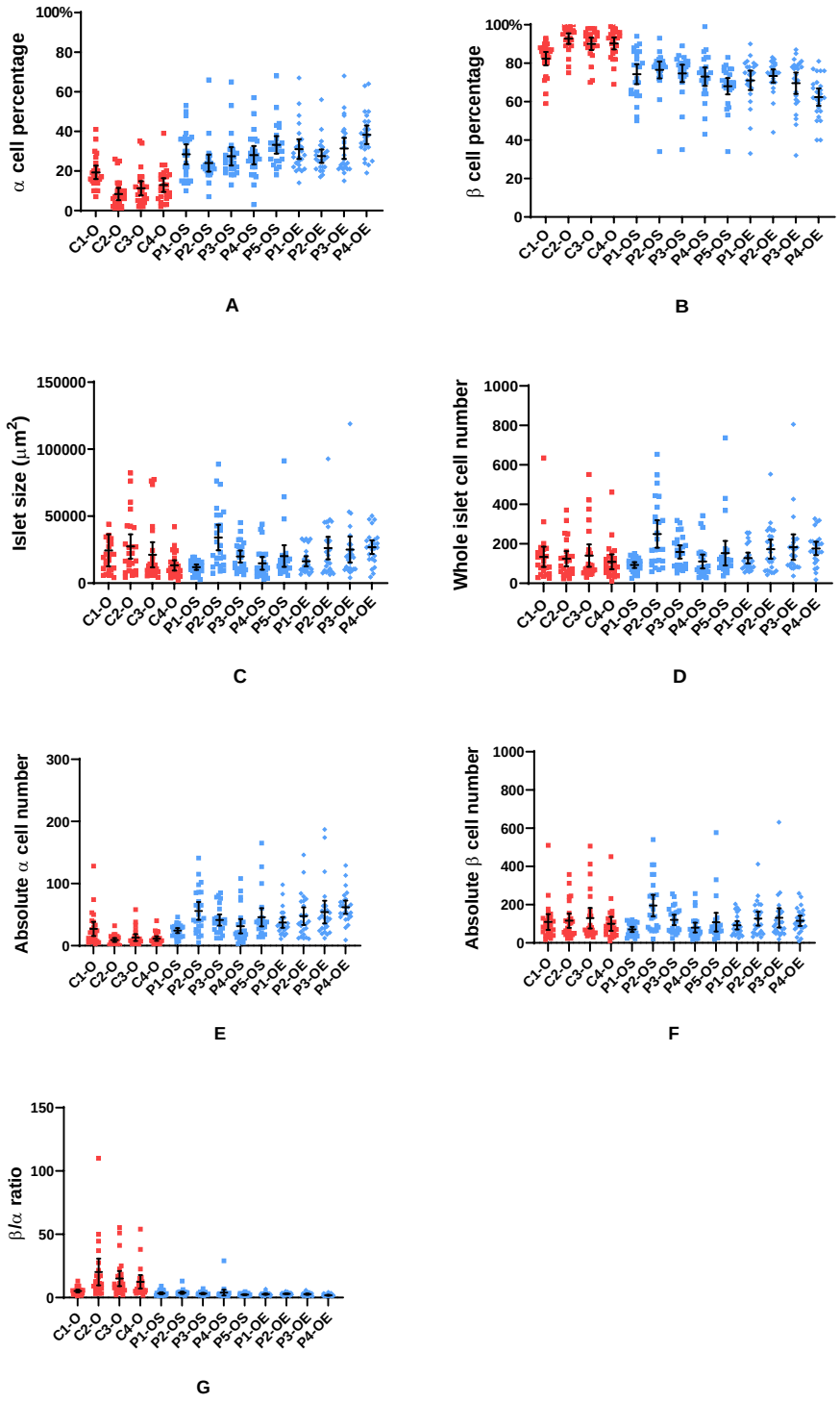

Figure 4-5. Islet cell composition summary in 11 month sacrificed mice. Data are presented as mean ± 95% CI. In all graphs, wild type mice (C1-O to C4-O); *PolgA*$^{mut/mut}$ sedentary mice (P1-OS to P5-OS); *PolgA*$^{mut/mut}$ exercise mice (P1-OE to P4-OE). 25 islets were studied per mouse and each dot represents one islet in the above graph. (A) α-cell percentage; (B) β-cell percentage; (C) Islet size; (D) Whole islet cell number; (E) Absolute α-cell number; (F) Absolute β-cell number; (G) β/α ratio.

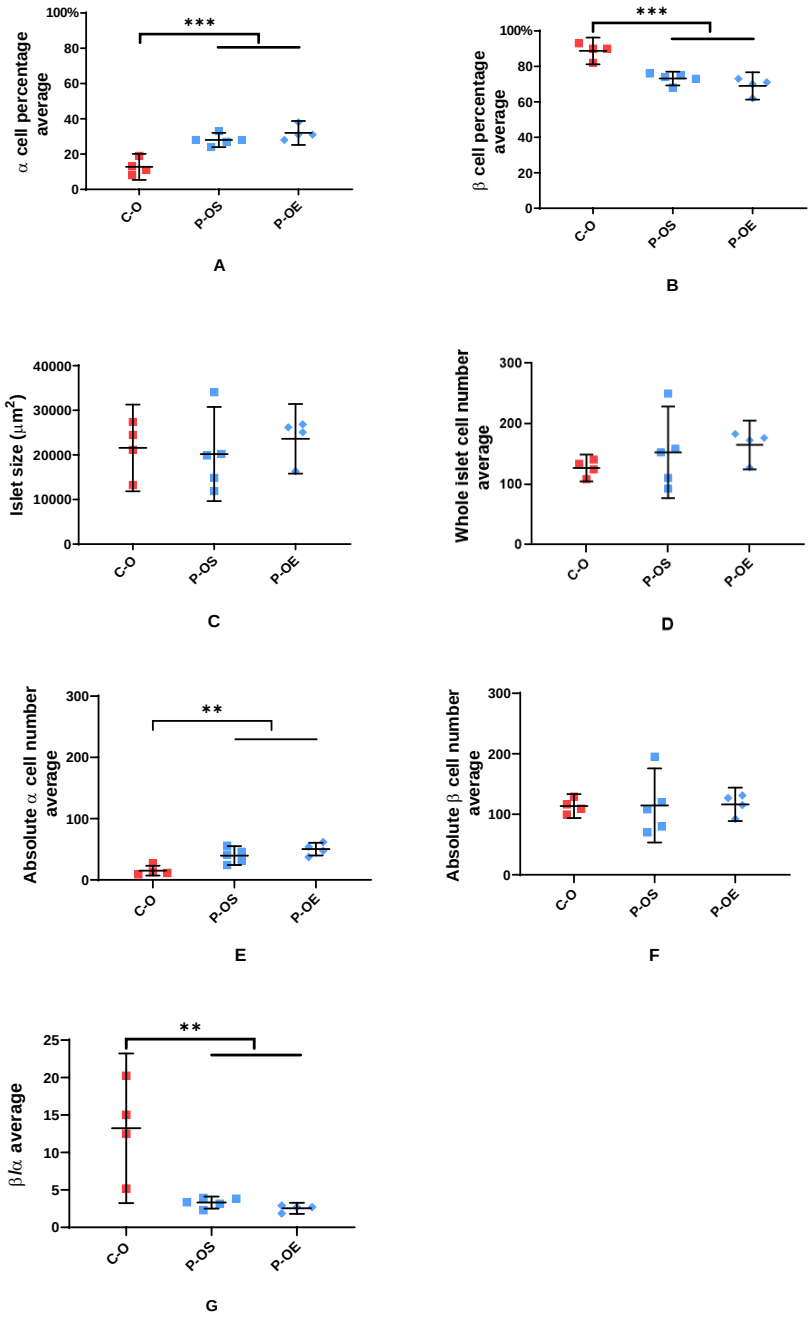

Figure 4-6. Average value of islet cell composition summary in 11 month sacrificed mice. Data are presented as mean ± 95% CI. In all graphs, wild type mice (C-O); *PolgA*$^{mut/mut}$ sedentary mice (P-OS); *PolgA*$^{mut/mut}$ exercise mice (P-OE). One dot represents the average value of 25 islets from each case. **(A) Average α-cell percentage.** Unpaired t-test between wild type and *PolgA*$^{mut/mut}$ mice, p<0.001; unpaired t-test between *PolgA*$^{mut/mut}$ sedentary and exercise, p>0.05. **(B) Average β-cell percentage.** Unpaired t-test between wild type and *PolgA*$^{mut/mut}$ mice, p<0.001; unpaired t-test between *PolgA*$^{mut/mut}$ sedentary and exercise, p>0.05. **(C) Average islet size.** Unpaired t-test, p>0.05; **(D) Average whole islet cell number.** Unpaired t-test, p>0.05; **(E) Average absolute α-cell number.** Unpaired t-test between WT and *PolgA*$^{mut/mut}$ mice, p<0.01; unpaired t-test between *PolgA*$^{mut/mut}$ sedentary and exercise, p>0.05. **(F) Average absolute β-cell number.** Unpaired t-test, p>0.05. **(G)Average β/α ratio.** Unpaired t-test between WT and *PolgA*$^{mut/mut}$ mice, p<0.01; unpaired t-test between *PolgA*$^{mut/mut}$ sedentary and exercise, p>0.05. **p<0.01. ***p<0.001.

4.3.3. Islet size, whole islet cell number and absolute β-cell number all increased significantly in wild type mice from 3-month to 11-month.

After I finished the comparison between genotypes at both ages, we analyzed the impact of ageing on pancreatic cell composition from 3 months to 11 months within each genotype. Looking at the wild-type mice first, the individual islet data are shown in ***Figure 4-7***. ***Figure 4-8*** shows the mean values for each animal and unpaired t-test was used for intergroup analysis. It is evident that the 11 month old wild type mice had significantly greater islet size (21570.8 ± 6098.73 vs 11494.58 ± 3620.20, mean±SEM, $P<0.05$), greater whole islet cell number (126.92 ± 13.98 vs 70.41 ± 12.82, mean±SEM, $P<0.01$), greater absolute β-cell number (113.71 ± 12.44 vs 56 ± 13.56, mean±SEM, $P<0.001$) and a higher β/α ratio (13.73 ± 5.44 vs 5.41 ± 1.94, mean±SEM, $P<0.05$) compared with the 3 month wild type mice.

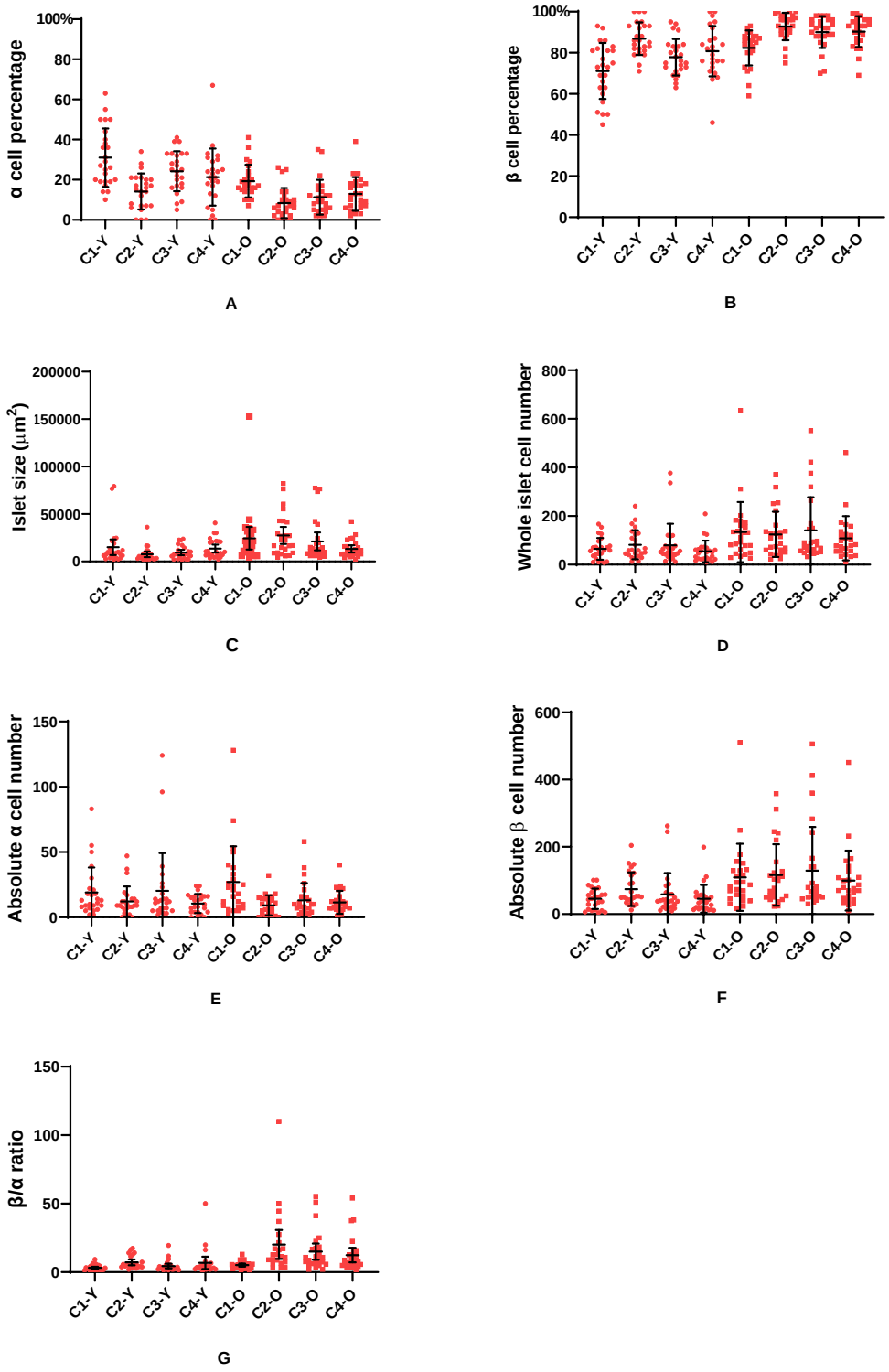

Figure 4-7. The islet cell composition comparison between two different ages in wild type mice. Data are presented as mean ± 95% CI. In all graphs, young mice (C1-Y to C4-Y); old mice (C1-O to C4-O). 25 islets were studied per mouse and each dot represents one islet in the above graph. (A) α-cell percentage; (B) β-cell percentage; (C) Islet size; (D) Whole islet cell number; (E) Absolute α-cell number; (F) Absolute β-cell number; (G) β/α ratio.

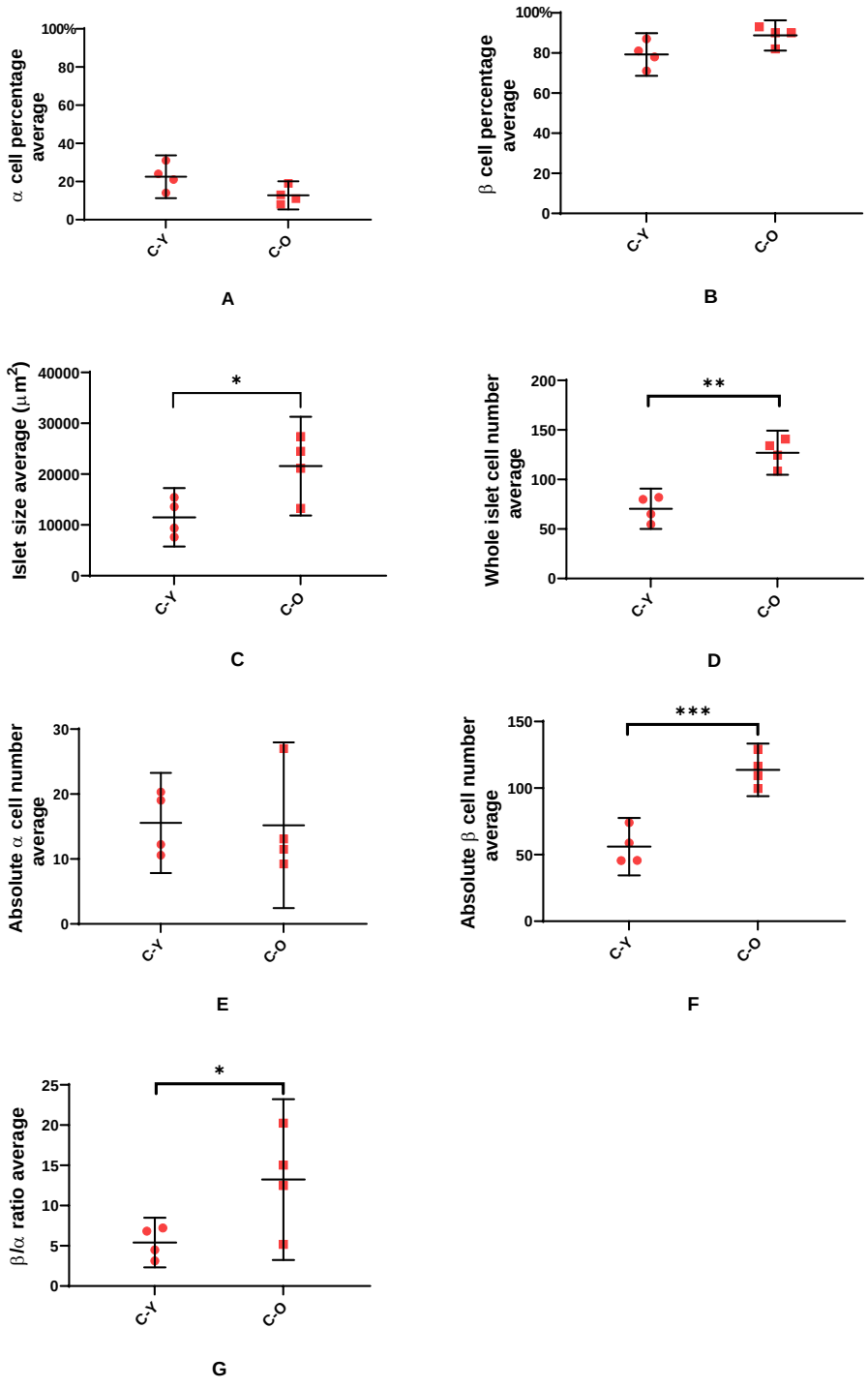

Figure 4-8. Average value of islet cell composition summary in wild type mice between two different ages. Data are presented as mean ± 95% CI. Young mice (C-Y); Old mice (C-O). One dot represents the average value of 25 islets from each case. (A) Average α-cell percentage. Unpaired t-test, p>0.05; (B) Average β-cell percentage. Unpaired t-test, p>0.05; (C) Average islet size. Unpaired t-test, p<0.05; (D) Average whole islet cell number. Unpaired t-test, p<0.01; (E) Average absolute α-cell number. Unpaired t-test, p>0.05; (F) Average absolute β-cell number. Unpaired t-test, p<0.001. (G) Average β/α ratio. Unpaired t-test, p<0.05. *p<0.05. **p<0.01. ***p<0.001

4.3.4. Islet size, whole islet cell number, absolute α and β cell number all increased significantly in *PolgA*$^{mut/mut}$ mice from 3-month to 11-month.

I then compared young and old *PolgA*$^{mut/mut}$ mice. ***Figure 4-9*** shows the individual islet data while ***Figure 4-10*** shows the mean values for each animal. From the staining images and the data analysis, I can conclude that 11-month *PolgA*$^{mut/mut}$ mice have significantly greater islet size (21714.91 ± 6956.9 vs 10276.02 ± 1707.79, mean±SEM, $P<0.01$), greater whole islet cell number (158.23 ± 46.33 vs 70.26 ± 11.29, mean±SEM, $P<0.01$), greater absolute α cell number (44.41 ± 12.14 vs 17.45 ± 5.96, mean±SEM, $P<0.01$) and greater absolute β cell number (115.46 ± 36.47 vs 53.25 ± 5.75, mean±SEM, $P<0.01$). However, the β/α ratio (2.97 ± 0.67 vs 4.16 ± 0.66, mean±SEM, $P<0.05$) was lower in the 11-month compared to the 3-month *PolgA*$^{mut/mut}$ mice.

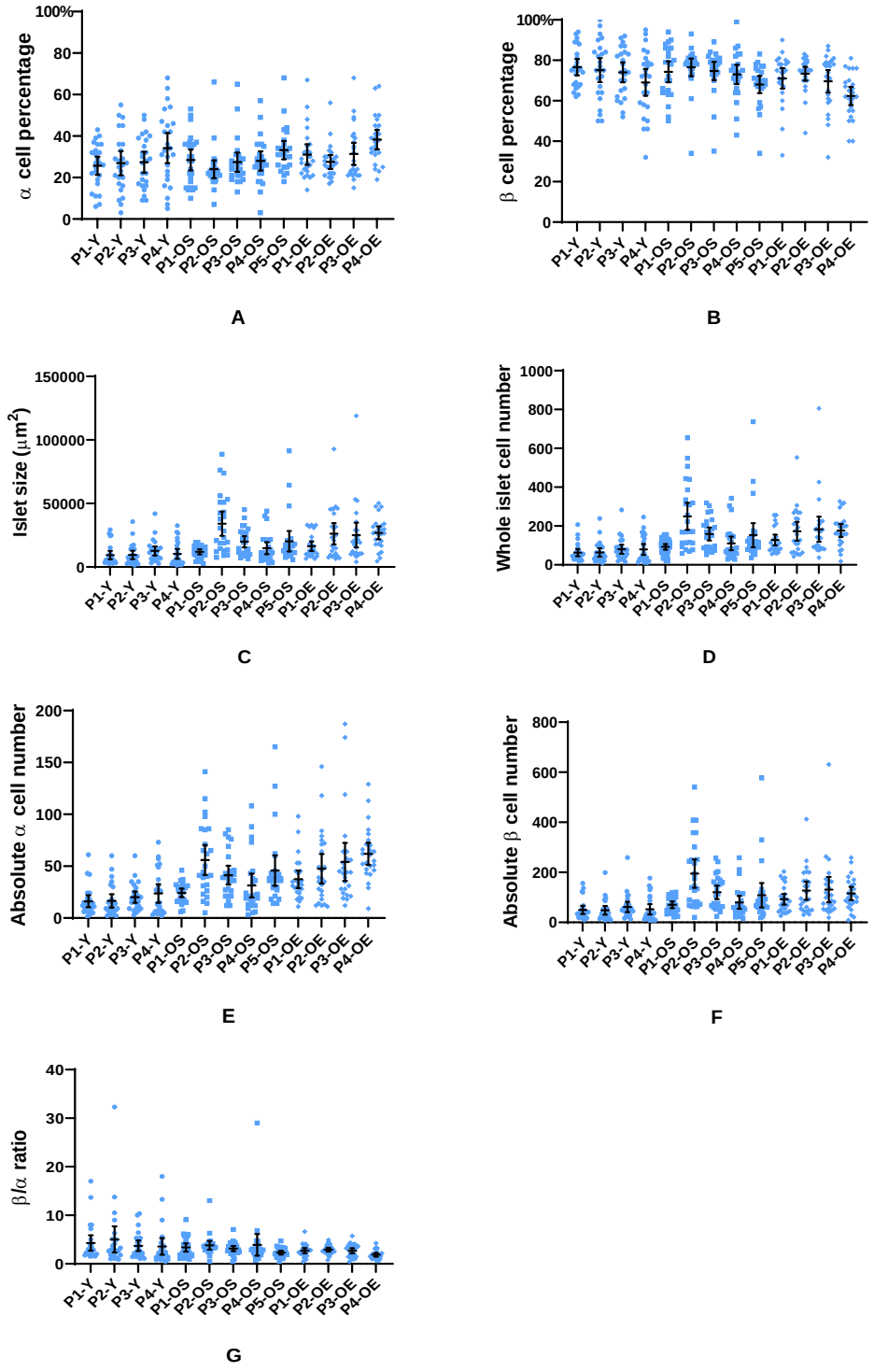

Figure 4-9. The islet cell composition comparison between two different ages in *PolgA*$^{mut/mut}$ mice. Data are presented as mean ± 95% CI. In all graphs, young *PolgA*$^{mut/mut}$ mice (P1-Y to PY-4); old *PolgA*$^{mut/mut}$ sedentary mice (P1-OS to P5-OS); old *PolgA*$^{mut/mut}$ exercise mice (P1-OE to P4-OE). 25 islets were studied per mouse and each dot represents one islet in the above graph. (A) α-cell percentage; (B) β-cell percentage; (C) Islet size; (D) Whole islet cell number; (E) Absolute α-cell number; (F) Absolute β-cell number; (G) β/α ratio.

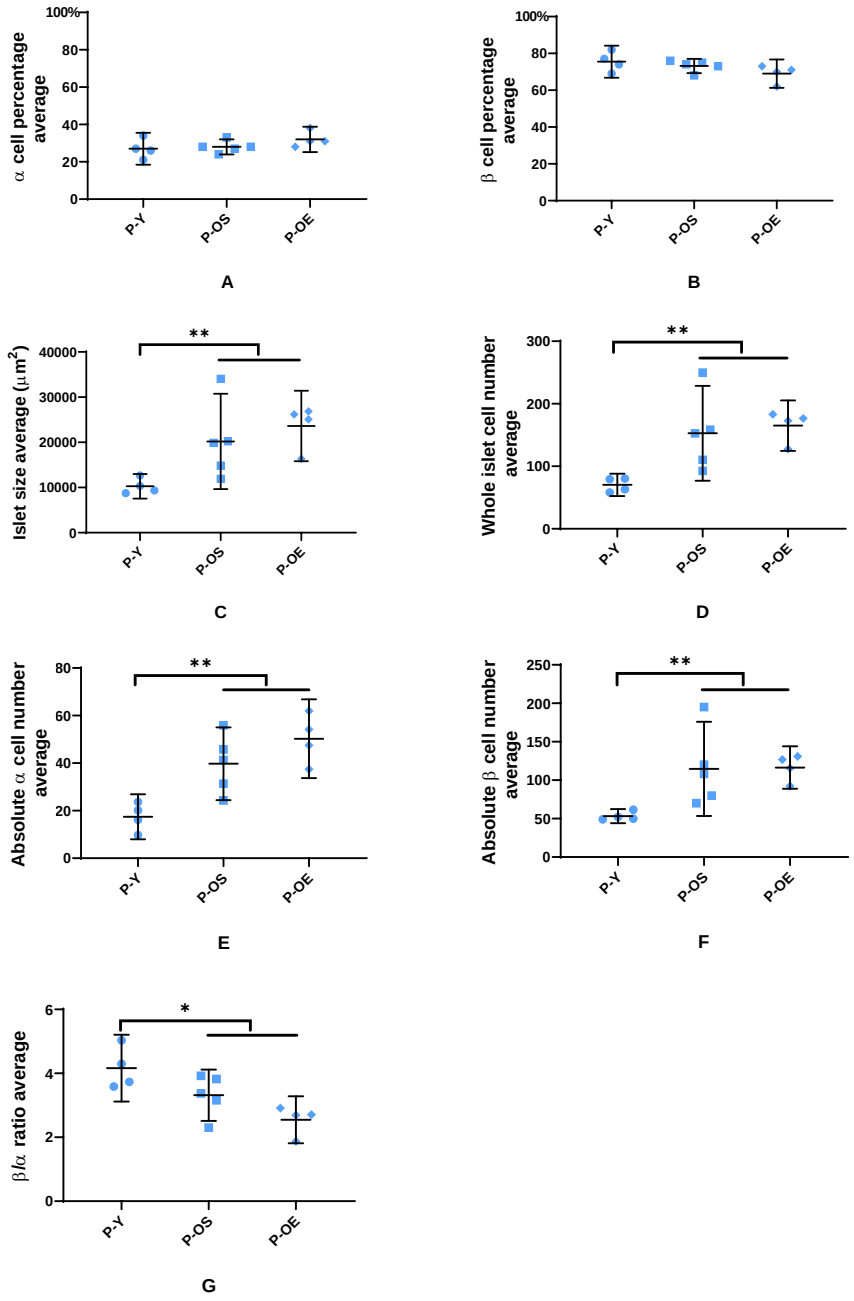

Figure 4-10. Average value of islet cell composition summary in *PolgA*$^{mut/mut}$ mice between two different ages. Data are presented as mean ± 95% CI. Young *PolgA*$^{mut/mut}$ mice (P-Y); old *PolgA*$^{mut/mut}$ sedentary mice (P-OS); old *PolgA*$^{mut/mut}$ exercise mice (P-OE). One dot represents the average value of 25 islets from each case. **(A) Average α-cell percentage.** Unpaired t-test, p>0.05; **(B) Average β-cell percentage.** Unpaired t-test, p>0.05; **(C) Average islet size.** Unpaired t-test between young and old *PolgA*$^{mut/mut}$ mice, p<0.01; Unpaired t-test between *PolgA*$^{mut/mut}$ sedentary and exercise, p>0.05. **(D) Average whole islet cell number.** Unpaired t-test between young and old *PolgA*$^{mut/mut}$ mice, p<0.01; Unpaired t-test between *PolgA*$^{mut/mut}$ sedentary and exercise, p>0.05. **(E) Average absolute α-cell number.** Unpaired t-test between young and old *PolgA*$^{mut/mut}$ mice, p<0.01; Unpaired t-test between *PolgA*$^{mut/mut}$ sedentary and exercise, p>0.05. **(F) Average absolute β-cell number.** Unpaired t-test young and old *PolgA*$^{mut/mut}$ mice, p<0.01; Unpaired t-test between *PolgA*$^{mut/mut}$ sedentary and exercise, p>0.05. **(G) Average β/α ratio.** Unpaired t-test young and old *PolgA*$^{mut/mut}$ mice, p<0.05; Unpaired t-test between *PolgA*$^{mut/mut}$ sedentary and exercise, p>0.05. *p<0.05. **p<0.01.

4.3.5. The overall comparison between *PolgA*$^{mut/mut}$ and WT mice in two different ages.

In the end of the islet cell composition analysis, data from two different types of mice in two different age groups were put together for the final analysis ***Figure 4-11***. It can be concluded that islet size and whole islet cell number both increase significantly with age in wild type and *PolgA*$^{mut/mut}$ mice. In wild type mice, only absolute β-cell number significantly increase from 3-month age to 11-month age, contributing to the increase of islet size and whole islet cell number. However, both absolute α- and β-cell number significantly increase in 11-month *PolgA*$^{mut/mut}$ mice compared to their young controls. As a consequence, the β/α cell ratio increases from 5.41 ± 1.94 to 13.73 ± 5.44 (mean ± SEM) with age in the wild type mice because of the absolute increase in β-cells. It conversely decreases from 4.16 ± 0.66 to 2.97 ± 0.67 (mean ± SEM) with age in the *PolgA*$^{mut/mut}$ mice due to the significantly increase of α-cells (***Table 4- 1***).

Table 4- 1. The β/α ratio in wild type and *PolgA*$^{mut/mut}$ mice at two different ages.

β/α ratio	WT	*PolgA*$^{mut/mut}$
3-month	5.41 ± 1.94	4.16 ± 0.66
11-month	13.73 ± 5.44	2.97 ± 0.67

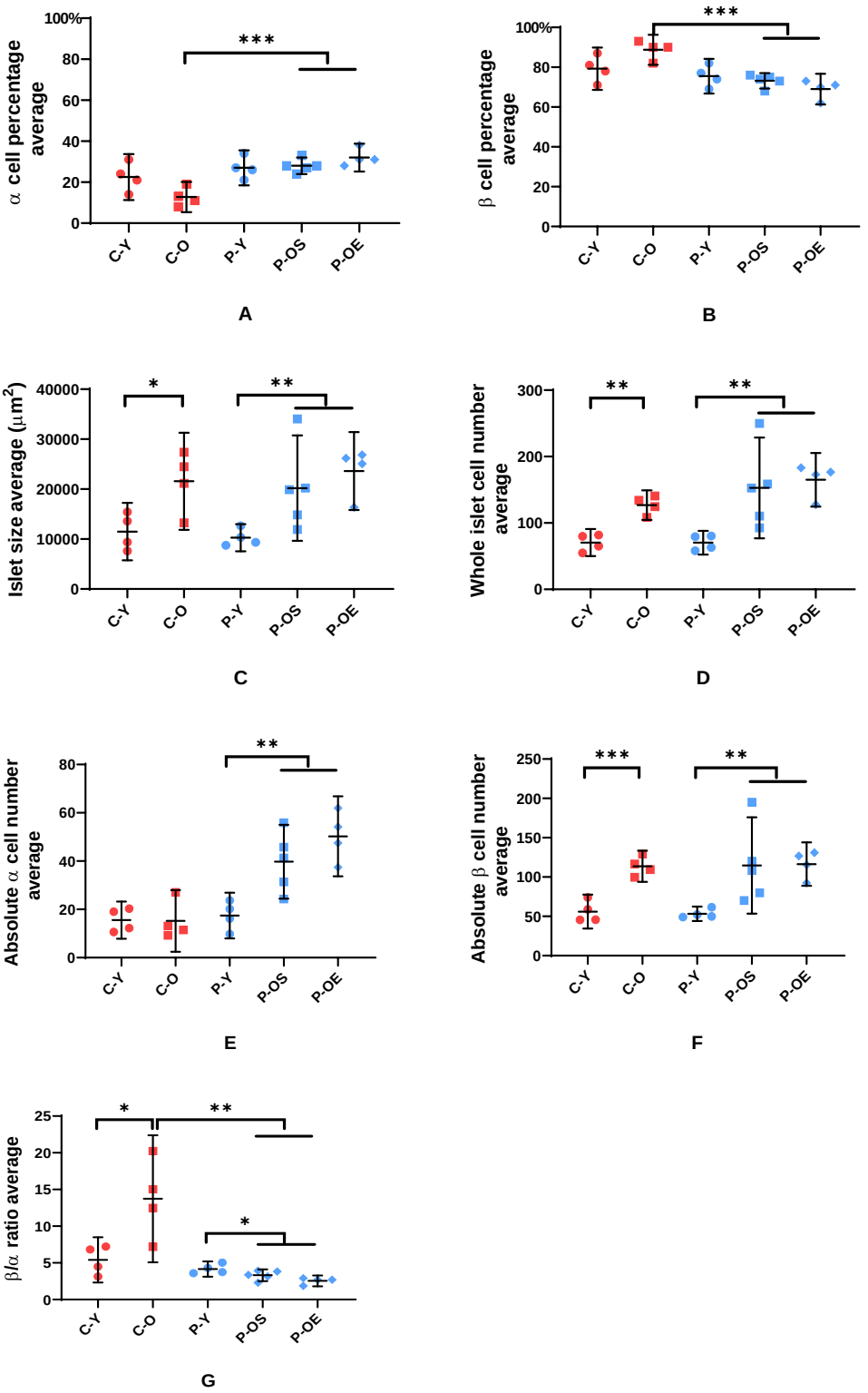

Figure 4-11. The comparison of islet cell composition in two different mice groups in two different age. Data are presented as mean ± 95% CI. In all graphs, young wild type mice (C-Y); Young *PolgA*$^{mut/mut}$ mice (P-Y); Old wild type mice (C-O); Old *PolgA*$^{mut/mut}$ sedentary mice (P-OS); Old *PolgA*$^{mut/mut}$ exercise mice (P-OE). *p<0.05. **p<0.01. ***p<0.001.

4.4. Summary

1. There is no significant difference in β- and α-cell percentage, islet size and whole islet cell number between 3-month *PolgA*$^{mut/mut}$ sedentary mice and age-matched wild type mice.

2. *PolgA*$^{mut/mut}$ mice had a significantly lower β-cell percentage, higher α-cell percentage, higher absolute α-cell number and lower β/α ratio versus their wild type controls at 11 months. There is no significant difference in islet size and whole islet cell number between 11-month *PolgA*$^{mut/mut}$ and wild type mice. In addition, there was no significant difference between *PolgA*$^{mut/mut}$ exercise and sedentary mice.

3. 11-month wild type mice have significantly bigger islet size, higher whole islet cell number, higher absolute β-cell number and higher β/α ratio compared to the 3-month wild type mice. However, there was no significant difference in α- and β-cell percentage between different ages in wild type mice.

4. 11-month *PolgA*$^{mut/mut}$ mice have significantly bigger islet size, higher whole islet cell number, higher absolute α- and β-cell number, lower β/α ratio compared to the 3-month *PolgA*$^{mut/mut}$ mice. However, there is no significant difference in α- and β-cell percentage between different ages in *PolgA*$^{mut/mut}$ mice.

4.5. Discussion

I started this part of study from 3-month *PolgA*$^{mut/mut}$ and wild type mice. It was found out that there was no significant difference in any of the islet cell indexes between 3-month *PolgA*$^{mut/mut}$ and wild type mice. The same comparisons were made for *PolgA*$^{mut/mut}$ and wild type mice at 11 months. It was reported for the first time in my study that 11-month pancreatic islets of this accelerated ageing mouse model have significantly higher α-cell percentage, lower β-cell percentage, higher absolute α-cell number and lower β/α ratio compared to their age-matched wild type control mice. Islets of wild type and *PolgA*$^{mut/mut}$ mice both changed significantly from 3 months to 11 months. In the two mice groups, islet size and whole islet cell number both significantly increased from 3 months to 11 months. Absolute β-cell number significantly increased in wild type mouse islets from 3 months to 11 months but there was no increase in α-cell number with age in wild type mice. This is in line with findings from previous studies that in normal mice or rats, the increment and replication of islet endocrine cells with ageing is selective for β-cells, while the growth of endocrine non-β-cells was limited to the initial stage of life (Montanya, Nacher et al. 2000, Poy, Hausser et al. 2009, Feng, Xiang et al. 2017). As a consequence, β/α ratio significantly increased with age in normal mice. However, the 11-month *PolgA*$^{mut/mut}$ mouse islets have a significantly higher absolute α- and β-cell number. The fold change of α-cells is higher compared to that of β-cells in *PolgA*$^{mut/mut}$ mice at 11 months, resulting in a lower β/α ratio compared to the 3-month *PolgA*$^{mut/mut}$. One previous study on isolated human and mice islets showed that the average β/α ratio for wild type mice aged 6 weeks was 7.46. This number was 4.24 in human donors aged between 25-45 years (Kharouta, Miller et al. 2009). Another study calculated that average β/α ratio for wild type mice aged between 20 to 23 weeks was around 10 (Mehta, Fine et al. 2016). These data are all in line with β/α ratio I achieved in my study (***Table 4-* 1**). In a previous β-cell specific TFAM-knock out mutant mice model, a comparable decrease in the islet β/α cell ratio was observed with age. However, this appeared to result from a decrease in β-cell mass rather than a specific increase in α-cell mass (Silva, Köhler et al. 2000).

The changes of islet cell composition in wild type and *PolgA*$^{mut/mut}$ mice in two age groups are shown schematically in ***Figure 4-12*** below.

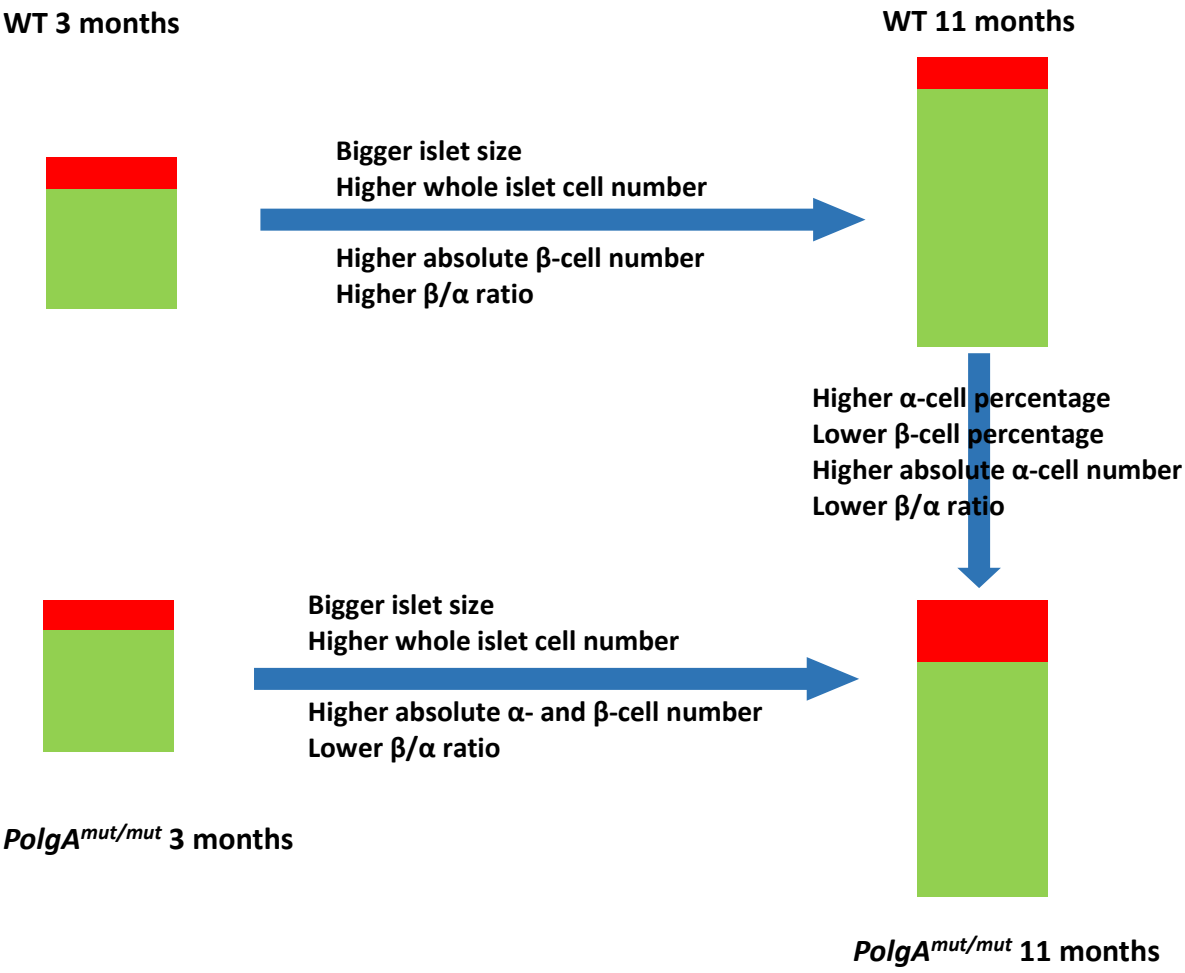

Figure 4-12. Schematic representation of the change of islet cell composition in wild type and *PolgA*$^{mut/mut}$ mice in two age groups. The whole block represents an islet. Red blot represents α-cell mass and green blot represents β-cell mass.

Previous investigation of the Lewis rat model indicated that, β-cell mass increased throughout the lifespan in the normal animal and it was closely correlated with the age-related increase in the body weight (Montanya, Nacher et al. 2000). The mass of β-cell can be modified to maintain normoglycemia and homeostasis when there is an increment in metabolic demand caused by ageing, obesity and pregnancy. In the young rats, both hypertrophy and hyperplasia of β-cells are contributing to increased β-cell mass but mainly β-cell hypertrophy was responsible for increased β-cell mass in old rats (Swenne 1983). Another study by Swenne and Andersson (Swenne and Andersson 1984) found out β-cell replication declines from 3 to 9 months of age in C57BL/6 mice. These facts indicate that although β-cell replication maintained throughout lifespan, it is reducing with ageing but it doesn't fall to 0 even in the late stage of life (Montanya, Nacher et al. 2000). These above studies gave a possible explanation about the increase of absolute β-cell number in wild type mice islets from 3 months to 11 months of age in our study.

As discussed in chapter 3, I also discovered that endurance exercise didn't have significant positive impact on islet cell composition in *PolgA*$^{mut/mut}$ mice islets. The impact of exercise on wild type mice islet was unknown because I didn't exercise my wild type mice. One previous study about the exercise on pancreatic islet in revealed that there was no significant difference in islet cell composition between the sedentary and exercised control rats (Rawal, Huang et al. 2013).

In this chapter, *PolgA*$^{mut/mut}$ mice were found to have a significantly lower β-cell percentage, higher α-cell percentage and higher absolute α-cell number compared to their wild type controls at 11 months. I want to further discover the potential drivers and mechanisms underlying changes in islet cell composition in the *PolgA*$^{mut/mut}$ mice.

CHAPTER 5. THE STUDY OF ENDOCRINE CELL SUBTYPES IN *POLGA*$^{MUT/MUT}$ MICE COMPARED TO AGE-MATCHED WILD TYPE MICE.

5.1. Introduction

As we know, pancreatic islets are mainly composed of α- and β-cells. Although α- and β-cells have similar embryonic origins and are equally exposed to metabolic and oxidative stress during the ageing process, they have different stress-induced response and final fates. It was reported by many studies before that β-cells are more prone to progress to apoptosis status or loss their cell identities compared to α-cells due to the metabolic and oxidative stress in the evolution of T1D and T2D compared to α -ells (Marroqui, Masini et al. 2015). Although I have already studied the mitochondrial complex expression in whole islets of *PolgA*$^{mut/mut}$ and wild type mice at 3 and 11 months of age, I wondered whether the different endocrine subtype cells show the same patterns of mitochondrial subunit expression in response to natural ageing and accelerated ageing in the *PolgA*$^{mut/mut}$ mice model. This level of analysis has never been done by any previous study, so my study has been the first one to study mitochondrial complex expression of different cell subtypes in pancreatic islets.

As summarized in chapter 4, 11-month *PolgA*$^{mut/mut}$ mice had significantly higher absolute α-cell number compared to the age-matched controls but there was no significant difference in absolute β-cell number between mice groups. It is reasonable to deduce that the significant increase of absolute α-cells of *PolgA*$^{mut/mut}$ compared to age-matched controls might be caused by the different response of endocrine α-cells towards the impact of ageing.

In order to study islet cell proliferation, I stained the islets for Ki67 proliferation marker. Ki67 is a nuclear protein, which is absent in resting phase of cell cycle (G_0) but present during the active phases of the cell cycle. Therefore, it is able to mark cells that undergo proliferating process (Gerdes, Schwab et al. 1983, Scholzen and Gerdes 2000, Perl, Kushner et al. 2010). In many cases, it was used in diagnosis of human tumours, such as prostate and breast cancer (Bettencourt, Bauer et al. 1996, Stattin, Damber et al. 1997).

The aims of the current chapter were to:

Study the potential drivers and mechanisms underlying changes in islet cell composition in the *PolgA*$^{mut/mut}$ mouse.

It can be further separated into following aims:

1. Study the driving factors behind the change of pancreatic cell composition in 11- month *PolgA*$^{mut/mut}$ mice.
2. Study the mitochondrial respiratory subunit expression in different islet cell subtypes.
3. Investigate the insulin expression in pancreatic β-cells from mtDNA mutator mice and age-matched wild type mice at two different ages.
4. Study the progression and endpoint values of blood weight, blood glucose level and blood HbA1c in *PolgA*$^{mut/mut}$ and wild type mice from 5-month age to 11-month age.

5.2. Methods

5.2.1. Mitochondrial complex expression analysis in different islet cell subtypes.

The mean signal intensity of mitochondrial complex expression in β-cells can be acquired directly from NIS-element analysis software by locating the insulin staining area. As for α-cell analysis, either mathematical method or drawing around method can be used to acquire the mean signal intensity of mitochondrial complex expression. The detailed analysis steps are in method chapter 2.3.4.3.

5.2.2. Proliferation assay immunofluorescence staining.

Quadruple immunofluorescence staining protocol was used for studying the cell proliferation in islets. Ki67, glucagon and insulin stains were excited under FITC, TRITC and Alexa fluor 647 separately. Stained sections were mounted with nuclei staining DAPI. After staining, 40 islets were counted for each case. I calculated the number of Ki67 (+) islets and divided it by the number of all islets in each case and generated a ratio of Ki67 (+) islet. I further calculated the number of islets with Ki67 (+) α-cells and Ki67 (+) β-cells and divided them by the number of all islets in each case, generating a ratio of islets with Ki67 (+) stained α-cells and a ratio of islets with Ki67 (+) β cells. Graphpad prism was used to generate graphs and different analysis.

5.2.3. Monthly blood glucose and body weight measurement.

Every month, after measuring mouse weight, I used Alphatrak glucometer (Abbott Laboratories) to determine blood glucose concentrations. This monthly blood glucose measurement started from March 2019 and stopped in September 2019 when these mice reached age of 11 months individually.

5.2.4. Endpoint HbA1c measurement.

For quantitatively determination of hemoglobin A1c (HbA1c) in mouse whole blood, an Elisa kit was used in my study (Crystal Chem, Cat 80310, USA). The detailed protocol was explained in method chapter 2.7.3.4.

5.3. Results

5.3.1. Increased α-cell proliferation in islets of 11-month *PolgA$^{mut/mut}$* mice compared to the age-matched wild type mice.

In my study, a triple immunofluorescence staining of Ki67, insulin and glucagon was applied to islets from 4 *PolgA$^{mut/mut}$* mice and 4 age-matched wild type mice. ***Figure 5-1*** and ***Figure 5-2*** are representative staining images from 11-month-old *PolgA$^{mut/mut}$* mice and age-matched wild type mice. Yellow arrows point out dividing cells with Ki67 stained nuclei. In order to compare the difference in number of Ki67 marked proliferating cells between wild type and *PolgA$^{mut/mut}$* mice, I stained and calculated at least 40 islets for each mouse case. I calculated the number of Ki67 (+) islets, number of islets with Ki67 (+) α-cells , number of islets with Ki67 (+) β-cells and number of all islets in each case (***Table 5-1***). Mean percentage of islets per case with ≥1 Ki67 (+) cells in *PolgA$^{mut/mut}$* and wild type mice was generated. It can be seen in ***Figure 5-3*** that 11-month-old *PolgA$^{mut/mut}$* mice have significantly higher Ki67 (+) stained islets (24.24% ± 7.01% vs 7.62% ± 6.02%, mean ± SEM, $P<0.05$) compared to the age-matched wild type mice.

The distribution of Ki67 (+) stained nuclei differs between different mouse genotypes. By simply doing an eyeball test between groups, Ki67(+) stained nuclei are more likely locating in α-cells in *PolgA$^{mut/mut}$* mice group, whereas Ki67(+) staining is more likely to exist in β-cells in wild type mice group. So apart from calculating the mean percentage of islets per case with ≥1 Ki67(+) cells, I further calculated the mean percentage of islets with Ki67 (+) stained α-cells and Ki67 (+) β-cells in both mice groups and generated mean percentages of islets per case with ≥1 Ki67(+) α-cells and with ≥1 Ki67(+) β-cells. Result are shown in the ***Figure 5-3.*** It can be seen that 11-month-old *PolgA$^{mut/mut}$* mice have significantly higher mean percentage of islets with ≥1 Ki67(+) α-cells compared to the age-matched wild type mice (16.2% ± 7.3% vs 2.2% ± 3.1%, mean±SEM, $P<0.05$). Conversely, there was no significant difference in mean percentage of islets with ≥1 Ki67 (+) β-cells between *PolgA$^{mut/mut}$* and age-matched wild type mice (8.1% ± 1.6% vs 7.0% ± 5.1%, mean±SEM, $P>0.05$). Based on the above analysis, I found

evidence of increased α-cell proliferation in islets from 11-month *PolgA*$^{mut/mut}$ mice compared to the age-matched wild type mice.

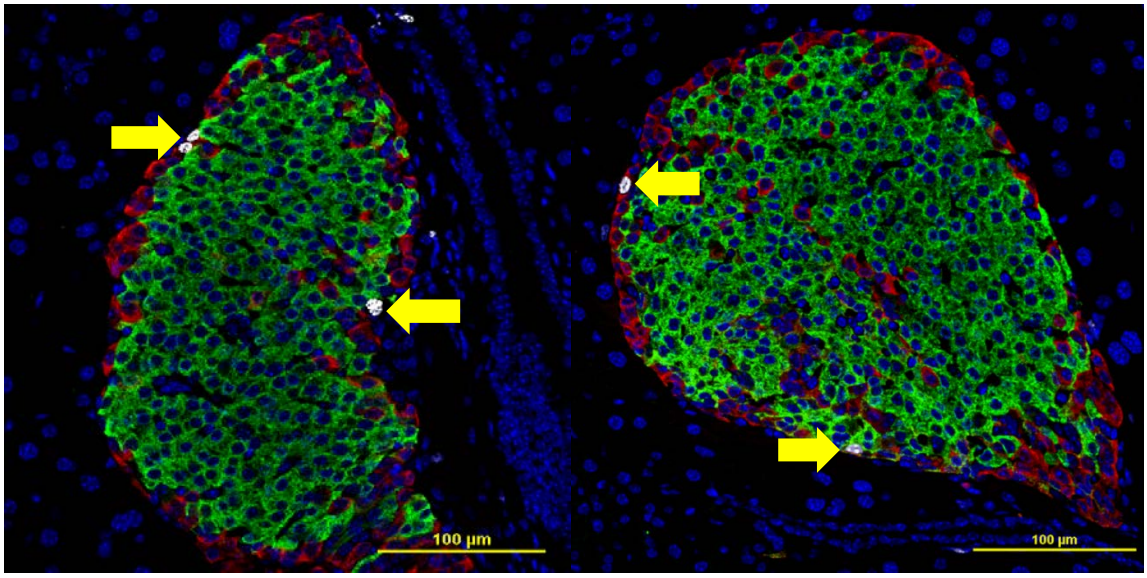

Figure 5-1. Representative image from 11 month old *PolgA*$^{mut/mut}$ mice. (left) LG0005; (Right), LG0024. DAPI stain for nucleus (blue); Ki67 stain for proliferating cell nuclei, Alexa fluor 488 (white); Glucagon stain for α-cells, Alexa fluor 568 (red); Insulin stain for β-cells, Alexa fluor 647 (green). Yellow arrows point out the proliferating cell with Ki67(+) stained nuclei. It can be observed that these Ki67(+) stained cells are all α-cells in 11-month *PolgA*$^{mut/mut}$ mice. Pictures were all taken by A1 confocal with 20× magnification.

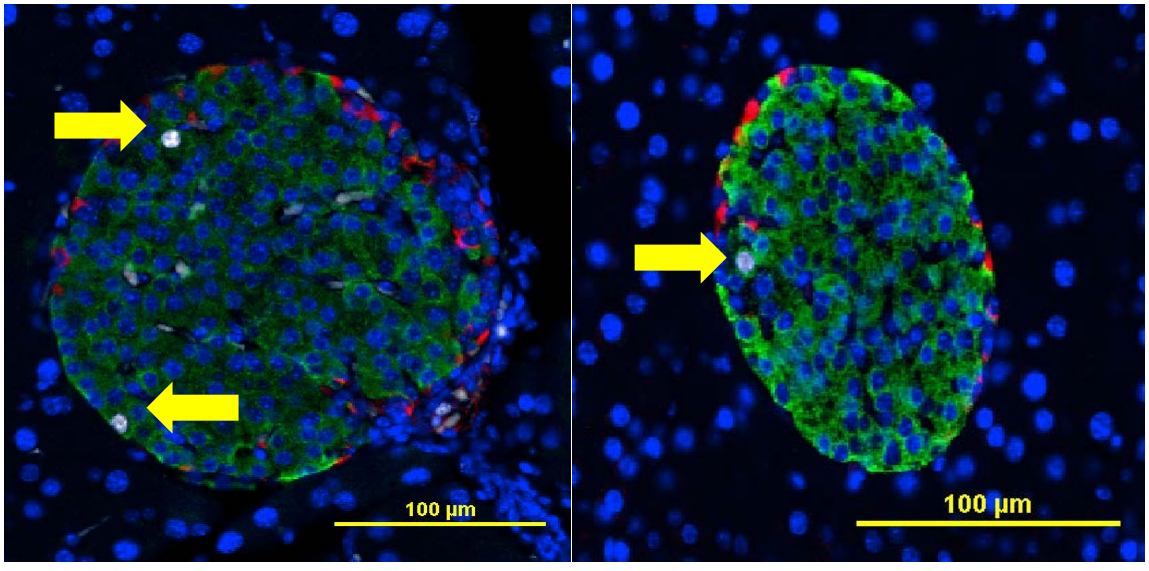

Figure 5-2. Representative image from 11-month wild type mice. (Left) GA0004; (Right) GA0007. DAPI stain for nucleus (blue); Ki67 stain for proliferating cell nuclei, Alexa fluor 488 (white); Glucagon stain for α-cells, Alexa fluor 568 (red); Insulin stain for β-cells, Alexa fluor 647 (green). Yellow arrows point out the proliferating cell with Ki67(+) stained nuclei. It can be observed that these Ki67(+) stained nuclei are mainly in β-cells of 11 month wild type mice islets. Pictures were all taken by A1 confocal with 20× magnification. Scale bar, 100µm.

Table 5-1. The number of Ki67 (+) islets in each mouse.

Case number	Label	No of Ki67(+) islets	No of islets with Ki67 (+) α-cells	No of islets with Ki67 (+) β-cells	No of islets counted
GA0004	WT1	6	1	5	41
GA0005	WT2	3	0	3	42
GA0007	WT3	0	0	0	42
GA0008	WT4	4	3	4	46
LG0005	PolG1	20	16	4	64
LG0024	PolG2	10	6	4	41
LG0032	PolG3	6	3	3	41
LG0037	PolG4	12	8	4	45

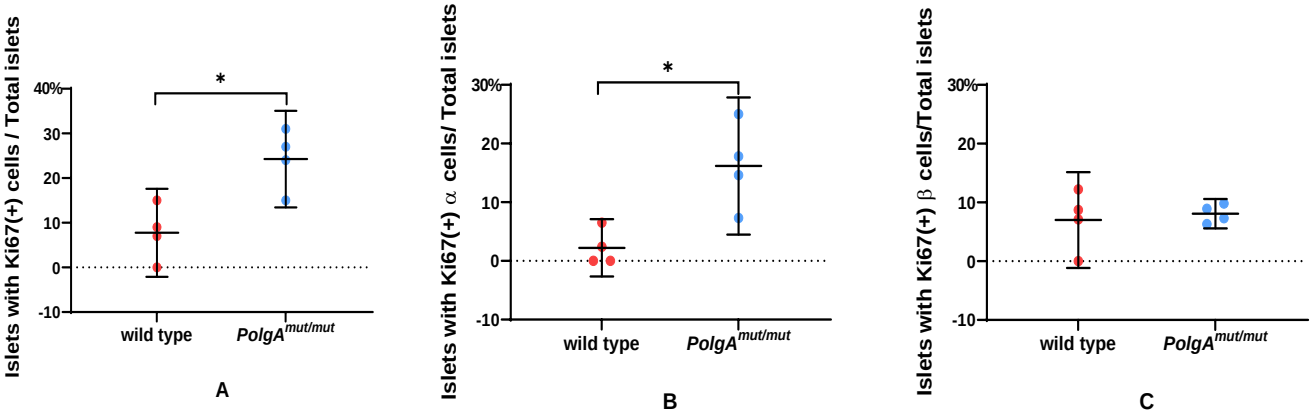

Figure 5-3. The comparison in ratio of Ki67 (+) islets between *PolgA*$^{mut/mut}$ and wild type mice groups. (A) Mean percentage of islets per case with ≥1 Ki67(+) cells in *PolgA*$^{mut/mut}$ and wild type mice. (B) Mean percentage of islets per case with ≥1 Ki67(+) α-cells in *PolgA*$^{mut/mut}$ and wild type mice. (C) Mean percentage of islets per case with ≥1 Ki67(+) β-cells in *PolgA*$^{mut/mut}$ and wild type mice. *p<0.05.

5.3.2. Endocrine cell sub-types react differently to normal ageing and premature ageing.

When I separately analyse the mitochondrial complex expression in α-and β-cells of WT and *PolgA*$^{mut/mut}$ islets at 11 months, significant differences were detected in mitochondrial complex expression between α-and β-cells. Again, 5 *PolgA*$^{mut/mut}$ mice and 5 WT mice were studied in this part and 50 islets were studied for each mouse. The results of mitochondrial mass marker and mitochondrial complex expression in α- and β- cells of *PolgA*$^{mut/mut}$ mice compared to α- and β-cells of WT mice islets are shown in ***Figure 5-4***. For comparative purposes, all data are expressed as z-scores relative to the β-cells in the wild type mice islets. I first compared mitochondrial subunit expression between α- and β-cell populations in islets of the old control mice. As shown in ***Figure 5-4***, Tomm20, Complex I and Complex IV expression levels were all lower in the α-cells compared with the β-cells in the old control islets (Unpaired t-test, all P<0.0001). The same pattern was seen when comparing α-cells with β-cells in the old *PolgA*$^{mut/mut}$ islets (Unpaired t-test, all P<0.001). I next compared mitochondrial complex expressions in β-cells from old *PolgA*$^{mut/mut}$ mice and their age-matched controls. There was a small decrease in Complex I (P<0.01), while Complex IV expression was markedly increased in the β-cells of the *PolgA*$^{mut/mut}$ mice (P<0.0001). The expression pattern was different for α-cells. There was a marked decrease in Complex I expression (P<0.0001) accompanied by a small increase Complex IV expression (P<0.001) in α-cells of the old *PolgA*$^{mut/mut}$ mice compared with the α-cells of the age-matched controls. To quantify the changing level of complex I and IV in α and β-cells of *PolgA*$^{mut/mut}$ mice, z-score expression of complex I was significantly lower in the *PolgA*$^{mut/mut}$ α-cells versus *PolgA*$^{mut/mut}$ β cells (-5.02±0.25 vs -0.65±0.23, mean ± SEM, p<0.0001), and z-score expression of complex IV was higher in the *PolgA*$^{mut/mut}$ β-cells versus *PolgA*$^{mut/mut}$ α-cells (2.84±0.53 vs -0.83±0.41, mean ± SEM, p<0.0001). These data show different patterns of mitochondrial subunit expression between pancreatic islet cell subtypes in this model of accelerated ageing.

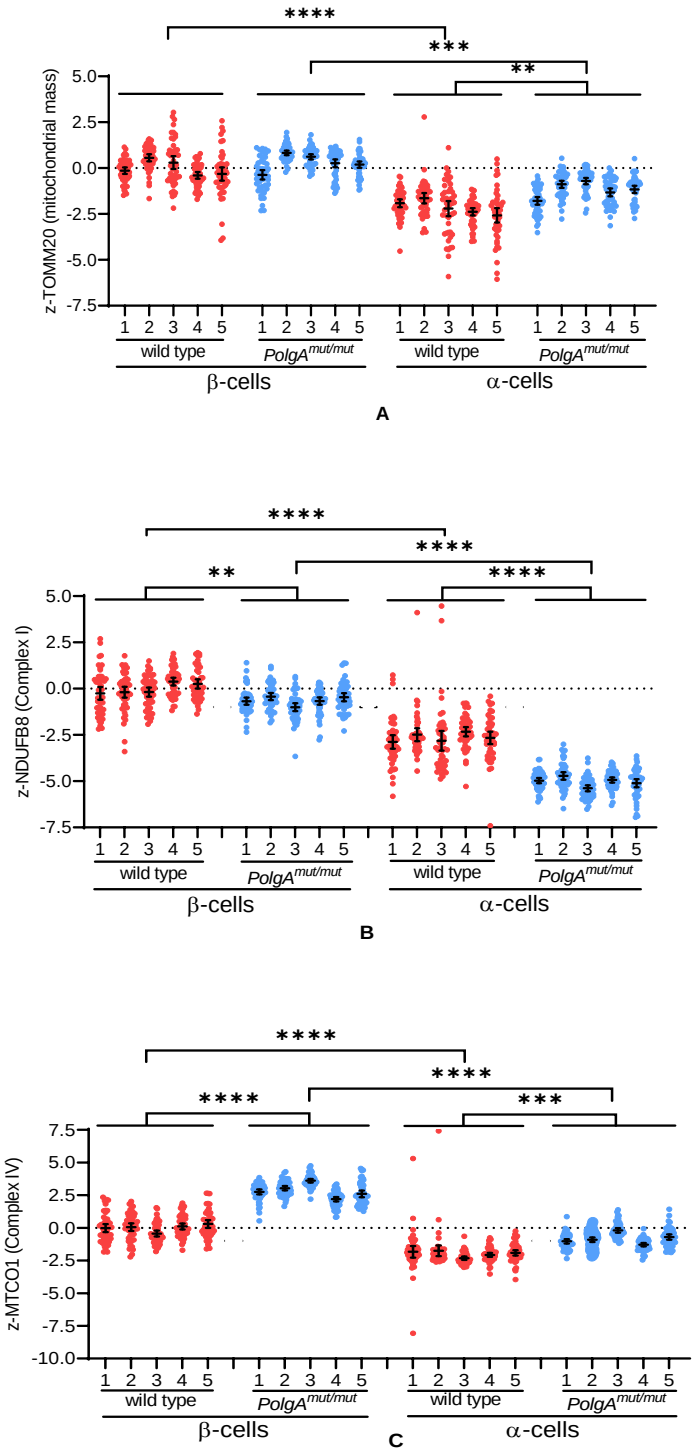

Figure 5-4. Different patterns of mitochondrial subunit expressions were found in different islet cell subtypes from *PolgA*$^{mut/mut}$ mice and the age-matched wild type mice at 44 weeks. Each point represents an individual islet with mean ± 95% CI. Wild type mice islets are shown in red and *PolgA*$^{mut/mut}$ mice islets are shown in blue. (A1) z-Tomm20. (B1) z-NDUFB8. (C1) z-MTCO1. **p<0.01. ***p<0.001. ****p<0.0001

5.3.3. Insulin expression in the pancreatic β-cells was significantly lower in the *PolgA$^{mut/mut}$* versus their wild type controls at 11 months.

In chapter 3, I have already analyzed the change of mitochondrial complex expression by using the quadruple immunofluorescence staining. However, in addition to the three mitochondrial channels (Tomm20, MTCO1 and NDUFB8), I also analyzed the signal intensity from the remaining 4th channel to understand insulin expression in the β-cells in *PolgA$^{mut/mut}$* and wild type mice in two different ages. 50 islets were studied for each case. Detailed analysis methods were explained in method chapter 2.3.4.2. At 3 months, there was no significant difference in insulin signal intensity between islets from the wild type and *PolgA$^{mut/mut}$* mice ($p>0.05$) (***Figure 5-5***). However, insulin expression in the pancreatic β-cells was significantly decreased in the *PolgA$^{mut/mut}$* versus their wild type controls at 11 months ($p<0.001$) (***Figure 5-6***). However, endurance exercise didn't significantly alter insulin expression in 11-month *PolgA$^{mut/mut}$* mice ($p>0.05$).

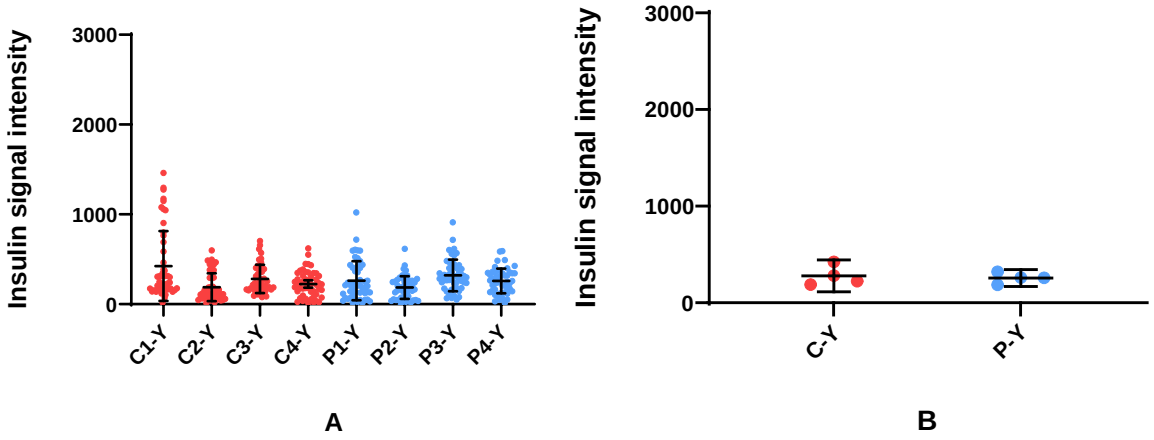

Figure 5-5. The insulin signal intensity summary in mice at 3 months. Data are presented as mean ± 95%CI**. (A) Insulin signal case comparison.** Wild type mice (C1-Y to C4-Y) and *PolgA*$^{mut/mut}$ sedentary mice (P1-Y to P4-Y). Each point represents data of 50 islets. **(B) Insulin signal intensity group comparison.** Wild type mice (C-Y), *PolgA*$^{mut/mut}$ sedentary mice (P-Y). Each point represents average data of 50 islets from one case. Unpaired t-test between wild type and *PolgA*$^{mut/mut}$ mice group, p>0.05.

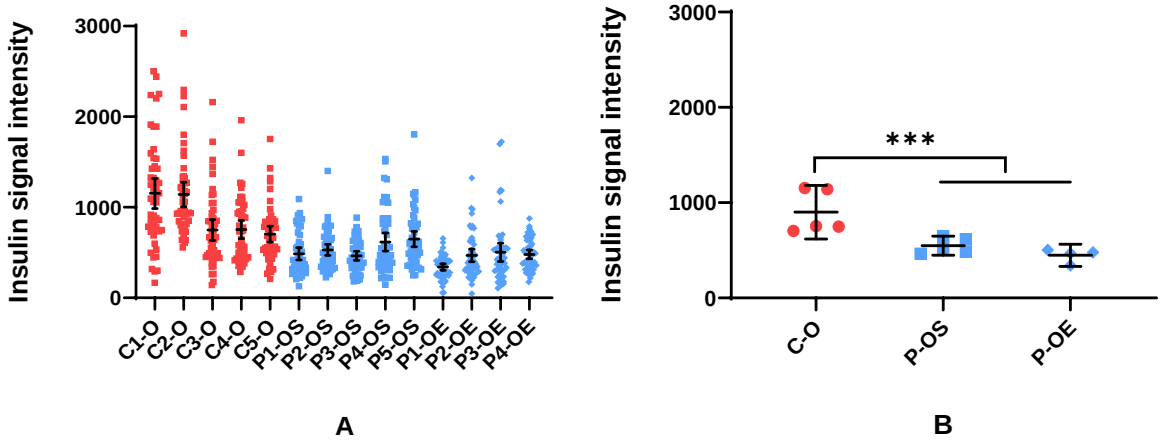

Figure 5-6. The insulin signal intensity summary in mice at 11 months. Data are shown in mean ± 95%CI. **(A) Insulin signal case comparison.** Wild type mice (C1-O to C5-O); *PolgA*$^{mut/mut}$ sedentary mice (P1-OS to P5-OS); *PolgA*$^{mut/mut}$ exercise mice (P1-OE to P4-OE). Each point represents data of 50 islets. **(B) Insulin signal intensity group comparison.** Wild type mice (C-O); *PolgA*$^{mut/mut}$ sedentary mice (P-OS); *PolgA*$^{mut/mut}$ exercise mice (P-OE). Each point represents average data of 50 islets from one case. Unpaired t-test between wild type and *PolgA*$^{mut/mut}$ mice group, P<0.001; Unpaired t-test between *PolgA*$^{mut/mut}$ sedentary and exercise groups, p>0.05. ***p<0.001.

5.3.4. No increase in blood glucose levels in the 11-month-old *PolgA*$^{mut/mut}$ mice with age.

Another 5 *PolgA*$^{mut/mut}$ mice and 5 wild type mice were included in our study. These 10 mice were raised in the same condition with the previous 11 mice which were studied for mitochondrial expression and cell composition (The endpoint body weight data of previous 11 mice were listed ***Table 8-1*** in Appendix). The body weight and blood glucose values of these new 10 mice were measured monthly (Detailed information is in the method chapter 2.6). Monthly glucose measurement results and body weight measurement results were listed in ***Table 8-2*** and ***Table 8-3*** separately in Appendix chapter. The endpoint blood glucose measurements of each mouse were plotted in ***Figure 5-7***. In ***Figure 5-7***, the unpaired t-test showed that there was no significant difference in endpoint blood glucose levels between the two groups (9.46 ± 1.17 mmol/l vs 8.9 ± 1.44 mmol/l, mean ± SEM, $P>0.05$). The changing trends of body weight measurements in *PolgA*$^{mut/mut}$ and wild type mice from March to September were plotted in ***Figure 5-8***. Green lines represent wild type mice and red lines represent *PolgA*$^{mut/mut}$ mice. It was shown that body weights of wild type mice gradually increase from March to September. However, *PolgA*$^{mut/mut}$ mice body weights didn't increase with the passage of time, most of the *PolgA*$^{mut/mut}$ mice weights even decreased monthly. The endpoint body weight of each mouse was plotted in ***Figure 5-9***. Unpaired t-test showed us that endpoint body weights of wild type mice were significantly higher compared to *PolgA*$^{mut/mut}$ mice groups (39.66 ± 6.06g vs 25.28 ± 3.64g, mean ± SEM, $P<0.01$). Every mouse has different date of birth, so they were sacrificed at different times. Mice were culled when they reached age of 11 month and their endpoint blood samples were collected in EDTA coated tubes (Detailed information was in method **chapter 2.7**) for following HbA1c% measurement. Graphpad prism graphs were generated in ***Figure 5-10*** based on the average HbA1c% measurement results. The average HbA1c results of wild type mice are significantly higher than those of *PolgA*$^{mut/mut}$ mice ($P<0.05$).

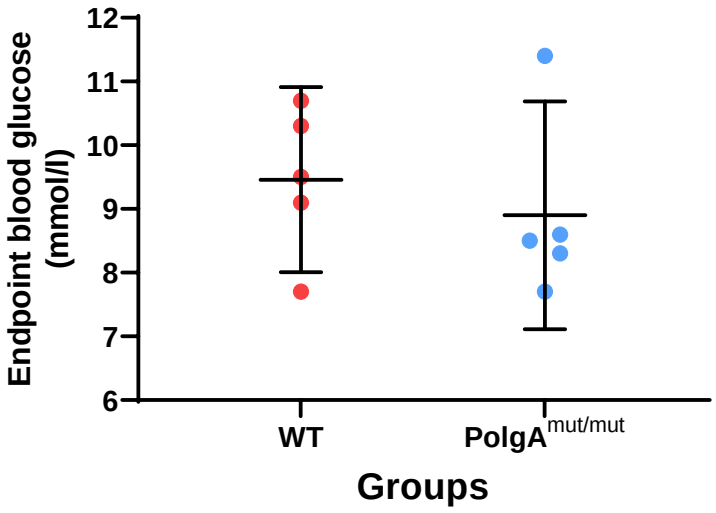

Figure 5-7. The comparison in endpoint blood glucose results between *PolgA*$^{mut/mut}$ and wild type mice. Data are shown in mean ± 95% CI. 11-month wild type mice (WT); 11-month *PolgA*$^{mut/mut}$ mice (PolgA$^{mut/mut}$). Unpaired t-test, p>0.05.

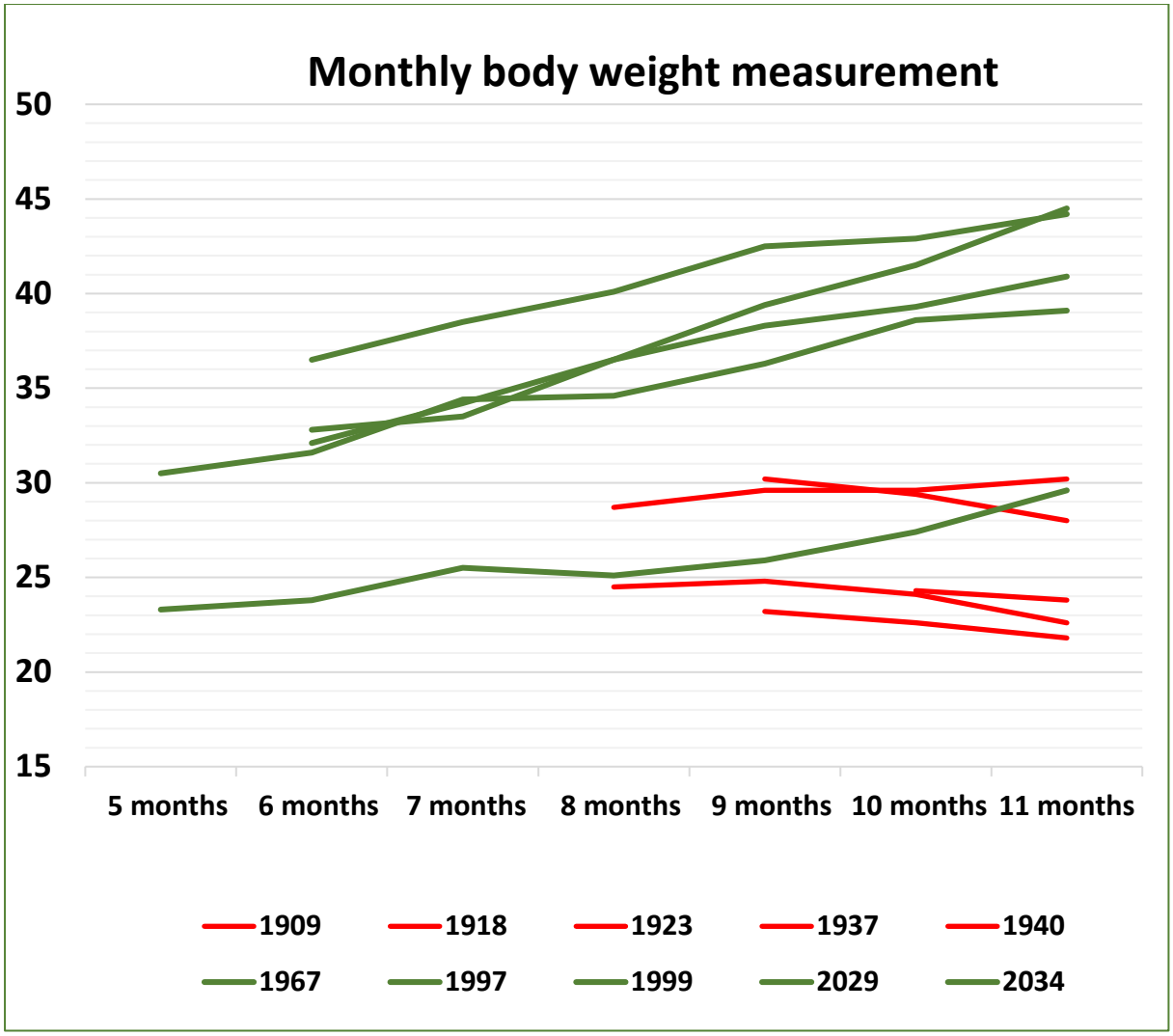

Figure 5-8. Monthly body weight measurement in wild type and *PolgA*$^{mut/mut}$ mice until 11 months of age. The green lines represent wild type mice. The red lines represent *PolgA*$^{mut/mut}$ mice.

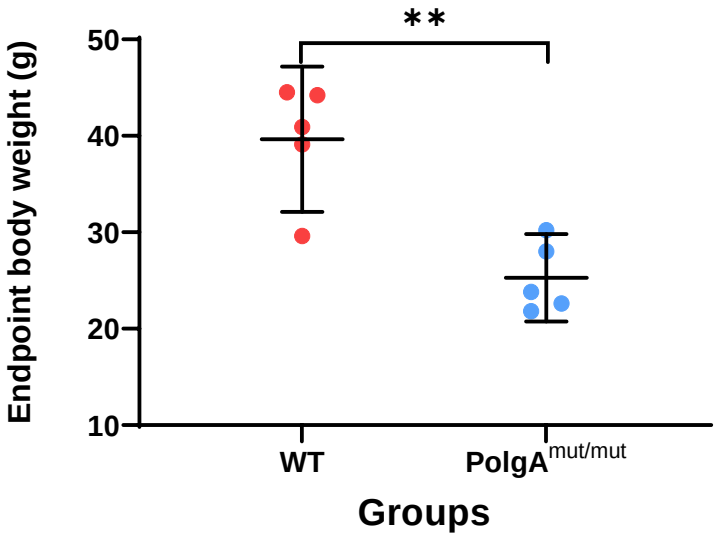

Figure 5-9. The comparison in endpoint body weight between *PolgA*$^{mut/mut}$ and wild type mice groups. Data are shown in mean ± 95% CI**.** 11-month wild type mice (WT); 11-month *PolgA*$^{mut/mut}$ mice (PolgA$^{mut/mut}$). Unpaired t-test, p<0.01. **p<0.01.

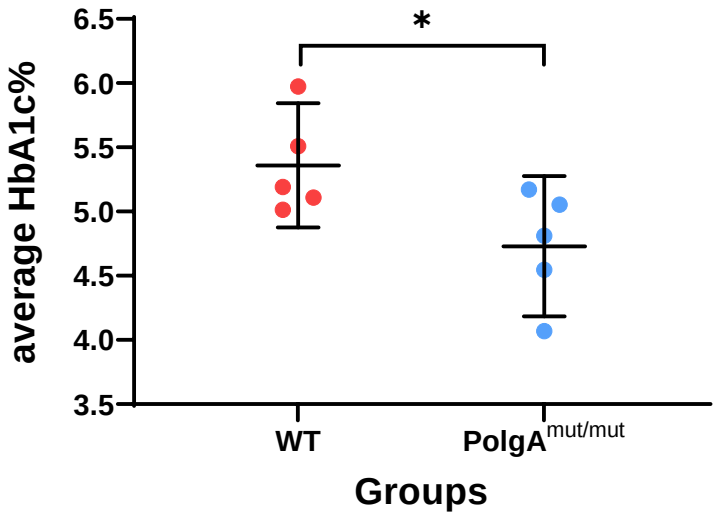

Figure 5-10. The average HbA1c% measurement result in endpoint whole blood samples from two groups of mice. 11-month wild type mice (WT); 11-month *PolgA*$^{mut/mut}$ mice (PolgA$^{-/-}$). Unpaired t-test, p<0.05. *p<0.05.

The endpoint mice body weight, HbA1c% and blood glucose measurement result summary were listed in ***Table 5-2*****.** We can conclude from the result that: firstly, wild type mice are generally heavier than *PolgA*$^{mut/mut}$ mice. Four out of five wild type mice can be categorized as overweight at the endpoint because their body weights exceed 30g, whereas all *PolgA*$^{mut/mut}$ mice have normal body weights. Secondly, most of the wild type mice endpoint HbA1c% and blood glucose values are generally higher than those of *PolgA*$^{mut/mut}$ mice. This can partly be explained by the higher body weight of wild type mice, and due to the fact that *PolgA*$^{mut/mut}$ mice have been reported to have macrocytic and hypochromic anaemia. (Trifunovic, Wredenberg et al. 2004). Thirdly, none of these mice can be diagnosed as diabetes when they were sacrificed at 11-month-old because these blood glucose level were all less than 13.3 mmol/l, the diagnostic cut off for diabetes (Surwit, Kuhn et al. 1988).

Table 5-2. The endpoint body weight, HbA1c% and blood glucose level result summary.

mouse	Genotype	Gender	Weight (g)	Status	Average HbA1c (%)	Endpoint blood glucose (mmol/l)
1909	*PolgA*$^{mut/mut}$	F	23.8	Normal	4.069081	8.5
1918	*PolgA*$^{mut/mut}$	M	28	Normal	4.81028	8.6
1923	*PolgA*$^{mut/mut}$	F	21.8	Normal	4.545349	7.7
1937	*PolgA*$^{mut/mut}$	M	30.2	Normal	5.054242	11.4
1940	*PolgA*$^{mut/mut}$	F	22.6	Normal	5.170925	8.3
1967	WT	M	44.2	Overweight	5.19097	9.5
1997	WT	M	40.9	Overweight	5.109294	7.7
1999	WT	M	44.5	Overweight	5.972855	10.3
2029	WT	F	29.6	Normal	5.014877	10.7
2034	WT	M	39.1	Overweight	5.509017	9.1

I can conclude that although *PolgA*$^{mut/mut}$ mice have mitochondrial dysfunction caused by knock-in mutation in proof-reading-deficient mtDNA polymerase gamma (POLG) gene at birth, they didn't develop diabetes with the increase of age. The significant changes of mitochondrial complex expression and cell composition in *PolgA*$^{mut/mut}$ mice are primarly caused by mtDNA mutation induced accelerated ageing but not secondary diabetes.

5.4. Summary

1. Different endocrine cell types have different responses towards the impact of ageing.
    - Tomm20, Complex I and Complex IV expression levels were all lower in α-cells compared with β-cells in both old control islets and old *PolgA*$^{mut/mut}$ islets.
    - There was a small decrease in Complex I, while Complex IV expression was markedly increased in β-cells of the old *PolgA*$^{mut/mut}$ mice compared with β-cells of the age-matched controls.
    - There was a marked decrease in Complex I, while Complex IV expression slightly increased in α-cells of the old *PolgA*$^{mut/mut}$ mice compared with α-cells of the age-matched controls.

2. Increased α-cell proliferation was evident in islets from 11-month-old *PolgA*$^{mut/mut}$ mice compared to the age-matched wild type controls.

3. Insulin expression in the pancreatic β-cells was significantly decreased in the *PolgA*$^{mut/mut}$ versus their wild type controls at 11 months.

4. Neither 11-month *PolgA*$^{mut/mut}$ mice nor wild type mice develop diabetes with increase of age, and there was no significant difference in end-point blood glucose between the two groups of mice.

5.5. Discussion

My results from chapter 4 showed that there was a comparable increase in whole islet cell and β-cell numbers with age in both wild type control and *PolgA*$^{mut/mut}$ mice. This is in line with findings from previous studies that in normal mice or rats, the increment and replication of islet endocrine cells with ageing is selective for β-cells, while the growth of endocrine non-β-cells was limited to the initial stage of life (Montanya, Nacher et al. 2000, Poy, Hausser et al. 2009, Feng, Xiang et al. 2017). However, I also found an increase in the absolute α-cell number in *PolgA*$^{mut/mut}$ mice islets from 3 months to 11 months of age and set out to explore the possible mechanisms. When I compare the staining images from *PolgA*$^{mut/mut}$ mice between two different ages, I saw a thicker α-cell ring on the peripheral side of the islets and many α cells have an abnormal location in the centre of the islets. It is even more obvious when you compare the images from 11-month *PolgA*$^{mut/mut}$ mice with age-matched wild type mice together (***Figure 4-4***). Similar changing trend of α-cell number was also observed in the β-cell specific TFAM knockout mouse model of mitochondrial diabetes but in this model there was an age-related decrease of insulin producing β-cells and islet size (Silva, Köhler et al. 2000). In order to solve this question, I applied the triple immunofluorescence assay with proliferation marker Ki67, insulin and glucagon using islets from 11-month-old *PolgA*$^{mut/mut}$ and wild type mice. The main findings were: first, *PolgA*$^{mut/mut}$ mice islets have significantly higher mean percentages of islets with ≥1 Ki67(+) cells compared to the age-matched wild type mice; second, *PolgA*$^{mut/mut}$ mice have significantly higher mean percentage of islets with ≥1 Ki67(+) α-cells compared to the age-matched wild type mice; and third, there was no significant difference in mean percentage of islets with ≥1 Ki67 (+) β-cells between *PolgA*$^{mut/mut}$ and age-matched wild type mice. The Ki67 (+) stained nuclei are located throughout islet cells but mainly belong to α-cells in *PolgA*$^{mut/mut}$ mice islets whereas Ki67 (+) nuclei are mainly located in β-cells in wild type mice islets. Based on the above analysis, I propose that increased α-cell proliferation contribute to the significantly higher absolute α-cell number in the 11-month *PolgA*$^{mut/mut}$ mice compared to the age-matched wild type mice. This in turn resulted in a significantly lower β/α cell percentage ratio in islets from the old *PolgA*$^{mut/mut}$ mice compared with the age-matched controls. In previous studies, Lam and

colleagues provided evidence that α-cells in islets from healthy mice primarily expand by self-renewal (ie proliferation of existing α-cells) rather from specialized progenitors, and that this process of α-cell renewal declined with age (Lam, Rankin et al. 2019). The increased proliferation and expanded α-cell mass in the islets of the old *PolgA*$^{mut/mut}$ mice would suggest a relaxation of an age-related constraining mechanism.

Considering the analysis of mitochondrial complex expression in islet cell subtypes, α- and β-cell area in the islets of 11-month *PolgA*$^{mut/mut}$ and age-matched wild type mice were separated and analyzed using the Nikon software. It was very surprising to see that α- and β-cells react differently towards the impact of ageing in both mice groups. As I known from the **chapter 3.3.2**, islets of *PolgA*$^{mut/mut}$ mice have significantly lower complex I expression but higher complex IV expression compared to the age-matched wild type mice islets. By comparing the mitochondrial complex expression in α- and β-cell area, it can be found out that Tomm20, Complex I and Complex IV expression levels were all lower in the α-cells compared with the β-cells in the 11-month wild type islets. The same pattern was seen when comparing α-cells with β-cells in the 11-month *PolgA*$^{mut/mut}$ islets. I next compared mitochondrial complex expressions in β-cells from 11-month *PolgA*$^{mut/mut}$ mice and the age-matched wild type mice. There was a small decrease in Complex I, while Complex IV expression was markedly increased in the β-cells of the 11-month *PolgA*$^{mut/mut}$ mice compared to the age-matched wild type mice. The expression pattern was different for α-cells. There was a marked decrease in Complex I expression accompanied by a small increase in Complex IV expression in α-cells of the 11-month *PolgA*$^{mut/mut}$ mice compared with the α-cells of the age-matched wild type mice. This can explain that the significant decrease of complex I expression in the whole islets of *PolgA*$^{mut/mut}$ mice compared to wild type mice was mainly driven by the complex I deficiency in α-cells of *PolgA*$^{mut/mut}$ mice whereas the maintenance of complex IV expression with age in the *PolgA*$^{mut/mut}$ islets mainly be caused by the increasing complex IV expression in β-cells of the *PolgA*$^{mut/mut}$ mice. These data show different patterns of mitochondrial subunit expression between pancreatic islet cell subtypes in wild type mice and *PolgA*$^{mut/mut}$ mice.

The phenotypic response to the mitochondrial stress differs between the cellular subtypes within the islet. β-cell mass increases normally with age, accompanied by an increase in complex IV expression. It is possible that the increased complex IV expression in the β-cells of the old *PolgA*$^{mut/mut}$ mice represents an adaptive response to the mitochondrial stress in the pancreatic β-cells in the *PolgA*$^{mut/mut}$ mice. This has been observed in other tissues in which there is an upregulation of components of the mitochondrial respiratory chain in response to complex I deficiency (DiMauro and Schon 2003, Picard, Zhang et al. 2014). However, α-cells of *PolgA*$^{mut/mut}$ mice islet also had marked complex I deficiency but they didn't present with complex IV compensation. The reason maybe because α- and β-cells compensate complex I deficiency in different ways, in which β-cells compensate by increasing complex IV expression whereas α-cells compensate by cell proliferation. The β-cell specific TFAM knockout model breeds more severe knock out and decreased mitochondrial gene expression with complex IV deficiency. It was concluded in this study that complex IV deficiency was related to the death of β-cells (Silva, Köhler et al. 2000). In addition, these animals developed marked hyperglycaemia and diabetes which may well have exerted secondary effects on islet cell mass and function. It proves my hypothesis from a different perspective that the increased complex IV expression in the β-cells of the old *PolgA*$^{mut/mut}$ mice in my study represents an adaptive response to the mitochondrial stress and it helps keeping β-cells alive with increase of age.

Conversely, the marked complex I deficiency in the α-cells in comparison both with the β-cells of the old *PolgA*$^{mut/mut}$ mice and with the α-cells of the old control islets can be the main mechanism of age-related increase in α-cell proliferation and cell number. One previous study reported that increased Knockdown of NDUFB9, a component of complex I, was shown to promote cell proliferation in a tumour cell-line and was accompanied by an increase in ROS generation (Li, Sun et al. 2015). Raised ROS levels have been implicated in promoting cell proliferation in non-tumour cell lines (Han, Kim et al. 2003). Using the same *PolgA*$^{mut/mut}$ mouse model, a recent study examined mitochondrial ROS generation *in vivo* (Logan,

Shabalina et al. 2014). ROS levels were normal in young mice despite marked mitochondrial dysfunction but increased as the animals aged. Together, these findings raise the possibility that the increased α-cell proliferation observed in old *PolgA*$^{mut/mut}$ mouse islets are a response to complex I deficiency and increased ROS generation. An alternative and complementary mechanism relates to the interaction between pancreatic β- and α-cells. The increase in α-cell number could be led by a compensatory response to altered β-cell mass and function. In other cases chronic hyperglucagonemia is also associated with α-cell hyperplasia in some models (Poy, Hausser et al. 2009). Streptozotocin induced diabetes in healthy mice was accompanied by decreased insulin and GABA expression in β-cells and an increase in α-cell mass (Feng, Xiang et al. 2017). GABA treatment reversed α-cell hyperplasia pointing to a link between β-cell function and α-cell mass. While GABA expression was not measured in this study, I did find evidence of decreased insulin expression consistent with impaired β-cell function in the pancreatic islets of the old *PolgA*$^{mut/mut}$ mice.

My mouse model created by inducing a point mutation in mtDNA polymerase gamma gene show many premature ageing phenotypes thus can be used as a model of ageing. MtDNA mutation can cause mitochondrial diabetes and it can also negatively affect pancreatic beta-cell function and cause decreased insulin secretion. The failure of blood glucose regulation caused by decreased insulin secretion is an important step before progressing to diabetes. So, an important question has arisen from our study, whether these mice have developed diabetes with ageing?

Firstly, I measured the insulin expression in the pancreatic β-cells by using the quadruple staining result. In addition to the Tomm20, MTCO1 and NDUFB8 staining, I also analyzed the signal intensity of insulin staining in order to understand insulin expression in the beta cells of *PolgA*$^{mut/mut}$ and wild type mice in two different ages. The insulin expression was significantly decreased in the *PolgA*$^{mut/mut}$ versus their wild type controls at 11 months. My result is in line with the findings of Li and colleagues who reported a decreased insulin secretory response to high glucose in isolated pancreatic islets from 40-week-old *PolgA*$^{mut/mut}$

mutator mice compared with age-matched wild type controls (Li, Trifunovic et al. 2014). The change of insulin signal intensity in *PolgA*$^{mut/mut}$ mice group at 11 months reveals a possibility that this mtDNA mutation mouse model has impaired β-cell function compared to the wild type as reported before (Safdar, Bourgeois et al. 2011). One of the previous studies reported that the β-cell specific TFAM knockout mutant mice developed diabetes from the age of approximately 5 weeks. (Silva, Köhler et al. 2000). Isolated islets from this mouse model showed impaired Ca^{2+} signaling and lower insulin release at 7~9 weeks of age (Silva, Köhler et al. 2000). However, I only did the measurement on insulin signal intensity within islet β-cells not the actual amount of insulin secreted from pancreatic islets. Taken together, my findings and previous findings show that mitochondrial dysfunction adversely affects pancreatic β-cell function and islet cell composition in response to ageing. These changes will predispose to impaired glucose tolerance, particularly under conditions of increased insulin resistance and increased secretory demand placed on the pancreatic β-cells. In order to further explore this question, I measured blood glucose levels and HbA1C in wild type and *PolgA*$^{mut/mut}$ mice at the time of sacrifice.

By the time I started thinking about this question, previous 11 *PolgA*$^{mut/mut}$ and wild type mice had been sacrificed, and their pancreas tissue had been paraben-embedded long time ago. I therefore recruited another 10 mice, among them 5 *PolgA*$^{mut/mut}$ mice and 5 wild type mice. They were kept under the same conditions and their blood glucose and body weight were measured monthly in order to know whether these *PolgA*$^{mut/mut}$ mice develop diabetes with ageing. At the endpoint, all the 10 mice were sacrificed at the same age as the original 11 mice. However, blood glucose test was done by tail puncture and blood glucose reading can be affected by many factors, such as stress that mice experienced during tail puncture, or even the amount of food mice intake on the measuring day (blood measurement is usually done in the afternoon between 1pm to 3pm, when mice were not fasting). In view of this concern, HbA1c% was also measured as an index of longer term glycaemia. After comparing the glucose and HbA1c result I achieved from mice in my study with the standard normal range, I can conclude none of our 11-month mice (from both mice groups) developed diabetes

with ageing. In both mice groups, there are a few blood glucose readings exceed the normal non-diabetic blood glucose range but still can't be considered as diabetic. The reason behind can be either stress caused by tail puncture or glucose intolerance. In my study, the endpoint HbA1c values of wild type mice were significantly higher compared to those of *PolgA*$^{mut/mut}$ mice. This could be explained by the fact that *PolgA*$^{mut/mut}$ mice have been reported to develop macrocytic and hypochromic anaemia which could lead to a falsely low HbA1c result (Trifunovic, Wredenberg et al. 2004). Although there was no significant difference in endpoint blood glucose level between mice groups, wild type mice still have higher blood glucose reading compared to *PolgA*$^{mut/mut}$ mice. This result was consistent with that of endpoint body weight. Wild type mice had significantly higher body weights when they were sacrificed at 11-months. In these 10 mice, all the body weights of wild type mice keep increasing with ageing whereas most of the *PolgA*$^{mut/mut}$ mice experienced decrease in body weight with the increase of age. Besides, wild type mice body weights are higher than that of *PolgA*$^{mut/mut}$ mice when they were measured at the same time point. I further looked for the endpoint body weight data from the 11 mice I used previously for mitochondrial complex expression and cell composition staining study (Data are listed in appendix ***Table 8-1*** and ***Figure 8-1***). The endpoint body weights of these 11 mice are comparable to those of 10 mice I used for blood glucose measurement. My findings are in keeping with the original description of the aged *PolgA*$^{mut/mut}$ mouse in which body weight decreased as they aged due to a specific decrease in whole body adiposity compared to age-matched healthy control mice (Trifunovic, Wredenberg et al. 2004). They observed that the body weights of *PolgA*$^{mut/mut}$ mice decreased with the passage of time whereas the body weights of wild type mice increased with age. Wild type mice body weights were significantly higher compared to the age-matched *PolgA*$^{mut/mut}$ mice. (Safdar, Bourgeois et al. 2011). This may well explain why the *PolgA*$^{mut/mut}$ mice at 11 months are protected from diabetes despite the changes in islet cell composition and decreased insulin expression. The normal mice blood glucose concentrations proved that neither *PolgA*$^{mut/mut}$ mice nor wild type mice develop diabetes. I can thus conclude that the change of pancreatic islet cell composition was solely driven by premature ageing caused by mtDNA mutation and are not secondary metabolic changes of diabetes. Moreover, I propose

that the restricted weight gain with age in the *PolgA$^{mut/mut}$* mice protected the animals from diabetes by lowering the insulin secretory with advancing age. This is clearly not the case in a model of islet specific mtDNA knockdown, where normal whole body growth with age would be predicted to exert an increased functional stress on the compromised islet increasing the risk of diabetes (Silva, Köhler et al. 2000).

It was discussed in previous studies that endurance exercise can protect *PolgA$^{mut/mut}$* mice, rescue progeroid ageing and help promoting mitochondrial biogenesis. Thus, it can be regarded as a non-pharmacological intervention systemically improve body condition and mitigate multisystem degeneration. It was the main reason why I induced endurance exercised *PolgA$^{mut/mut}$* mice in my study (Menshikova, Ritov et al. 2006, Safdar, Bourgeois et al. 2011). In the previous study, endurance exercise was proved to promote systemic mitochondrial biogenesis, increase multi-system rejuvenation and multi-organ oxidative capacity, contributing to the complete phenotypic protection and reducing the morbidity and mortality of the *PolgA$^{mut/mut}$* mice. They also discovered that the endurance exercise attenuated the decline in body weight and body condition in *PolgA$^{mut/mut}$* mice (Safdar, Bourgeois et al. 2011). However, this improvement of endurance exercise was not observed in my study although I used the same mutator mice species and followed the same exercise protocol. Similar results were reported by my colleague Dr. Ghazaleh Alimohammadiha, she agreed that endurance exercise didn't extend the lifespan of *PolgA$^{mut/mut}$* mice and didn't provide physiological benefits to *PolgA$^{mut/mut}$* mice, especially to the cardiac function. Both of our results are contrasting with Safdar's research despite we used the mice originating from the same colony with the same age and exercise protocol. The only difference in the experiment design is Safdar et al singly housed their mice to keep away external factors such as case fights whereas we did the group housing; the husbandry of mice such as diet, lighting and temperature are different between two studies; Safdar generated wild type control mice (*PolgA$^{+/+}$*) from *PolgA$^{mut/+}$* mice whereas we purchased C57BL/6J mice from a different laboratory. The individual response to external stimuli such as endurance exercise can be significantly impacted by different genetic background of mice (Skinner 2005). 11-month wild

type mice have significantly higher endpoint body weight compared to the 11-month *PolgA*$^{mut/mut}$ sedentary and exercise mice. However, *PolgA*$^{mut/mut}$ mice that had endurance exercise training didn't have significant difference in endpoint body weight compared to the sedentary *PolgA*$^{mut/mut}$ mice (Data are listed in appendix ***Table 8-1*** and ***Figure 8-1***). Similar to the results I got in the chapter 3 and 4, endurance exercise didn't have significant impact on the endpoint weight of *PolgA*$^{mut/mut}$ mice compared to the sedentary ones.

This part of our study has some potential limitations. First I should further study whether transdifferentiation processes happen in my study. Instead of one single mechanism contributing to the change of islet cell composition, it is more possible that cell proliferation, transdifferentiation and even apoptosis are working together to achieve the significant difference in islet cell composition between wild type and *PolgA*$^{mut/mut}$ mice at 11 months (Cinti, Bouchi et al. 2016). Second, decreased insulin staining intensity is a novel observation but it needs verification using an alternative measure of insulin expression. Third, the blood glucose measurements were not fasting but random measurements taken during a fixed time interval each day.

After discovering the driver and mechanisms underlying changes in islet cell composition in the *PolgA*$^{mut/mut}$ mice islets, I want to further discover the mitochondrial complex expression and islet cell composition change in ageing human islets.

CHAPTER 6. STUDY THE IMPACT OF AGEING ON MITOCHONDRIAL RESPIRATORY CHAIN FUNCTION AND ISLET CELL COMPOSITION IN NON-DIABETIC HUMAN PANCREATIC ISLETS.

6.1. Introduction

After studying the mitochondrial expression and cell composition in islets from *PolgA*$^{mut/mut}$ mice and age-matched wild-type controls, I applied the same analytical protocol to non-diabetic human samples to study the impact of ageing on mitochondrial complex expression and cell composition in human islets.

Long term physiological and pathological demands such as ageing, pregnancy, excessive nutrition and obesity can accumulate stress and trigger morphological and functional compensations of beta cells in mice. Obese non-diabetic human subjects have higher β-cell mass, lower insulin sensitivity and increased insulin secretion compared to the lean controls (Polonsky, Given et al. 1988, Kahn, Prigeon et al. 1993, Ferrannini, Natali et al. 1997, Cnop, Igoillo-Esteve et al. 2011). Ageing is also associated with impaired mitochondrial function, glucose intolerance, insulin resistance and defect islet secretory function in human. In adult humans, pancreatic β-cell mass has certain degree of plasticity and can expand to compensate for insulin resistance (Gregg, Moore et al. 2012). (DeFronzo 1979, DeFronzo 1981, Fink, Kolterman et al. 1983, Chen, Bergman et al. 1985, Kahn, Larson et al. 1992, Ihm, Matsumoto et al. 2006). These indexes are also affected by other age-related variations in dietary habits, exercise, lean body mass and total body fat (Rowe, Minaker et al. 1983). The change of body composition such as the decrease in lean body mass and increases in total body fat can accompany normal human ageing (Rowe, Minaker et al. 1983) and impair insulin action. Endurance exercise can improve the degree of insulin sensitivity (Rowe, Minaker et al. 1983).

In human islets, islet cell composition and islet cell mass change with the increase of age but different studies have different conclusions about this change. In a recent study, both β-and α-cell mass increased gradually with age from 1-5 days to 5-10 years (Hart, Aramandla et al. 2014). In another human study with donor age range between 16 to 66 years, found that

older donors' islets have more β-cells relative to α-cells (Blodgett, Carroll et al. 2013). In a recent Japanese study, the number of β-cells per islet decreased from the fifth decade of life (40-49yrs age) to the eighth decade of life (70-79yrs age) (Mizukami, Takahashi et al. 2014). Compared to rodent donors, human islets have greater variability and lower β: α cell ratio (4 in rodent islets). There is also greater donor-to-donor variability in human donors (Blodgett, Carroll et al. 2013).

If stresses on the islets persist, the exhaustion of stressed β-cells can trigger accelerated hyperglycemia progression and quickly progress to the final T2DM status (Chang-Chen, Mullur et al. 2008). Pancreas from 109 human cases (non-diabetic: 52 vs T2DM: 57) were studied and the mean β-cell mass has shown to have an average of 24% loss in patients with 5 years of diabetes onset, this number increases to 54% in patients diagnosed with diabetes for more than 15 years. It shows us a positive correlation between the reduction of β-cell mass and the diabetes duration (Rahier, Guiot et al. 2008). The β-cell mass is also determined by combined factors in humans with T2DM. For example, obese T2DM patients have larger deficit of β-cell volume compared to lean T2DM patients (63% vs 41%)(Butler, Janson et al. 2003). It is reported that there is a significant decrease of β-cells but significant increase of α-cells in diabetic versus non-diabetic donors. This causes a decrease in β: α cell ratio in diabetic donors (Cinti, Bouchi et al. 2016). Apart from the β-cell mass reduction, many human studies showed that insulin secretion capacity in T2D patients reduced 50%-97%, revealing the existence of β-cell dysfunction (Butler, Janson et al. 2003, Chen, Cohrs et al. 2017).

The aim of the current chapter was:

Characterize the differences in mitochondrial ETC complex expression and islets cell composition in pancreatic islets from "young" (<40yrs age) and "old" (>60yrs age) non-diabetic human donors.

6.2. Methods

6.2.1. Human sample procurement.

In our study I used a total of 12 non-diabetic human samples. Among them, 2 young non-diabetic human donors (aged 31y and 24y) and 4 old non-diabetic human donors (aged 68y, 72y, 75y and 85y) were kindly given by Professor Piero Marchetti (University of Pisa). Another 3 young non-diabetic human pancreas blots (aged 27y, 35y and 39y) and 3 old non-diabetic human pancreas blots (aged 63y, 71y and 71y) were kindly given by Professor James Shaw from Newcastle University. These donors can be divided into two age groups which are young age (20~40y, 5 cases) and old age (60~90y, 7 cases). Their donor information is listed in ***Table 2-3*** and ***Table 2-4*** in Method chapter.

6.2.2. Quadruple mitochondrial immunofluorescence staining on human pancreas sections.

The same quadruple immunofluorescence staining protocol (chapter 3) was applied on human pancreas sections. After staining, Nikon A1 upright confocal was used to image the slides with 20 times magnification. The camera settings remain the same between cases and between different batches of experiments. 50 islets were imaged and analysed per case. Nikon A1 analysis software and OXPHOS quadruple immunofluorescence analysis software were used for getting the raw signal intensity value and z-score of signal intensity value. After that, Graphpad Prism8 was used to generate graphs and different analysis.

6.2.3. Triple immunofluorescence staining on human pancreas sections.

Same triple immunofluorescence staining protocol which elaborated in chapter 4 was applied on human pancreas sections. After staining, β-cells can be counted when I overlap insulin and DAPI channel and α-cells can be counted when I overlap glucagon and DAPI channel. In this study, only α-and β-cells are counted in each islet and other endocrine cell types are not counted. 25 islets were counted for each case. Graphpad prism was used to generate graphs and different analysis.

6.3. Results

6.3.1. There was no significant difference in BMI or gender between old and young non-diabetic donors.

I grouped all the human donors into young (20~40yrs, 5 cases) and old (70~ 90yrs, 7 cases) age groups separately. The BMI and gender information of these donors are listed in the ***Table 6-1*** below. In order to see if old age non-diabetic donors had significantly higher BMI compared to the young human controls, unpaired t-test was carried out and it showed there was no significant difference in BMI value between old and young non-diabetic human donors (P>0.05). The distribution of male and female donors across the old and young age groups is shown in ***Table 6-2***. While the 2 age grous were not exactly matched for gender. Fisher exact test showed there was no significant difference in the portion of male and female donors in different age groups (P>0.05).

Table 6-1. The age, BMI and gender information of human non-diabetic donors.

Young			Old		
Age	BMI	Gender	Age	BMI	Gender
31	23.1	M	68	27.3	F
24	27.8	M	72	22	F
27	26	M	75	23.4	F
35	29.98	F	85	24.7	F
39	-	M	63	24	F
			71	26.73	M
			71	30.86	M

Table 6-2. The gender distribution in old and young age donors.

	Young	Old	Row total
Male	4	2	6
Female	1	5	6
Column total	5	7	12

6.3.2. The expression of mitochondrial mass marker (Tomm20) is significantly higher in islets from old versus young non-diabetic human donors.

I applied the same quadruple immunofluorescence staining protocol on pancreas slides and signal intensities of 50 islets were studied per human case. The composite and separate staining images are shown in the ***Figure 6-1***. The z-score analysis results were shown in ***Figure 6-2***. Unpaired t-test showed that there was significant difference in Tomm20 expression between old age non-diabetic and young age non-diabetic groups ($p<0.01$). It indicated that Tomm20 expression was significantly higher in islets from old age non-diabetic donors compared to the young age non-diabetic donors. There were no significant differences between the 2 groups for complex I and complex IV expression. The signal intensity comparison and graphs of are listed in ***Figure 8-6*** in Appendix chapter.

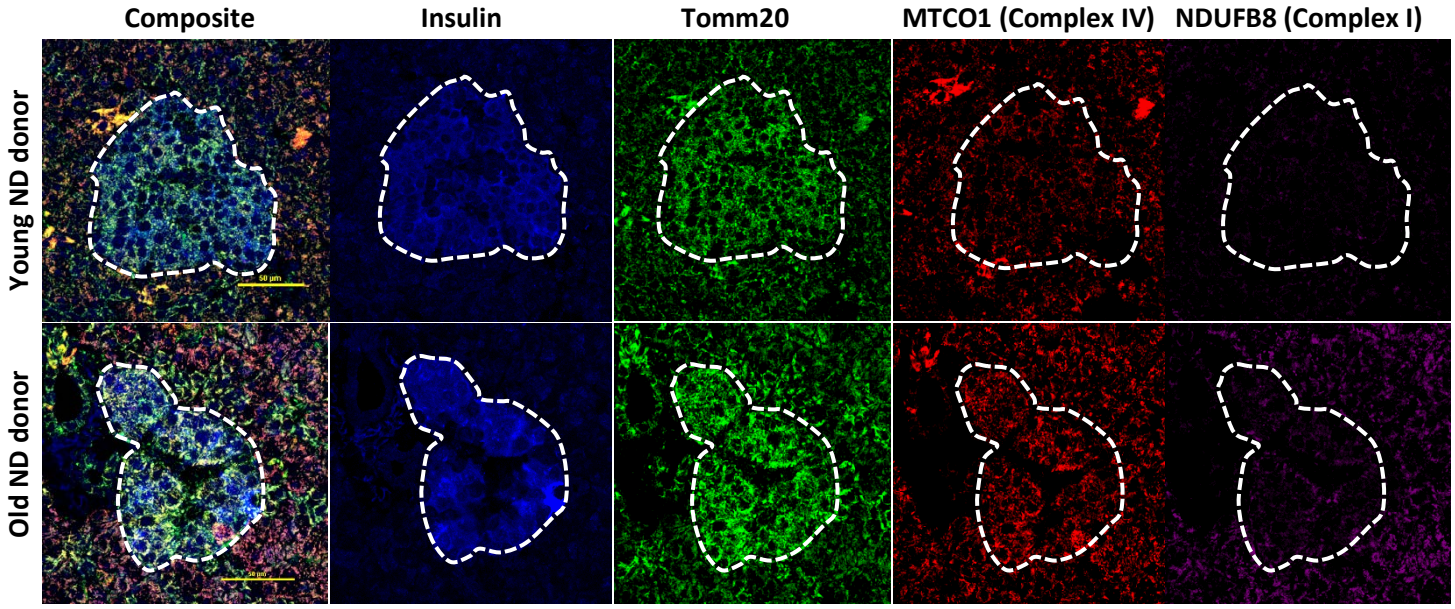

Figure 6-1. The composite and separate quadruple mitochondrial immunofluorescence in human pancreatic islets. (Top) young non-diabetic donor LDIS158; (Bottom) old non-diabetic donor LDIS174. Immunofluorescence labelling from left to right. Insulin (Alexa fluor 405), Tomm20 (Alexa fluor 488), Complex IV (MTCO1, Alexa fluor 546) and Complex I (NDUFB8, Alexa fluor 647). Pictures were taken by A1 confocal with 20 times magnification. Yellow label marks the 50µm length. Scale bar, 50µm.

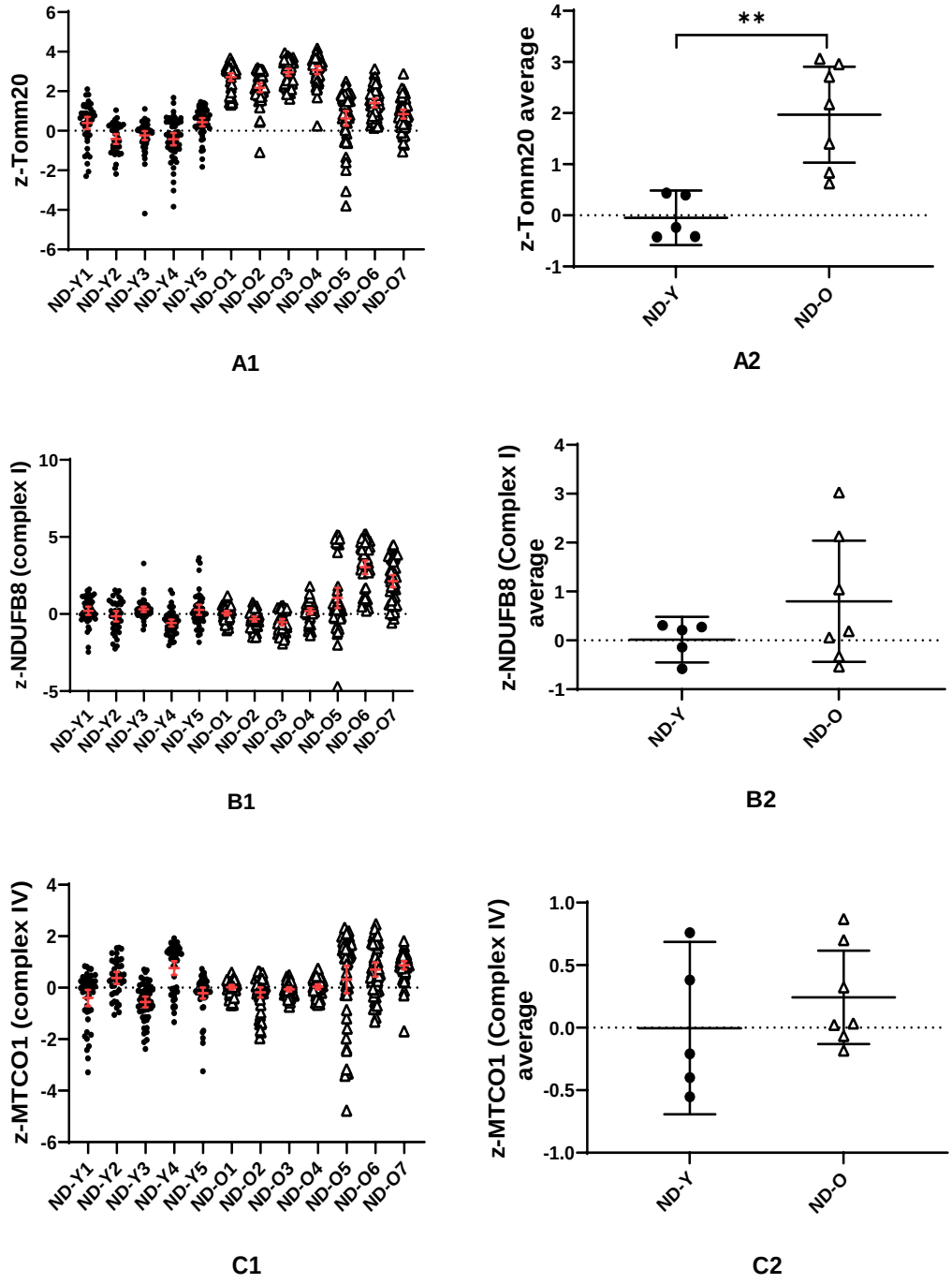

Figure 6-2. Changes of z-score expression in Tomm20 (mitochondrial mass), NDUFB8 (complex I) and MTCO1 (complex IV) in old age non-diabetic human donors compared to young non-diabetic human donors. Mean ± 95% CI. (A1, B1, C1) Z-score case comparison. Young non-diabetic donors (ND-Y1 to ND-Y5); old non-diabetic donors (ND-O1 to ND-O7). Each dot represents one islet and 50 islets were studied for one case. (A1) z-Tomm20; (B1) z- NDUFB8; (C1) z- MTCO1. **(A2, B2, C2) Z-score group average comparison.** Young non-diabetic donors (ND-Y); old non-diabetic donors (ND-O). Each point represents an average data of 50 islets. (A2) z-Tomm20 group average; (B2) z-NDUFB8 group average; (C2) z-MTCO1 group average. **p<0.01.

6.3.3. Old human non-diabetic donors have significantly lower whole islet cell number and absolute β-cell number compared to the young non-diabetic donors.

After testing the mitochondrial complex expression in young and old non-diabetic human donor samples, I further studied the islet cell composition in our human pancreas sections. 5 young non-diabetic human samples and 7 old non-diabetic human samples which I used to study mitochondrial complex expression in **section 6.3.2** were studied in this part and 25 islets were studied per human case. The composite and separate staining images are listed in ***Figure 6-3***. The islet cell composition results for individual islets from different donors are shown in ***Figure 6-4***. The average islet cell composition for each group are shown in ***Figure 6-5***. Unpaired t-test showed that old non-diabetic human samples had significantly lower whole islet cell number ($P<0.05$) and lower absolute β-cell number ($P<0.01$) compared to the young human samples. There were non-significant trends for increased α-cell percentage, decreased β-cell percentage and decreased islet size with the increase of age in the human donors.

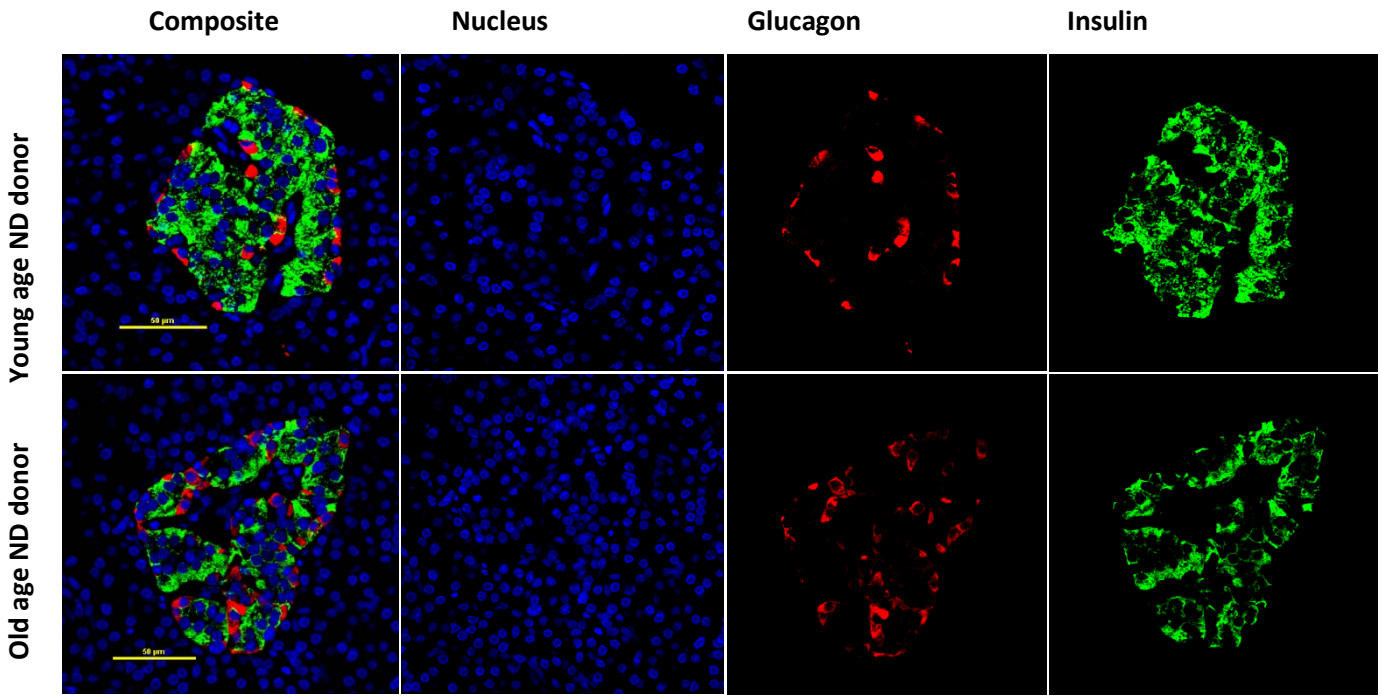

Figure 6-3. The separate and composite triple immunofluorescence staining images for endocrine hormones in pancreatic islets human non-diabetic donors. (Top) Young non-diabetic donor (LDIS087); (Bottom) Old non-diabetic donor (LDIS193). DAPI stain for nucleus; Glucagon stain for α cells, Alexa fluor 568; Insulin stain for β cells, Alexa fluor 488. Pictures were all taken by A1 confocal with 20 times magnification. Scale bar, 50μm.

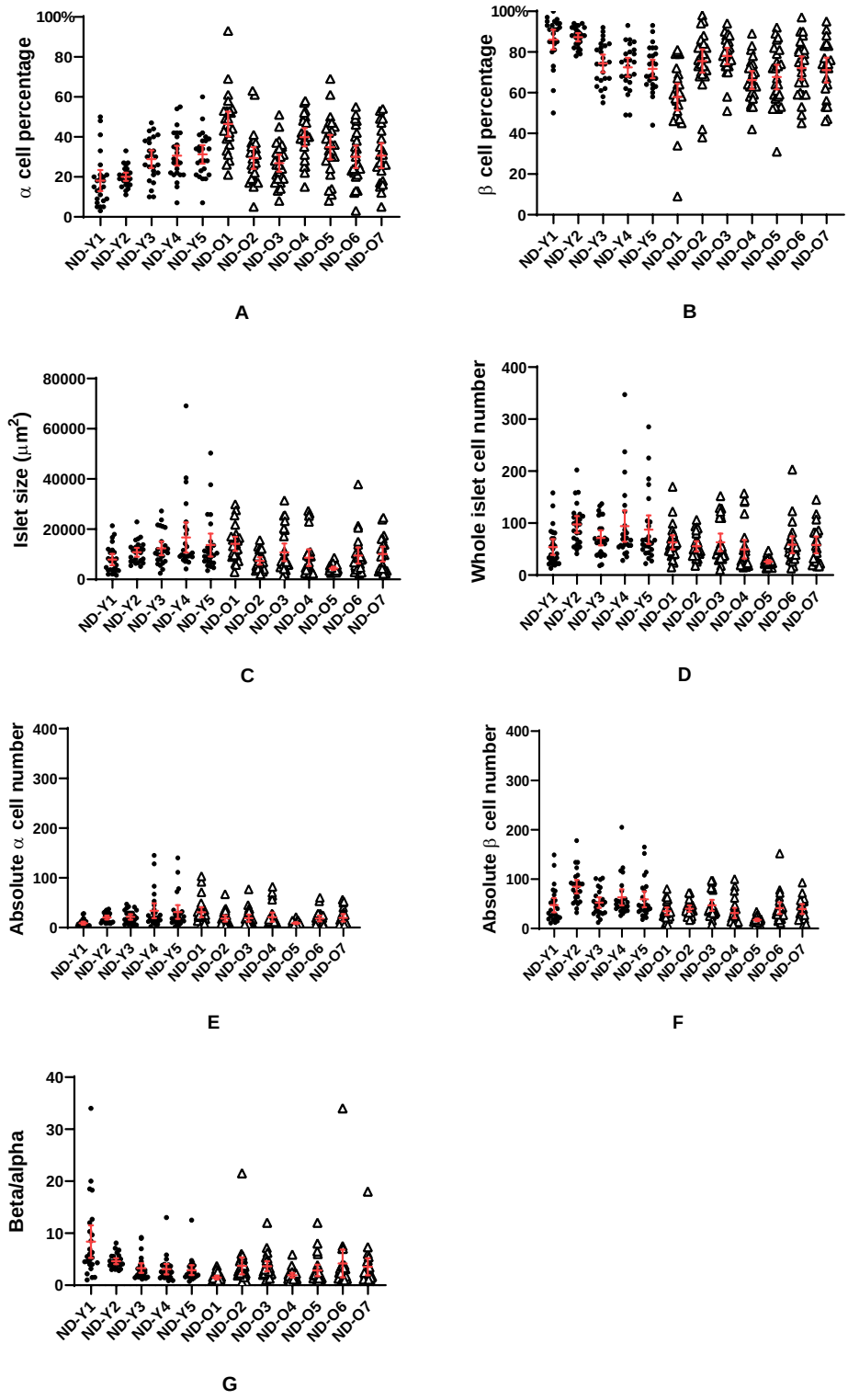

Figure 6-4. Islet cell composition summary in young and old non-diabetic donors. Mean ± 95% CI. Young non-diabetic donors (ND-Y1 to ND-Y5); old non-diabetic donors (ND-O1 to ND-O7). Each dot represents one islet and 25 islets were studied per case. (A) α cell percentage; (B) β cell percentage.; (C) Islet size; (D) Whole islet cell number; (E) Absolute α cell number; (F) Absolute β cell number; (G) β/α ratio.

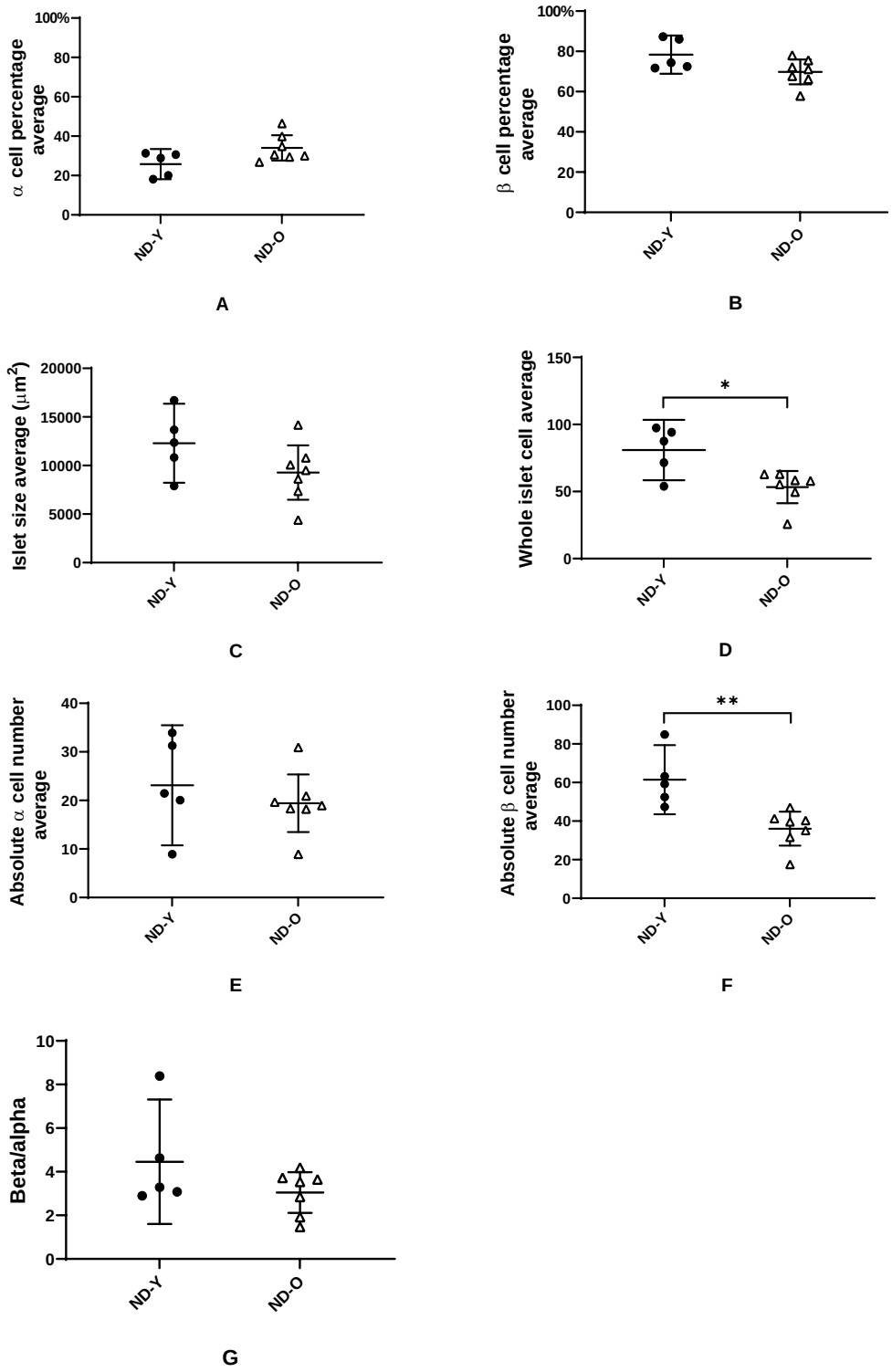

Figure 6-5. Average Islet cell composition summary in young and old non-diabetic donors. Mean ± 95% CI. Young non-diabetic donors (ND-Y); old non-diabetic donors (ND-O). One dot represents an average value of 25 islets. (A) Average α cell percentage; (B) Average β cell percentage; (C) Average islet size; (D) Average whole islet cell number; (E) Average absolute α cell number; (F) Average absolute β cell number; (G) Average β/α ratio. *p<0.05. **p<0.01.

6.4. Summary

1. The expression of Tomm20 was significantly higher in islets from old versus young human non-diabetic donors.

2. Old human non-diabetic donors have significantly lower whole islet cell number and absolute β-cell number compared with the young non-diabetic donors.

6.5. Discussion

Due to the mosaic pattern of deficiency, oxidative phosphorylation defects in human tissues are often challenging to quantify. A unique quadruple immunofluorescence technique enabling the quantification of key respiratory chain subunits of complexes I and IV, together with mitochondrial mass was developed and first used on mice tissue. This technique was further applied on the human tissue, helping to improve the diagnosis of mitochondrial disease and to study the mechanisms underlying mitochondrial abnormalities in disease (Rocha, Grady et al. 2015).

Previous human studies have applied the quadruple immunofluorescence staining protocol to many tissues before. For example, patients with single, large-scale mtDNA deletions show a simultaneous loss of both complex I and complex IV in myofibres (Rocha, Grady et al. 2015). Another study reported a significant decrease in complex II activity with age in human skin fibroblasts but complex IV activity didn't have a significant change with increase of age (Bowman and Birch-Machin 2016). A study which used quantitative skeletal muscle proteome analysis in skeletal muscle revealed that most of the mitochondrial complex proteins declined from young and old healthy person. Among them, 16 proteins which consisted of complex I to V were significantly lower in the older age group (Ubaida-Mohien, Lyashkov et al. 2019). It was quite surprising for us to see significant higher mitochondrial signal expression in pancreatic islets from old non-diabetic donors compared to the young non-diabetic donors. I discussed the changes in mitochondrial complex expression in islets from mice in chapter 3. I discovered that the expression of Tomm20 increases significantly in *PolgA*$^{mut/mut}$ mice with increase of age. In wild type mice, the expression of Tomm20 shows an increasing trend in wild type mice with increase of age although it was not significant.

The increase of Tomm20 expression in human samples with age is consistent with what I observed in mice. The reason behind this increment of Tomm20 signal expression with increase of age can be explained by mitochondrial biogenesis. Tomm20 is a nuclear encoded protein located on the mitochondrial outer membrane and can be studied as a marker of

mitochondrial mass. The significant increase in Tomm20 expression is the evidence of mitochondrial biogenesis. Mitochondrial biogenesis is the expansion of mitochondria by either increasing in mitochondrial mass or increasing mitochondrial number. It can be regarded as an efficient strategy to delay mitochondrial ageing (Chistiakov, Sobenin et al. 2014). Mitochondrial biogenesis is a well-known process that cells use to adjust their metabolic processes to meet different energetic requirements of tissues, especially under circumstances of decreased fuel supply or increased energy demand (Adaes 2019). It is well known that there is an age-related decline in intracellular ATP metabolism and mitochondrial function in islets, especially in β-cells. Decreased mitochondrial function and decreased ATP generation are related to a decrease of glucose stimulated insulin secretion. Also, insulin sensitivity which decreases with age can accelerate the situation of glucose intolerance (Chen, Bergman et al. 1985). In order to maintain the blood glucose homeostasis and normal insulin secretory capacity, it is predicted that islet cells upregulate their ATP generating capacity and enhance their energy producing machinery by mitochondrial biogenesis. Also, although mitochondrial DNA encodes a small number of OXPHOS subunits, the abundance of mtDNA is tightly regulated and the relative abundance broadly correlates with respiratory activity across tissues. Mitochondrial biogenesis contributes to a larger number of mtDNA genome which can buffer the mitochondrial dysfunction caused by mtDNA mutations. Mitochondrial biogenesis helps to maintain mitochondrial mass and function through these two mechanisms in human β-cells (Kaufman, Li et al. 2015). In many studies, mitochondrial biogenesis has been shown to have an age-related decline. PGC-1α is the key regulator of mitochondrial biogenesis. One study observed a decline in PGC-1α expression with advancing age in healthy human neurons (Chen, Vincent et al. 2019). Mitochondrial biogenesis is still required for healthy ageing because cells need to renew the mitochondrial network, remove defective mitochondria and replace them with ones that are fully functional (Kauppila, Kauppila et al. 2017). This process can consequently improve mitochondrial function, slow down the cascade of damage caused by mitochondrial dysfunction. This might explain why the expression of mitochondrial mass and complexes significantly increase in my non-diabetic ageing donors. However, because complex I and IV expression were not higher in the old

human, it is also possible that increased Tomm20 expression serve to be a response to main normal level of complex I and IV in the old human islets.

One of my previous studies revealed that mtDNA copy number of pancreatic islets decreased with age (Cree, Patel et al. 2008). Old age healthy human donors have significantly lower mtDNA copy number compared to the young age controls. The reasons behind different results caused by impact of ageing can be explained as follow: firstly, the islets I used in the previous study were isolated islets from human pancreas tissue whereas in the current study I used paraben-embedded pancreas section; Secondly, the experiment method I performed for the previous study is to use real time PCR to calculate mtDNA copy number whereas in the current study I used quantitative staining to measure the signal intensity of mitochondrial mass marker (Tomm20). It is difficult to compare results carried by different experiment methods. However, which index can better illustrate the impact of ageing? Is it mtDNA or mitochondrial mass marker? In a study carried by Steen Larsen in 2012, mtDNA abundance was found to be a poor biomarker of mitochondrial content because it is more susceptible to oxidative damage and mutation. Nuclear encoded protein such as citrate synthase and Tomm20 along with complex I are biomarkers that exhibit the strongest association with mitochondrial content (Larsen, Nielsen et al. 2012). Another study of human breast cancer metastasis also pointed out that Tomm20 can serve as an established marker for mitochondrial mass and biogenesis (Sotgia, Whitaker-Menezes et al. 2012). In conclusion, Tomm20 staining can better illustrate mitochondrial content, thus can be regarded as a good index for studying the impact of ageing on mitochondrial expression and function in human islets.

The human baseline β-cell population is established before 5 years of age (Gregg, Moore et al. 2012). The replication of human α- and β-cell is largely completed by the age of 20 (Perl, Kushner et al. 2010, Hart, Aramandla et al. 2014). Human β-cells turn over very slowly, estimated to be once every 25 years (Gregg, Moore et al. 2012). In my study, the ages of young non-diabetic donors are all higher than 20 years which means the development of

human islet endocrine cells would have finished in my young donors. And the results of this part of study will accurately reflect the impact of ageing on islet cell without being affected by early age islet cell replication and development. It was stated before in an American study with donor age range between 16 to 66 years, the average β: α ratio is 1.3 in donors aged <40 years and 1.8 in donors aged 40 or older. The result suggested older donors' islets have more β-cells relative to α-cells (Blodgett, Carroll et al. 2013). However, in a Japanese study, average β-cell size (calculated by dividing the β-cell area by the number of β-cells) increased from 83.3 μm^2 in the first decade of life (0-9yrs age) to 129.4 μm^2 in the eighth decade of life (70- 79yrs age). The β-cell occupancy (calculated by dividing the β-cell area by the total islet area) started from 54.4% in the first decade (0-9yrs age) kept increasing to 66.0% in the fifth decade (40-49yrs age) and then went down to 60.2% in eighth decade (70-79yrs age). As a result, the number of β-cells per islet decreased from the fifth decade of life (40-49yrs age) to eighth decade of life (70-79yrs age) (Mizukami, Takahashi et al. 2014). There are two possible reasons behind the different islet cell composition results: firstly, human islets have bigger donor-to-donor variability; secondly, it was agreed by one study previously that ethnicity and different lifestyles can yield different results on islet cell composition (Mizukami, Takahashi et al. 2014).

I used donors which came from Italy and United Kingdom in our study. They are five young non-diabetic donors and seven old non-diabetic donors. It was found out that old non-diabetic human samples had significantly lower whole islet cell number and absolute β-cell number compared to the young human samples (both $p<0.05$). In the old age donor group, 5 female donors and 2 male donors were used. Female human islets have more β-cells relative to α-cells compared to male according to a human study. The decrease of absolute β-cells in the old non-diabetic donors is therefore unlikely to be the result of gender. There were no significant differences in α-cell percentage, β-cell percentage, islet size, absolute α-cell number and β/α ratio between old and young age non-diabetic donors. In conclusion, the decline of absolute β-cells with ageing lead to the reduction of whole islet cell number in the old age non-diabetic donors.

The reason why I can observe a decrease in whole islet cell number but not in the islet size maybe explained by comparing the staining images of young and old donors. We know that unlike the islet structure of mice, the endocrine cells of human and some primate islets have a more complex and random pattern. More recently human Islets were described as lobulated with mantle-core lobules. B-cells usually locate along microvasculatures which penetrate into the islets and the normal functions of β-cells depend oxygen and nutrition provided by vessels (Bonner-Weir, Sullivan et al. 2015). Although I didn't stain for intraislet vasculature in our study, the vessles appear as black spaces between cells as shown in ***Figure 6-6***. It can be seen from my islet images that old age non-diabetic donors have bigger vasculature space in the middle of islets compared to the young donors. When I measure the islet size, I only draw the region of interest based on the outside of islets without excluding the vessel space. That could explain why islet size didn't reduce along with the reduction of whole islet cell number. Also other reasons including the existence of more non-α and non-β cells in old age donors are also possible. In order to fully understand this question, more donors are better to be recruited for future study.

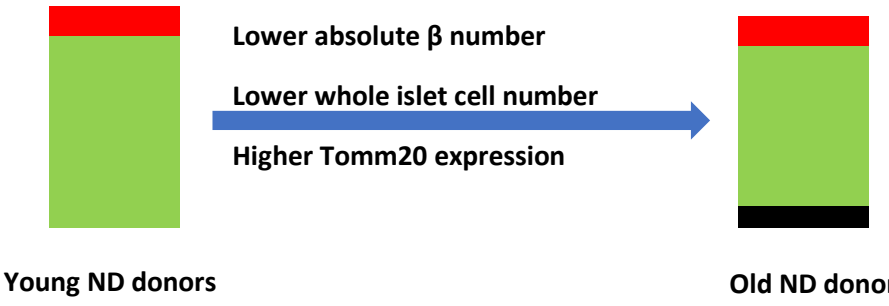

Figure 6-6. The schematic representation of the change of mitochondrial complex expression and islet cell composition in non-diabetic donors in two age groups. The whole block represents an islet. Red blot represents α-cell mass and green blot represents β-cell mass. Black blot represents intraislet vasculature mass.

The Schematic representations of the change of mitochondrial complex expression and islet cell composition in non-diabetic donors in two age groups are summarised in ***Figure 6-6.*** It can be concluded from the schematic figure that the expression of Tomm20 increases with the reduction of islet β-cells. The reason behind can be explained in this way: the lower absolute β-cell number in the old age donors is related to a decrease of GSIS. In order to maintain a normal insulin secretory response and blood glucose homeostasis, islet cells need to upregulate their ATP generating capacity and enhance their energy producing machinery by increasing the expression of Tomm20.

After I tested the impact of ageing on mitochondrial complex expression and islet cell composition on ND human samples, I'm very keen to explore these indexes in islets from old age T2DM human donors. Professor Piero Marchetti kindly donated us some T2DM human samples aged between 70-80 years. My next step will be carrying on the same quadruple immunofluorescence staining protocol on these T2DM donors and their age-matched ND control donors to see the impact of T2DM on mitochondrial complex expression and islet cell composition.

CHAPTER 7. GENERAL DISCUSSION

7.1. Discussion

The aim of this thesis was to investigate the impact of ageing on mitochondrial function and islet cell composition by using the mtDNA mutator mice model and ageing human donors. Mitochondrial dysfunction can affect pancreatic β-cell function and islet cell composition in response to ageing.

7.1.1. Is *PolgA$^{mut/mut}$* mice a good ageing model?

In human, mtDNA mutations accumulate throughout a lifetime, albeit at extremely low levels. The mutation loads vary in different tissues and they are especially high in postmitotic tissues such as the brain, heart and muscle (Khaidakov, Heflich et al. 2003, Schon, Dimauro et al. 2012). To enable the study of ageing, mice model are widely used firstly because of their phylogenetic relatedness and physiological similarity to humans (Perlman 2016). Many age-related diseases such as T2DM, cancer, heart disease, arthritis, osteoporosis and cognitive decline have been modeled in mice (Wallace 1999, Muller, Liu et al. 2008, Li, Jiao et al. 2016). Secondly, mice age much faster than humans. 14- 15 month old C57BL/6 are considered as middle-aged corresponding to 38-47 years old humans (Laboratory). This enables the investigation of mitochondrial dysfunction and ageing within a short period.

The homozygous knock-in *PolgA$^{mut/mut}$* mice model I used in my study have 3 to 5-fold increase in mtDNA point mutations and an increase in mtDNA deletions compared to their age-matched controls (Trifunovic, Wredenberg et al. 2004). These high-level mtDNA mutations can cause mitochondrial dysfunction which has been shown to be associated with reduced lifespan and the onset of premature ageing phenotypes. Thus, *PolgA$^{mut/mut}$* mice has been widely regarded as an ideal ageing model and the mitochondrial complex expressions have been studied before in different body organs of *PolgA$^{mut/mut}$* mice, including but not limited to the bone, heart, colon and brain tissues (Trifunovic, Wredenberg et al. 2004, Vermulst, Wanagat et al. 2008, Dobson, Rocha et al. 2016). Compared to age-matched wild type

controls, the osteoblast cells of 11-month *PolgA*$^{mut/mut}$ mice have significant deficiency in both complex I and IV expression (Dobson, Rocha et al. 2016); 15 month *PolgA*$^{mut/mut}$ mice have many complex IV deficient cells in the duodenum, heart and brain tissue (Vermulst, Wanagat et al. 2008); some cardiomyocytes from 11-month *PolgA*$^{mut/mut}$ mice have complex IV deficiency, leading to a mosaic pattern in the heart muscle staining (Trifunovic, Wredenberg et al. 2004). My study was the first to study mitochondrial complex expression in pancreatic islets of *PolgA*$^{mut/mut}$ mice. A key finding was that complex I deficiency was clearly present in the islets of *PolgA*$^{mut/mut}$ mice compared to the age-matched wild type mice at 3 months and this deficiency persisted in the *PolgA*$^{mut/mut}$ through to 11 months. Complex IV expression was significantly higher in islets of 11-month *PolgA*$^{mut/mut}$ mice compared to the age-matched wild type mice.

However, it was reported before that in the *PolgA*$^{mut/mut}$ mice, the accumulation of mtDNA mutation starts from the embryonic/fetal period. The mutation load sharply accumulates and reaches a substantially high level in different tissues compared to the age-matched wild type controls by 2 months of age. This level of mutation appears to remain stable afterward, leading to the onset of various premature ageing phenotypes at around 6 months of age (Trifunovic, Wredenberg et al. 2004, Kujoth, Hiona et al. 2005). However, in the normal ageing process, mtDNA mutations steadily and gradually increase with age. Besides, this model is a 'whole body' mutator mice model, mtDNA mutation remains equally between different tissues within the mice which is different from normal ageing (Greaves and Turnbull 2009). *PolgA*$^{mut/mut}$ mice cannot be regarded as a good ageing model because of this difference in the growth and allocation of mtDNA mutations compared to normal ageing (***Figure 7-1***). Nonetheless, it has illustrated that mitochondrial dysfunction promotes tissue dysfunction and premature ageing.

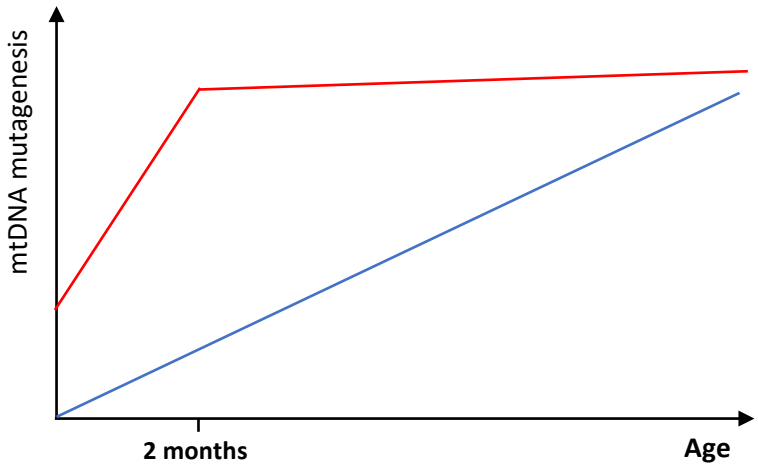

Figure 7-1. Different changing trend of mtDNA mutations between PolgA mutated ageing and normal ageing. Red line represent PolgA mutated ageing and blue line represents normal ageing.

7.1.2. The difference in mitochondrial complex expression between α and β cells.

As discussed in chapter 5, Tomm20, complex I and complex IV expression levels were all lower in α-cells compared with β-cells in the old *PolgA*$^{mut/mut}$ islets. The same pattern was seen when comparing α-cells with β-cells in the old control islets. What could be the reasons behind this lower mitochondrial complex expression in α-cells?

Blood glucose levels rise after a meal and glucose is the primary stimulus for insulin secretion. Hyperglycemia and the resulting high intercellular ATP inhibits K_{ATP} channel activity. This results in the membrane depolarization and the subsequent opening of voltage-gated Ca^{2+} channels of β-cells. The influx of Ca^{2+} leads to an increase of cytosolic calcium, inducing the migration and fusion of insulin containing granules to the β-cell membrane surface and insulin secretion. When this elevation of blood glucose activates insulin secretion, it leads to suppression of glucagon secretion in healthy α-cells (Briant, Salehi et al. 2016). On the contrary, hypoglycemia and resulting low intracellular ATP levels in α-cells is the primary trigger for exocytosis of glucagon granules from the α-cells. Müller stated that glucagon may regulate its own secretion indirectly via a stimulatory effect on β-cells to secrete insulin (Müller, Finan et al. 2017). This was also proved by Ishihara that there was a coupling of metabolism and secretion between α- and β-cells in isolated islets (Ishihara, Maechler et al. 2003). It can be deduced that the secretory functions are quite different between α and β-cells. β-cells require periodic high energy provision for the post-meal insulin secretory bursts, while glucagon secretion is under long term tonic control with periods of secretory shut-down post-meal. These different energy demands might explain why Tomm20, complex I and complex IV expression are all lower in α-cells compared to β-cells in both mice groups.

7.1.3. Altered pancreatic islet cell composition of *PolgA*$^{mut/mut}$ mice result from different mitochondrial complex expression in different endocrine cells.

When comparing the mitochondrial complex expression in the same endocrine cells between different mouse groups, complex I expression was decreased while complex IV expression was markedly increased in β-cells of the *PolgA*$^{mut/mut}$ mice compared with the β-cell of the

age-matched controls. The expression pattern was different for α-cells. There was a marked decrease in complex I expression accompanied by a small increase in complex IV expression in α-cells of the old *PolgA*$^{mut/mut}$ mice compared with α-cells of the age-matched controls.

While there was no difference in β-cell number between the old *PolgA*$^{mut/mut}$ mice compared with the age-matched controls, there was evidence of decreased insulin expression in the 11-month *PolgA*$^{mut/mut}$ mice. It is possible that the increased complex IV expression in the β-cells of the old *PolgA*$^{mut/mut}$ mice represents an adaptive and protective response to the mitochondrial stress to try to maintain the β-cell function in the *PolgA*$^{mut/mut}$ mice islets with age. This phenomenon has been observed in other tissues in which there is an upregulation of components of the mitochondrial respiratory chain in response to complex I deficiency (DiMauro and Schon 2003, Picard, Zhang et al. 2014).

Conversely, the marked complex I deficiency in α-cells in comparison with both the β-cells of the old *PolgA*$^{mut/mut}$ mice and with α-cells of the old control islets may be the main mechanism of age-related increase in α-cell proliferation and cell number. One previous study reported that knockdown of NDUFB9 (a component of complex I) was shown to promote cell proliferation in a tumour cell-line and was accompanied by an increase in ROS generation (Li, Sun et al. 2015). ROS levels are normal in young mice but increase as the animal age. Raised ROS levels have been implicated in promoting cell proliferation in non-tumour cell lines (Kim, Okamoto et al. 2017). Together, these findings raise the possibility that the increased α-cell proliferation observed in old *PolgA*$^{mut/mut}$ mouse islets are a response to complex I deficiency and increased ROS generation. Taken together, it can be concluded that α-and β-cells have different adaptations towards complex I deficiency. α-cells compensate by α-cell proliferation whereas β-cells adapt by increasing complex IV expression in β-cells.

7.1.4. *PolgA*$^{mut/mut}$ mice model compared to TFAM β-cell specific knockdown mice model.

As discussed in chapter 4 and 5, 11-month *PolgA*$^{mut/mut}$ mice are presented with an increase in absolute α-cell number, a decreased β/α cell ratio, decreased insulin expression and

decreased body weight. The endpoint blood glucose measurements show they didn't develop diabetes at 11-month. In another mitochondrial mouse model, β-cell-specific TFAM- knock out mutant mice, there was a comparable decrease in the islet β/α cell ratio with age. However, this altered cell ratio was caused by extensive loss of β-cell mass at 39 weeks. These mice developed diabetes from the age of approximately 5 weeks with normal body weight (Silva, Köhler et al. 2000). Isolated islets from this mouse model showed impaired Ca^{2+} signaling and lower insulin release at 7~9 weeks of age (Silva, Köhler et al. 2000). The β-cell-specific TFAM knockout model breeds more severe knockout and decreased mitochondrial gene expression with complex IV deficiency along with the reduction of β-cell mass (Silva, Köhler et al. 2000). The final islet phenotype will have resulted from a combination of mitochondrial dysfunction and the secondary effects of chronic hyperglycaemia. In my study, the *PolgA*$^{mut/mut}$ mice did not develop diabetes, probably because the restricted increase in body mass limited the insulin secretory demand. As a consequence, the changes in islet cell composition observed in the *PolgA*$^{mut/mut}$ mice with age appear to be directly related to mitochondrial dysfunction and independent of changes in glycaemic status. A detailed comparison between the two mice models are summarised in ***Table 7-1***.

Table 7-1. The comparison between *PolgA*$^{mut/mut}$ mice and TFAM β cell specific knockdown mice.

	PolgA$^{mut/mut}$ mice	TFAM β cell knockdown mice
Absolute α cell number	↑	
Absolute β cell number		↓
β/α ratio	↓	↓
Insulin secretion	↓	↓
Complex IV expression in islet	↓	↑
Body weight	↓	↔
Diabetes	No	Yes

7.1.5. The longitudinal comparison in mitochondrial complex expression and islet cell composition between human and mice.

Table 7-2. The age related changes in mitochondrial complex expression in mice and human islets.

	Mouse		Human
	Wild type	*PolgA*$^{mut/mut}$	
Tomm20 (mito mass)	↑	↑	↑
NDUFB8 (Complex I)	↔	↔*	↔
MTCO1 (Complex IV)	↓	↔	↔

* The complex I expression started at low base level at 3 months and persistent till 11 months.

I found some similarities and some differences in terms of mitochondrial complex expression when I compare the results of mice and humans longitudinally. With the increase of age, the expression of Tomm20 (mitochondrial mass) increases in islets of wild-type mice, *PolgA*$^{mut/mut}$ mice and humans. This can be explained by a compensatory response to maintain the normal mitochondrial function by mitochondrial biogenesis in pancreatic islets with age. This result is in consistent with the latest study about mitochondrial adaptation in human skeletal muscle. They discovered that the expression of Tomm20 is higher in skeletal muscle of the older age group compared to that of the younger age group (Buso, Comelli et al. 2019). Another study that uses male C57BL/6J mice reported that the Tomm20 expression is higher in 16-20 month mice compared to 2-3 month mice (Del Campo, Contreras-Hernández et al. 2018).

However, the change of complex I was not observed in the normal ageing process, but it was observed in the *PolgA*$^{mut/mut}$ mice compared to their age-matched controls at a young age and persisted till 11 months. The age-related decrease in Complex IV expression was only observed in the islets of wild type mice but not in the *PolgA*$^{mut/mut}$ mice and humans. Similar results were also reported in different tissues of normal mice before: one study showed that complex IV activity in the auditory cortex of the normal mice gradually decrease by 13% between 1 and 15 months of age (Zhong, Hu et al. 2012); another study showed that

mitochondrial complex IV activity is specifically decreased in white adipocytes in the ageing normal mice (Soro-Arnaiz, Li et al. 2016).

It's important to recap that the mice and human studies address different questions. The *PolgA*$^{mut/mut}$ mice model was used to study the impact of mitochondrial dysfunction on islet cell composition in response to age, whereas the human study explored whether mitochondrial subunit expression changed with age in pancreatic islet cells.

Table 7-3. The age-related changes in islet cell composition in mice and human.

	Mouse		Human
	Wild type	*PolgA*$^{mut/mut}$	
Islet size	↑	↑	↔
Whole islet cell number	↑	↑	↓
Absolute α cell number	↔	↑	↔
Absolute β cell number	↑	↑	↓
β/α ratio	↑	↓	↔

When compared the results of mice and human in terms of islet cell composition, I see a different age-related change in whole islet cell number and absolute β-cell number. In the mice study, I observed an increase of whole islet cell number and the increase of absolute β-cell number in wild type mice islets from 3 months to 11 months of age. The body weights of our wild type mice went from nearly 30g at 5 months to nearly 40g at 11 months (Detailed chart is in appendix chapter). Similar growth rate was also reported in another study that the body weight of C56BL/6 mice was nearly doubled from 2.5 months of age to 10 months of age (Kehm, König et al. 2018). My results is consistent with a previous literature using the Lewis rat model. β-cell mass increased with age in the normal Lewis rat and was closely correlated with the age-related increase in the body weight (Montanya, Nacher et al. 2000). Another study that emphasized on the impact of ageing on islet size and composition showed a similar age-related change of islet size as shown in my study, in which islet size doubled in

normal C57BL/6 mice from 2.5 months to 21 months. During this time period, the mice average body weight increased from 23 ± 3.8g to 41.5 ± 5g (Kehm, König et al. 2018).

It can be concluded that the increase of β-cell mass in wild type mice is driven by combinative factors of normal ageing and the increment of metabolic demand. However, as for *PolgA*$^{mut/mut}$ mice, their islet size and whole islet cell number increase even under the circumstance of the age-related decrease of body weight. I can conclude that the increase of islet size and whole islet cell number in *PolgA*$^{mut/mut}$ mice was solely driven by mtDNA mutations induced accelerated ageing. Although there were no significant difference in islet size and whole islet cell number between wild type and *PolgA*$^{mut/mut}$ mice at 11 months, the 11-month islet cell composition is different between two groups of mice. The reason is because the increment of islet cell with age was mainly caused by the increase of β-cells in the wild type mice, whereas α- and β-cell number both increase in *PolgA*$^{mut/mut}$ mice. The increasing extent of β-cells is not as significant as that of α-cells in *PolgA*$^{mut/mut}$ mice. This difference was also shown in the β/α ratio, the value of 11-month wild type mice increased longitudinally whereas the value of *PolgA*$^{mut/mut}$ mice decreased with the increase of age.

In islets of human samples, an age-related decrease in whole islet cell number and absolute β-cell number were observed in old age non-diabetic donors. The change of the whole islet and β-cell number was driven solely by the increase of age but not the change of metabolic demand. In mice, a marked increase of body weight drives the significant increase of β-cell number to maintain metabolic homeostasis with an increase of age. As for humans, body growth is largely complete by the age of 20, although adiposity can increase with time. In this study, the young and old islet tissue donors were matched for BMI, so the differences in islet cell composition were not driven by body growth.

7.2. Mitochondrial dysfunction and islet cell composition

It can be concluded that mitochondrial mutation caused mitochondrial dysfunction can impact islet cell composition in mice and humans through following mechanisms (***Figure 7-2***).

7.2.1. Ageing

According to the mitochondrial theory of ageing, ageing is the driver and consequence of mitochondrial dysfunction. As mentioned in the **chapter 1.2.6** that normal ageing has been associated with impaired glucose tolerance, insulin resistance, hyperinsulinemia, defect islet β-cell function and changes of islet endocrine cells composition. The change of body composition such as decrease of lean body mass and increase of total body fat which accompany normal human ageing can impair insulin secretion and action. Rodent pancreatic β-cell mass has a certain degree of plasticity and can expand to compensate for insulin resistance with age.

7.2.2. T2DM.

Apart from causing mitochondrial diabetes, mitochondrial dysfunction also contributes to the pancreatic β-cell dysfunction and decreased insulin secretion in T2DM. As mentioned in **Chapter 1.3.3**, T2DM can negatively impact β-cell mass, function and islet cell identity.

7.2.3. The interaction between ageing and T2DM.

T2DM prevalence increases with age. Firstly, the generation of ROS from age-related mitochondrial dysfunction can activate β-cell apoptosis, β-cell dysfunction and insulin resistance which are closely related to the onset, progression and pathological consequences of diabetes. Also, there is significant evidence that mtDNA mutations and mitochondrial dysfunction play a role in diabetes pathogenesis. Maternally inherited diabetes and deafness (MIDD) is the most common manifestation of the m.3243A>G mutation (Nesbitt, Pitceathly et al. 2013) with particularly high levels of the mutation detected in islets (Kobayashi, Nakanishi et al. 1997) and a mosaic pattern of pancreatic β-cell loss, probably due to low tolerance of mitochondrial dysfunction in these cells (Otabe, Yasuda et al. 1999). Vice versa,

the chronic hyperglycaemia status of diabetes can increase glucose metabolism through oxidative phosphorylation which further increases the production of ROS with age. This vicious cycle can mass generate ROS and activate the progression of important diabetes-related metabolic disorders. Secondly, age-related mitochondrial dysfunction can cause the respiratory chain complex blockage which inhibits glucose stimulated insulin secretion. This strong interaction between T2DM and ageing will further accelerate the change of islet cell composition.

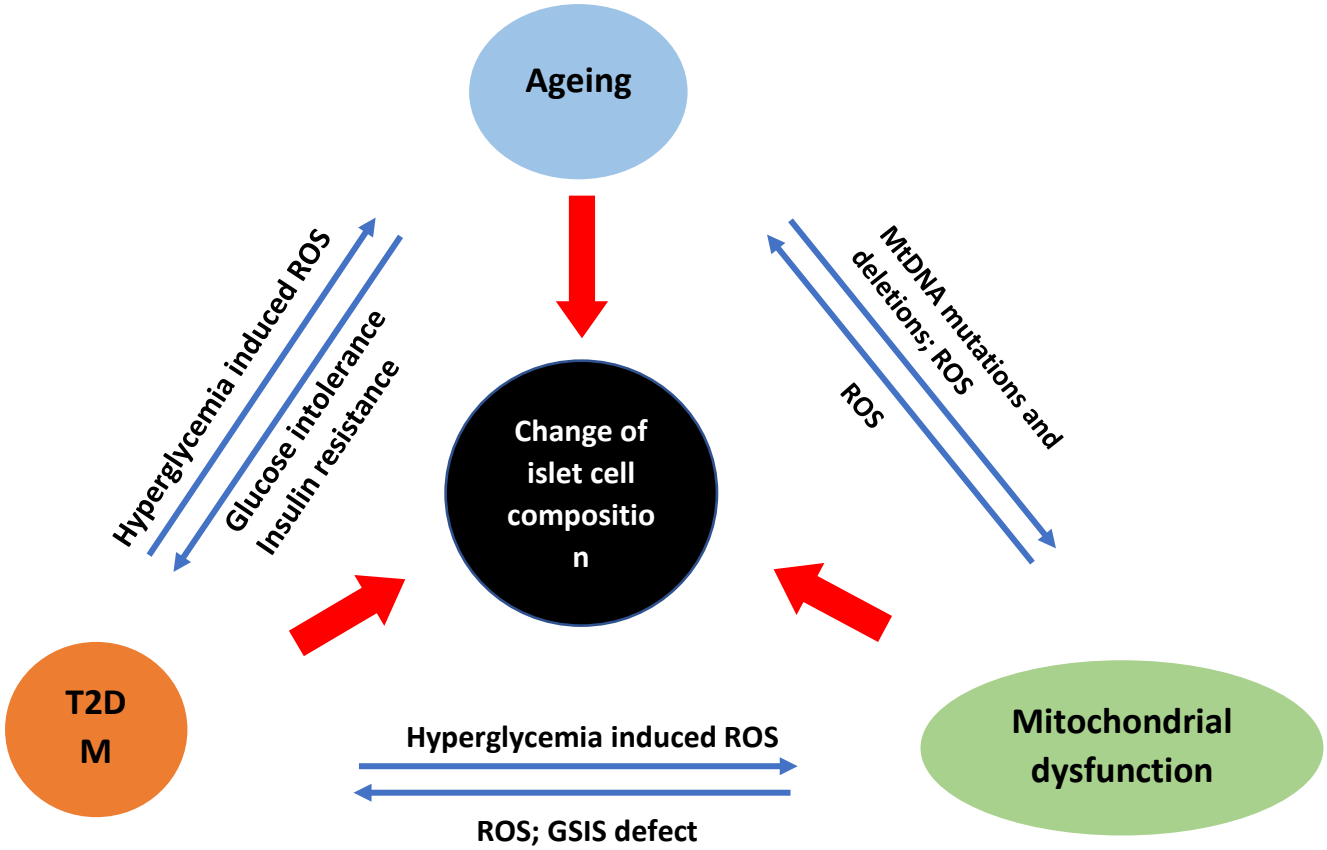

Figure 7-2. The possible mechanisms behind the change of islet cell composition.

7.3. Innovations

The main focus of this PhD study is the impact of ageing on islet mitochondrial respiratory chain complex expression and islet cell composition by using a mtDNA mutator mice model and ageing human pancreas samples. It has many innovations, firstly, although studies about *PolgA*$^{mut/mut}$ mice have been published worldwide for many years, it's the first one to study the mitochondrial complex expression and cell composition in pancreatic islets of *PolgA*$^{mut/mut}$ mice. Secondly, my study is the first study which quantitatively measures mitochondrial complex expression in pancreatic whole islet and islet cell subtypes by using a novel quadruple immunofluorescence staining protocol. Thirdly, this is the first study that applied quadruple mitochondrial staining protocol on ageing human pancreas samples and quantitatively analyzed mitochondrial complex expression in human pancreatic islets with an increase of age.

7.4. Limitations

In the cell composition study of *PolgA*$^{mut/mut}$ mice. Firstly, instead of one mechanism solely contributing to the increment of α- and β-cells in different mice groups, I believe it's more likely that several different mechanisms are working together to achieve the islet cell composition results. Some classic differentiation, transdifferentiation or even apoptosis markers are also worth studying in my case. Secondly, apart from counting α-and β-cell number, I can also count colocalized cells that secrete both insulin and glucagon. The existence of colocalized cells is also solid evidence that some endocrine cells are undergoing transdifferentiation. Thirdly, it was reported in the Kehm study that there was an age-dependent decrease in Ki67 proliferation capacity from 2.5 months to 21 months. However, I haven't applied the Ki67 staining on 3 months *PolgA*$^{mut/mut}$ and wild type mice to further prove this discovery.

A previous study showed that blood glucose, plasma insulin level of healthy C57BL/6 mice are very stable throughout ages. However, the plasma proinsulin level decreases but the conversion rate of proinsulin to insulin increases in C57BL/6 mice with age, indicating a better

glucose homeostasis management with age in C57BL/6 mice (Kehm, König et al. 2018). Ideally, I would have periodically measured proinsulin and insulin secretion in my mice. Secondly, due to the restrictions of the animal experiment license, I was not allowed to perform blood glucose measurements when mice were fasting. Instead, I measured the blood glucose in a certain time period (1pm – 3pm) in the afternoon monthly. It will be more accurate if I can measure blood glucose in the morning after overnight fasting. Overnight fasting nearly depletes liver glycogen stores in the mouse and has the advantage of reducing variability in baseline blood glucose (Ayala, Samuel et al. 2010).

7.5. Future work

As I discussed in the limitation part, it is more likely that different mechanisms are contributing together for the change of islet cell composition in the 11-month *PolgA*$^{mut/mut}$ mice. Apart from proliferation marker Ki67, some classic transdifferentiation markers (such as PDX1, NKX6.1) and apoptosis assays (such as TUNEL and caspase activation assays) are also worthy to be further studied. RNA sequencing can be used to look at the gene expression of Ki67, PDX1 and NKX6.1 to further validate the result we achieved from immunofluorescence.

Given the importance of mitochondrial dysfunction for GSIS in β-cells, it is possible that a selective mutation of mtDNA polymerase in β-cells will lead to an impaired glucose homeostasis and impaired GSIS. Bensch and his team generated a Tg mouse model which expresses a proofreading-deficit D181A poly only in β-cells. An elevated blood glucose level was observed as early as 4 weeks in Tg mice. They also concluded that the glucose intolerance in these mice is not related to defects in β-cell mitochondrial oxidative metabolism but is associated with β-cell apoptosis (Bensch, Degraaf et al. 2007). It will be very interesting if I can apply our quadruple mitochondrial immunofluorescence staining protocol on this mice model of selective mutation of mtDNA polymerase in β-cells and further study the changes of mitochondrial complex expression.

I studied islets from non-diabetic young age and old age donors and compare the impact of normal ageing on mitochondrial complex expression and cell composition. Tissue samples from type 2 diabetes donors which are age-matched with old age non-diabetics were kindly given by Professor Piero Marchetti. It will be interesting to analyse mitochondrial subunit expression and islet cell composition in these samples to see what changes occur as the beta-cells fail and diabetes develops.

7.6. Conclusion

By using a novel quadruple mitochondrial immunofluorescence assay, it's the first study which quantitatively measured mitochondrial complex expression within pancreatic islets. In this study I have shown that age-associated defects in mitochondrial complex I protein expression cause a significant decrease in β-cell insulin staining intensity and alter pancreatic islet cell composition in aged *PolgA*$^{mut/mut}$ mice. I show a significant increase in the proportion of α-cells per islet and provide evidence that is due to increased α-cell proliferation. My findings in the pancreatic islets are consistent with the original Trifnovic's observations, with evidence of a marked decrease in mitochondrial expression in islets from young *PolgA*$^{mut/mut}$ mice but with no premature ageing phenotypes. The impact of mitochondrial dysfunction only became apparent as the animals aged. In normal ageing human islets, the age-associated change of mitochondrial expression also leads to the change of islet cell composition.

Taken together, my findings show that mitochondrial dysfunction adversely affects pancreatic β-cell function and islet cell composition in response to ageing.

CHAPTER 8. APPENDIX

Table 8-1. The endpoint body weight of 11 month *PolgA*$^{mut/mut}$ mice and wild type mice which used for mitochondrial expression and islet cell composition studies.

	Genotype	Status	Endpoint body weight (g)
GA0002	WT	Sedentary	41.6
GA0004	WT	Sedentary	40.8
GA0005	WT	Sedentary	37.2
GA0007	WT	Sedentary	36.4
GA0008	WT	Sedentary	40.7
LG0002	HOM	Sedentary	29.4
LG0004	HOM	Sedentary	27.5
LG0006	HOM	Sedentary	27.5
LG0011	HOM	Sedentary	28.2
LG0036	HOM	Sedentary	30.7
LG0005	HOM	Exercise	26.4
LG0009	HOM	Exercise	28.9
LG0023	HOM	Exercise	31.4
LG0024	HOM	Exercise	34.7

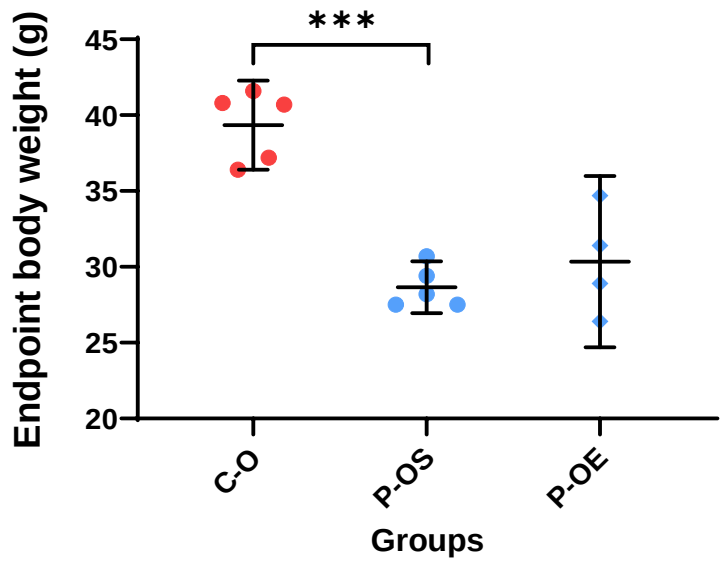

Figure 8-1. The endpoint body weight of 11 month PolgA$^{mut/mut}$ sedentary and exercise mice and wild type mice. Mean ± 95% CI. 11 month wild type mice (WT); 11 month *PolgA*$^{mut/mut}$ sedentary mice (P-OS); 11 month *PolgA*$^{mut/mut}$ (P-OE). Unpaired t-test between wild type and *PolgA*$^{mut/mut}$ mice, $p<0.01$; Unpaired t-test between *PolgA*$^{mut/mut}$ sedentary and exercise, $p>0.05$.

Table 8-2. Monthly glucose measurement results in newly recruited 5 *PolgA*$^{mut/mut}$ mice and 5 wild type mice (mmol/l).

	Genotype	14/03/19	17/04/19	15/05/19	18/06/19	16/07/19	14/08/19	17/09/19
1909	HOM	9.8	8.5					
1918	HOM	9.9	9.5	8.6				
1923	HOM	8.8	6.3	7.7				
1937	HOM	11.8/10.6	9.6	9.4	11.4			
1940	HOM	9.4	9.6	11.9/11.1	8.3			
1967	WT	9.6	11.7	11.5	13.3/10.2	11.9/10.3	9.5	
1997	WT	9.1	8.8	10.2	11.9/9.7	9.7	7.7	
1999	WT	9.3	15.9/9.6	9.6	12.8/11.1	10.7/10.1	10.3	
2029	WT	9.3	9.3	15.2/10.3	11.5	11.3/11.5	8.7	10.7
2034	WT	9.6	8.6	9.4	10.7	10.2	9.1	9.1

Table 8-3. Monthly body weight measurement results in newly recruited *PolgA*$^{mut/mut}$ mice and wild type mice (g).

	Genotype	14/03/19	17/04/19	15/05/19	18/06/19	16/07/19	14/08/19	17/09/19
1909	HOM	24.3	23.8					
1918	HOM	30.2	29.4	28				
1923	HOM	23.2	22.6	21.8				
1937	HOM	28.7	29.6	29.6	30.2			
1940	HOM	24.5	24.8	24.1	22.6			
1967	WT	36.5	38.5	40.1	42.5	42.9	44.2	
1997	WT	32.1	34.2	36.5	38.3	39.3	40.9	
1999	WT	32.8	33.5	36.5	39.4	41.5	44.5	
2029	WT	23.3	23.8	25.5	25.1	25.9	27.4	29.6
2034	WT	30.5	31.6	34.4	34.6	36.3	38.6	39.1

Table 8-4. Two times of HbA1c% measurement and average HbA1c% result in endpoint whole blood samples from newly recruited 5 *PolgA*$^{mut/mut}$ and 5 wild type mice.

	Genotype	1st	2nd	average
1909	HOM	4.063378	4.074783	4.069081
1918	HOM	5.21062	4.409941	4.81028
1923	HOM	4.822117	4.268582	4.545349
1937	HOM	5.656363	4.45212	5.054242
1940	HOM	5.68681	4.655039	5.170925
1967	WT	5.761101	4.620839	5.19097
1997	WT	5.399391	4.819197	5.109294
1999	WT	6.25556	5.69015	5.972855
2029	WT	5.708732	4.321021	5.014877
2034	WT	5.992498	5.025536	5.509017

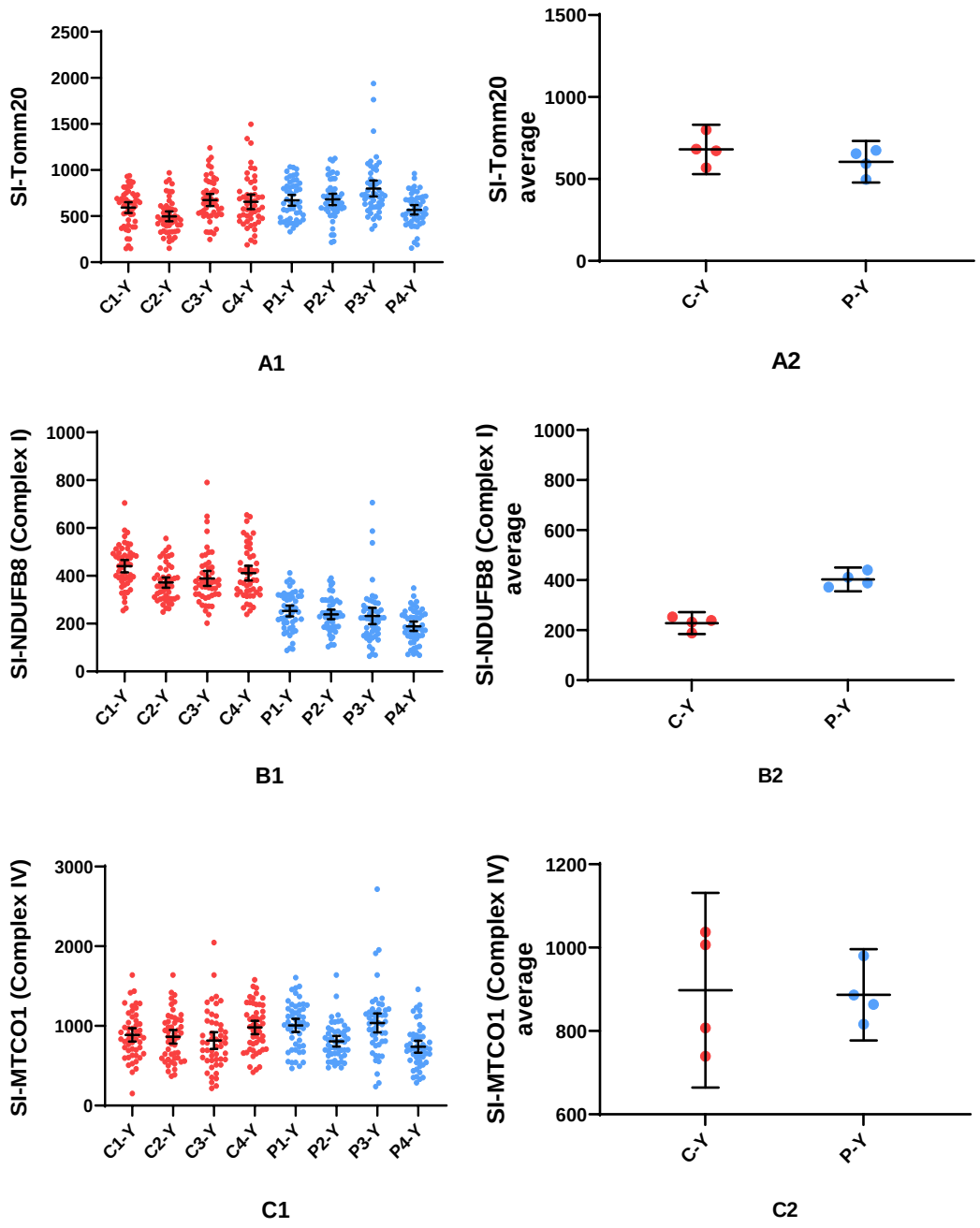

Figure 8-2. Changes of signal intensity in mitochondrial mass marker, complex I (NDUFB8) and complex IV (MTCO1) in 3-month sacrificed *PolgA*$^{mut/mut}$ mice compared to age-matched wild type mice. Mean ± 95% CI. (A1, B1, C1) Signal intensity case comparison. In all graphs: wild type mice (C1-Y to C4-Y) and *PolgA*$^{mut/mut}$ sedentary mice (P1-Y to P4-Y). Each point consists of 50 islet data. (A1) SI-Tomm20, One-way ANOVA, $p<0.01$; (B1) SI- NDUFB8, One-way ANOVA, $p<0.01$; (C1) SI- MTCO1. One-way ANOVA, $p<0.01$. **(A2, B2, C2) Signal intensity group average comparison.** In all graphs, wild type mice (C-Y), *PolgA*$^{mut/mut}$ sedentary mice (P-Y). Each point represents average data of 50 islets from one group. (A2) SI-Tomm20 group average. Unpaired t-test, $p>0.05$. (B2) SI-NDUFB8 group average. Unpaired t-test, $p<0.01$; (C2) SI-MTCO1 group average. Unpaired t-test, $p>0.05$.

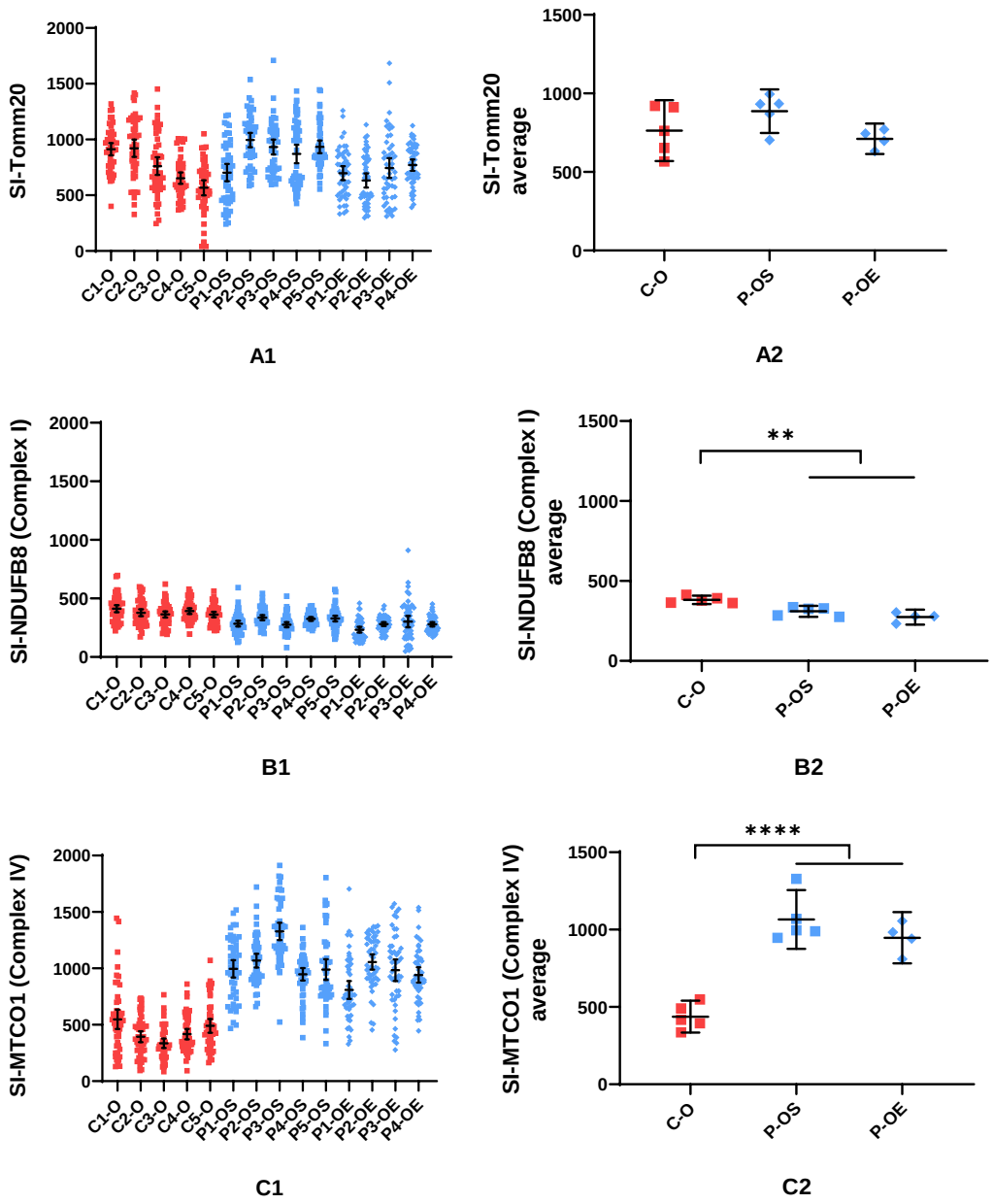

Figure 8-3. Changes of signal intensity in mitochondrial mass marker, complex I (NDUFB8) and complex IV (MTCO1) in 11-month sacrificed *PolgA*$^{mut/mut}$ mice compared to age-matched wild type mice. Mean ± 95% CI. (A1, B1, C1) Signal intensity case comparison. Wild type mice (C1-O to C5-O); *PolgA*$^{mut/mut}$ sedentary mice (P1-OS to P5-OS); *PolgA*$^{mut/mut}$ exercise mice (P1-OE to P4-OE). Each point consists of 50 islets data. (A1) SI-Tomm20; (B) SI-NDUFB8; (C) SI-MTCO1. One-way ANOVA, all P<0.01. **(A2, B2, C2) Signal intensity group average comparison.** Wild type mice (C-O); *PolgA*$^{mut/mut}$ sedentary mice (P-OS); *PolgA*$^{mut/mut}$ exercise mice (P-OE). Each point represents average data of 50 islets from one case. (A2) SI-Tomm20 group average. Unpaired t-test, p>0.05. (B2) SI-NDUFB8 group average. Unpaired t-test between wild type and *PolgA*$^{mut/mut}$ group, p<0.01; Unpaired t-test between *PolgA*$^{mut/mut}$ sedentary and exercise group, p>0.05; (C2) SI-MTCO1 group average. Unpaired t-test between wild type and *PolgA*$^{mut/mut}$ mice group, p<0.01; Unpaired t-test between *PolgA*$^{mut/mut}$ sedentary and exercise group, p>0.05.

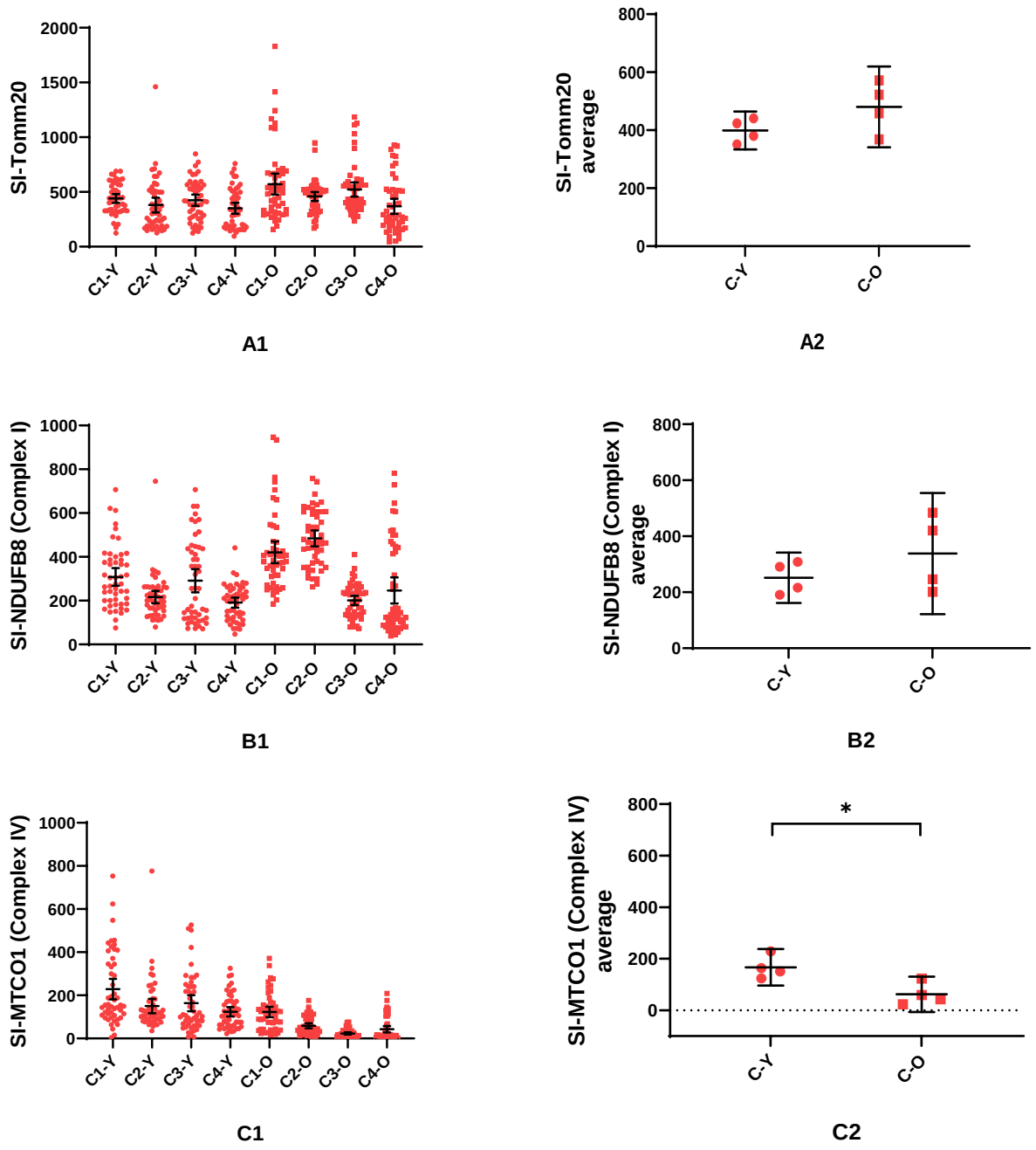

Figure 8-4. Changes of signal intensity in mitochondrial mass marker, complex I (NDUFB8) and IV (MTCO1) in 11-month wild type mice compared to 3-month wild type mice. Mean ± 95% CI. (A1, B1, C1) Signal intensity case comparison. Young mice (3 month) C1-Y to C4-Y; old mice (11 month) C1-O to C4-O. Each point consists of 25 islet data. (A1) SI-Tomm20; (B1) SI-NDUFB8; (C1) SI-MTCO1. All one-way ANOVA, $p<0.01$. **(A2, B2, C2) Signal intensity group average comparison.** Young mice (3 month) C-Y; Old mice (11 month) C-O. Each point represents average data of 25 islets from one case. (A2) SI-Tomm20 group average. Unpaired t-test, $p>0.05$. (B2) SI-NDUFB8 group average. Unpaired t-test, $p>0.05$; (C2) SI-MTCO1 group average. Unpaired t-test, $p<0.05$.

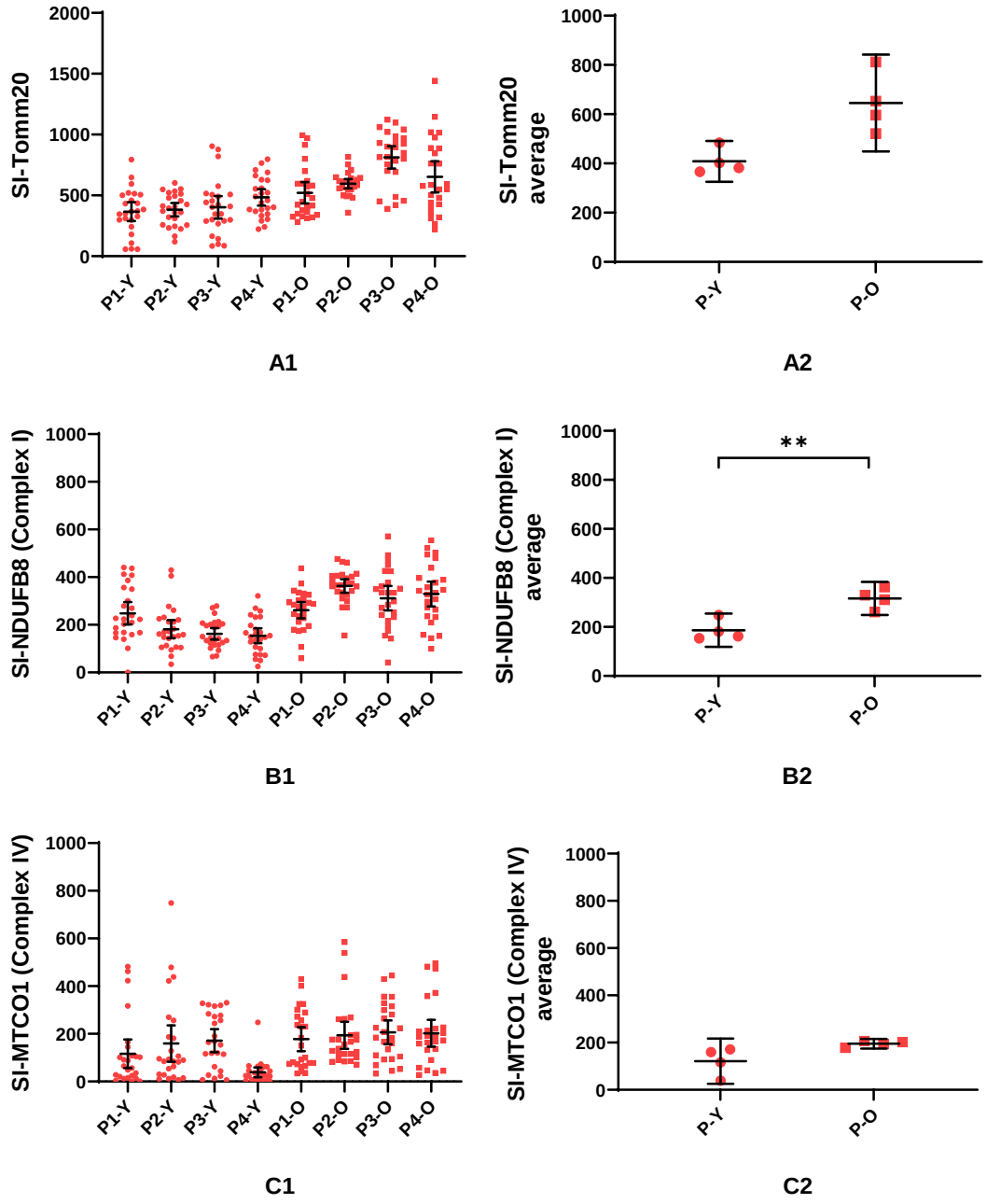

Figure 8-5. Changes of signal intensity in mitochondrial mass marker, complex I (NDUFB8) and IV (MTCO1) in 11-month *PolgA*$^{mut/mut}$ mice compared to 3-month *PolgA*$^{mut/mut}$ mice. Mean ± 95% CI. (A1, B1, C1) Signal intensity case comparison. Young (3 month) PolgAmut/mut mice (P1-Y to PY-4); old (11 month) *PolgA*$^{mut/mut}$ sedentary mice (P1-OS to P5-OS); old (11 month) *PolgA*$^{mut/mut}$ exercise mice (P1-OE to P4-OE). Each point represents 25 islets data. (A1) SI-Tomm20; (B1) SI-NDUFB8; (C1) SI-MTCO1. One-way ANOVA, p<0.01 **(A2, B2, C2) Signal intensity group average comparison.** Young (3 month) *PolgA*$^{mut/mut}$ mice (P-Y); old (11 month) *PolgA*$^{mut/mut}$ sedentary mice (P-OS); old (11 month) *PolgA*$^{mut/mut}$ exercise mice (P-OE). Each point represents average data of 25 islets from one case. (A2) SI-Tomm20 group average. Unpaired t-test, p>0.05. (B2) SI-NDUFB8 group average. Unpaired t-test, p<0.01; (C2) SI-MTCO1 group average. Unpaired t-test, p>0.05.

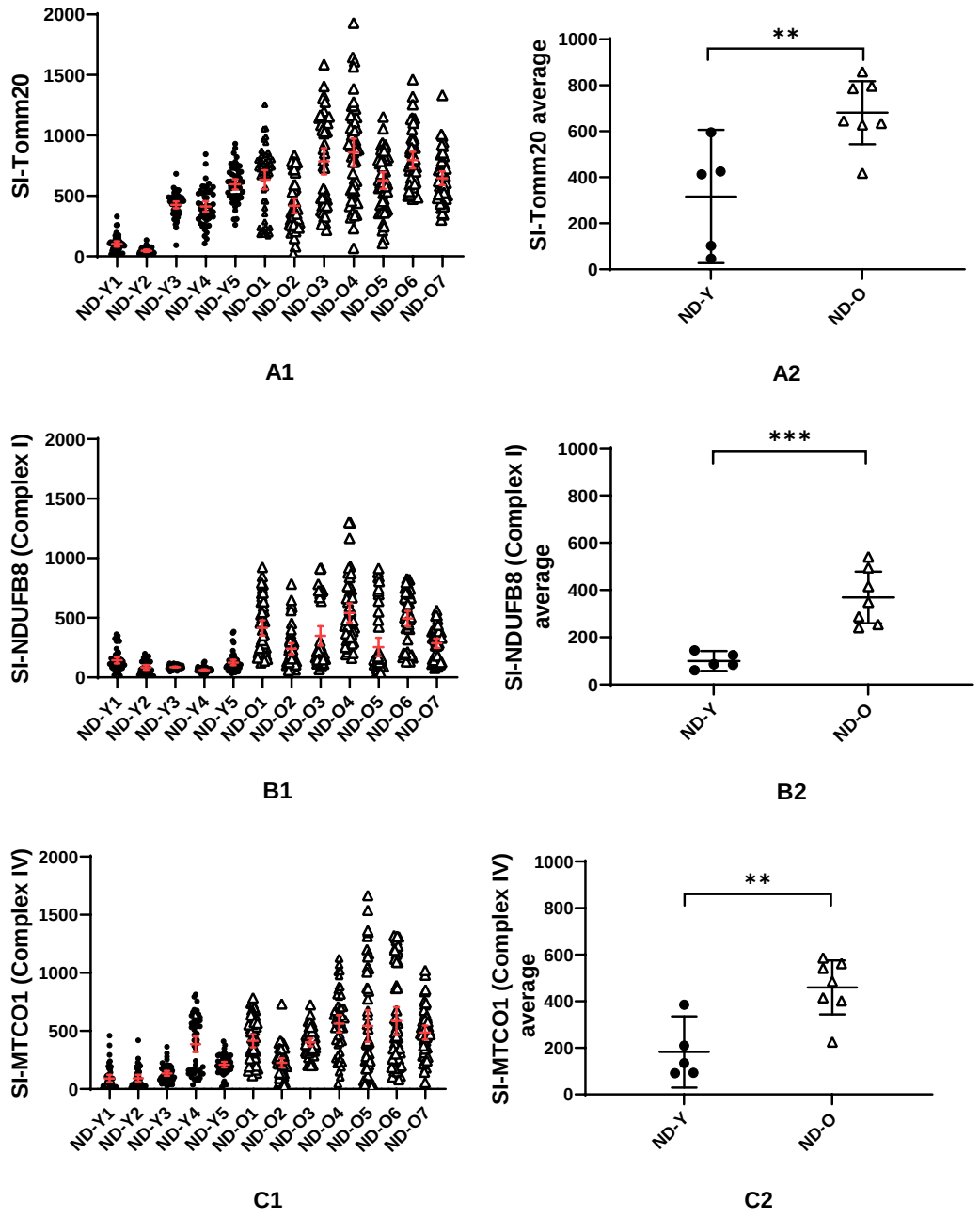

Figure 8-6. Changes of signal intensity in Tomm20 (mitochondrial mass), NDUFB8 (complex I) and MTCO1 (complex IV) in old age non-diabetic human donors compared to young non-diabetic human donors. Mean ± 95% CI. (A1, B1, C1) Signal intensity case comparison. Young non-diabetic donors (ND-Y1 to ND-Y5); old non-diabetic donors (ND-O1 to ND-O7). Each dot represents one islet and 50 islets were studied for one case. (A1) SI-Tomm20. One-way ANOVA, $p<0.01$; (B1) SI-NDUFB8. One-way ANOVA, $p<0.01$; (C1) SI-MTCO1. One-way ANOVA, $p<0.01$. **(A2, B2, C2) Signal intensity group average comparison.** Young non-diabetic donors (ND-Y); old non-diabetic donors (ND-O). Each point represents an average data of 50 islets. (A2) SI-Tomm20 group average. Unpaired t-test, $p<0.01$. (B2) SI-NDUFB8 group average. Unpaired t-test, $p>0.05$; (C2) SI-MTCO1 group average. Unpaired t-test, $p>0.05$.

REFERENCES

Adaes, S. (2019). "What is Mitochondrial Biogenesis? Benefits & Effects ".

Alagiakrishnan, K. and L. Mereu (2010). "Approach to managing hypoglycemia in elderly patients with diabetes." Postgraduate Medicine **122**(3): 129-137.

Aranda-Anzaldo, A. (2012). "The post-mitotic state in neurons correlates with a stable nuclear higher-order structure." Communicative & integrative biology **5**(2): 134-139.

Arrojo e Drigo, R., et al. (2015). "New insights into the architecture of the islet of Langerhans: a focused cross-species assessment." Diabetologia **58**(10): 2218-2228.

Attardi, G. and G. Schatz (1988). "BIOGENESIS OF MITOCHONDRIA." Annual Review of Cell Biology **4**: 289-333.

Avila, J. J., et al. (2017). "Differences in exercise capacity and responses to training in 24 inbred mouse strains." Frontiers in Physiology **8**: 974.

Ayala, J. E., et al. (2010). "Standard operating procedures for describing and performing metabolic tests of glucose homeostasis in mice." Disease models & mechanisms **3**(9-10): 525-534.

Baines, H. L., et al. (2014). "Similar patterns of clonally expanded somatic mtDNA mutations in the colon of heterozygous mtDNA mutator mice and ageing humans." Mechanisms of Ageing and Development **139**: 22-30.

Baines, H. L., et al. (2014). "Human stem cell aging: do mitochondrial DNA mutations have a causal role?" Aging Cell **13**(2): 201-205.

Balaban, R. S., et al. (2005). "Mitochondria, Oxidants, and Aging." Cell **120**(4): 483-495.

Barja, G. and A. Herrero (2000). "Oxidative damage to mitochondrial DNA is inversely related to maximum life span in the heart and brain of mammals." Faseb Journal **14**(2): 312-318.

Beckman, K. B. and B. N. Ames (1998). "The free radical theory of aging matures." Physiological Reviews **78**(2): 547-581.

Bensch, K., et al. (2007). "A transgenic model to study the pathogenesis of somatic mtDNA mutation accumulation in β - cells." Diabetes, Obesity and Metabolism **9**: 74-80.

Bensellam, M., et al. (2018). "Mechanisms of beta-cell dedifferentiation in diabetes: recent findings and future research directions." Journal of Endocrinology **236**(2): R109-R143.

Bettencourt, M.-C., et al. (1996). "Ki-67 expression is a prognostic marker of prostate cancer recurrence after radical prostatectomy." The Journal of urology **156**(3): 1064-1068.

Blodgett, D. M., et al. (2013). Age and Gender Effects on Human Islet Cell Composition. Diabetes, AMER DIABETES ASSOC 1701 N BEAUREGARD ST, ALEXANDRIA, VA 22311-1717 USA.

Bonner-Weir, S., et al. (2010). "beta-Cell Growth and Regeneration: Replication Is Only Part of the Story." Diabetes **59**(10): 2340-2348.

Bonner-Weir, S., et al. (2015). "Human islet morphology revisited: human and rodent islets are not so different after all." Journal of Histochemistry & Cytochemistry **63**(8): 604-612.

Bonner-Weir, S., et al. (2000). "In vitro cultivation of human islets from expanded ductal tissue." Proceedings of the National Academy of Sciences of the United States of America **97**(14): 7999-8004.

Booth, F. W. and D. B. Thomason (1991). "Molecular and cellular adaptation of muscle in response to exercise: perspectives of various models." Physiological Reviews **71**(2): 541-585.

Bouwens, L. and I. Rooman (2005). "Regulation of pancreatic beta-cell mass." Physiological Reviews **85**(4): 1255-1270.

Boveris, A. and A. Navarro (2008). "Systemic and mitochondrial adaptive responses to moderate exercise in rodents." Free Radical Biology and Medicine **44**(2): 224-229.

Bowman, A. and M. A. Birch-Machin (2016). "Age-Dependent Decrease of Mitochondrial Complex II Activity in Human Skin Fibroblasts." Journal of Investigative Dermatology **136**(5): 912-919.

Brandt, U. (2006). "Energy converting NADH : Quinone oxidoreductase (Complex I)." Annual Review of Biochemistry **75**: 69-92.

Briant, L., et al. (2016). "Glucagon secretion from pancreatic α-cells." Upsala journal of medical sciences **121**(2): 113-119.

Buso, A., et al. (2019). "Mitochondrial Adaptations in Elderly and Young Men Skeletal Muscle Following 2 Weeks of Bed Rest and Rehabilitation." Frontiers in Physiology **10**(474).

Butler, A. E., et al. (2003). "beta-cell deficit and increased beta-cell apoptosis in humans with type 2 diabetes." Diabetes **52**(1): 102-110.

Byrne, M. M., et al. (1996). "Elevated plasma glucose 2 h postchallenge predicts defects in beta-cell function." American Journal of Physiology-Endocrinology and Metabolism **270**(4): E572-E579.

Cabrera, O., et al. (2006). "The unique cytoarchitecture of human pancreatic islets has implications for islet cell function." Proceedings of the National Academy of Sciences of the United States of America **103**(7): 2334-2339.

Care, D. (2004). "Diagnosis and classification of diabetes mellitus." Diabetes Care **27**.

Cecchini, G., et al. (2002). "Succinate dehydrogenase and fumarate reductase from Escherichia coli." Biochimica Et Biophysica Acta-Bioenergetics **1553**(1-2): 140-157.

Chang-Chen, K. J., et al. (2008). "beta-cell failure as a complication of diabetes." Reviews in Endocrine & Metabolic Disorders **9**(4): 329-343.

Chang, A. M. and J. B. Halter (2003). "Aging and insulin secretion." American Journal of Physiology-Endocrinology and Metabolism **284**(1): E7-E12.

Chen, C., et al. (2019). "Investigation of mitochondrial biogenesis defects in single substantia nigra neurons using post-mortem human tissues." Neurobiology of disease: 104631.

Chen, C. G., et al. (2017). "Human beta cell mass and function in diabetes: Recent advances in knowledge and technologies to understand disease pathogenesis." Molecular Metabolism **6**(9): 943-957.

Chen, M., et al. (1985). "Pathogenesis of age-related glucose intolerance in man: insulin resistance and decreased β-cell function." The Journal of Clinical Endocrinology & Metabolism **60**(1): 13-20.

Chistiakov, D. A., et al. (2014). "Mitochondrial aging and age-related dysfunction of mitochondria." BioMed research international **2014**.

Cinti, F., et al. (2016). "Evidence of β-cell dedifferentiation in human type 2 diabetes." The Journal of Clinical Endocrinology & Metabolism **101**(3): 1044-1054.

Clapham, D. E. (2007). "Calcium Signaling." Cell **131**(6): 1047-1058.

Clark, A. (2008). The Metabolic Syndrome: Epidemiology, Clinical Treatment, and Underlying mechanisms. B. C. Hansen, Bray, George A, Humana Press.

Cnop, M., et al. (2011). "Longevity of human islet alpha- and beta-cells." Diabetes Obesity & Metabolism **13**: 39-46.

Coller, H. A., et al. (2001). "High frequency of homoplasmic mitochondrial DNA mutations in human tumors can be explained without selection." Nature Genetics **28**(2): 147.

Cree, L. M., et al. (2008). "Age-related decline in mitochondrial DNA copy number in isolated human pancreatic islets." Diabetologia **51**(8): 1440-1443.

Davies, K. J., et al. (1982). "Free radicals and tissue damage produced by exercise." Biochemical and Biophysical Research Communications **107**(4): 1198-1205.

De Biase, C., et al. (2014). "Effects of physical activity on endothelial progenitor cells (EPCs)." Frontiers in Physiology **4**: 414.

DeFronzo, R. A. (1979). "Glucose Intolerance and Aging: Evidence for Tissue Insensitivity to Insulin." Diabetes **28**(12): 1095-1101.

DeFronzo, R. A. (1981). "Glucose intolerance and aging." Diabetes Care **4**(4): 493-501.

DeFronzo, R. A. (2004). "Pathogenesis of type 2 diabetes mellitus." Medical Clinics **88**(4): 787-835.

DeFronzo, R. A., et al. (2015). International textbook of diabetes mellitus, 2 volume set, John Wiley & Sons.

Del Campo, A., et al. (2018). "Muscle function decline and mitochondria changes in middle age precede sarcopenia in mice." Aging (Albany NY) **10**(1): 34.

Dhawan, S., et al. (2007). "Formation and regeneration of the endocrine pancreas." Current opinion in cell biology **19**(6): 634-645.

Diabetes, U. Diabetes: facts and stats. Dec 2015.

DiMauro, S. and E. A. Schon (2003). "Mitochondrial respiratory-chain diseases." New England Journal of Medicine **348**(26): 2656-2668.

Dobson, P. F., et al. (2016). "Unique quadruple immunofluorescence assay demonstrates mitochondrial respiratory chain dysfunction in osteoblasts of aged and PolgA−/− mice." Scientific reports **6**: 31907.

Dolenšek, J., et al. (2015). "Structural similarities and differences between the human and the mouse pancreas." Islets **7**(1): e1024405.

E, L., et al. (2014). "Effect of high-intensity exercise on aged mouse brain mitochondria, neurogenesis, and inflammation." Neurobiology of Aging **35**(11): 2574-2583.

Elston, T., et al. (1998). "Energy transduction in ATP synthase." Nature **391**(6666): 510-513.

Erlandsen, S. L., et al. (1976). "Pancreatic islet cell hormones distribution of cell types in the islet and evidence for the presence of somatostatin and gastrin within the D cell." Journal of Histochemistry & Cytochemistry **24**(7): 883-897.

Falkenberg, M., et al. (2007). DNA replication and transcription in mammalian mitochondria. Annual Review of Biochemistry. **76:** 679-699.

Faxen, K., et al. (2005). "A mechanistic principle for proton pumping by cytochrome c oxidase." Nature **437**(7056): 286-289.

Feng, A. L., et al. (2017). "Paracrine GABA and insulin regulate pancreatic alpha cell proliferation in a mouse model of type 1 diabetes." Diabetologia **60**(6): 1033-1042.

Ferrannini, E., et al. (1997). "Insulin resistance and hypersecretion in obesity." Journal of Clinical Investigation **100**(5): 1166-1173.

Fink, R. I., et al. (1983). "Mechanisms of Insulin Resistance in Aging." The Journal of clinical investigation **71**(6): 1523-1535.

Finsterer, J. (2004). "Mitochondriopathies." European Journal of Neurology **11**(3): 163-186.

Fox, J. G., et al. (2006). The mouse in biomedical research: normative biology, husbandry, and models, Elsevier.

Gerdes, J., et al. (1983). "Production of a mouse monoclonal antibody reactive with a human nuclear antigen associated with cell proliferation." International journal of cancer **31**(1): 13-20.

Greaves, L. C. and R. W. Taylor (2006). "Mitochondrial DNA mutations in human disease." Iubmb Life **58**(3): 143-151.

Greaves, L. C. and D. M. Turnbull (2009). "Mitochondrial DNA mutations and ageing." Biochimica Et Biophysica Acta-General Subjects **1790**(10): 1015-1020.

Gregg, B. E., et al. (2012). "Formation of a Human beta-Cell Population within Pancreatic Islets Is Set Early in Life." Journal of Clinical Endocrinology & Metabolism **97**(9): 3197-3206.

Group, U. P. D. S. (1995). "UK Prospective Diabetes Study 16: overview of 6 years' therapy of type II diabetes: a progressive disease." Diabetes **44**(11): 1249-1258.

Güssow, D., et al. (1987). "The human beta 2-microglobulin gene. Primary structure and definition of the transcriptional unit." The Journal of Immunology **139**(9): 3132-3138.

Han, M.-J., et al. (2003). "Cell proliferation induced by reactive oxygen species is mediated via mitogen-activated protein kinase in Chinese hamster lung fibroblast (V79) cells." Molecules and cells **15**(1): 94-101.

Harris, M. and C. Thompson (2000). "The role of the Bcl-2 family in the regulation of outer mitochondrial membrane permeability." Cell Death & Differentiation **7**(12): 1182-1191.

Hart, N. J., et al. (2014). Age-related Changes in Islet Cell Composition, Proliferation, and Mass in Human Pancreas. Diabetes, AMER DIABETES ASSOC 1701 N BEAUREGARD ST, ALEXANDRIA, VA 22311-1717 USA.

Holloszy, J. O. and F. W. Booth (1976). "Biochemical adaptations to endurance exercise in muscle." Annual Review of Physiology **38**(1): 273-291.

Houghton, D., et al. (2017). "Impact of age-related mitochondrial dysfunction and exercise on intestinal microbiota composition." The Journals of Gerontology: Series A **73**(5): 571-578.

Huttemann, M., et al. (2011). "The multiple functions of cytochrome c and their regulation in life and death decisions of the mammalian cell: From respiration to apoptosis." Mitochondrion **11**(3): 369-381.

Ihm, S.-H., et al. (2006). "Effect of donor age on function of isolated human islets." Diabetes **55**(5): 1361-1368.

Ishihara, H., et al. (2003). "Islet β-cell secretion determines glucagon release from neighbouring α-cells." Nature cell biology **5**(4): 330-335.

Janssen, R. J., et al. (2006). "Mitochondrial complex I: structure, function and pathology." J Inherit Metab Dis **29**(4): 499-515.

Jia, Y. B. (2012). Real-Time PCR. Laboratory Methods in Cell Biology: Biochemistry and Cell Culture. P. M. Conn. **112:** 55-68.

Johannsen, D. L. and E. Ravussin (2009). "The role of mitochondria in health and disease." Current opinion in pharmacology **9**(6): 780-786.

Kaaman, M., et al. (2007). "Strong association between mitochondrial DNA copy number and lipogenesis in human white adipose tissue." Diabetologia **50**(12): 2526-2533.

Kahn, S. E., et al. (1992). "Exercise training delineates the importance of B-cell dysfunction to the glucose intolerance of human aging." The Journal of Clinical Endocrinology & Metabolism **74**(6): 1336-1342.

Kahn, S. E., et al. (1993). "QUANTIFICATION OF THE RELATIONSHIP BETWEEN INSULIN SENSITIVITY AND BETA-CELL FUNCTION IN HUMAN-SUBJECTS - EVIDENCE FOR A HYPERBOLIC FUNCTION." Diabetes **42**(11): 1663-1672.

Kassem, S. A., et al. (2000). "beta-cell proliferation and apoptosis in the developing normal human pancreas and in hyperinsulinism of infancy." Diabetes **49**(8): 1325-1333.

Kaufman, B. A., et al. (2015). "Mitochondrial regulation of β-cell function: Maintaining the momentum for insulin release." Molecular Aspects of Medicine **42**: 91-104.

Kauppila, J. H. K., et al. (2016). "A Phenotype-Driven Approach to Generate Mouse Models with Pathogenic mtDNA Mutations Causing Mitochondrial Disease." Cell Reports **16**(11): 2980-2990.

Kauppila, T. E. S., et al. (2017). "Mammalian Mitochondria and Aging: An Update." Cell Metabolism **25**(1): 57-71.

Kehm, R., et al. (2018). "Age-related oxidative changes in pancreatic islets are predominantly located in the vascular system." Redox biology **15**: 387-393.

Kemi, O. J., et al. (2002). "Intensity-controlled treadmill running in mice: cardiac and skeletal muscle hypertrophy." Journal of applied physiology **93**(4): 1301-1309.

Kerr, J. F., et al. (1972). "Apoptosis: a basic biological phenomenon with wideranging implications in tissue kinetics." British journal of cancer **26**(4): 239.

Khaidakov, M., et al. (2003). "Accumulation of point mutations in mitochondrial DNA of aging mice." Mutation Research/Fundamental and Molecular Mechanisms of Mutagenesis **526**(1-2): 1-7.

Kharouta, M., et al. (2009). "No mantle formation in rodent islets—the prototype of islet revisited." Diabetes Research and Clinical Practice **85**(3): 252-257.

Kim, J., et al. (2017). "Amino acid transporter Slc38a5 controls glucagon receptor inhibition-induced pancreatic α cell hyperplasia in mice." Cell Metabolism **25**(6): 1348-1361. e1348.

Kirichok, Y., et al. (2004). "The mitochondrial calcium uniporter is a highly selective ion channel." Nature **427**(6972): 360.

Kobayashi, T., et al. (1997). "In situ characterization of islets in diabetes with a mitochondrial DNA mutation at nucleotide position 3243." Diabetes **46**(10): 1567-1571.

Kroemer, G., et al. (1998). "The mitochondrial death/life regulator in apoptosis and necrosis." Annual Review of Physiology **60**: 619-642.

Ku, H.-H., et al. (1993). "Relationship between mitochondrial superoxide and hydrogen peroxide production and longevity of mammalian species." Free Radical Biology and Medicine **15**(6): 621-627.

Kujoth, G. C., et al. (2005). "Mitochondrial DNA mutations, oxidative stress, and apoptosis in mammalian aging." Science **309**(5733): 481-484.

Laboratory, H. Life span as a biomarker.

Lam, C. J., et al. (2019). "Glucagon Receptor Antagonist–Stimulated α-Cell Proliferation Is Severely Restricted With Advanced Age." Diabetes **68**(5): 963-974.

Larsen, S., et al. (2012). "Biomarkers of mitochondrial content in skeletal muscle of healthy young human subjects." The Journal of physiology **590**(14): 3349-3360.

Larsson, N. G., et al. (1998). "Mitochondrial transcription factor A is necessary for mtDNA maintenance and embryogenesis in mice." Nature Genetics **18**(3): 231-236.

Li, L.-D., et al. (2015). "Down-regulation of NDUFB9 promotes breast cancer cell proliferation, metastasis by mediating mitochondrial metabolism." PLoS One **10**(12): e0144441.

Li, L. S., et al. (2014). "Defects in beta-Cell Ca2+ Dynamics in Age-Induced Diabetes." Diabetes **63**(12): 4100-4114.

Li, T., et al. (2016). "Sex effect on insulin secretion and mitochondrial function in pancreatic beta cells of elderly Wistar rats." Endocrine research **41**(3): 167-179.

Liesa, M. and O. S. Shirihai (2013). "Mitochondrial dynamics in the regulation of nutrient utilization and energy expenditure." Cell Metabolism **17**(4): 491-506.

Linnane, A., et al. (1989). "Mitochondrial DNA mutations as an important contributor to ageing and degenerative diseases." The Lancet **333**(8639): 642-645.

Logan, A., et al. (2014). "In vivo levels of mitochondrial hydrogen peroxide increase with age in mt DNA mutator mice." Aging Cell **13**(4): 765-768.

Loschen, G., et al. (1974). "Superoxide radicals as precursors of mitochondrial hydrogen peroxide." Febs Letters **42**(1): 68-72.

Lowell, B. B. and G. I. Shulman (2005). "Mitochondrial Dysfunction and Type 2 Diabetes." Science **307**(5708): 384-387.

Luzi, L. and R. A. DeFronzo (1989). "Effect of loss of first-phase insulin secretion on hepatic glucose production and tissue glucose disposal in humans." American Journal of Physiology-Endocrinology and Metabolism **257**(2): E241-E246.

Lynn, S., et al. (2003). "Heteroplasmic ratio of the A3243G mitochondrial DNA mutation in single pancreatic beta cells." Diabetologia **46**(2): 296-299.

Maechler, P., et al. (1999). "Hydrogen peroxide alters mitochondrial activation and insulin secretion in pancreatic beta cells." Journal of Biological Chemistry **274**(39): 27905-27913.

Maechler, P. and C. B. Wollheim (2001). "Mitochondrial function in normal and diabetic [beta]-cells." Nature **414**(6865): 807-812.

Mannella, C. A. (2008). "Structural diversity of mitochondria: functional implications." Ann N Y Acad Sci **1147**: 171-179.

Marroqui, L., et al. (2015). "Pancreatic α cells are resistant to metabolic stress-induced apoptosis in type 2 diabetes." EBioMedicine **2**(5): 378-385.

Mattson, M. P. and S. L. Chan (2003). "Calcium orchestrates apoptosis." Nature cell biology **5**(12): 1041.

Mehta, Z. B., et al. (2016). "Changes in the expression of the type 2 diabetes-associated gene VPS13C in the β-cell are associated with glucose intolerance in humans and mice." American Journal of Physiology-Endocrinology and Metabolism **311**(2): E488-E507.

Mejia, E. M. and G. M. Hatch (2016). "Mitochondrial phospholipids: role in mitochondrial function." Journal of Bioenergetics and Biomembranes **48**(2): 99-112.

Menshikova, E. V., et al. (2006). "Effects of exercise on mitochondrial content and function in aging human skeletal muscle." The Journals of Gerontology Series A: Biological Sciences and Medical Sciences **61**(6): 534-540.

Miller, F. J., et al. (2003). "Precise determination of mitochondrial DNA copy number in human skeletal and cardiac muscle by a PCR-based assay: lack of change of copy number with age." Nucleic Acids Research **31**(11).

Miller, K., et al. (2009). "Islet formation during the neonatal development in mice." PLoS One **4**(11): e7739.

Mimaki, M., et al. (2012). "Understanding mitochondrial complex I assembly in health and disease." Biochimica et Biophysica Acta (BBA) - Bioenergetics **1817**(6): 851-862.

Mitchell, P. (1975). "PROTONMOTIVE REDOX MECHANISM OF CYTOCHROME-B-C1 COMPLEX IN RESPIRATORY-CHAIN - PROTONMOTIVE UBIQUINONE CYCLE." Febs Letters **56**(1): 1-6.

Mito, T., et al. (2013). "Mitochondrial DNA mutations in mutator mice confer respiration defects and B-cell lymphoma development." PLoS One **8**(2): e55789.

Mizukami, H., et al. (2014). "Age-associated changes of islet endocrine cells and the effects of body mass index in Japanese." Journal of diabetes investigation **5**(1): 38-47.

Montanya, E., et al. (2000). "Linear correlation between beta-cell mass and body weight throughout the lifespan in Lewis rats: role of beta-cell hyperplasia and hypertrophy." Diabetes **49**(8): 1341-1346.

Moser, C. C., et al. (2006). "Electron tunneling chains of mitochondria." Biochimica et Biophysica Acta (BBA) - Bioenergetics **1757**(9): 1096-1109.

Muller, F. L., et al. (2008). "High rates of superoxide production in skeletal-muscle mitochondria respiring on both complex I-and complex II-linked substrates." Biochemical Journal **409**(2): 491-499.

Müller, T., et al. (2017). "The new biology and pharmacology of glucagon." Physiological Reviews **97**(2): 721-766.

Murphy, E., et al. (2016). "Mitochondrial function, biology, and role in disease: a scientific statement from the American Heart Association." Circulation research **118**(12): 1960-1991.

Murphy, M. P. (2009). "How mitochondria produce reactive oxygen species." Biochemical Journal **417**: 1-13.

Narath, E., et al. (2001). "Voluntary and forced exercise influence the survival and body composition of ageing male rats differently." Experimental gerontology **36**(10): 1699-1711.

Nebiker, L., et al. (2018). "Moderating Effects of Exercise Duration and Intensity in Neuromuscular vs. Endurance Exercise Interventions for the Treatment of Depression: A Meta-Analytical Review." Frontiers in psychiatry **9**: 305-305.

Nesbitt, V., et al. (2013). "The UK MRC Mitochondrial Disease Patient Cohort Study: clinical phenotypes associated with the m. 3243A> G mutation—implications for diagnosis and management." Journal of Neurology, Neurosurgery & Psychiatry **84**(8): 936-938.

Old, S. L. and M. A. Johnson (1989). "Methods of microphotometric assay of succinate dehydrogenase and cytochromec oxidase activities for use on human skeletal muscle." The Histochemical Journal **21**(9): 545-555.

Olver, T. D., et al. (2015). Molecular mechanisms for exercise training-induced changes in vascular structure and function: skeletal muscle, cardiac muscle, and the brain. Progress in molecular biology and translational science, Elsevier. **135:** 227-257.

Organization, W. H. (2006). "Definition and diagnosis of diabetes mellitus and intermediate hyperglycaemia: report of a WHO/IDF consultation."

Otabe, S., et al. (1999). "Molecular and histological evaluation of pancreata from patients with a mitochondrial gene mutation associated with impaired insulin secretion." Biochemical and Biophysical Research Communications **259**(1): 149-156.

Ouziel-Yahalom, L., et al. (2006). "Expansion and redifferentiation of adult human pancreatic islet cells." Biochemical and Biophysical Research Communications **341**(2): 291-298.

Palade, G. E. (1952). "The fine structure of mitochondria." The Anatomical Record **114**(3): 427-451.

Perl, S., et al. (2010). "Significant human β-cell turnover is limited to the first three decades of life as determined by in vivo thymidine analog incorporation and radiocarbon dating." The Journal of Clinical Endocrinology & Metabolism **95**(10): E234-E239.

Perlman, R. L. (2016). "Mouse models of human disease: An evolutionary perspective." Evolution, medicine, and public health **2016**(1): 170-176.

Picard, M., et al. (2014). "Progressive increase in mtDNA 3243A> G heteroplasmy causes abrupt transcriptional reprogramming." Proceedings of the National Academy of Sciences **111**(38): E4033-E4042.

Polonsky, K. S., et al. (1988). "24-HOUR PROFILES AND PULSATILE PATTERNS OF INSULIN-SECRETION IN NORMAL AND OBESE SUBJECTS." Journal of Clinical Investigation **81**(2): 442-448.

Poy, M. N., et al. (2009). "miR-375 maintains normal pancreatic α-and β-cell mass." Proceedings of the National Academy of Sciences **106**(14): 5813-5818.

Prevention., C. f. D. C. a. (2017). "National Diabetes Statistics Report, 2017.".

Proskuryakov, S. Y., et al. (2003). "Necrosis: a specific form of programmed cell death?" Experimental Cell Research **283**(1): 1-16.

Puri, S. and M. Hebrok (2012). Diabetic beta Cells: To Be or Not To Be?

Rahier, J., et al. (2008). "Pancreatic beta-cell mass in European subjects with type 2 diabetes." Diabetes Obesity & Metabolism **10**: 32-42.

Rajamanickam, C., et al. (1979). "Changes in mitochondrial DNA in cardiac hypertrophy in the rat." Circulation research **45**(4): 505-515.

Ramiya, V. K., et al. (2000). "Reversal of insulin-dependent diabetes using islets generated in vitro from pancreatic stem cells." Nature Medicine **6**(3): 278-282.

Rampelt, H., et al. (2017). "Role of the mitochondrial contact site and cristae organizing system in membrane architecture and dynamics." Biochimica et Biophysica Acta (BBA) - Molecular Cell Research **1864**(4): 737-746.

Rankin, M. M. and J. A. Kushner (2009). "Adaptive beta-cell Proliferation Is Severely Restricted With Advanced Age." Diabetes **58**(6): 1365-1372.

Rawal, S., et al. (2013). "Effect of Exercise on Pancreatic Islets in Zucker Diabetic Fatty Rats." Journal of Diabetes & Metabolism **S10**: 007.

Rich, P. R. (2003). "The molecular machinery of Keilin's respiratory chain." Biochemical Society Transactions **31**: 1095-1105.

Robertson., O. (1933). "The islands of langerhans in 19 cases of obesity." The Journal of Pathology and Bacteriology **37**(3): 473-481.

Rocha, M. C., et al. (2015). "A novel immunofluorescent assay to investigate oxidative phosphorylation deficiency in mitochondrial myopathy: understanding mechanisms and improving diagnosis." Scientific reports **5**: 15037.

Rooman, I., et al. (2002). "Gastrin stimulates beta-cell neogenesis and increases islet mass from transdifferentiated but not from normal exocrine pancreas tissue." Diabetes **51**(3): 686-690.

Rosenberg, L., et al. (1996). "Islet-cell regeneration in the diabetic hamster pancreas with restoration of normoglycaemia can be induced by a local growth factor (s)." Diabetologia **39**(3): 256-262.

Ross, J. M., et al. (2014). "Maternally transmitted mitochondrial DNA mutations can reduce lifespan." Scientific reports **4**(1): 6569.

Rowe, J., et al. (1983). "Characterization of the insulin resistance of aging." The Journal of clinical investigation **71**(6): 1581-1587.

Rygiel, K. A., et al. (2015). "Mitochondrial and inflammatory changes in sporadic inclusion body myositis." Neuropathol Appl Neurobiol **41**(3): 288-303.

Safdar, A., et al. (2009). "miRNA in the Regulation of Skeletal Muscle Adaptation to Acute Endurance Exercise in C57Bl/6J Male Mice." PLoS One **4**(5): e5610.

Safdar, A., et al. (2011). "Endurance exercise rescues progeroid aging and induces systemic mitochondrial rejuvenation in mtDNA mutator mice." Proceedings of the National Academy of Sciences **108**(10): 4135-4140.

Sanz, A. (2017). "OP-20 - Mitochondrial ROS and ageing." Free Radical Biology and Medicine **108**: S9.

Sarabia Marín, J. M., et al. (2018). "Influence of the exercise frequency, intensity, time and type according to different training modalities on the cardiac rehabilitation programs." European Journal of Human Movement **41**.

Sastre, J., et al. (2000). "Mitochondrial oxidative stress plays a key role in aging and apoptosis." Iubmb Life **49**(5): 427-435.

Scholzen, T. and J. Gerdes (2000). "The Ki‐67 protein: from the known and the unknown." Journal of cellular physiology **182**(3): 311-322.

Schon, E. A., et al. (2012). "Human mitochondrial DNA: roles of inherited and somatic mutations." Nature Reviews Genetics **13**(12): 878-890.

Sciacco, M. and E. Bonilla (1996). "Cytochemistry and immunocytochemistry of mitochondria in tissue sections." Methods Enzymol **264**: 509-521.

Sena, L. A. and N. S. Chandel (2012). "Physiological roles of mitochondrial reactive oxygen species." Molecular cell **48**(2): 158-167.

Silva, J. P., et al. (2000). "Impaired insulin secretion and β-cell loss in tissue-specific knockout mice with mitochondrial diabetes." Nature Genetics **26**(3): 336.

Skinner, J. S. (2005). "Influence of genetic factors on exercise and training.".

Sohal, R. S. (2002). "Role of oxidative stress and protein oxidation in the aging process." Free Radical Biology and Medicine **33**(1): 37-44.

Song, D. H., et al. (2013). "Biophysical significance of the inner mitochondrial membrane structure on the electrochemical potential of mitochondria." Physical review. E, Statistical, nonlinear, and soft matter physics **88**(6): 062723-062723.

Soro-Arnaiz, I., et al. (2016). "Role of Mitochondrial Complex IV in Age-Dependent Obesity." Cell Reports **16**(11): 2991-3002.

Sotgia, F., et al. (2012). "Mitochondrial metabolism in cancer metastasis: visualizing tumor cell mitochondria and the “reverse Warburg effect” in positive lymph node tissue." Cell Cycle **11**(7): 1445-1454.

Stattin, P., et al. (1997). "Cell proliferation assessed by Ki-67 immunoreactivity on formalin fixed tissues is a predictive factor for survival in prostate cancer." The Journal of urology **157**(1): 219-222.

Surwit, R. S., et al. (1988). "Diet-Induced Type II Diabetes in C57BL/6J Mice." Diabetes **37**(9): 1163.

Sutherland, L. N., et al. (2009). "Exercise and adrenaline increase PGC‐1α mRNA expression in rat adipose tissue." The Journal of physiology **587**(7): 1607-1617.

Svensson, M., et al. (2016). "Forced treadmill exercise can induce stress and increase neuronal damage in a mouse model of global cerebral ischemia." Neurobiology of stress **5**: 8-18.

Swenne, I. (1983). "Effects of aging on the regenerative capacity of the pancreatic B-cell of the rat." Diabetes **32**(1): 14-19.

Swenne, I. and A. Andersson (1984). "Effect of genetic background on the capacity for islet cell replication in mice." Diabetologia **27**(4): 464-467.

Tadaishi, M., et al. (2011). "Skeletal muscle-specific expression of PGC-1α-b, an exercise-responsive isoform, increases exercise capacity and peak oxygen uptake." PLoS One **6**(12): e28290.

Talchai, C., et al. (2012). "Pancreatic beta Cell Dedifferentiation as a Mechanism of Diabetic beta Cell Failure." Cell **150**(6): 1223-1234.

Taylor, R. W., et al. (2003). "Mitochondrial DNA mutations in human colonic crypt stem cells." The Journal of clinical investigation **112**(9): 1351-1360.

Thorel, F., et al. (2010). "Conversion of adult pancreatic alpha-cells to beta-cells after extreme beta-cell loss." Nature **464**(7292): 1149-1154.

Tondera, D., et al. (2009). "SLP‐2 is required for stress‐induced mitochondrial hyperfusion." The EMBO journal **28**(11): 1589-1600.

Trifunovic, A., et al. (2004). "Premature ageing in mice expressing defective mitochondrial DNA polymerase." Nature **429**(6990): 417-423.

Truscott, K. N., et al. (2003). "Mechanisms of Protein Import into Mitochondria." Current Biology **13**(8): R326-R337.

Tsukihara, T., et al. (1996). "The whole structure of the 13-subunit oxidized cytochrome c oxidase at 2.8 angstrom." Science **272**(5265): 1136-1144.

Tuomilehto, J., et al. (2001). "Prevention of Type 2 Diabetes Mellitus by Changes in Lifestyle among Subjects with Impaired Glucose Tolerance." New England Journal of Medicine **344**(18): 1343-1350.

Ubaida-Mohien, C., et al. (2019). "Discovery proteomics in aging human skeletal muscle finds change in spliceosome, immunity, proteostasis and mitochondria." eLife **8**.

Vermulst, M., et al. (2008). "DNA deletions and clonal mutations drive premature aging in mitochondrial mutator mice." Nature Genetics **40**(4): 392.

Vogel, F., et al. (2006). "Dynamic subcompartmentalization of the mitochondrial inner membrane." The Journal of cell biology **175**(2): 237-247.

Wajchenberg, B. L. (2007). "beta-cell failure in diabetes and preservation by clinical treatment." Endocrine Reviews **28**(2): 187-218.

Wallace, D. C. (1992). "Diseases of the mitochondrial DNA." Annual Review of Biochemistry **61**(1): 1175-1212.

Wallace, D. C. (1999). "Mitochondrial diseases in man and mouse." Science **283**(5407): 1482-1488.

Walther, D. M. and D. Rapaport (2009). "Biogenesis of mitochondrial outer membrane proteins." Biochimica Et Biophysica Acta-Molecular Cell Research **1793**(1): 42-51.

Wang, R. N., et al. (1996). "Beta-cell growth in adolescent and adult rats treated with streptozotocin during the neonatal period." Diabetologia **39**(5): 548-557.

Warburton, D. E., et al. (2010). "A systematic review of the evidence for Canada's Physical Activity Guidelines for Adults." International Journal of Behavioral Nutrition and Physical Activity **7**(1): 39.

Wei, M. C., et al. (2001). "Proapoptotic BAX and BAK: a requisite gateway to mitochondrial dysfunction and death." Science **292**(5517): 727-730.

Welle, S., et al. (2004). "Skeletal muscle gene expression profiles in 20–29 year old and 65–71 year old women." Experimental gerontology **39**(3): 369-377.

WHO (2016). "Global report on diabetes.".

Yankovskaya, V., et al. (2003). "Architecture of Succinate Dehydrogenase and Reactive Oxygen Species Generation." Science **299**(5607): 700-704.

Youle, R. J. and A. M. Van Der Bliek (2012). "Mitochondrial fission, fusion, and stress." Science **337**(6098): 1062-1065.

Zhao, R. Z., et al. (2019). "Mitochondrial electron transport chain, ROS generation and uncoupling (Review)." Int J Mol Med **44**(1): 3-15.

Zheng, L. M., et al. (1991). "Extracellular ATP as a trigger for apoptosis or programmed cell death." The Journal of cell biology **112**(2): 279-288.

Zheng, W., et al. (2006). "Origins of human mitochondrial point mutations as DNA polymerase γ-mediated errors." Mutation Research/Fundamental and Molecular Mechanisms of Mutagenesis **599**(1-2): 11-20.

Zhong, Y., et al. (2012). "Age-related decline of the cytochrome c oxidase subunit expression in the auditory cortex of the mimetic aging rat model associated with the common deletion." Hear Res **294**(1-2): 40-48.